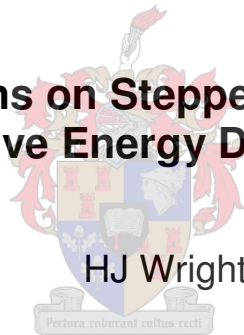




Thesis

**Protrusions on Stepped Spillways to
Improve Energy Dissipation**



HJ Wright

13304348

December 2006

Protrusions on Stepped Spillways to Improve Energy Dissipation

By

Henry-John Wright

13304348



Thesis presented in partial fulfilment of the requirements for the degree of
Master of Engineering Sciences (Civil) at Stellenbosch University

Prof GR Basson
Study Leader

Stellenbosch
December 2006

Declaration

I, the undersigned, hereby declare that the work contained in this thesis is my own original work and that I have not previously in its entirety or in part submitted it at any university for a degree.

Signed:

Date:



Acknowledgements

Thanks to the Lord for giving me the strength to do this research project.

I would like to thank the following persons for their advice, patience and guidance:

- Prof GR Basson (University of Stellenbosch);
- Mr NJ van Deventer (Department of Water Affairs: Hydraulic Studies);
- Mr HFWM Druyts (Department of Water Affairs: Earth- and Rockfill Dams);
- Mr GP Otto (Department of Water Affairs: Laboratory Services);
- Mr V Balintulo (Department of Water Affairs: Laboratory Services) and the personnel at the Hydraulic Laboratory who was responsible for the construction of the models; and
- Messrs N du Buisson, R Ras, J van Niekerk and H Muller (Department of Water Affairs: Directorate: Construction).

I would also like to thank the following institution:

- Department of Water Affairs and Forestry for the use of the Hydraulic Laboratory, the funding of the project and the permission to use the data obtained from the tests.

I would also like to thank all my friends and family for their support.

Synopsis

Stepped spillways constructed of roller compacted concrete (RCC) is a hydraulic and cost effective measure to dissipate energy of large water flows over the spillway of a dam. Stepped spillways, like other spillway types, have its limitations and a measure to improve the energy dissipation effectiveness is proposed.

Two hydraulic models were constructed at the hydraulics laboratory of the Department of Water Affairs and Forestry (DWAF) in Pretoria, South Africa. The scales of the models were 1:20 and 1:30.

The study proposes the use of triangular protrusions applied over the spillway surface. The protrusions have the same height as the steps, with the width of the protrusions varying. The triangular protrusions deflect the water sideways resulting in higher energy losses.

The results indicate that the protrusions reduce scouring at the toe of the dam, thus increasing the roughness of the steps. It also indicate that aeration occur earlier than with normal stepped spillways. An optimal spacing, lateral and across the steps, are proposed. The construction of the protrusions is also discussed, as well as the cost implications.

It is concluded that the protrusions are effective at a unit discharge up to 35 m³/s.m. This value is however dependent on the configuration of the apron downstream of the toe of the dam. It is proposed that protrusions be added on the downstream face of the dam on every second step, with one protrusion and then no protrusion alternating in the flow path. It is recommended that the protrusions be cast in situ.

Samevatting

Trapoorlope uit rolbeton is 'n hidrouliese en koste effektiewe manier van energie dissipering. Trapoorlope, soos enige ander oorloop, het egter sy beperkinge. 'n Metode om meer effektiewe energie dissipering te verkry word voorgestel.

Twee hidrouliese skaalmodelle is gebou in die hidroulika laboratorium van die Departement van Waterwese en Bosbou in Pretoria, Suid-Afrika. Die skaal van die modelle was onderskeidelik 1:20 en 1:30.

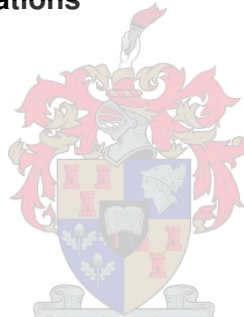
Die studie stel die gebruik van driehoekige "uitstulpings" oor die trapoorloop oppervlak voor. Die uitstulping (English: protrusion) het dieselfde hoogte as die trap, met die wydte van die uitstulping wat varieer. Die uitstulping deflekteer die water sydelings met meer energieverlies wat plaasvind.

Die resultate van die studie dui daarop dat die uitstulping uitskuring verminder by die toon van die dam en dus verhoog die ruheid van die trappe. Dit dui ook aan dat belugting vroeër begin as met normale trapoorlope. 'n Optimale spasiëring, lateraal en oor die wydte van die oorloop, word voorgestel. Die konstruksie van die uitstulpings word bespreek, asook die koste daaraan verbonde.

Daar word aanbeveel dat die uitstulpings 'n effektiewe manier van energie dissipering is vir 'n eenheidsdeurstroming van tot $35 \text{ m}^3/\text{s.m}$. Hierdie waarde is steeds afhanklik van die konfigurasie van die skort by die toon van die dam. Daar word voorgestel dat die uitstulpings op elke tweede trap van die oorloop gebruik word, met afwisselend een uitstulping en dan geen uitstulping. Daar word aanbeveel dat die uitstulpings in-situ gegiet word.

TABLE OF CONTENTS

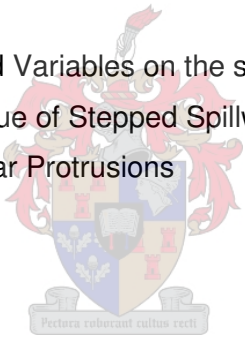
	Page
Declaration	i
Acknowledgements	ii
Synopsis	iii
Samevatting	iv
List of Figures	ix
List of Photographs	xiv
List of Tables	xvi
List of Acronyms and Abbreviations	xvii
List of Symbols	xviii
1 INTRODUCTION	1-1
1.1 Background	1-1
1.2 History of Dams	1-1
1.3 Spillways and Energy Dissipation Measures	1-10
1.4 Stepped Roller Compacted Concrete Spillways	1-11
1.5 Modeling of Spillways	1-13
1.6 Proposed Protrusions	1-13
1.7 Motivation for Research	1-14
2 LITERATURE STUDY	2-1
2.1 Definitions	2-2
2.2 Estimation of Roughness Values (f)	2-6
2.3 Air Inception	2-16
2.4 The Influence of Model Scales	2-23
2.5 Residual Energy	2-25



3	REVIEW OF LITERATURE	3-1
3.1	Flow Parameters	3-1
3.2	Roughness	3-2
3.3	Air Inception	3-6
4	EXPERIMENTAL WORK/PHYSICAL MODELING	4-1
4.1	De Hoop Dam	4-1
4.2	De Hoop Dam Model Studies	4-1
4.3	The Models	4-3
4.4	The First Model (Scale 1:20)	4-4
4.5	The Second Model (Scale 1:30)	4-9
4.6	Measurements	4-10
4.7	Protrusions	4-13
4.8	Spacing of Protrusions	4-15
4.9	Ratio between the Area of Protrusions	4-36
4.10	Hydraulic Jump Calculation and Flow Profile Calculation	4-38
5	HYDRAULIC MODEL TEST RESULTS	5-1
5.1	Standard Steps	5-1
5.2	The First Model (Scale1:20)	5-9
5.3	The Second Model (Scale 1:30)	5-18
5.4	Combined Roughness of both Models	5-28
5.5	Combined Length of Inception of both Models	5-29
5.6	Scouring at Both Models	5-31
6	DISCUSSION OF RESULTS	6-1
6.1	Variables	6-1
6.2	Protrusion Spacing	6-3
6.3	The Effect of Scale	6-9



6.4	The Effect of the Triangular Protrusions on the Spillway design of the De Hoop Dam	6-9
7	CONSTRUCTION ASPECTS AND COST	7-1
7.1	Normal RCC Placement	7-1
7.2	Construction Options	7-11
7.3	Cost of Adding the Protrusions	7-14
7.4	Cost of Standard Stilling Basins	7-14
8	CONCLUSIONS	8-1
8.1	Scale Effects	8-1
8.2	The Effect of the Identified Variables on the standard Steps	8-1
8.3	Prototype Roughness Value of Stepped Spillways	8-1
8.4	The Effect of the Triangular Protrusions	8-2
8.5	Summary	8-2
9	RECOMMENDATIONS	9-1
	REFERENCES	



APPENDICES

Appendix A: Graphs

Appendix B: Ogee and Apron Dimensions

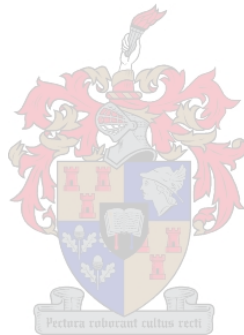
Appendix C: Photographs

Appendix D: Scour Drawings

Appendix E: De Hoop Dam background

Appendix F: Drawings of Models

Appendix G: Data



LIST OF FIGURES

	Page
Figure 1.1: Cross-section through Sadd el-Kafara Dam (Courtesy Fahlbusch, 2001)	1-3
Figure 1.2: Slope protection of Sadd el-Kafara Dam (Courtesy Fahlbusch, 2001)	1-4
Figure 1.3: The 60 m high Gouffre d'Enfer Dam in Paris (Courtesy Schnitter, 1994)	1-6
Figure 1.4: Layout of proposed protrusions	1-14
Figure 2.1: Section through a typical stepped spillway (DWAF, 2005)	2-2
Figure 2.2: Skim flow (Courtesy Rajaratnam, 1990)	2-3
Figure 2.3: Nappe flow (Courtesy Rajaratnam, 1990)	2-4
Figure 2.4: Point of inception (PI) (Courtesy Chanson, 2002)	2-5
Figure 2.5: Data by Tozzi of f versus Y/k (1994)	2-8
Figure 2.6: Re-analysis of data by Chanson et al (2000)	2-10
Figure 2.7: Friction factors for two downstream slopes according to Boes & Minor (2002)	2-11
Figure 2.8: Friction coefficient C_f versus k / Y by Chamani and Rajaratnam (1999)	2-12
Figure 2.9: Point of inception as defined by Wood et al (1983)	2-18
Figure 2.10: Mean air concentration at the point of inception as determined by Matos et al (2000)	2-19
Figure 2.11: The influence of scale on model results by Pegram et al (1999)	2-24
Figure 3.1: Tozzi's friction factor (1994)	3-2
Figure 3.2: Comparison between friction factors of Boes & Minor (2002) and Tozzi (1994)	3-3
Figure 3.3: Chamani's & Rajaratnam's (1999) data converted to a friction factor f and compared with Tozzi (1994) and Boes & Minor (2002)	3-4
Figure 3.4: Pegram et al (1999) and Tozzi's (1994) data converted to be depended only on Y_c	3-5

Figure 3.5:	Point of inception (PI) as determined by Chanson (1994), Matos (1999), Matos et al (2000) and Boes & Minor (2002)	3-7
Figure 4.1:	Dimension of the First Model (Scale 1:20)	4-5
Figure 4.2:	Location of the point of inception	4-13
Figure 4.3:	Protrusions for the First Model (Scale 1:20)	4-14
Figure 4.4:	Protrusions for the Second Model (Scale 1:30)	4-15
Figure 4.5:	Layouts tested by Van Deventer (2006)	4-16
Figure 4.6:	Plan of layout of Protrusion1 Layout 1 (Scale 1:20)	4-17
Figure 4.7:	Plan of layout of Protrusion1 Layout 2 (Scale 1:20)	4-18
Figure 4.8:	Plan of layout of Protrusion 1 Layout 3 (Scale 1:20)	4-19
Figure 4.9:	Plan of layout of Protrusion 1 Layout 4 (Scale 1:20)	4-20
Figure 4.10:	Plan of layout of Protrusion 2 Layout 1 (Scale 1:20)	4-22
Figure 4.11:	Plan of layout of Protrusion 2 Layout 2 (Scale 1:20)	4-23
Figure 4.12:	Plan of layout of Protrusion 2 Layout 3 (Scale 1:20)	4-25
Figure 4.13:	Plan of layout of Protrusion 2 Layout 4 (Scale 1:20)	4-25
Figure 4.14:	Plan of layout of Protrusion 1 Layout 1 (Scale 1:30)	4-27
Figure 4.15:	Plan of layout of Protrusion 1 Layout 2 (Scale 1:30)	4-28
Figure 4.16:	Plan of layout of Protrusion 1 Layout 3 (Scale 1:30)	4-29
Figure 4.17:	Plan of layout of Protrusion 1 Layout 4 (Scale 1:30)	4-30
Figure 4.18:	Plan of layout of Protrusion 1 Layout 5 (Scale 1:30)	4-31
Figure 4.19:	Plan of layout of Protrusion 2 Layout 1 (Scale 1:30)	4-31
Figure 4.20:	Plan of layout of Protrusion 2 Layout 2 (Scale 1:30)	4-33
Figure 4.21:	Plan of layout of Protrusion 2 Layout 3 (Scale 1:30)	4-34
Figure 4.22:	Plan of layout of Protrusion 2 Layout 4 (Scale 1:30)	4-35
Figure 4.23:	Measuring line on model	4-38
Figure 5.1:	Sequent depth measurements for both models	5-2
Figure 5.2:	Roughness of standard steps for both models obtained from modeling	5-3
Figure 5.3:	Data of roughness of standard steps compared with Tozzi (1994), Chamani et al (2000) and Boes & Minor (2002)	5-4
Figure 5.4:	Inception length for both models obtained from modeling	5-5

Figure 5.5:	Length of inception of standard steps for both models compared with Boes & Minor (2002), Chanson (1994), Matos (1999) and Matos et al (2000)	5-6
Figure 5.6:	Length of inception of standard steps combined for both models compared with Boes & Minor (2002), Chanson (1994), Matos (1999) and Matos et al (2000)	5-7
Figure 5.7:	Scour measurements	5-8
Figure 5.8:	Sequent depth measurements for Model 1 Protrusion 1 (Scale 1:20)	5-9
Figure 5.9:	Sequent depth measurements for Model 1 Protrusion 2 (Scale 1:20)	5-9
Figure 5.10:	Roughness of Model 1 Protrusion 1 (Scale 1:20) obtained from modeling	5-10
Figure 5.11:	Roughness of Model 1 Protrusion 2 (Scale 1:20) obtained from modeling	5-10
Figure 5.12:	Model data for Model 1 (Scale 1:20) compared with Tozzi (1994) and Pegram et al (1999)	5-11
Figure 5.13:	Comparison of observed roughness data for Model 1 Protrusion 1 (Scale 1:20) with Tozzi (1994), Chamani et al (2000) and Boes & Minor (2002)	5-12
Figure 5.14:	Comparison of observed roughness data for Model 1 Protrusion 2 (Scale 1:20) with Tozzi (1994), Chamani et al (2000) and Boes & Minor (2002)	5-12
Figure 5.15:	Comparison of observed roughness data for protrusions with Tozzi (1994), Chamani et al (2000) and Boes & Minor (2002) for Scale 1:20 Model	5-13
Figure 5.16:	Length of inception for Scale 1:20 Model for Protrusion 1	5-14
Figure 5.17:	Length of inception for Scale 1:20 Model for Protrusion 2	5-15
Figure 5.18:	Comparison of model data for Protrusion 1 (Scale 1:20) with Boes & Minor (2002), Chanson (1994), Matos (1999) and Matos et al (2000) for L_i	5-16
Figure 5.19:	Comparison of model data for Protrusion 2 (Scale 1:20) with Boes & Minor (2002), Chanson (1994), Matos (1999) and Matos et al (2000) for L_i	5-16

Figure 5.20: Combined Point of Inception for Model 1 (Scale 1:20) compared with Boes & Minor (2002), Chanson (1994), Matos (1999) and Matos et al (2000) for L_i	5-18
Figure 5.21: Sequent depth measurements for Model 2 Protrusion 1 (Scale 1:30)	5-19
Figure 5.22: Sequent depth measurements for Model 2 Protrusion 1 (Scale 1:30)	5-19
Figure 5.23: Roughness of Model 2 Protrusion 1 (Scale 1:30) obtained from modeling	5-20
Figure 5.24: Roughness of Model 2 Protrusion 1 (Scale 1:30) obtained from modeling	5-20
Figure 5.25: Model data for Model 2 (Scale 1:30) compared with Tozzi (1994) and Pegram et al (1999)	5-21
Figure 5.26: Comparison of observed roughness data for Model 2 Protrusion 1 (Scale 1:30) with Tozzi (1994), Chamani et al (2000) and Boes & Minor (2002)	5-22
Figure 5.27: Comparison of observed roughness data for Model 2 Protrusion 2 (Scale 1:30) with Tozzi (1994), Chamani et al (2000) and Boes & Minor (2002)	5-22
Figure 5.28: Comparison of observed roughness data for protrusions with Tozzi (1994), Chamani et al (2000) and Boes & Minor (2002) for Scale 1:30 Model	5-23
Figure 5.29: Length of inception for Scale 1:30 Model for Protrusion 1	5-24
Figure 5.30: Length of inception for Scale 1:30 Model for Protrusion 2	5-25
Figure 5.31: Comparison of model data for Protrusion 1 (Scale 1:30) with Boes & Minor (2002), Chanson (1994), Matos (1999) and Matos et al (2000) for L_i	5-26
Figure 5.32: Comparison of model data for Protrusion 2 (Scale 1:30) with Boes & Minor (2002), Chanson (1994), Matos (1999) and Matos et al (2000) for L_i	5-26
Figure 5.33: Combined Point of Inception for Model 2 (Scale 1:30) compared with Boes & Minor (2002), Chanson (1994), Matos (1999) and Matos et al (2000) for L_i	5-28
Figure 5.34: Comparison of observed data for protrusions and standard steps with Tozzi (1994), Chamani et al (2000) and Boes & Minor (2000)	5-29

Figure 5.35:	Point of Inception for both models compared with Boes & Minor (2002), Matos (1999), Matos et al (2000) and Chanson (1994)	5-30
Figure 5.36:	Combined Point of Inception for both models compared with Boes & Minor (2002), Matos (1999), Matos et al (2000) and Chanson (1994)	5-31
Figure 5.37:	Scour depths obtained for triangular protrusions and standard steps for both models at a prototype unit discharge of $q = 25 \text{ m}^3/\text{s.m}$ (RMF)	5-31
Figure 6.1:	Relative roughness of the protrusions for both models	6-5
Figure 6.2:	Scour depths and relative roughness of triangular protrusions for both models	6-6
Figure 6.3:	Schematical scour effect for unit discharges larger than $35 \text{ m}^3/\text{s.m}$	6-6
Figure 6.4:	Relative length of inception for both models	6-7
Figure 6.5:	Prototype position of point of inception observed from Model 2 (Scale 1:30)	6-10
Figure 6.6:	Velocities at the point of inception observed from Model 2 (Scale 1:30)	6-11
Figure 7.1:	RCC Placement Procedure (Courtesy DWAF, 2005)	7-7
Figure 7.2:	Sloped Layer RCC Placement (Courtesy DWAF, 2005)	7-8
Figure 7.3:	Non-continuous RCC Layer Placement (Courtesy DWAF, 2005)	7-9
Figure 7.4:	Crack Director Installation after RCC Compaction (Courtesy DWAF)	7-10
Figure 7.5:	Protrusion 1 converted to De Hoop Dam dimensions	7-12
Figure 7.6:	USBR Type II Stilling Basin (Courtesy USBR, 1987)	7-15
Figure 7.7:	Determination of Length of Stilling Basin (Courtesy USBR, 1987)	7-16
Figure 7.8:	Type II Basin Length for Protrusion P 1(1)	7-19

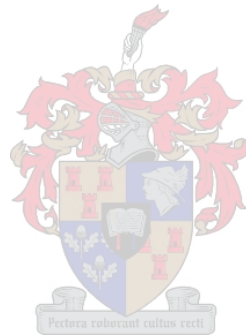
LIST OF PHOTOGRAPHS

	Page
Photograph 4.1: Flag Boshielo Dam apron splitters (Courtesy DWAF, 2005)	4-3
Photograph 4.2: The First Model (Scale 1:20) without protrusions	4-6
Photograph 4.3: Sluice gate and gate valve to adjust tailwater levels	4-6
Photograph 4.4: Connection from pumps	4-7
Photograph 4.5: Apron and shutter board at toe of spillway	4-7
Photograph 4.6: Flow stabilisers	4-8
Photograph 4.7: The Second Model (Scale 1:30) without protrusions	4-10
Photograph 4.8: Protrusion 1 Layout 1 (Scale 1:20)	4-18
Photograph 4.9: Protrusion 1 Layout 2 (Scale 1:20)	4-19
Photograph 4.10: Protrusion 1 Layout 4 (view 1) (Scale 1:20)	4-20
Photograph 4.11: Protrusion 1 Layout 4 (view 2) (Scale 1:20)	4-20
Photograph 4.12: Protrusion 2 Layout 1 (Scale 1:20)	4-22
Photograph 4.13: Protrusion 2 Layout 2 (Scale 1:20)	4-24
Photograph 4.14: Protrusion 2 Layout 4 (Scale 1:20)	4-26
Photograph 4.15: Protrusion 1 Layout 1 (Scale 1:30)	4-27
Photograph 4.16: Protrusion 1 Layout 2 (Scale 1:30)	4-28
Photograph 4.17: Protrusion 1 Layout 3 (Scale 1:30)	4-29
Photograph 4.18: Protrusion 1 Layout 4 (Scale 1:30)	4-30
Photograph 4.19: Protrusion 2 Layout 1 (Scale 1:30)	4-32
Photograph 4.20: Protrusion 2 Layout 2 (Scale 1:30)	4-33
Photograph 4.21: Protrusion 2 Layout 3 (Scale 1:30)	4-34
Photograph 4.22: Protrusion 2 Layout 4 (Scale 1:30)	4-35
Photograph 7.1: Conveyor system with self-propelled crawler placer (Courtesy US Corps of Engineers, 2000)	7-4
Photograph 7.2: Conveyor system with mobile side discharge belt (Courtesy US Corps of Engineers, 2000)	7-4
Photograph 7.3: Installation of waterstop, joint drain and crack initiator (Courtesy US Corps of Engineers, 2000)	7-5

LIST OF TABLES

		Page
Table 1.1:	List of ancient dams (Courtesy Schnitter, 1994)	1-2
Table 1.2:	Recorded periods of operation of ancient dams (Courtesy Schnitter, 1994)	1-2
Table 1.3:	Examples of gravity dams constructed of rubble masonry (Courtesy Schnitter, 1994)	1-6
Table 1.4:	Examples of gravity dams constructed of concrete (Courtesy Schnitter, 1994)	1-8
Table 4.1:	Protrusion Density for Model 1 (Scale 1:20)	4-37
Table 4.2:	Protrusion Density for Model 2 (Scale 1:30)	4-37
Table 5.1:	Roughness values for the standard steps for both models	5-2
Table 5.2:	Inception Length L_i for the standard steps for both models	5-5
Table 5.3:	Scour depths for the standard steps for the three models	5-8
Table 5.4:	Inception Length (L_i) for Protrusion 1 for Scale 1:20 Model	5-14
Table 5.5:	Inception Length (L_i) for Protrusion 2 for Scale 1:20 Model	5-15
Table 5.6:	Inception Length (L_i) for Protrusion 1 for Scale 1:30 Model	5-24
Table 5.7:	Inception Length (L_i) for Protrusion 2 for Scale 1:30 Model	5-25
Table 5.8:	Scour measurement at both models	5-31
Table 6.1:	Relative roughness of the Triangular Protrusions	6-4
Table 6.2:	Point of inception of the Triangular Protrusions	6-8
Table 7.1:	Sequent depth for all tested protrusion configurations	7-18
Table 7.2:	Reduction of stilling basin length for Scale 1:20 Model	7-19
Table 7.3:	Reduction of stilling basin length for Scale 1:30 Model	7-20
Table 7.4:	Reduction in sequent depth and basin depth for Scale 1:20 Model	7-20
Table 7.5:	Reduction in sequent depth and basin depth for Scale 1:30 Model	7-20

Table 8.1:	Friction, length of inception and protrusion density ratio's for Scale 1:20 Model tests	8-4
Table 8.2:	Friction, length of inception and protrusion density ratio's for Scale 1:30 Model tests	8-7



LIST OF ACRONYMS AND ABBREVIATIONS

AD	Anno Domini (used to indicate that a date comes the specified number of years after the traditional date of Christ's birth)
BC	Before Christ
DWAF	Department of Water Affairs and Forestry
EDR	Energy Dissipation ration
m	Metre
mm	Millimetres
NOC	Non-overflow Crest
PEL	Potential Economic Loss
PI	Point of Inception
PLL	Potential Loss of Life
RCC	Roller Compacted Concrete
RDF	Recommended Design Flood
SANCOLD	South African National Committee on Large Dams
SEF	Safety Evaluation Flood
USBR	United States Bureau of Reclamation

LIST OF SYMBOLS

A	Cross section area (m ²)
a ₁	Constant depending on chute slope
a ₂	Constant depending on chute slope
B	Width of chute (m)
b ₁	Constant
b ₂	Constant
C _a	Average air concentration (m ³ /m ³) defined as $C_a = (Y_{90} - Y) / Y_{90}$
C _f	Skin friction coefficient (dimensionless)
C _{mean}	Mean air concentration at point of inception
D	Hydraulic diameter (m) defined as $D = 4 R$
D ₂	Downstream sequent depth at hydraulic jump
d	Uniform flow depth (m)
d	Flow depth at inception point (m)
d _i	Flow depth at point of inception (m)
E	Specific energy head (m) defined as $E = Y \cos \theta + \alpha v^2 / 2 g$
E _c	Specific energy head for critical flow (m) defined as $E_c = 1,5 Y_c$
E _{res}	Specific energy at the toe of the spillway (m)
Fr	Froude number (dimensionless) defined as $Fr^2 = v^2 / g d_m$ with $d_m = A/T$
F	Roughness Froude number
F _n	Froude roughness number defined as $F_n^2 = q^2 / (g \sin \theta h^3) = Y_c^3 / (\sin \theta h^3)$
F _i	Inception Froude number defined as $F_i = q / \sqrt{g} (h / l) k^3$
F _k	Froude roughness number defined as $F_k^2 = q^2 / (g \sin \theta k^3) = Y_c^3 / (\sin \theta k^3)$
f	Darcy friction factor (dimensionless)
g	Acceleration due to gravity (m/s ²)
H	Total head (m) defined as $H = Z + P/Y + \alpha v^2 / 2 g$
H	Dam height (m)
H _A	Design head of spillway (m)
H _s	Depth from the upstream total energy line to the local water surface (m)
h	Step height (m)

h	Flow depth at the toe of the spillway (m)
h_c	Critical depth (m)
h_v	Velocity head (m) defined as $h_v = v^2 / 2g$
h_{mi}	Flow depth at the inception point (m)
I	Inception point
K_s	Uniform roughness
k	Roughness of steps (m) defined as $k = h \cos \theta$
k	Height of step normal to the bed (m)
k_s	Step dimension (m) normal to the flow as $k_s = h \cos \theta$
k_s	Surface roughness (m)
L	Length measured along bed of channel (m)
L	Distance from the crest (m)
L	Length of the stilling basin (m)
L_i	Length of inception (m)
L_k	Length between roughness peaks in the flow direction defined as $L_k = 2k / \sin 2\theta$
l	Length of the step thread (m)
n	Number
P	Hydrostatic pressure
P	Wetted perimeter (m)
Q	Discharge (m^3/s)
q	Unit discharge (discharge per unit width) ($m^3/s/m$)
R	Hydraulic Radius (m) defined as $R = A / P$
S_f	Friction slope (dimensionless) defined as $S_f = \Delta H / \Delta L$
S_o	Bed slope (dimensionless) defined as $S_o = \sin \theta$
s	Step height (m)
T	Triangle
TP	Triangular Protrusion
t	Tread of step (m)
u	Normal flow
v	Velocity (m/s)
v_0	Mean Velocity (m/s)
v_c	Critical velocity (m/s)
x	Horizontal distance (m)



x	Distance along the profile of the crest (m)
y_0	Normal depth (m)
Y	Depth of flow (m) for one phase flow
Y_{90}	Characteristic depth (m) where the air concentration is 90 %
Y_c	Critical flow depth (m)
Y_2	Downstream sequent depth at hydraulic jump
Z	Vertical distance (m) from crest of the spillway to any point
Z	Vertical distance (m) of any point above the horizontal datum line
Δ	Kinetic energy coefficient
ΔL	Difference in length along channel (m)
ΔZ	Potential energy head (m)
Δx	Inception point as the location measured along the channel invert (m)
\emptyset	Downstream slope of spillway
δ	Boundary layer thickness
γ	Specific weight (N/m^3)
Δ	Difference
ρ	Density (kg/m^3)
α	Kinetic energy correction factor



1 INTRODUCTION

A stepped spillway constructed of roller compacted concrete (RCC) is a hydraulic and cost effective measure to dissipate energy of large water flows over the spillway of a dam. Stepped spillways, like other spillway types, have their limitations and a measure to improve the energy dissipation effectiveness is proposed. The use of triangular protrusions is investigated and the benefit thereof is reported on.

1.1 Background

Large floods that need to be accommodated by the spillway of a dam require energy dissipation measures. Normally these are provided either near the spillway crest or at the toe of the dam. The amount of energy needed to be dissipated varies with the height of the dam and the flow rate that must be accommodated. Large floods tend to erode the area downstream of the toe of the dam, which in turn could cause failure if undermining of the structure occurs. The use of a stepped spillway can lead to a reduction in the dimensions of an energy dissipater structure at the toe of the dam. The amount of scouring must be dealt with during the design stage of the dam. Model studies are normally conducted to predict the severity of scouring.

Stepped spillways dissipate energy better than smooth surfaces. The rough face of stepped spillways can dissipate a portion of the energy. The more efficient energy can be dissipated on the steps, the lower the velocities will be at the toe of the spillway which results in a smaller energy dissipater structure at the toe of the dam. This saves cost and can lead to less complicated construction.

1.2 A History of Dams

1.2.1 General

A list of the oldest dams in the world is shown in Table 1.1. From the table it is evident that dam engineering started during the first half of the third millennium before Christ (BC). The purposes of the dams included water supply, flood control and water and soil conservation. Dams for irrigation purposes only became a priority one millennium later.

Table 1.1: List of ancient dams (Courtesy Schnitter, 1994)

Year Completed	Country	Name of Dam	Type	Purpose
3 000 BC	Jordan	Jawa	Gravity	Water supply
2 600 BC	Egypt	Sadd el-Kafara	Embankment	Flood control
2 500 BC	Baluchistan	Gabarbands	Gravity	Conservation
1 500 BC	Yemen	Marib	Embankment	Irrigation
1 260 BC	Greece	Kofini	Embankment	Flood control
1 250 BC	Turkey	Karakuyu	Embankment	Water supply
950 BC	Israel	Shiloah	Unknown	Water supply
703 BC	Iraq	Kisiri	Gravity	Irrigation
700 BC	Mexico	Purron	Embankment	Irrigation
581 BC	China	Anfengtang	Embankment	Irrigation
370 BC	Sri Lanka	Panda	Embankment	Irrigation
275 BC	Sudan	Musawwarat	Embankment	Water supply

The structural characteristics of ancient dams varied, but all of them had to resist the water pressure by the weight of the construction material. The dams were mainly embankment or gravity dams, as classified in modern terms. Most of the embankment dams were homogeneous (thus not zoned). Three main types of gravity dams existed, namely solid masonry walls, masonry walls with a central earth core and a masonry wall with a fill section downstream. It is speculated that the highest dam in the first century Anno Domini (AD) was 19 m high and the highest dam for the next 1 200 years was 34 m. Considerable reservoir capacities were achieved with this relatively low wall heights.

Some dams were in operation for long periods of time (See Table 1.2). Some fell into ruin mainly because of floods or earthquakes and problems occurring due to technical defects. The neglect of some dams also lead to their failure.

Table 1.2: Recorded periods of operation of ancient dams (Courtesy Schnitter, 1994)

Country	Name of Dam	Period of Operation	
		Years	End
Egypt	Lala'a	3 600	1900 AD
Greece	Kofini	3 300	In operation
Turkey	Keşiş Gölü	2 600	1891 AD
China	Anfengtang	2 600	In operation
Sri Lanka	Bassawak	2 300	Operating again
Sri Lanka	Tissa	2 300	Operating again
China	Tianping	2 200	In operation
Sri Lanka	Pavat	2 200	Operating again
Sri Lanka	Vavuni	2 200	Operating again
Yemen	Marib	2 100	630 AD
Sri Lanka	Nuwara	2 100	Operating again
Israel	Solomon Pools	2 000	In operation

1.2.2 The World's Oldest Dam

Some publications state that the Sadd el-Kafara Dam in Egypt is the oldest dam, while others (and Table 1.1, obtained from Schnitter, 1994) state that the Jawa Dam in Jordan is the oldest. A brief background of both dams is given in subsequent paragraphs.

The first known dam to exist was built in Egypt south of Cairo between the period 2750 and 2950 BC. The dam was called Sadd el-Kafara, which means "Dam of the Pagans" in Arabic. The dam was constructed for flood retention. The dam was 14 m high, 56 m wide at the crest, 98 m wide at the bottom and 113 m long. According to ancient hydrology, the capacity was estimated at 0,5 million cubic metres. The dam consisted of a silty sand and gravelly impervious core with rockfill shells. Resistance against erosion and wave action was provided on the upstream face by means of placed limestone blocks. The dam took nearly 10 years to construct. The dam failed and Egyptian engineers waited nearly eight centuries before attempting to build another dam. Figure 1.1 shows a cross section of the dam with Figure 1.2 showing the upstream slope protection.

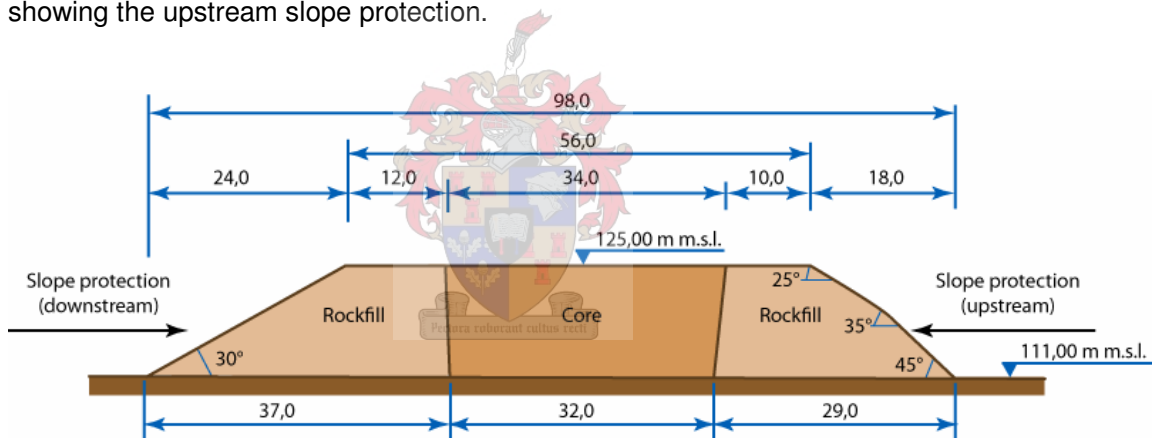


Figure 1.1: Cross section through Sadd el-Kafara Dam (Courtesy Fahlbusch, 2001)

The Jawa Dam was situated approximately 100 km northeast of the Jordan capital city of Amman. The dam supplied water for the town Jawa. The city is located in a desert and had 2 000 inhabitants. The dam site was favourable and selected on the basis of defence of the city. The primary purpose was to supply water. Five reservoirs were built in the Rajil River, with the biggest reservoir being 4,5 m high and 80 m long, called the Jawa Dam. The structure of the dam was complex, comprising of two dry masonry walls with a 2 m thick earth core providing the water retaining function. An impervious blanket was supplied in front of the upstream heel. A downstream embankment ensured stability of the structure. The structure

was designed to be raised by 1 m, but work was never started. The city and thus the dam were abandoned within one generation.



Figure 1.2: Slope protection of Sadd el-Kafara Dam (Courtesy Fahlbusch, 2001)

1.2.3 Historical Development of Dams

Dams can be classified according to their use, the material the dam is constructed from and according to the dam safety legislation.

Dams may be classified according to the broad functions they serve. It includes storage dams, flood detention dams and non-overflow dams.

The most common classification used for purpose of discussion of design procedures is based upon the materials comprising the structure. Examples are as follows:

- Earthfill dams;
- Rockfill dams;
- Concrete faced rockfill dams;
- Concrete gravity dams;

- Concrete arch dams;
- Concrete buttress dams; and
- Composite dams.

The category classification of the dam is based on the size of the dam and the hazard potential rating. Hazard potential is a qualitative indication of the potential loss of life (PLL) and the potential economical loss (PEL) that may result from failure of a dam. The classification is defined in the Dam Safety Regulations (DWAf, 1986).

Since this project is concerned with dissipating energy down a stepped spillway, the history of gravity dams is given. A stepped spillway is a gravity structure with a variable downstream slope. The slope depends on the stability of the structure. Earth- and rockfill dams will be briefly discussed. These structures can also be used with a gravity stepped spillway section or with an alternative spillway arrangement, as will be discussed under Section 1.3.

Gravity Dams

A gravity dam is a masonry or solid mass concrete structure. It resists the imposed forces by its own mass. The gravity dam is the most common concrete dam and the simplest to design and to construct. As with other dam types geological information, hydrological information, seismic data, foundation data and material investigations must be conducted before detail design can commence. Detail design includes the layout and structural analysis. Stresses in the structure and safety against sliding and overturning are then determined. Different spillway options can be used with a gravity dam, as discussed under Section 1.3. The most common type used with gravity dams is a spillway which forms part of the gravity structure. To meet the stability requirements as set by the design engineer, the downstream slope varies depending on the uplift conditions. A battered upstream slope can be used to increase the stability of the structure, but this is more difficult to construct than a vertical upstream slope. The crest width varies from dam to dam, but is normally wide enough to accommodate inspection and maintenance vehicles.

The analysis of the stresses in structures in their elastic condition and the concepts of the modulus of elasticity was introduced in 1826 by Professor LMH Navier. Linear distribution of stresses developed on the base of the dam was used to show that the most optimum profile of a gravity dam is a triangle with a vertical upstream face. Some early dams were inclined on the upstream face, while others proved to be unstable upon impoundment and drastic

measures had to be taken to ensure stability. In France a 60 m high gravity dam was built from 1859 to 1866. The Gouffre d'Enfer Dam had a base width of 82 % of the height, with the maximum compressive stress limited to 0,6 MPa. Figure 1.3 shows a cross section of the Gouffre d'Enfer Dam. The dam was also curved in plan. Most of the gravity dams were constructed of rubble masonry up to World War I, with Portland cement being used nowadays. Table 1.3 shows gravity dams constructed of rubble masonry.

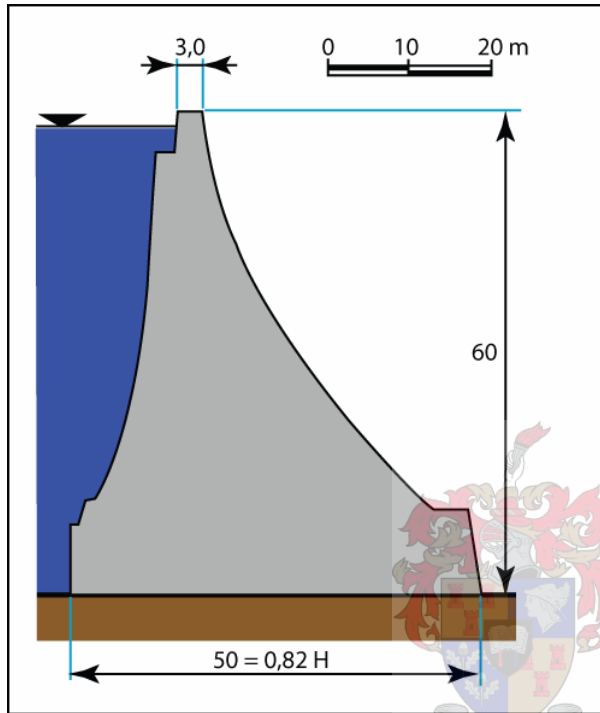


Figure 1.3: The 60 m high Gouffre d'Enfer Dam in Paris (Courtesy Schnitter, 1994)

Table 1.3: Gravity dams constructed of rubble masonry (Courtesy Schnitter, 1994)

Year of completion	Name of Dam	Country	Height (m)	Length (m)	Masonry volume (1 000 m ³)	Purpose
1866	Gouffre d'Enfer	France	60	102	40	Flood control
1875	Gileppe	Belgium	52	235	249	Water supply
1879	Khadakvasla	India	40	1 471	290	Irrigation/Water supply
1892	Tansa	India	41	2 804	312	Water supply
1902	Aswan	Egypt	39	1 950	545	Irrigation
1904	Cheeseman	USA	72	216	79	Water supply
1906	New Croton	USA	91	329	516	Water supply
1912	Aswan	Egypt	44	1 982	1 057	Irrigation
1934	Mettur	India	70	1 615	1 545	Irrigation/Power generation
1974	Nagarjuna	India	125	1 450	5 635	Irrigation/Power generation

The Gileppe Dam in Belgium required almost 250 000 m³ of masonry due to the cross-section. The conservative base width of 132 % of the height of the dam was due to concern of the design engineers regarding the water seeping through the dam and the foundation creating uplift forces. The engineers assumed that the whole dam would act as if it were submerged. In Germany the 25 m high Alfeld Dam was designed with the uplift pressure at the heel of the dam decreasing linearly from the full water pressure to zero at the downstream toe.

Foundation drainage was first introduced during the construction of the 40 m high Vyrnwy Dam southwest of Liverpool in Britain during 1882 to 1890. Transverse drains which ended in vertical shafts were used. The shafts led to a longitudinal gallery above the tailwater level and this was connected by a transversal gallery to the downstream face. An uplift pressure equal to the reservoir head was assumed for the section up to the drainage holes with uplift pressure equal to the tailwater head used for the rest of the dam.

More than one generation passed before this early work on uplift forces was fully understood by the dam building community. Drainage provisions were refined and used with success in the 107 m high Arrowrock Dam in the Idaho State (United States of America) from 1911 to 1915.

Concrete manufactured using Portland cement was used for the first time for the construction of the Boyds Corner Dam near New York from 1866 to 1872. It was also used in Switzerland at the Pérolles Dam during the same time. During the construction of the Lower Crystal Spring Dam south of San Francisco attention was given to the ratio between water and cement and the influence on the strength of the concrete. It was found that the lower the water/cement ratio the better the quality of the concrete. This includes higher strength, better impermeability and durability of the concrete. However the water content ensures workability of concrete while too much cement can cause increased heat generation and result in cracking. Cooling of concrete soon became necessary, as well as the provision of vertical contraction joints. Special cement as well as the use of pozzolans was later used to reduce heat generation within the concrete. Table 1.4 shows gravity dams constructed of concrete.

Table 1.4: Gravity dams constructed of concrete (Courtesy Schnitter, 1994)

Year of completion	Name of Dam	Country	Height (m)	Length (m)	Concrete volume (1 000 m ³)	Purpose
1872	Boyds Corner	USA	24	204	20	Water supply
1872	Pérolles	Switzerland	21	195	32	Power generation
1890	Crystal Springs	USA	45	183	120	Water supply
1897	Periyar	India	54	439	140	Irrigation/Power generation
1915	Arrowrock	USA	105	351	486	Irrigation/Flood control
1916	Kensico	USA	94	562	738	Water supply
1924	Schrah	Switzerland	112	156	237	Power generation
1924	Wilson	USA	42	1 384	981	Multipurpose
1932	Owyhee	USA	127	254	411	Irrigation
1934	Chambon	France	136	294	295	Power generation
1936	Hoover	USA	221	379	2 486	Multipurpose
1942	Grand Coulee	USA	168	1 272	7 450	Multipurpose
1961	Grande Dixence	Switzerland	285	695	5 957	Power generation
1983	Sayano	Russia	245	1 066	9 075	Power generation

Some form of Roller Compacted Concrete (RCC) was introduced in Switzerland during the 1950's. Section 1.4 deals with RCC construction and the relevance to this project.

Embankment and Rockfill Dams

An earthfill dam is the most common type of dam. Their construction involves the use of the materials in their natural state requiring only minimal processing [Druyts, 2005]. The foundation requirements for earthfill dams are also less stringent than for other types of dams. In determining the optimal cross section, the available materials at the site and the foundation conditions must be borne in mind. Virtually all kinds of foundations can be used to construct an embankment dam, provided that proper foundation treatment is done. Most embankment dams are zoned to take full advantage of the available materials at the specific site.

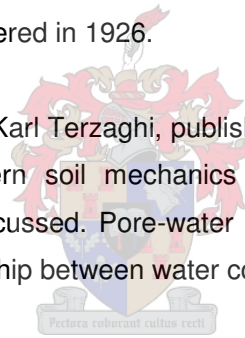
Slope protection to prevent washing away of the embankment due to wave action is provided on the upstream side. Downstream erosion protection is also provided. A properly designed internal drainage system must be used at all times. Different spillway options can be used with an embankment dam, as discussed under Section 1.3. The crest width varies from dam to dam, but it is normally wide enough to accommodate inspection vehicles and to provide comfortable placing of material.

The engineering study of slope stability in excavations as well as embankments was initiated in 1769 by JR Perronet in France. He already investigated boring and pit tests for design and construction of earthworks. In 1776 CA Coulomb published a paper in limit equilibrium analysis in soil mechanics. Embankment dams in Britain were designed and constructed based on empirical knowledge. The Entwistle reservoir constructed in 1837 was the highest dam in the world until 1882, initially 33 m high and later raised to 38 m. Over 260 embankments over 15 m in height were built in Great Britain until 1930. In the USA 360 embankments over 15 m in height were constructed.

The first pure rockfill dam was built for irrigation purposes. The Otay Dam southeast of San Diego consisted of an impermeable core with loose rocks sloping on both faces. Upon completion in 1886 it was the highest embankment dam in the world with a height of 49 m.

Later HPG Darcy determined soil permeability, colonial engineers studied the allowable velocity of seepage flow to avoid internal erosion of the soil (known as piping), and JS Beresford introduced the use of filters as safeguard against piping. The circular slip failure stability analysis was rediscovered in 1926.

The father of soil mechanics, Karl Terzaghi, published the book 'Principles of Soil Mechanics' in 1926. Principles of modern soil mechanics including effective stress concepts and consolidation theory were discussed. Pore-water pressure was discovered in 1940. Proctor established the basic relationship between water content and compaction in 1933.



The development of big earth moving equipment and rollers for compaction increased the popularity of embankment dams. The use of bitumen as the impervious core and concrete faced rockfill dams became more popular from the late 1930's. The highest embankment dam in the world until 1980 was the 300 m high Nurek Dam in Tajikistan.

Embankment dams can be used with RCC spillway sections. A number of composite embankment dams with concrete spillways exist in South Africa, e.g. Nandoni and Inyaka Dams. The interface between the concrete and embankment needs special attention, but various design methods are available to ensure watertightness.

1.3 Spillways and Energy Dissipation Measures

The main purpose of a spillway of a dam is to safely pass small to moderate floods and to prevent failure of the dam during major floods. The design inflow flood is not necessarily the flow that needs to be catered for by the spillway. The spillway designer must provide a structure that complies with all dam safety requirements. In terms of the regulations by the South African National Committee on Large Dams (SANCOLD, 1991) the spillway has to pass the Recommended Design Flood (RDF) with adequate freeboard. No damage is allowed. When the spillway passes the Safety Evaluation Flood (SEF), it must not bring the dam to failure although some damage to the structure and surroundings is allowed.

Spillways can be classified according to their use, namely normal service spillways and auxiliary (emergency) spillways [Chemaly, 2001]. Service spillways are also known as primary spillways, which are frequently used while the auxiliary spillway is used more infrequently. The auxiliary spillway is a secondary spillway that passes floodwater during rare extreme flood events and it may be expected that expensive repair after such events will be necessary.

The choice of spillway type depends on a number of factors, including the dam type, topography of the dam site, flood discharge and frequency and duration of overflows. The main components of spillways are the entrance channel, the control structure, the discharge carrier, the energy dissipater and the outlet channel. The control structure and energy dissipater are relevant for this thesis.

Spillway types include ogee, free overfall, gated, chute, side channel, morning glory, siphon and labyrinth spillways [Shand, 2005]. For gravity type structures ogee and labyrinth spillways are used with downstream steps. Many examples for the design of these spillway types are available, with only the ogee spillway modelled for this thesis.

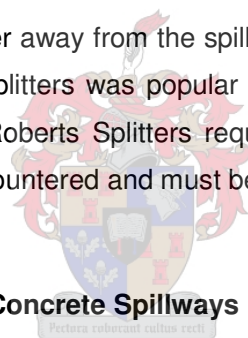
In order to dissipate kinetic energy of the spillway discharge, a terminating structure is required to convert the excess energy into heat and potential energy at tailwater level. The most frequently used energy dissipaters are hydraulic jump stilling basins, roller buckets, ski-jumps and Roberts Splitters. As mentioned earlier, the downstream surface is stepped due to the preferred method of construction. This feature is then made use of for energy dissipation. This has the advantage of a smaller terminating structure at the toe of the dam.

The hydraulic jump stilling basin is an expensive but effective measure [Chow, 1959]. It effectively converts supercritical flow in the discharge carrier to subcritical flow. Recently designers have tended to move away from this structure due to the delicate construction process which includes drainage or anchorage and the relative wide sections required.

Where the tailwater at the toe of a dam is too great to form a hydraulic jump, a roller bucket can be built. The bucket uses a forward and reverse roller to dissipate energy before it returns to the subcritical flow state. The bucket can have either solid or slotted ends.

Ski-jumps can also provide an economical way of dissipating energy, depending on the topography of the dam site. The discharge from the ski-jump at the end of the chute leaves the structure as a free discharging jet, directed upwards. A plunge pool is created downstream of the toe of the dam. In many cases the pools are unlined and they attain a natural equilibrium depth. The main advantage is that the pool is sufficiently far away from the dam wall to minimise or prevent damage to the dam wall.

Roberts Splitters projects water away from the spillway. A high degree of aeration is normally obtained. The use of these splitters was popular for gravity dam design in DWAF until the arrival of RCC. The use of Roberts Splitters requires smooth downstream slopes. Severe spray of water is normally encountered and must be accommodated in the design.



1.4 Stepped Roller Compacted Concrete Spillways

There is no strict definition of roller compacted concrete (RCC), but a general definition would be as follows: a primary concrete intended for the use of construction of large structures by placement with bulk earth placing equipment that is normally used for fills. Proper compaction is achieved using heavy vibratory rollers. Higher construction rates can be achieved with RCC. But, as with all other products, it does have limitations.

RCC was developed in the early 1950's in Switzerland. Bulldozers were used to spread concrete while vibrators were attached to tractors. Independent blocks could no longer be used and thus transverse contraction joints were cut into the concrete after placement. The cement content in the mix design was considerably reduced whilst milled granulated blast furnace slag was included. In the middle 1970's vibratory rollers were introduced to compact the concrete rather than vibrators mounted on tractors. The first true rollcrete dam was the Willow Creek Dam completed in Oregon, United States of America, in 1982. The acceleration

of the construction of gravity dams due to the use of RCC made this an economical solution which could compare with the construction rates achieved for rockfill dams.

The Department of Water Affairs (DWA) first used rollcrete on an experimental section in a conventional concrete gravity dam, the Braam Raubenheimer Dam, in 1979 [Hollingworth and Druyts, 1990]. The first large RCC dam in South Africa, the De Mistkraal Diversion Dam with a maximum height of 30 m, was completed in 1986. Zaaihoek Dam with a maximum height of 50 m was completed in 1987. In 1988 and 1989 the Knellpoort and Wolwedans Dams were completed. These were the world's first RCC arch/gravity dams. Subsequently 22 large dams up to 1996 were constructed of RCC in South Africa [Geringer, 1995].

Stepped spillways are used for RCC gravity and arch dams due to the considerable cost saving associated with the construction techniques [French National Research Project BaCaRa, 1997]. This involves the placement of horizontal layers of concrete from one abutment of the dam to the other. Step heights vary according to the thickness of the concrete layers. At the start of the RCC method, step heights varied between 0,6 m and 1,0 m. Steps consisting of four 250 mm thick layers achieved a height of 1,0 m. Recently 300 mm thick layers are also used to form 1,2 m high steps, as will be the case at the De Hoop Dam to be constructed from 2007 in the Limpopo Province.

Benefits of stepped spillways include:

- High energy dissipation is obtained from the highly aerated flow. This results in a more economical design of a spillway apron or terminating structure at the toe of the dam.
- The creation of steps suits the construction technique to such extent that the construction programme is not affected by the construction technique.

However, a negative aspect of stepped spillways is the risk of cavitation when negative pressures develop due to high water velocities. If the water is not sufficiently aerated, velocities can easily approach 20 m/s at high unit discharges. At some distance downstream from the crest of the spillway, water becomes more aerated and thus serious cavitation of concrete is prevented. With unit discharges up to 30 m³/s.m no serious cavitation problems should occur.

The design of a stepped spillway is influenced by the flow per metre width of the spillway or the unit discharge q (m³/s.m). Unit discharges of up to 30 m³/s.m are accepted internationally, with a number of dams constructed with higher unit discharges such as Wolwedans Dam

($q = 34 \text{ m}^3/\text{s.m}$) and Nandoni Dam ($q = 32 \text{ m}^3/\text{s.m}$). Model tests show that the top steps should be recessed in the spillway profile to prevent separation of the water curve which can in turn lead to cavitation. Various publications on this topic are available.

Facing concrete is placed and compacted normally before the placement of RCC. Section 7 will deal with the placement of RCC including the proposed protrusions.

1.5 Modeling of Spillways

Scale models of free surface flow to different scales, normally to the capacity of the hydraulic laboratory, are used to simulate flow patterns over spillways. Froude similarity is used to determine scale for lengths, velocities and flow rates. Modeling of aerated flow, also called two-phase flow, is more difficult since differences between the model and the prototype exist. Two-phase flow is flow that contains both air and water portions.

The size of air bubbles at two-phase is not influenced by the scale of the hydraulic model. However, due to the presence of air bubbles, it can be said that the model would not behave as the prototype.

Published data can be used to determine the effect of scale. Many authors did not state whether or not allowance was made for scale effect. It is concluded that in most cases no correction for scale was made. Measurement techniques and the interpretation of known hydraulic equations by authors also differ. This makes comparison of data difficult and to calculate the effect of scale.

Results obtained from models used for this study are assumed to represent the model. The results will not necessarily represent the prototype. The model gives an indication of what values on the prototype may be.

1.6 Proposed Protrusions

As mentioned earlier, entrainment of air as early as possible in the water mass flowing over the spillway is a necessity. This reduces the risk of cavitation. The Roberts Splitters (Section 1.3) is an example where air is entrained very early.

This research proposes the use of triangular protrusions (in plan) applied over the spillway surface. The protrusions have the same height as the steps, with the width of the protrusions varying. The triangular protrusions deflect the water sideways resulting in more friction and energy losses. Early studies by Mr NJ van Deventer (DWAF) indicate that the protrusions reduce scouring at the toe of the dam. It also indicated that aeration occurs earlier than with normal stepped spillways. An optimal spacing, lateral and across the steps, is studied. The construction of the protrusions will also be discussed. Figure 1.4 shows the difference between a normal stepped spillway and the stepped spillway with protrusions.

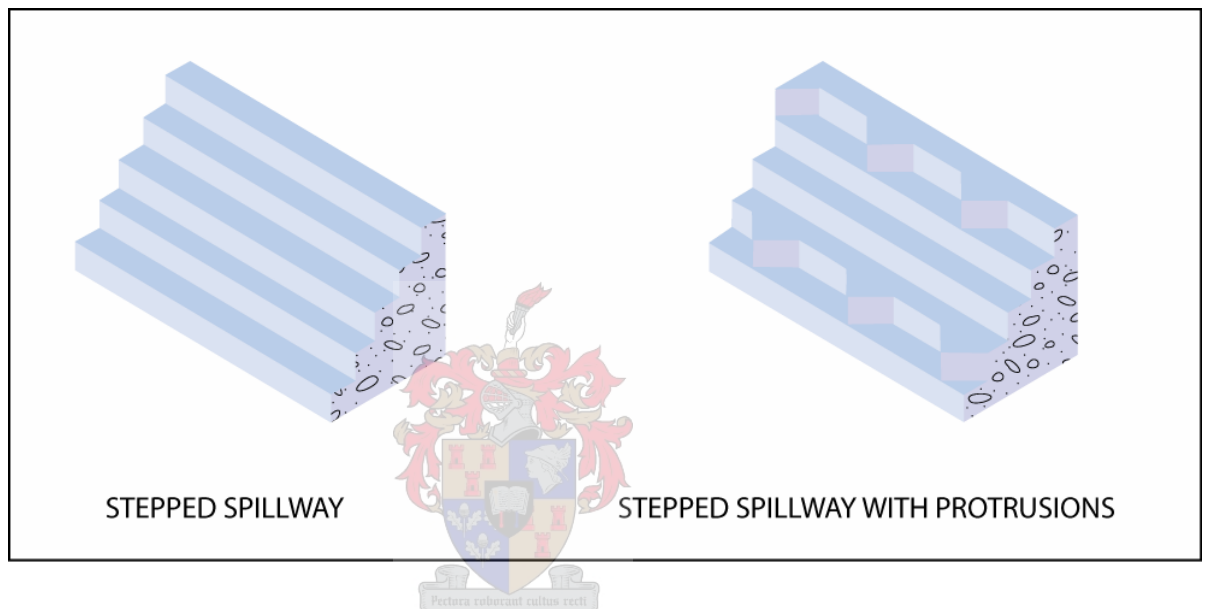


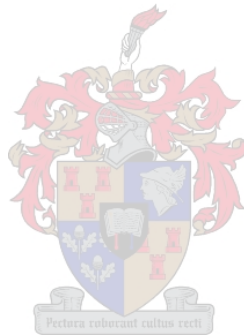
Figure 1.4: Layout of proposed protrusions

1.7 Motivation for Research

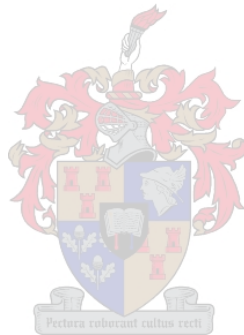
The aims of the research are as follows:

- Verify aspects of previous work done on stepped spillways;
- Investigate if an increase in roughness is obtained on the downstream slope of the stepped spillway by adding triangular protrusions on the downstream slope of a stepped spillway;
- Investigate if a reduction in scour downstream of a stepped spillway stilling basin can be obtained with the addition of triangular protrusions on the downstream slope of a stepped spillway;

- Investigate if earlier air entrainment is possible on a stepped spillway with the aid of triangular protrusions;
- Report on possible construction constraints and consider alternative construction methods for the construction of protrusions; and
- Report if this results in a more cost effective energy dissipation structure at the toe of the spillway.



1 INTRODUCTION



2 LITERATURE STUDY

Various studies have been conducted to try to understand the hydraulics of stepped spillways. This section deals with published literature including data obtained from numerous model studies conducted across the world. Various experts on stepped spillways have emerged, and their literature is reviewed and commented on in Section 3.

General relationships between the main variables involved in hydraulics of flow over stepped spillways have not yet been established. From the literature described below, it is found that the following variables have an influence on the energy dissipation of stepped spillways:

Unit discharge (q) in cubic metres per second per metre ($\text{m}^3/\text{s}\cdot\text{m}$);

Flow depth (y) in metres (m);

Step height (h) in metres (m);

Dam height (H) in metres (m); and

Downstream slope of dam (\emptyset) in degrees ($^\circ$).

This specific study aims to prove that a stepped spillway with extra roughness being provided through the arrangement of protrusions (triangles) to change the direction of flow gives better energy dissipation at the downstream toe of the dam. In order to show that providing extra roughness on the steps is practical and economical, the data obtained from the model study conducted at the Hydraulics Laboratory of the Department of Water Affairs and Forestry (DWAF), Pretoria, South Africa, had to be reworked into a measurable international standard. In order to do this, published literature were reviewed, and conclusions drawn from the model study had to be measured against published data to prove an improvement in energy dissipation.

Various literature concerning spillway slopes varying between 15° and 60° above the horizontal are available. Typical downstream slopes of Roller Compacted Concrete (RCC) gravity dams vary from 1: 0,7 (vertical: horizontal) to 1: 0,8 (vertical: horizontal), which relates to spillway slopes varying from 51° to 55° from the horizontal. This is relevant slopes for the study and literature concerning flatter slopes is only referred to. The proposed De Hoop Dam situated in the Limpopo Province has a downstream slope of 1: 0,8 (vertical: horizontal).

2.1 Definitions

In order to understand the literature, the following definitions are given:

Stepped spillway:

This is a spillway constructed to mobilise the method of Roller Compacted Concrete (RCC) placement. RCC is placed in layers of thickness ranging normally 250 mm to 300 mm thick. Dams with steps ranging from 600 mm to 2 000 mm have been constructed. The spillway helps to dissipate the energy of water and reduces the size of energy dissipation structures downstream of the toe of the dam. Figure 2.1 shows a section through a typical stepped spillway. The RCC method of construction will be discussed in Section 7.

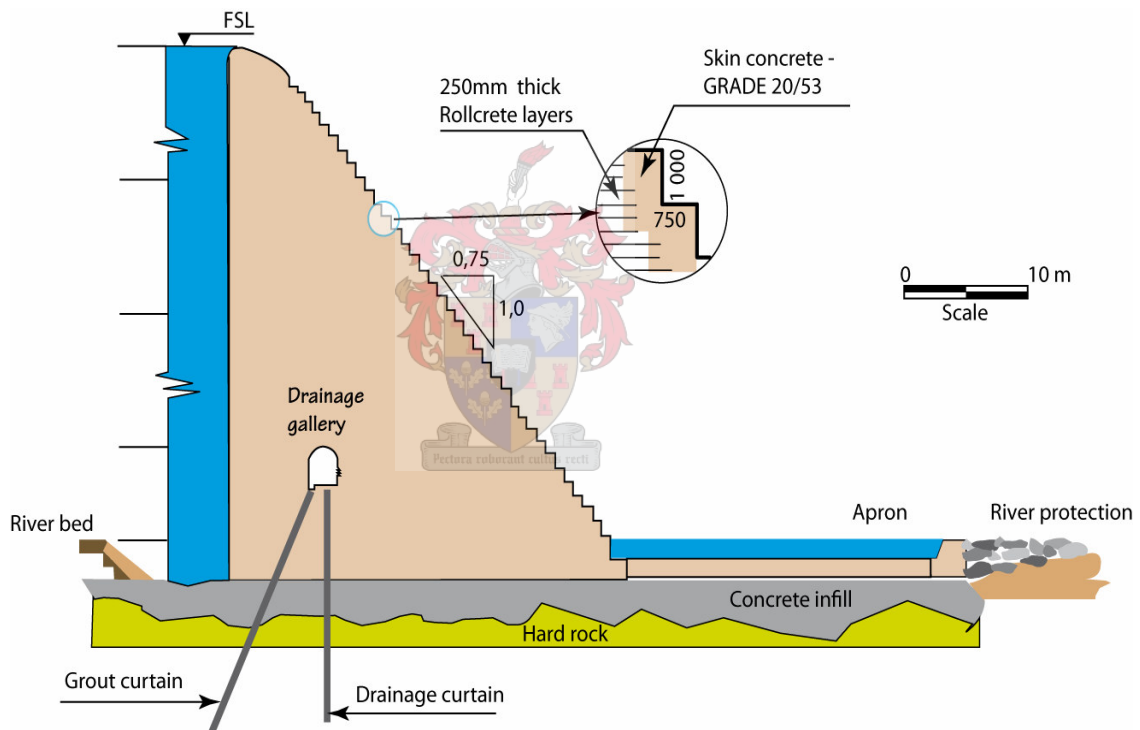


Figure 2.1: Section through a typical stepped spillway (Courtesy DWAF, 2005)

For large RCC dams the following flow types can be distinguished, namely skim, nappe and transition flow.

Skim flow:

Skim flow occurs if the depth of water flow is large when compared to the step height. The flow is normally highly aerated, and moves down the steps without “touching” the steps (as if there were no steps present, just like the spillway of a normal conventional concrete dam with a smooth downstream face). The flow in the space between the steps and the main flow is filled with aerated water, rotating in a vortex. The water after circulation in the vortex is ejected back into the main flow. This does not happen uniformly, and some water and air from the main stream water turn on the steps and then after a while it is ejected back to the main stream. Skim flow occurs when the critical flow depth (Y_c) to step height (h) ratio Y_c / h is larger than 0,8. Figure 2.2 shows skimming flow. This type of flow is mainly observed at high unit discharges, and is of relevance to the study.

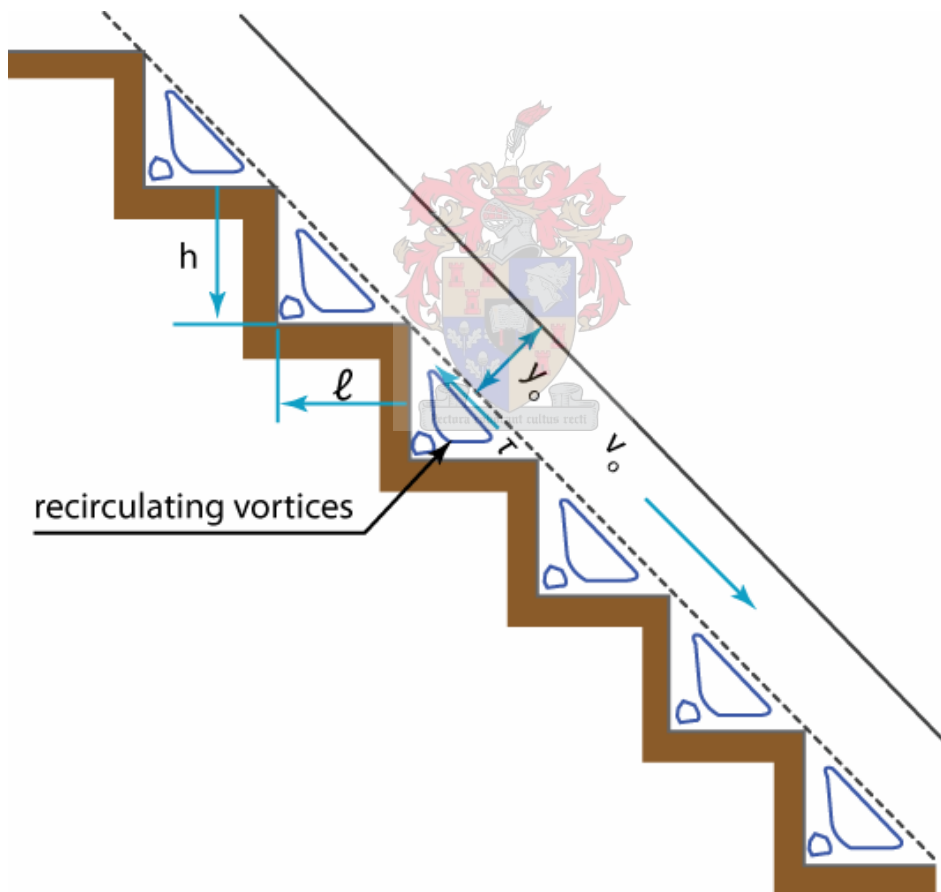


Figure 2.2: Skim flow (Courtesy Rajaratnam, 1990)

Nappe flow:

Nappe flow is the opposite of skim flow. This occurs usually at low flows on steep stepped spillways and over a large range of flows on flat slopes. Flow from the upper step “impinges” on the tread of the lower step and cascades from step to step down the spillway in a series of free nappes. Nappe flow occurs when the Y_c / h ratio is smaller than 0,4. Figure 2.3 shows nappe flow.

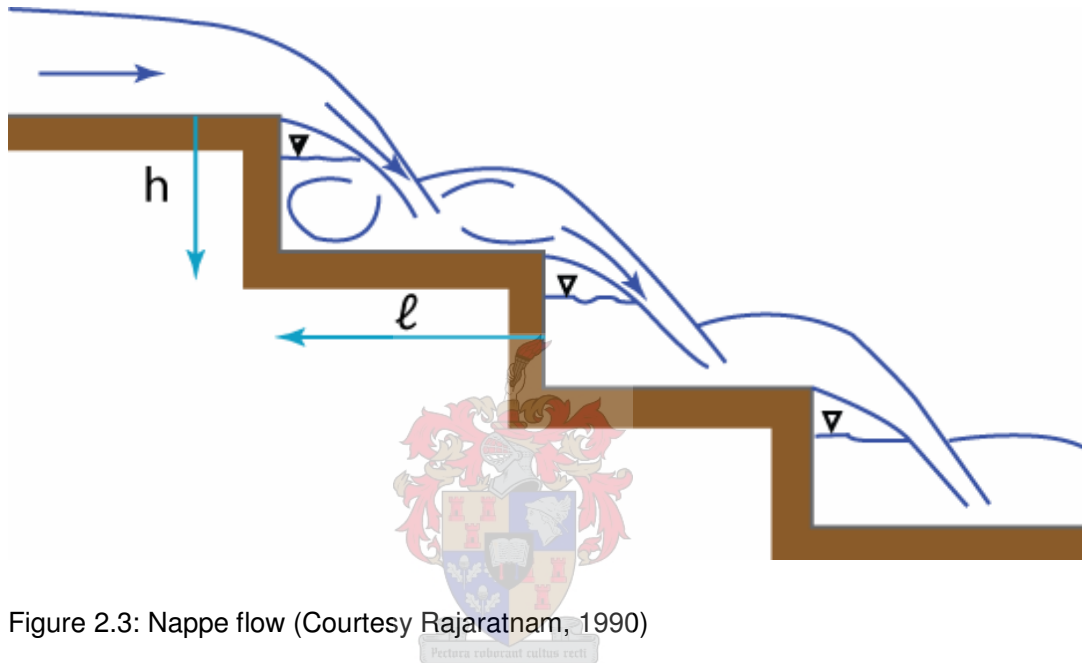


Figure 2.3: Nappe flow (Courtesy Rajaratnam, 1990)

Transitional flow:

Flow rates in between skim and nappe flow is called transitional flow. The water partially skims over the steps and partially falls on the next downstream step.

Point of inception (PI):

The location of the start of air entrainment is called the point of inception. Downstream of the point of inception, the flow is fully developed and free-surface aeration is observed. Further downstream the flow will reach uniform equilibrium and for a given discharge the flow depth, air concentration and velocity distributions will not vary. Upstream of the point of inception, the free water surface is smooth. Turbulence is generated and a boundary layer develops. When the outer edge of the boundary layer reaches the free surface, the turbulence initiates natural free aeration. Figure 2.4 shows the point of inception.

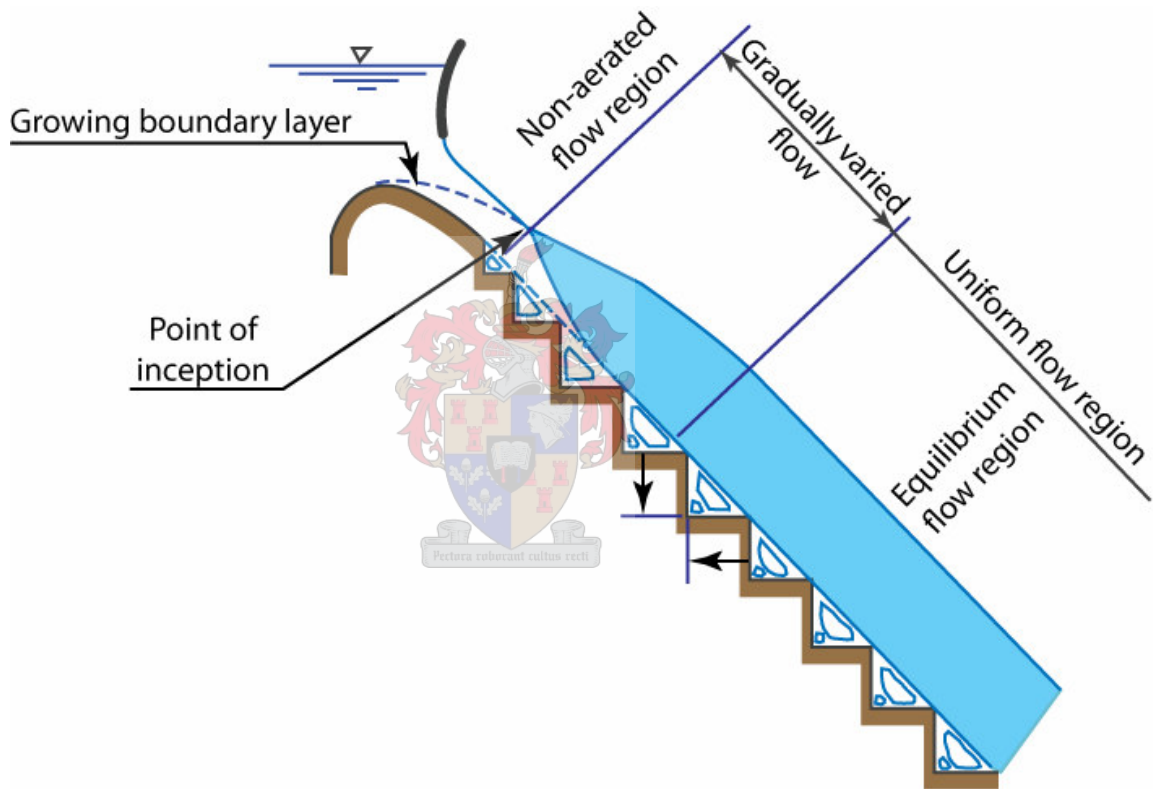


Figure 2.4: Point of inception (PI) (Courtesy Chanson, 2002)

Aeration:

Aeration is when air starts to mix with the water. The objective of energy dissipation down stepped spillways is to entrain air as early as possible and as close to the crest of the spillway as possible.

Normal flow:

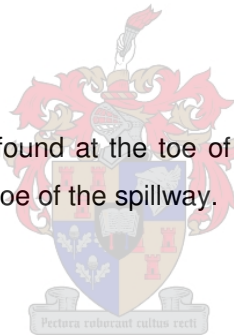
This flow state can only be reached when the loss in potential energy head ΔZ equals the friction loss $\Delta L \times S_f$, where ΔL is the difference in length and S_f friction slope. At normal flow the friction slope is equal to the bed slope $S_f = \sin \theta$ where θ is the downstream slope of the spillway measured from the horizontal. Most dams are too low to make it possible that high unit discharges reach the normal flow state. Normal flow velocities can be derived from measured toe velocities, with some adjustments needed.

Friction factor:

Energy dissipation is directly related to the specific discharge of the flow (q) and to the size (h) of the steps. A general law for the friction factor 'f' of the Darcy-Weisbach equation (1966) has been established.

Residual energy:

It is the specific energy (E_{res}) found at the toe of the spillway. It is a function of the friction factor 'f' and velocity (v) at the toe of the spillway.



2.2 Estimation of Roughness Values (f)

Various writers have published roughness values (f) over stepped spillways. Work of Tozzi (1994), Pegram et al (1999), Boes and Minor (2002), Chamani and Rajaratnam (1999) and Chanson et al (2000) provide a good understanding of the variation of the roughness value f. Their work covers a wide range of unit flow rates (q) and step heights (h).

2.2.1 Darcy's Friction Loss Equation

The relationship between the dimensionless friction factor f and other flow parameters from Henderson (1966) reads:

$$S_f = f v^2 / (8 g Y) \dots\dots\dots (2.1)$$

with:

- S_f = Friction slope;
- f = Darcy friction factor;
- v = Velocity;
- g = Acceleration due to gravity; and
- y = Depth of flow.

With $y = q / v$ and $S_f = \text{Sin } \emptyset$, the equation can be transformed to read:

$$f = 8 g \text{Sin } \emptyset q / v^3 \dots\dots\dots (2.2)$$

with:

- \emptyset = Downstream slope of spillway; and
- q = Unit discharge.

Also, the equation can be rearranged to read:

$$8 S_f / f = v^2 / (g y) \dots\dots\dots (2.3)$$

The term to the right of the equation contains the dimensionless Froude number

$Fr = v / \sqrt{g y}$. This implies that the Froude similitude for determination of model scales is valid.

It must be noted that the friction factor f is inversely proportional to the third order of the velocity. The determination of the velocity thus needs special attention during model testing, as a small error in the velocity can lead to a big error in die friction factor f .

2.2.2 Tozzi, MJ (1994)

Tozzi provided a method for evaluating residual energy downstream of the toe of the dam. This is useful in the design of stilling basins or other energy dissipation measures downstream of the dam. A 1:15 scale model of 2,2 m height was used. Five different step sizes were used with unit flow rates ranging from 80 l/s to 210 l/s. Tozzi states that the dissipation of energy is directly related to the specific discharge of the flow and to the size of

the steps. The author developed a relationship between the friction factor, the step geometry and depth of flow. According to Tozzi the depth of flow is related to the specific discharge. The friction factor 'f' of the well known Darcy-Weisbach equation was used. The published data shows that the depth of water decreases as water descends from the crest to the point of inception or air entrainment. After this point is reached, the depth of flow increases towards the spillway toe, due to the air entrained. Tozzi published three different angles of stepped spillways, of which only the steepest slope (1V: 0,75 H), is of worth for this study. From the data published by Tozzi can be seen that the friction factor becomes constant for low flows. Figure 2.5 shows the relationship derived by Tozzi. The following equation applies to Figure 2.5:

$$f = [2,16 + 1,14 \text{ Log } (Y / k)]^{-2} \dots\dots\dots (2.4)$$

when $Y / k < 1,8$ the friction factor stays constant at $f = 0,163$

with:

Y = Depth of flow; and

k = Roughness of steps.



Figure 2.5: Data by Tozzi of f versus Y / k (1994)

2.2.3 Pegram et al (1999)

The authors studied two sets of stepped spillway models with a downstream slope of 1H: 0,6 V with a range of steps sizes. A 3 m high model to scales of 1:10 and 1:20 were modelled. Unit discharges varied from 10 l/s to 240 l/s. Pegram et al found that the residual specific energy is independent of steps sizes and that the residual specific energy for stepped spillways is smaller than for similar smooth spillways. The authors stated that the hydraulics of skimmed flow over stepped spillways is best described using the amount of residual specific force at the base of the spillway to quantify the effectiveness of the steps. The sequent depth or tailwater downstream of the hydraulic jump formed at the base of the spillway is normally used to describe the specific energy. The authors collected measurements from the models and derived general relationships between the residual specific energy and step height, discussed the influence of scale and compared the energy dissipation ratio of stepped spillways and smooth spillways. The authors concluded that the sequent depth is independent of the step size. A reduction in friction with increasing unit discharge is observed for both smooth and stepped spillways. An energy dissipation ratio (EDR), expressed in terms of the specific energy of a smooth downstream spillway face versus the specific energy of a stepped downstream spillway face (See Section 2.5), of 50 % can be expected for stepped spillways and the ratio decreases the higher the flow over the spillway. The energy dissipation ratio is independent of step height. The results are used in Section 3 to derive a value for the friction factor f . The authors also concluded that “models with scales of 1:20 and larger can faithfully represent the prototype behaviour of stepped spillways” with results “converging rather quickly as the scale gets bigger than 1:15”. The effect of scale will be discussed in Section 2.4.

2.2.4 Chanson et al (2000)

Chanson et al re-analysed more than 35 model studies and investigated 4 prototype studies. From the combined analysis of steep and flat sloped chutes can be seen that flow resistance is more for stepped chutes. Steep sloped chute data however show very little correlation. From the study it is also evident that there is a difference in procedure adopted by various authors. Measurement techniques and data processing techniques differ from author to author. From the re-analysed data a Darcy friction factor of 0,2 is recommend for use. The factor can be as high as 0,3 for prototypes. Figure 2.6 shows the re-analysis of the data.

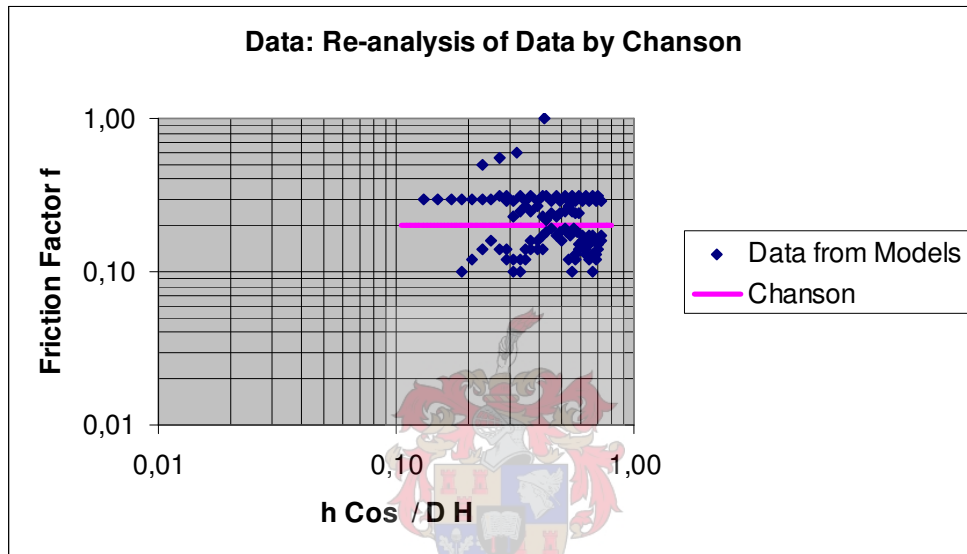


Figure 2.6: Re-analysis of data by Chanson et al (2000)

2.2.5 Boes R and Minor HE (2002)

The authors discuss general hydraulic design of stepped spillways. They studied various models and gave equations for determining the location of the inception point, the inception flow depth, the point where uniform flow is reached and flow depths at uniform flow.

The following relationship for roughness f has been established:

$$1 / \sqrt{f} = A (1 + 0,25 \text{ Log } (k / 4 Y)) \dots\dots\dots(2.5)$$

with:

$$A = 1 / [0,5 - 0,42 \text{ Sin } (2 \varnothing)]^{0,5} \dots\dots\dots(2.6)$$

For this thesis slopes (\emptyset) between 51° and 55° (vertical to horizontal ratio's of 1: 0,70 and 1: 0,80) are investigated. Figure 2.7 shows the friction factor f for different downstream slopes of dams. The location of the inception point and uniform flow depths as proposed by the authors will be discussed in subsequent sections.

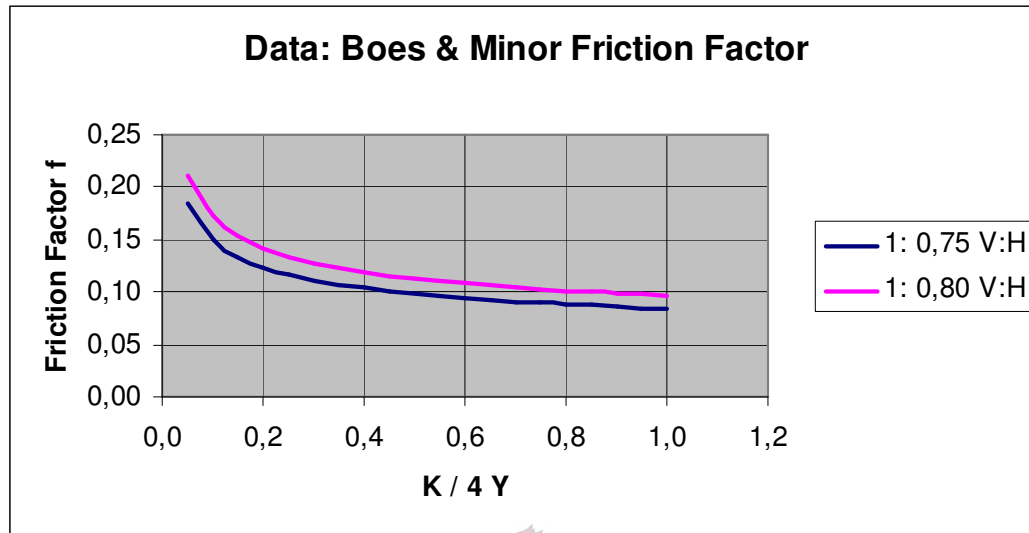


Figure 2.7: Friction factors for two different downstream slopes according to Boes & Minor (2002)

2.2.6 Chamani MR and Rajaratnam N (1999)

The authors studied fully developed skimming flow on a large scale model. They presented air concentration and velocities for skimming flow, and made an assessment of the energy dissipation on stepped spillways. They also reported on aeration on stepped spillways, the influence of scale and the lack of experimental observations of air concentration. Step heights of prototypes from 0,36 m to 3,8 m were investigated on flat and steep slopes. A 2,5 m high model with width of 0,3 m was altered for different step heights. The discharge varied between 21 l/s to 62 l/s.

The authors measured the depth where about 90 % air is contained. This is referred to as the $Y_{0,9}$ depth. This depth was used to determine a friction coefficient C_f defined as:

$$C_f = (2 g Y_{0,9} \sin \varnothing) / v^2 \dots\dots\dots(2.7)$$

with:

$Y_{0,9}$ = Characteristic depth where the air concentration is 90%.

For experiments with small flows C_f is found to be between 0,25 and 0,28, while for larger flows in the skim flow state C_f varies from 0,11 to 0,2.

By using data from various other authors a general equation for the skin friction coefficient (see Figure 2.8) was developed:

$$1 / \sqrt{C_f} = 3,53 + 3,85 \text{ Log } (Y_{0,9} / k) \dots\dots\dots(2.8)$$

To convert C_f to f is difficult due to the uncertainty regarding the clearwater depth Y . This will be discussed in Section 3.

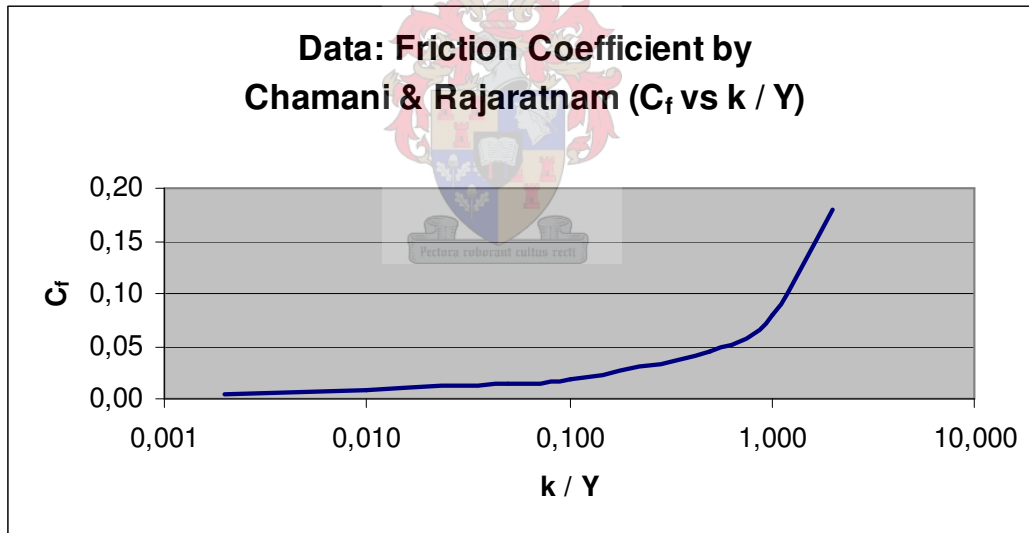


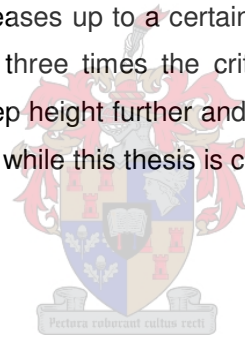
Figure 2.8: Friction coefficient C_f versus k / Y by Chamani and Rajaratnam (1999)

2.2.7 Chanson H (2002)

The author did a lot of experimental work on flat slopes ($\theta < 12^\circ$) where the flow regime is nappe flow (See section 2.1). For the flat slopes the data show an increase of the Darcy friction factor with the relative roughness (k_s / D) with k_s is the step dimension normal to the flow and D is the hydraulic diameter. For steep slopes (relevant to this thesis) there is little correlation between the flow resistance, the relative roughness and the channel slope. A friction factor of 0,17 to 5 is obtained with a mean value of 1,0. The author emphasised that the experimental data were analysed with negligence of air entrainment effects. This explains the high friction factor.

2.2.8 Stephenson D (1991)

The author experimented with a range of downstream slopes and came to the conclusion that maximum energy dissipation down stepped spillways for skimming flow is achieved with wide steps. Energy dissipation increases up to a certain limit as the step sizes increase. The step size can be increased up to three times the critical depth, after it becomes hydraulically unattractive to increase the step height further and construction becomes difficult. The author tested very low unit flow rates, while this thesis is concerned with larger unit flow rates.



2.2.9 Diez-Cascon et al (1991)

The authors presented a theoretical-experimental approach to the hydraulic behaviour of stepped spillways. A 1:10 scale model using different step heights was built. Unit flow rates of prototypes up to $8,85 \text{ m}^3/\text{s.m}$ were tested. The unit rates are too low for use in this thesis.

2.2.10 Christodoulou GC (1999)

The author presented a design approach for effective stepped spillways based on theoretical considerations and experimental results available. Further work is proposed on the effect of the downstream slope on the relationship between the friction factor and the relative step roughness.

A general formula for the friction factor as derived from Chanson (1995), Chamani and Rajaratnam (1999) and Tozzi (1994) is proposed:

$$1 / \sqrt{f} = a \text{Log} (Y / k) + b = a \text{Log} (B Y / k_s) \dots\dots\dots (2.9)$$

with:

The constants a and b are dependable on the slope \emptyset and $b = \text{Log} B / a$; and

B = Width of chute.

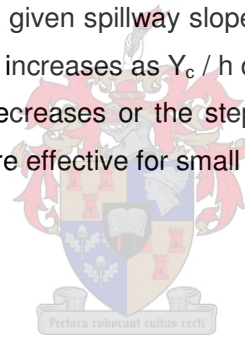
This equation can be rewritten to:

$$1 / \sqrt{f} = a \text{Log} [K f^{1/3} (q^2 / g)^{1/3} / h] = a \text{Log} [K f^{1/3} (Y_c / h)] \dots\dots\dots (2.10)$$

with:

$$K = K (\emptyset) = B / [2 \text{Cos} \emptyset (\text{Sin} \emptyset)^{1/3}] \dots\dots\dots (2.11)$$

This equation shows that for a given spillway slope the Darcy friction factor f depends on the ratio Y_c / h . The friction factor f increases as Y_c / h decreases, meaning that the friction factor f increases as the discharge decreases or the step height increases. This confirms that the stepped spillway becomes more effective for small discharges and/or large step heights.



2.2.11 Yildiz D and Kas I (1998)

Three 2D models were constructed and the hydraulic behavior of skimming flow was observed. Different step sizes were modeled with the discharge varying between 20 l/s and 120 l/s. The recirculating vortices forming and filling on the steps was found to play a major role in energy dissipation. As confirmed by many other studies, the length of the terminating structure is considerably reduced by the use of a stepped spillway. The study focused on the degree of energy dissipation compared to normal spillways, with no friction factor proposed.

2.2.12 Elviro V and Mateos C (1995)

Research done in Spain included the modeling of the stepped spillways of three dams. The downstream slopes of the dams varied with similar step heights. Unit discharges up to 14 m³/s.m were modeled. The effects of aeration and downstream slope were studied. One

configuration was tested at scales of 1:15, 1:10 and 1:6. Cavitation damage was also studied. A friction coefficient f according to Darcy-Weisbach was proposed when uniform flow develops, namely:

$$f = 8 g \sin \theta Y / v^2 \dots\dots\dots (2.12)$$

The main discrepancy in the formula is the difference in measurement of depth which in turn influences the velocity v .

2.2.13 Frantino U and Piccinni AF (2000)

The authors studied the behaviour of skimming flow with the aid of models. A maximum flow of 0,05 m³/s.m was used. The λ parameter is defined according to the friction characteristics resulting from the steps that determine the water flow. The friction factor according to Darcy-Weisbach is:

$$f = 8 g \sin \theta d^2 / q^2 \times R / 4 \dots\dots\dots (2.13)$$

with:

R = Hydraulic radius.

The authors compared data from Rajaratnam (1990), Chanson (1995), Ohtsu & Yasuda (2004), with correlation found on some tests. The authors observed a reduction in dissipation efficiency when the discharge increased or the channel slope increased for a fixed discharge. An indirect evaluation of the friction factor was performed during the tests. The water depths at several points along the structure were measured from where uniform flow was reached. The authors confirmed that the friction factor f is dependable on the discharge and channel slope. Also, energy dissipation increases with flatter slopes.

2.2.14 Chatila JG and Jurdi BR (2004)

The authors examined the hydraulics of ogee-profiled stepped spillways. A scale model was constructed and comparisons were made with smooth spillways. Reductions in terminal velocities and total energy were observed. The authors stated that stepped spillways proved to be efficient in terms of energy dissipation for flows in the region of the design head or lower

of the spillway. For flows higher than the design head (up to 1,4 times the design head) the dissipation reduces significantly. The authors did not propose a friction factor.

2.2.15 Ohtsu et al (2004)

The authors investigated the skimming flow conditions under a wide range of experimental conditions. A new approach to determine the flow characteristics and the friction factor is proposed, and energy dissipation clarified. Both flat and steep slopes were investigated. The authors stated that clarification of the friction factor and the residual energy requires a proper estimation of the depth of the flow in the stepped channel. A method for determining the relationship between the velocity of aerated flow and the velocity obtained according to the clear water depth of a stepped channel is outlined. A friction factor is expressed in terms of the channel slope and the relative step height. The relative step height depends on the Froude number. The authors propose a Darcy friction factor of between 5,5 and 13 times the friction factor of a normal non-stepped surface (smooth downstream face). This gives a friction factor in the region of 0,2. The obtained friction factors correlate well with the data of Chamani and Rajaratnam (1999) and Boes (2000).

2.3 Air Inception

The point of inception was defined in section 2.1 and Figure 2.4. Air entrainment reduces the risk of cavitation of the downstream slope. This is the reason for air entrainment as early as possible into the flow of water. Various studies have been conducted to determine the point of inception and increase the entrainment of air.

2.3.1 Wood et al (1983)

From Figure 2.9 the authors show that the gradually varied flow region is divided into a partially aerated flow region and the fully aerated flow region. This is before the uniform flow region is reached. Cain and Wood (1981) derived a formula for the calculation of the point of inception on uniform sloping spillways. Keller and Rastogi (1977) modified the equation and with a regression analysis determined a formula for the determination of the point of inception:

$$\delta / x = 0,0212 (x / H_s)^{0,11} (x / k_s)^{-0,10} \dots\dots\dots(2.14)$$

with:

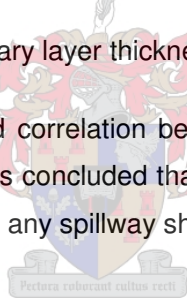
x = distance along the profile of the crest;

H_s = depth from the upstream total energy line to the local water surface;

k_s = surface roughness; and

δ = boundary layer thickness.

The authors believe that a good correlation between laboratory and field-scale data at the point of inception is obtained. It is concluded that the proposed equation can locate the point of inception for air entrainment of any spillway shape.



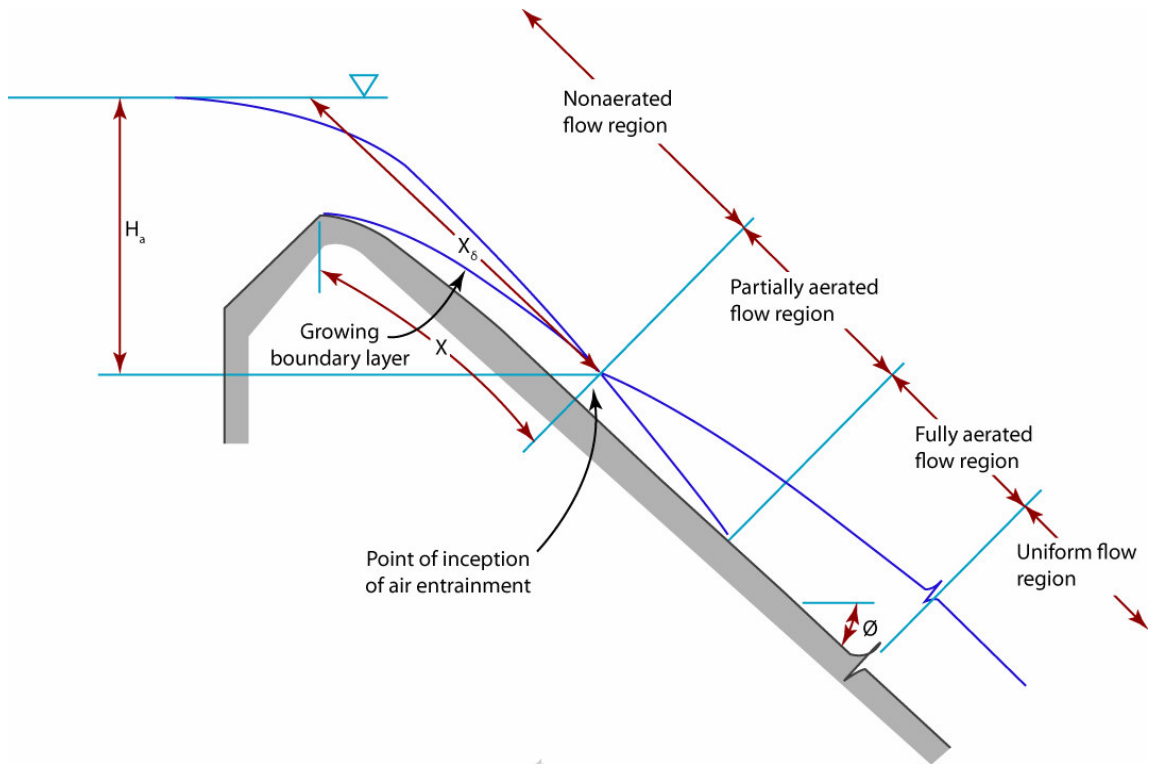


Figure 2.9: Point of inception as defined by Wood et al (1983)

2.3.2 Matos et al (2000)

A 2,90 m high model with a downstream slope of 1: 0,75 (V: H), width of 1,0 m and step height of 0,08 m was built. Discharges up to 200 l/s were tested. Equations to predict the location, corresponding equivalent clear water depth and mean air concentration at the point of inception have been proposed. An equation for the location of the point of inception is:

$$L_1 / k = a_1 F^{b_1} \dots\dots\dots (2.15)$$

with: L_1 = length of inception (x in Figure 2.9);

a_1 = 6,289 determined experimentally;

b_1 = 0,734 determined experimentally; and

F = roughness Froude number; and

k = Roughness of steps.

The equation for the clear water flow depth at the point of inception:

$$d_i / k = a_2 F^{b_2} \dots\dots\dots(2.16)$$

with: d_i = clear water depth;

k = Roughness of steps;

$a_2 = 0,361$ determined experimentally; and

$b_2 = 0,606$ determined experimentally.

The Froude number F is expressed as:

$$F = q / [g \sin \theta k^3]^{0.5} \dots\dots\dots (2.17)$$

Several authors' experimental data were also analysed to obtain values for the constants a_1 , a_2 , b_1 and b_2 .

From Figure 2.10 the mean air concentration (C_{mean}) at the point of inception is found to be 22 % and can be expressed as:

$$C_{mean} = 0,163 F^{0,154} \dots\dots\dots (2.18)$$

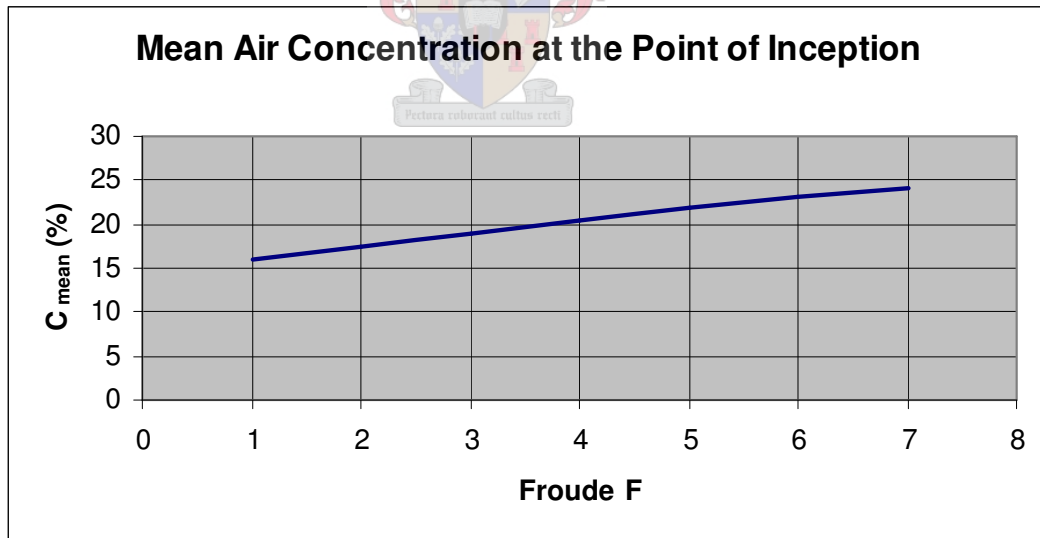


Figure 2.10: Mean air concentration at the point of inception as determined by Matos et al (2000)

2.3.3 Chanson H (2002)

Two variables are defined to characterize the point of inception. The distance from the start of the growth of the boundary layer is known as L_i and the depth of the flow at the point of inception is d_i . The point of inception is primarily a function of the discharge and step roughness. The equation is as follows:

$$d_i / L_i = 0,06106 (\sin \theta)^{0,133} (L_i / h \cos \theta)^{+0,17} \dots\dots\dots (2.19)$$

L_i and d_i can also be expressed in terms of the Froude number F . The location of the inception point moves downstream with increasing discharges. The author states that the type of crest profile does not influence the point of inception, provided that no deflecting jet is observed. The equations are based on experimental data with slopes between 20° and 55° . The flow is fully developed downstream of the inception point and substantial air entrainment is observed. There is an increase in the mean air concentration.

2.3.4 Chamani MR (2000)

A physical model was constructed. Four different step heights were tested. The author concluded that point of inception for a stepped spillway is reached before the point of inception for a smooth spillway. An equation for the position of the point of inception is expressed in terms of a Froude inception number and is derived as:

$$L_i / k = 8,29 F_i^{0,85} \dots\dots\dots (2.20)$$

with:

$$F_i = q / \sqrt{g (h / l) k^3}$$

with:

k = the height of the step relative to the bed;

h = Step height; and

l = Length of the step thread.

2.3.5 Boes R and Minor HE (2002)

The authors developed general design guidelines for the design of stepped spillways. Studies showed the location of the point of inception can be expressed in terms of length of the water reach or by the vertical distance from the spillway crest. According to the authors the length of inception L_i can be defined as:

$$L_i = 5,90 h_c^{1,2} / (\text{Sin } \emptyset)^{1,4} s^{0,2} \dots\dots\dots (2.21)$$

with:

h_c = critical depth; and

s = step height.

From the above equation can be seen that the critical depth h_c or the unit discharge q governs the value of L_i . The steeper the slope of the spillway, the further upstream the water becomes aerated. The depth of flow at the point of inception (H_{mi}) can be defined as:

$$H_{mi} = 0,40 h_c^{0,9} s^{0,1} / (\text{Sin } \emptyset)^{0,3} \dots\dots\dots (2.22)$$

The critical depth has a great influence on the depth of flow at the point of inception.



2.3.6 Chanson H (1994)

The author discussed practical applications of RCC stepped spillways. The inception of air was discussed, but no formula proposed for the point where inception starts. The author stated that self-aeration of the water increases with decreasing water discharge for a constant channel slope. He also stated further that the aeration efficiency is at the maximum for channel slopes ranging between 45° and 60° for a given discharge. A decrease in water discharge reduces the length of unaerated flow.

2.3.7 Christodoulou GC (1999)

The author developed a practical procedure for the design of an effective stepped spillway. Wood et al (1983) determined the length from the crest up to the point where the boundary layer reaches the free surface. Christodoulou manipulated the equation and obtained:

$$L = 11,34 F^{4,15} q^{11,15} / k_s^{0,10} (\text{Sin } \emptyset)^{4,15} \dots\dots\dots (2.23)$$

The equation shows that the length L mainly depends on the discharge, where it is only slightly dependent on the slope \emptyset .

2.3.8 Elviro V and Mateos C (1995)

The authors studied certain dams at different scales to comment on the influence of scale of models. The authors restated the uncertainty between the extrapolation of model data to prototype values. One dam was modeled at three different scales to determine how the scale influences the aeration of water. A formula to define the point of inception was proposed as follows:

$$d / L = A \text{ Sin } \emptyset B (L / k_s)^C \dots\dots\dots (2.24)$$

with:

d = flow depth at the inception point;

L = distance from the crest; and

k_s = step size function; and

A, B and C = constants varying from author to author.

2.3.9 Ferrando AM and Rico JRR (2002)

The authors studied the work of Wood et al (1983) and applied a multiple regression analysis on the provided results. A physical model with unit discharge up to 20 m³/s.m with slopes varying between 5° and 70° were tested. The authors studied the influence of the slope, the surface roughness and unit discharge on the location of the point of inception.

The following equation for the point of inception was proposed:

$$\Delta x = (q / 0,05642 K_s^{0,056} (\text{Sin } \emptyset)^{0,34})^F \dots\dots\dots (2.25)$$

with:

$$F = (1,46443 K_s^{0,0054} (\text{Sin } \emptyset)^{0,0027})^{-3} \dots\dots\dots (2.26)$$

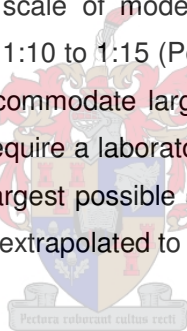
with:

K_s = uniform roughness.

Good correlation between the proposed formula and data from Wood et al (1983) was found. The equation is relevant for steep slopes.

2.4 The Influence of Model Scales

Many authors believe that the scale of models have an influence on the friction factor. Researchers state that scales of 1:10 to 1:15 (Pegram et al, 1999) will not deviate much from prototype values. Dams that accommodate large unit flow rates (up to 40 m³/s.m) that are modeled at a scale of 1:10 will require a laboratory with a capacity of at least 1,0 m³/s.m. It is thus proposed to model at the largest possible scale to be accommodated by the laboratory to ensure that the results can be extrapolated to prototype values.



2.4.1 Pegram et al (1999)

Two models were used and various aspects of skimming flow were discussed. The data was compared to that of Tozzi (1994). The slopes of the models studied by the authors and that of Tozzi (1994) were not the same. The sequent depth at the toe of the spillway was compared. Trend lines were fitted and a difference between the 1:10 scale model and Tozzi's (1994) data was found to be 3%, whereas a difference of 8 % was found between the 1:20 scale model and Tozzi's (1994) data. The results are shown in Figure 2.11. The authors also concluded that “models with scales of 1:20 and larger can faithfully represent the prototype behaviour of stepped spillways” with results “converging rather quickly as the scale gets bigger than 1:15”.

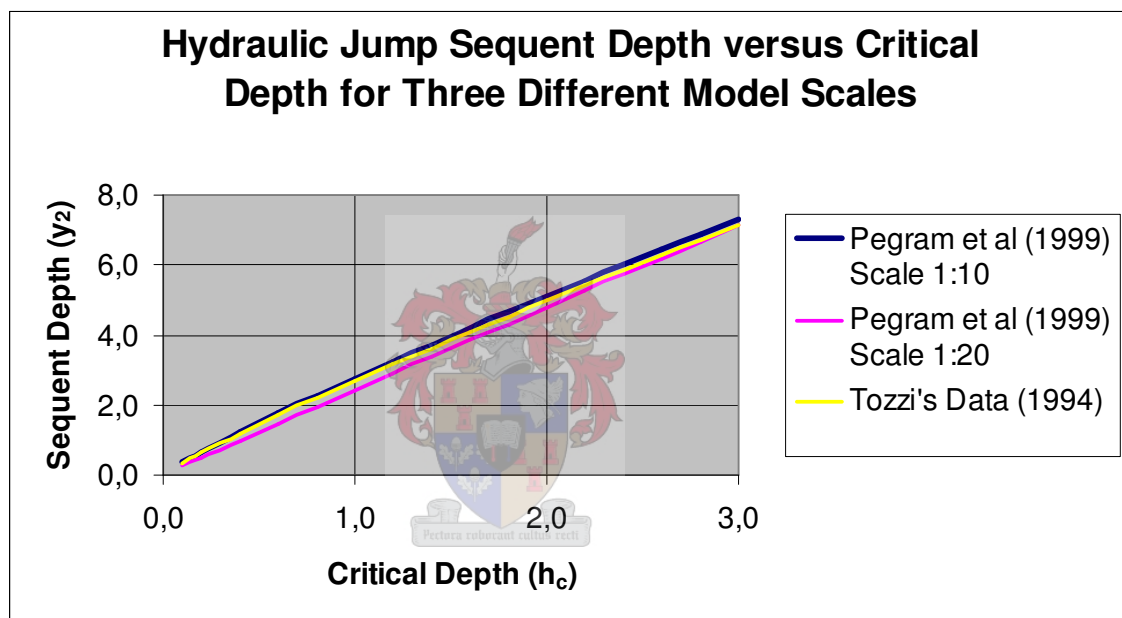


Figure 2.11: The influence of scale on model results by Pegram et al (1999)

2.4.2 Boes RM (2000)

The author states that a common way to estimate scale effects is to use geometrically similar models with different scales. Generally scale effects decrease with increasing model scales. Pinto (1984) suggested a model scale of 1:15 for the modelling of spillway aerators while Speerli (1999) suggested the use of a scale of 1:20 for two-phase flow modelling. Other authors suggested values for Reynolds and Weber numbers to neglect surface tension. Bayat (1991), Tozzi (1994) and Yildiz & Kas (1998) used spillway models with two or more different

step heights and scales. Unfortunately no reliable conclusions can be drawn on the effect of viscosity or surface tension. Results from Chamani & Rajaratnam (1999) indicate that aerated flow parameters depend on the model scale with no mention being made of scaling factors and limiting values for the Reynolds and Weber numbers. Air concentration and velocity profiles were studied. The author concluded that small-scale models can be scaled to prototype dimensions by the Froude similarity law with negligible scale effects. He proposes a minimum scale of 1:10 to 1:15 for spillways with unit discharges of 20 m³/s.m. Smaller scale models will have an increase in scale effects due to viscosity and surface tension effects. Smaller scales give more conservative answers for design purposes, thus achieving a safer design.

2.5 Residual Energy

Various authors stated that the effectiveness of stepped spillways can be determined by comparing the stepped spillway with a normal smooth spillway. Studies show that the residual energy found at the toe of the stepped spillway is less than for a smooth spillway. An increase of dissipation up to 30 % is proposed for stepped spillways by some authors.

Tozzi (1994) proposed the theoretical residual energy (E_t) as:

$$E_t = h + \alpha q^2 / (2 g h^2) \dots\dots\dots (2.27)$$

with:

α = kinetic energy correction factor = 1,10; and

h = flow depth at the toe of the spillway.

According to Pegram et al (1999) the Energy dissipation Ratio (EDR) can be defined as:

$$EDR = (E^{\text{smooth}} - E^{\text{stepped}}) / E^{\text{smooth}}$$

with:

E = Specific energy on the slope of a spillway.

An EDR value of 60 % was reached.

Chamani and Rajaratnam (1999) observed a relative energy loss in the range of 48% to 63%.

1 INTRODUCTION

2 LITERATURE STUDY



3 REVIEW OF LITERATURE

From the work done to date by various authors as shown in the previous section, uncertainties on the hydraulics of stepped spillways still exist. Keeping these uncertainties in mind, a more effective method of energy dissipation is proposed in Section 4.

3.1 Flow Parameters

As mentioned in Section 2, the following parameters have an influence on the friction factor:

- Slope \emptyset ($S = \sin \emptyset$):

As mentioned, this research focussed on slopes between 51° and 55° above the horizontal.

- Roughness of steps ($k = h \cos \emptyset$):

The depth of flow (Y) and critical flow depth (Y_c) influences the roughness of the steps. The parameters Y/k and Y_c/k are used. The parameters are dimensionless.

- Air concentration (C_a):

Y is used to define the roughness factor f , thus C_a is not used. The air concentration helps with the dissipation of energy, although the exact amount of air entrained in the water mass is still uncertain. Measurement of the volume of air entrained is normally done with the aid of probes.

- Unit discharge or flow depth (q or Y_c):

The unit flow rate (q) or critical depth of flow (Y_c) influence the amount of energy dissipation down the stepped spillway. From literature in Section 2 it was generally found that smaller unit discharges result in higher energy dissipation.

3.2 Roughness

3.2.1 Tozzi MJ (1994)

Section 2.2.2 described the model used from which Tozzi obtained his data. From the results it can be seen that two ranges for Y / k influence the roughness f . A clear correlation between f and q cannot be seen due to a small variation in q . Figure 3.1 shows the relationship between f and Y / k as derived by Tozzi.

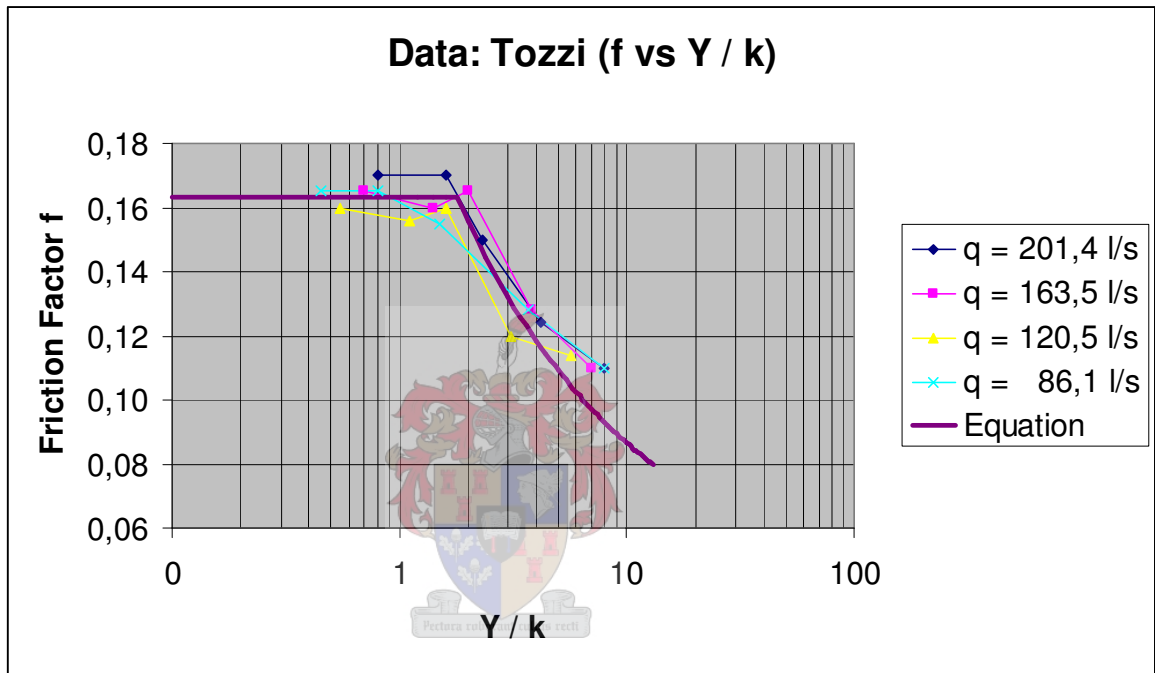


Figure 3.1: Tozzi's friction factor (1994)

3.2.2 Comparing the Boes RM & Minor HE (2002) friction factor with that of Tozzi (1994)

The authors proposed the following equation for roughness f :

$$1 / \sqrt{f} = A (1 + 0,25 \text{ Log } (k / 4 Y)) \dots\dots\dots (3.1)$$

with:

$$A = 1 / [0,5 - 0,42 \text{ Sin } (2 \varnothing)]^{0,5} \dots\dots\dots (3.2)$$

For a slope of 0,75:1 (V: H), the angle $\varnothing = 53,13^\circ$. Substituting into equations 3.1 and 3.2, a value of 3,222 is obtained for A. The equation for f becomes:

$$1/\sqrt{f} = 3,222 (1 + 0,25 \text{ Log } (k / 4 Y)) \dots\dots\dots (3.3)$$

Figure 3.2 shows the relationship between f and Y / k as derived by Boes & Minor (2002).

The values for f obtained by Boes & Minor (2002) are lower than those of Tozzi (1994). Possible reasons are as follows:

- A large scatter of data was obtained by Boes & Minor (2002).
- The average air concentration could be over estimated.
- Lower unit discharges were modelled.

Boes & Minor (2002) did not have separate ranges for f. The reason is probably the large scatter in data.

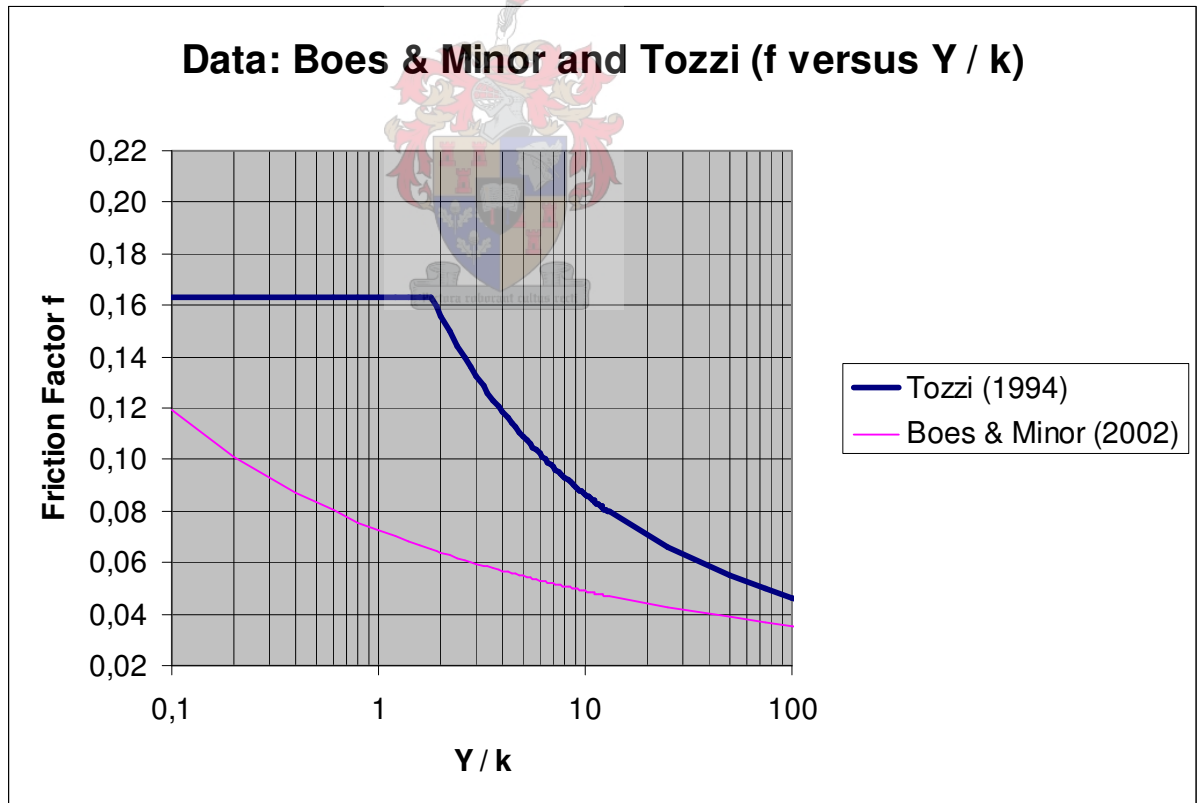


Figure 3.2: Comparison between friction factors of Boes & Minor (2002) and Tozzi (1994)

3.2.3 Comparing friction factors of Chamani MR & Rajaratnam N (1999) with Tozzi (1994) and Boes & Minor (2002)

The authors measured the depth where about 90 % air is contained. This is referred to as the $Y_{0,9}$ depth. This depth was used to determine a friction coefficient C_f defined as:

$$C_f = (2 g Y_{0,9} \sin \theta) / v^2 \dots\dots\dots (3.4)$$

For experiments with small flows C_f is found to be between 0,25 and 0,28, while for larger flows in the skim flow state C_f varies from 0,11 to 0,2.

By using data from various other authors, a general equation for the skin friction coefficient (see Figure 2.8) was developed by Chamani & Rajaratnam (1999):

$$1 / \sqrt{C_f} = 3,53 + 3,85 \text{ Log } (Y_{0,9} / k) \dots\dots\dots (3.5)$$

To convert C_f to f is difficult due to the uncertainty regarding the clearwater depth Y . C_f was however reworked to obtain a friction factor f . This was done by determining the velocity at the toe of the stepped spillway, with known discharge and calculated water depth (New Y). The water depth without air entrained (New Y) was calculated by converting the measured water depth with 90 % air entrained ($Y_{0,9}$) to a depth by using the measured percentage of air in the water (C_T). The water depth was converted to a critical depth Y_c .

Figure 3.3 compares the data by Chamani with those of Tozzi and Boes & Minor with the parameter Y_c/k . Chamani obtained higher values for the friction factor f . The reason for this (as mentioned) is the uncertainty regarding the clearwater depth Y .

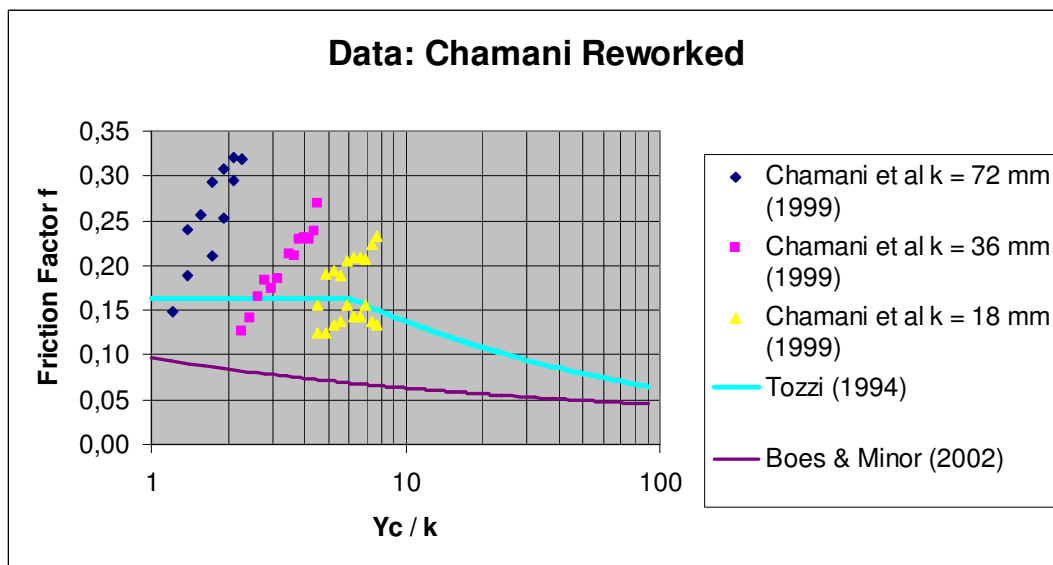


Figure 3.3: Chamani & Rajaratnam’s (1999) data converted to a friction factor f and compared with Tozzi (1994) and Boes & Minor (2002)

3.2.4 Comparing Pegram et al (1999) with Tozzi (1994)

The sequent depth measured by Pegram et al (1999) was used to determine the velocity at the toe of the spillway and was converted to a roughness value f . This is shown in Figure 3.4. Pegram et al only used Y_c as parameter to determine f , thus ignoring Y_c / k . A curve was fitted through the data of Pegram et al (1999) and compared with that of Tozzi (1994). Tozzi's (1994) data was converted to be only dependent on Y_c .

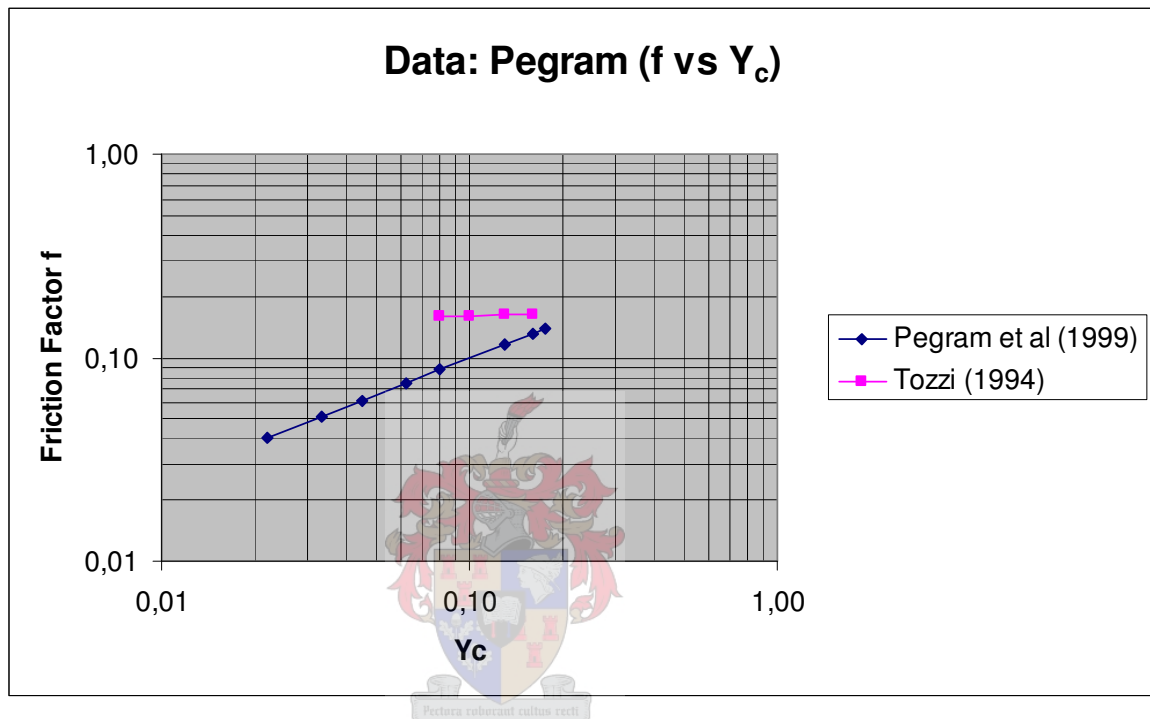


Figure 3.4: Pegram et al (1999) and Tozzi (1994) data converted to be dependent only on Y_c

From Figure 3.4 can be seen that the values of Tozzi (1994) are higher than that of Pegram et al (1999). It can also be seen that the values of Pegram will overtake the values of Tozzi at approximately $Y_c = 0.4$. From the Pegram et al (1999) data no flattening of the roughness value f is foreseen, with further work needed to ensure that the trend is accurate.

3.2.5 Conclusion on Roughness

From the above discussions and from Chapter 2, it seems that a value of f of lower than 0.2 may be reasonable to use.

3.3 Air inception

As discussed in Section 2.3, various equations to locate the point of inception have been developed. Data from the authors can be used to obtain a friction factor f . Data from Matos et al (2000) (Section 2.3.2) can be used to develop a constant friction factor f from the crest to the point of inception (PI) by using the standard step method. The Y/k value is higher at the crest than close to the PI. The energy slope close to the crest is relatively flat due to the relatively low flow velocities, while the energy head loss takes place towards the PI where the Y/k is not varying significantly.

It can be concluded that information regarding the location of the PI can be used to determine a friction factor f . Of importance to this thesis is the location of the PI, whilst it will be assumed that that friction factor f stays constant on the downstream slope from the PI to the toe of the dam.

Figure 3.5 shows the point of inception (L_i) reworked into the following format:

$$L_i/Y_c = A (Y_c / k)^n$$

where A and n are constants for different data sets.

Data by Matos (1999), Matos et al (2000), Boes en Minor (2002) and Chanson (1994) were used. Data obtained from the model tests have been compared to the above mentioned authors' data (see Section 5) as indicated in Figure 3.5.

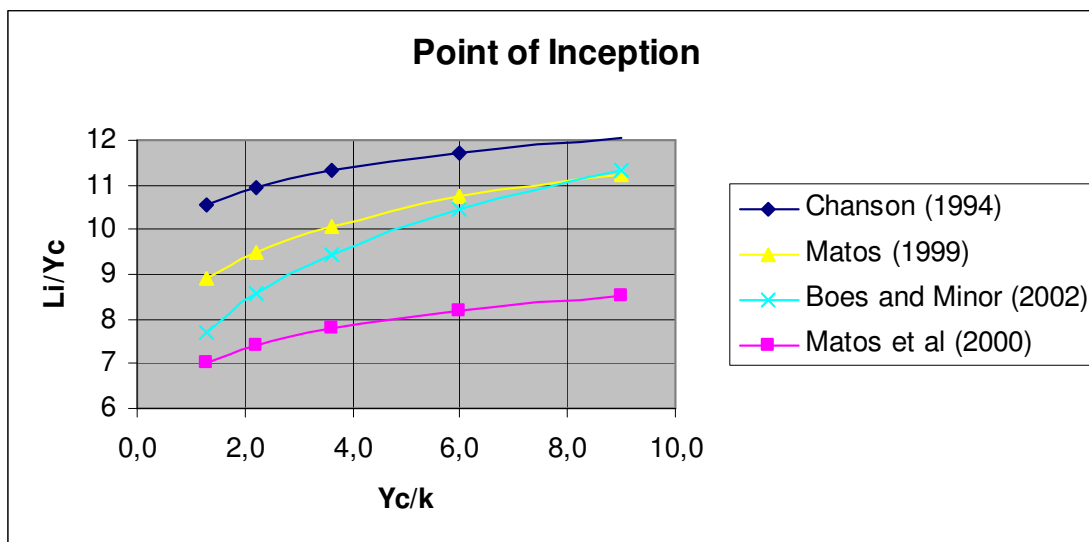
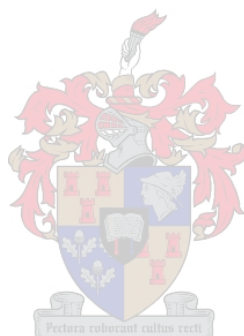


Figure 3.5: Point of inception as determined Chanson (1994), Matos (1999), Matos et al (2000) and Boes & Minor (2002)



1 INTRODUCTION

2 LITERATURE STUDY

3 REVIEW OF LITERATURE



4 EXPERIMENTAL WORK/PHYSICAL MODELING

Two physical models were constructed at the Department of Water Affairs and Forestry's Hydraulic Laboratory in Carl Street, Pretoria West. The standard stepped spillway was firstly modelled to ensure that a comparison can be made with published data on stepped spillways. The data was used as reference to compare the benefit of the proposed protrusions.

A brief background on the De Hoop Dam project is given, with attention to the model tests conducted for the dam, and the use of the data for this thesis.

4.1 De Hoop Dam

Cabinet has previously announced the approval of the Olifants River Water Resources Development Project (ORWRDP), Phase 2. Phase 2 comprises sub phases A – G, of which Phase 2A is the construction of the De Hoop Dam.

The proposed De Hoop Dam is situated on the Steelpoort River, a tributary of the Olifants River in the Limpopo Province. The dam will supply water mainly for mining activities, but water will also be supplied to surrounding towns and industries in the area as well as for poorly serviced rural communities. The dam will comprise a central roller compacted concrete (RCC) stepped spillway section in the river section, a RCC right bank and a RCC left bank, both with stepped downstream faces. An outlet block capable of supplying 20 m³/s is situated on the right bank. Appendix E gives background information on the De Hoop Dam.

The height of the dam will be 75 metres from the lowest foundation level. The RCC Dam will have a spillway with a length of 110 m with a 6 m freeboard. Overtopping of 0,5 m over the left bank non overspill crest (NOC) is allowed in the case of the Safety Evaluation Flood (SEF).

4.2 De Hoop Dam Model Studies

A hydraulic model study was commissioned as the hydraulic behaviour of the spillway and apron could not be theoretically predicted with sufficient accuracy. At the start of the model study, the Dam Type Selection Study (DTSS) was still under revision and it was decided to construct a three dimensional (3D) model rather than a two dimensional (2D) model. The

model can be easily changed to accommodate a side (return) chute if it was considered necessary [DWAF, 2006].

The principal aims of the study were therefore to:

- Determine the effectiveness of the energy dissipating downstream steps;
- Optimise the dimensions of the apron and end sill;
- Observe the flow regime on the stepped face at all flow rates;
- Determine the necessary height of the training wall needed to contain the maximum anticipated discharge; and
- Estimate the amount of scouring downstream of the apron for the different flood magnitudes.

It was later decided to study the entrainment of air at high floods. An alternative to ensure air entrainment at an earlier stage is to provide the downstream steps with extra protrusions, in this case triangular protrusions. This method not only ensures the early entrainment of air into the spillway, but is also more effective in dissipating energy and studies to date prove that 30% less scouring at the toe of the dam is observed (Van Deventer, 2006). A 2D model was then commissioned to refine these preliminary findings. The 3D model could not be used to accurately model air entrainment, due to the scale of 1:60.

Two different apron and end sill configurations were proposed for De Hoop Dam. A 6,75 m long horizontal apron was tested with two different solid end wall heights. The alternative was a 6,75 m long horizontal apron with alternating apron splitters, as is the case at Flag Boshielo Dam (See Photograph 4.1). It was concluded that the design length of the apron would ensure effective energy dissipation, as been obtained from previous model studies. From the 3D model study, a solid 2,0 m high end sill with a 1 V: 0,375 H sloping upstream face was found to work most effectively.



Photograph 4.1: Flag Boshielo Dam apron splitters (Courtesy DWAf, 2005)

4.3 The Models

Before it was decided to study the entrainment of air at high floods at De Hoop Dam, the Hydraulics Laboratory commenced with the construction of a 3 metre high model for this and other research projects. The model had a downstream slope of 0,75 H : 1 V, with a step height of 60 mm. The pump capacity of the laboratory determined the scale of the model, which was anticipated at 1:20. The prototype dam would then have a height of 60 metres. This model was later altered to have a height of 3,5 metres, corresponding to a height of 75 metres, as De Hoop Dam will have. This model was then used to refine the work on adding protrusions to the downstream face of the stepped spillway. The model was later changed to accommodate larger flow rates, as will be described in subsequent sections.

Three methods of determining the efficiency of the protrusions were used, firstly scour measurement with a fixed apron and end sill configuration, secondly sequent depth measurement and thirdly the location of the point of inception. Scour measurements were done to evaluate the effectiveness of the energy dissipation at the toe of the dam. Use was also made of a hydraulic jump (sequent depth measurement) to determine the friction factor f of the downstream slope (as used in Sections 2 and 3). Comparison of the scour depth at the

toe of the spillway in the case where protrusions were used and not used, the increase in relative roughness of the spillway, as well as the length of inception was used to evaluate the benefit of the protrusions.

4.4 The First Model (Scale 1:20)

A complete set of drawings of the model was drawn according to departmental (DWAF) standards and is attached in Appendix F.

Firstly, as described in Section 4.3, a 1:20 scale model of the De Hoop Dam was constructed. The model was 0,45 m wide by 12 m long and 3,5 m high. (This indicates a prototype height of 70 m, but due to the height of the apron and the amount of scour obtained from the 3D model, this height was sufficient to ensure comparable scour results since the scour does not reach the lowest foundation level). It consisted of a 0,45 m wide intake basin with flow stabilisers on the upstream end and a 0,45 m wide flow channel. Figure 4.1 shows the layout of the model. The width of the model was calculated to accommodate the maximum flow capacity of the pumps at the laboratory. The main advantage of the model was that observation of the flow over the steps and apron was possible as a sectional view was created, unlike the 3D model of De Hoop Dam.

Gravel was placed downstream of the spillway and apron to simulate the rocks in the river. 13 mm aggregate was used, simulating the rock at the dam site. This equivalent rock size would produce conservative results, because the rock would probably break up into much larger blocks or boulders. It would, however, be very difficult to estimate the size of the blocks into which the solid rock would break.

The size of the 1,2 m steps in the prototype is 60 mm high with a tread of 45 mm. The downstream slope of De Hoop Dam is 1 V: 0,8 H, but the model was constructed with a 1 V: 0,75 H slope (53°). An adjustment for the slope difference was made for the comparison of the results of the 3D model of De Hoop Dam, as stated in the Hydraulic Model Study Report of De Hoop Dam (DWAF, 2006).

The steps and ogee of the model was made of wood. The design head of the ogee was taken as 5,0 metres, with the ogee crest shape being designed in accordance with the design principles of the USBR publication, the Design of Small Dams [Reference 44]. Appendix B shows the ogee profile for the De Hoop Dam, and this profile scaled to the 1:20 and 1:30 models respectively. Perspex was used at the sides of the model to ensure that photographs

could be taken in the sectional view. The downstream return channel consisted of plastered bricks. A sluice gate and gate valve were used to adjust tailwater levels.

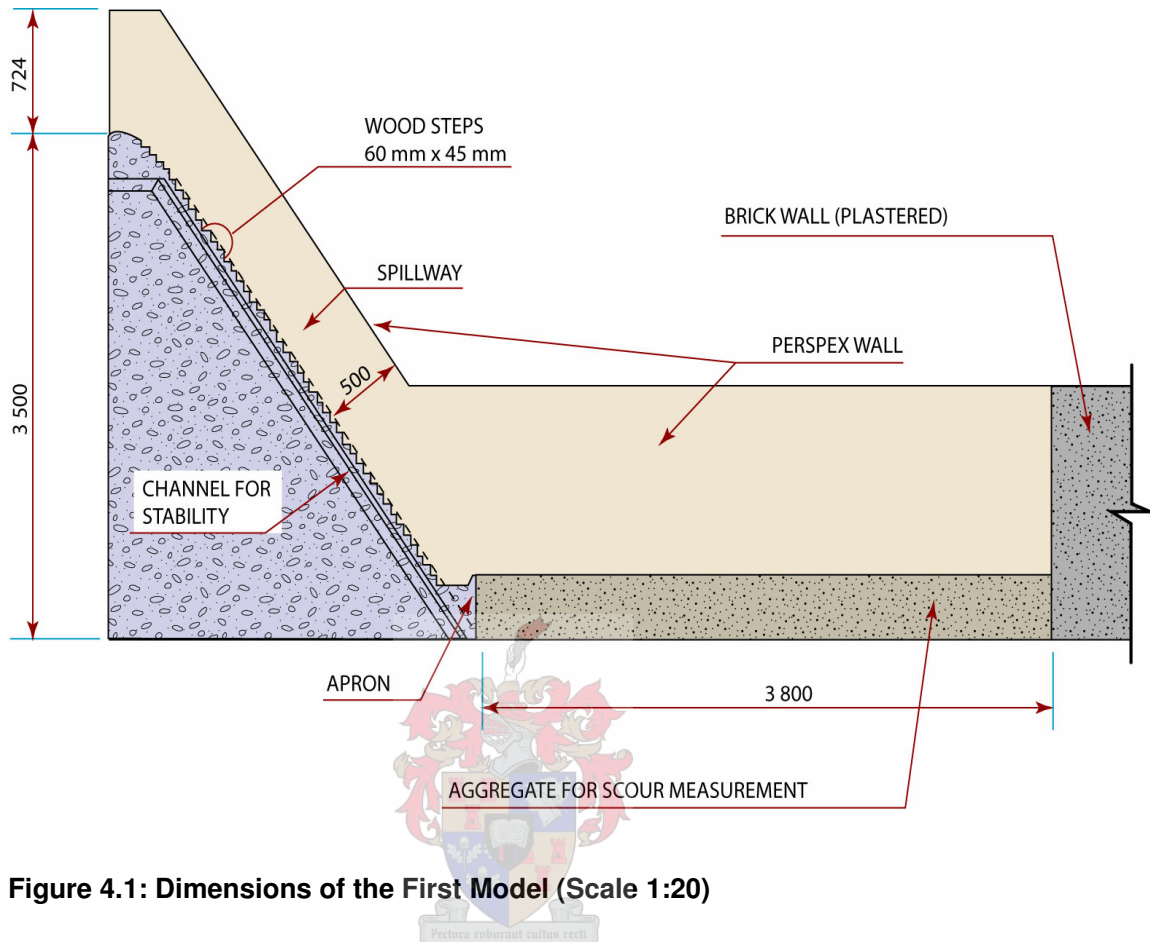


Figure 4.1: Dimensions of the First Model (Scale 1:20)

The apron configuration as described in Section 4.2 was used in the 1:20 scale model. Refer to Appendix B for the dimensions for the De Hoop Dam.



Photograph 4.2: The First Model (Scale 1:20) without protrusions



Sluice gate



Gate valve

Photograph 4.3: Sluice gate and gate valve to adjust tailwater levels



Connection from laboratory pumps



Connection from pump to intake basin

Photograph 4.4: Connection from pumps

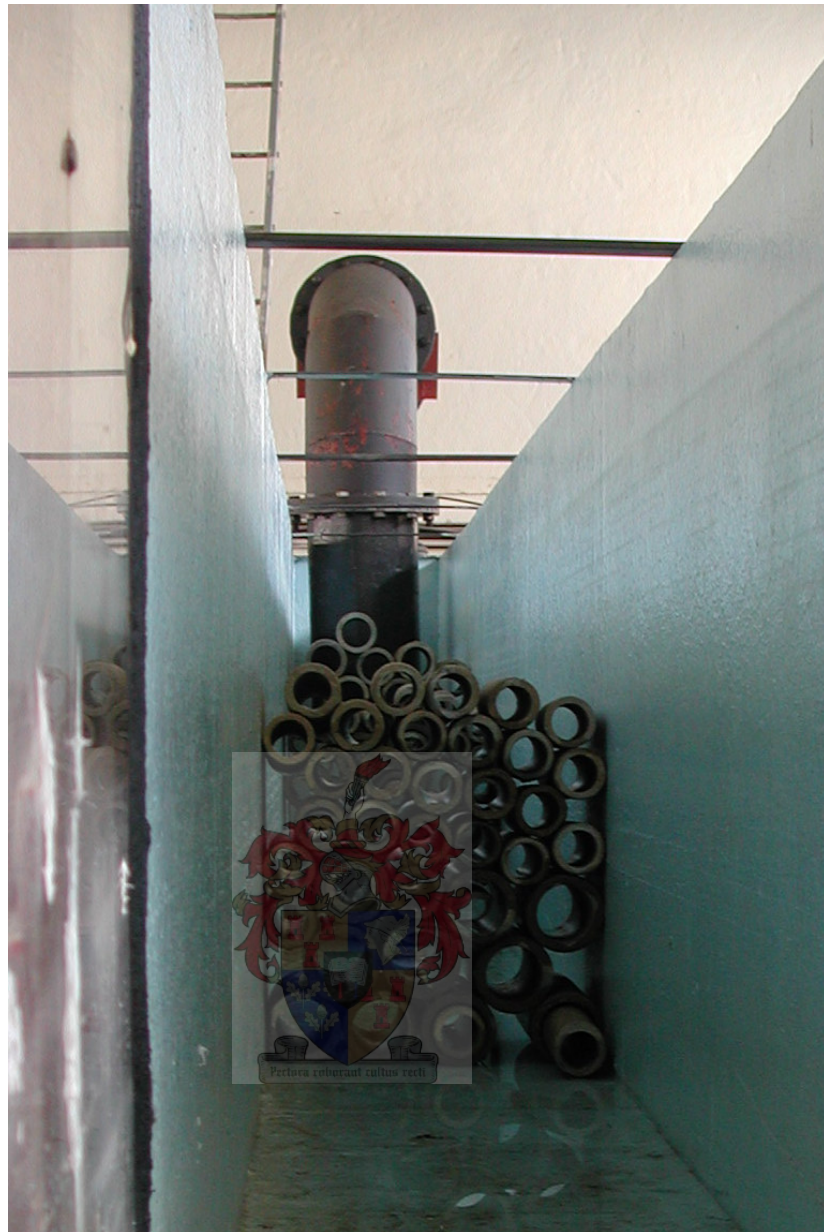


Apron of De Hoop Dam



Shutter board for hydraulic jump

Photograph 4.5: Apron and shutter board at toe of spillway



Photograph 4.6: Flow stabilisers

As mentioned previously, scale has a substantial influence on the modelling of hydraulic scale models. The limiting factor for the model scale was the pump capacity at the DWAF Hydraulics Laboratory. The maximum flow was given as approximately 180 l/s.

A Froude-model was built on an undistorted scale of 1:20 due to the limitation of the available supply capacity of the Hydraulics Laboratory. The scale was determined using Froude's law of similarity. Later a 1:30 scale model was built to accommodate larger flow rates.

The maximum yield of the pumps at 3,5 metre pressure head at the laboratory is however 140 l/s.

Modelling only a 0,45 m wide section at scale 1:20:

$$q_m = \frac{0,140}{0,450} = 0,311 \text{ m}^3/\text{s.m}$$

Flow in the prototype:

$$q_p = 20^{1,5} \times 0,311 \approx 30 \text{ m}^3/\text{s.m}$$

The flow in the prototype according to the 1:20 scale model is smaller than the maximum unit discharge of 37 m³/s.m for De Hoop Dam. Thus the capacity of the laboratory was only enough to ensure that enough water could be delivered at a scale of 1:20 to test up to the Regional Maximum Flood (RMF) equal to 2 700 m³/s at the De Hoop Dam site.

The model was then altered during April 2006 to a scale of 1:30 to test up to the Safety Evaluation Flood (SEF) equal to 4 500 m³/s at De Hoop Dam site.

4.5 The Second Model (Scale 1:30)

As mentioned, the first model was altered to obtain a smaller scale. This ensured that the author had more freedom with lateral spacing of the protrusions. The model was 2,5 metres high, with the rest of the dimensions (width, flow channel length) the same as the 1:20 scale model. The sluice gate and gate valve stayed the same. The apron dimensions were altered to reflect a 1:30 scale (Refer to Appendix B for the De Hoop dam dimensions). The size of the 1,2 m steps in the prototype is 40 mm high with a tread of 30 mm. The model was constructed with a 1 V: 0,75 H slope (53°).

Modelling only a 0,45 m wide section at scale 1:30:

$$q_m = \frac{0,140}{0,450} = 0,311 \text{ m}^3/\text{s.m}$$

Flow in the prototype:

$$q_p = 30^{1,5} \times 0,311 \approx 50 \text{ m}^3/\text{s.m}$$

Unit discharges of up to 40 m³/s.m were tested.

The 1:20 scale model was then modelled up to the RMF and the 1:30 scale model was modelled for the full range of flows. This gave the author two sets of data for lower flows to correlate and obtain the effect of scale on models.



Photograph 4.7: The Second Model (Scale 1:30) without protrusions

4.6 Measurements

As mentioned, scour depths, sequent depths and the location of the point of inception were measured.

For the De Hoop Dam model the apron length and end sill height as described in Section 4.2 were used (refer to Appendix B). The Recommended Design Discharge (RDD) and RMF

were tested and the amount of scour quantified for the 1:20 scale model. For the 1:30 scale model the RDD, RMF and SED were tested and the depth of scour quantified. The schematic layout for scour measurement is shown in Figure 5.7 and is described in Section 5.1.4.

The process for testing was as follows:

- Survey the gravel downstream of the apron in the normal position.
- Close the downstream sluice and valve.
- Fill the tank with water and let water run over the spillway at a slow rate (5 l/s) until the tailwater is close to the required level (as determined).
- Increase the flow to the required value (RDD, RMF or SED) and adjust the sluice and/or valve to maintain the correct tailwater level.
- Let the water run for 45 minutes to ensure that equilibrium conditions is achieved.
- Take measurements of flow depths.
- Stop the water flow and let the tailwater subside gradually.
- Survey the scouring of the gravel.
- Repeat the process for the other floods without disturbing the scour pattern during filling.

This sequence was used where gravel was present downstream of the end sill for the De Hoop Dam studies.

A configuration was set up (with or without protrusions) and then firstly the scour tests were done. A 4,0 metre long shutter board was then used to cover the apron and end sill. This served as the bed where upon a hydraulic jump could be stabilised and the sequent depth measured. No scoop was utilised at the toe of the dam. It was assumed that no losses occurred at the downstream toe of the dam.

The process for testing where the shutter board was present was as follows:

- Close the downstream sluice and valve.
- Fill the tank with water and let water run over the spillway at a slow rate (5 l/s) until the flow channel is filled with water.
- Increase the flow to the required value (see flows below) and adjust the sluice and/or valve to ensure that a stable hydraulic jump is formed as close to the toe of the spillway as possible.
- Take measurements of flow depths and sequent depth.
- Increase the flow to the required value and repeat measurements.

The following flows were tested for the first model where the shutter board was present and sequent depths were measured from it:

- 20 l/s corresponding to a prototype unit discharge of $4 \text{ m}^3/\text{s.m}$
- 40 l/s corresponding to a prototype unit discharge of $8 \text{ m}^3/\text{s.m}$
- 55 l/s corresponding to a prototype unit discharge of $11 \text{ m}^3/\text{s.m}$
- 70 l/s corresponding to a prototype unit discharge of $14 \text{ m}^3/\text{s.m}$
- 80 l/s corresponding to a prototype unit discharge of $16 \text{ m}^3/\text{s.m}$
- 95 l/s corresponding to a prototype unit discharge of $19 \text{ m}^3/\text{s.m}$
- 110 l/s corresponding to a prototype unit discharge of $22 \text{ m}^3/\text{s.m}$
- 120 l/s corresponding to a prototype unit discharge of $24 \text{ m}^3/\text{s.m}$
- 135 l/s corresponding to a prototype unit discharge of $28 \text{ m}^3/\text{s.m}$

The following flows were tested for the second model where the shutter board was present and sequent depths were measured from it:

- 22 l/s corresponding to a prototype unit discharge of $8 \text{ m}^3/\text{s.m}$
- 30 l/s corresponding to a prototype unit discharge of $11 \text{ m}^3/\text{s.m}$
- 41 l/s corresponding to a prototype unit discharge of $16 \text{ m}^3/\text{s.m}$
- 52 l/s corresponding to a prototype unit discharge of $19 \text{ m}^3/\text{s.m}$
- 66 l/s corresponding to a prototype unit discharge of $24 \text{ m}^3/\text{s.m}$
- 77 l/s corresponding to a prototype unit discharge of $28 \text{ m}^3/\text{s.m}$
- 88 l/s corresponding to a prototype unit discharge of $32 \text{ m}^3/\text{s.m}$
- 99 l/s corresponding to a prototype unit discharge of $36 \text{ m}^3/\text{s.m}$
- 110 l/s corresponding to a prototype unit discharge of $40 \text{ m}^3/\text{s.m}$
- 120 l/s corresponding to a prototype unit discharge of $44 \text{ m}^3/\text{s.m}$

The position where the sequent depths were measured were approximately 3,8 metres downstream of the toe of the spillway (See Figure 4.22).

Two methods for locating the point of inception are described by Boes (2000) and Matos et al (2000). The first method is locating the point of inception by visual examination where air is started to be seen in the skimming flow. (Refer to Figure 2.4 and Appendix C). The depth of inception (d_i) can then be measured from the top of the ogee cap. This distance can be reworked to the length of inception (L_i) with the ogee profile known. The second method to locate the point of inception is the measurement of air concentration, velocities and depth profiles along the spillway with the aid of optical fibre probes. Measurements show that the point of inception as achieved by the measurement of profiles occurs upstream of the location indicated by visual observation.

The location of the point of inception for this thesis was visually observed. This gives a more conservative answer and the DWAF Hydraulics Laboratory also does not have the luxury of optical fibre probes.

4.7 Protrusions

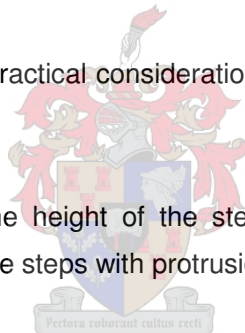
As mentioned, protrusions on the downstream steps in the form of triangles were added (Refer to Figure 1.4). Lateral deflection of water is obtained, with the deflected water also mixing with the horizontally deflected water. This increases the roughness of the downstream steps, thus dissipating more energy and decreasing the scour downstream of the apron. It also entrains air earlier into the model.

Two different protrusion sizes were used (see Figures 4.2 and 4.3):

- A triangle with two 45 degree angles and one 90 degree angle.
- A triangle with two 30 degree angles and one 120 degree angle.

The sizes were governed by practical considerations, whilst cracking should not occur at the edges of the protrusions.

The tread of the step and the height of the step stayed fixed for both protrusions. The configurations and results of the steps with protrusions are discussed below.



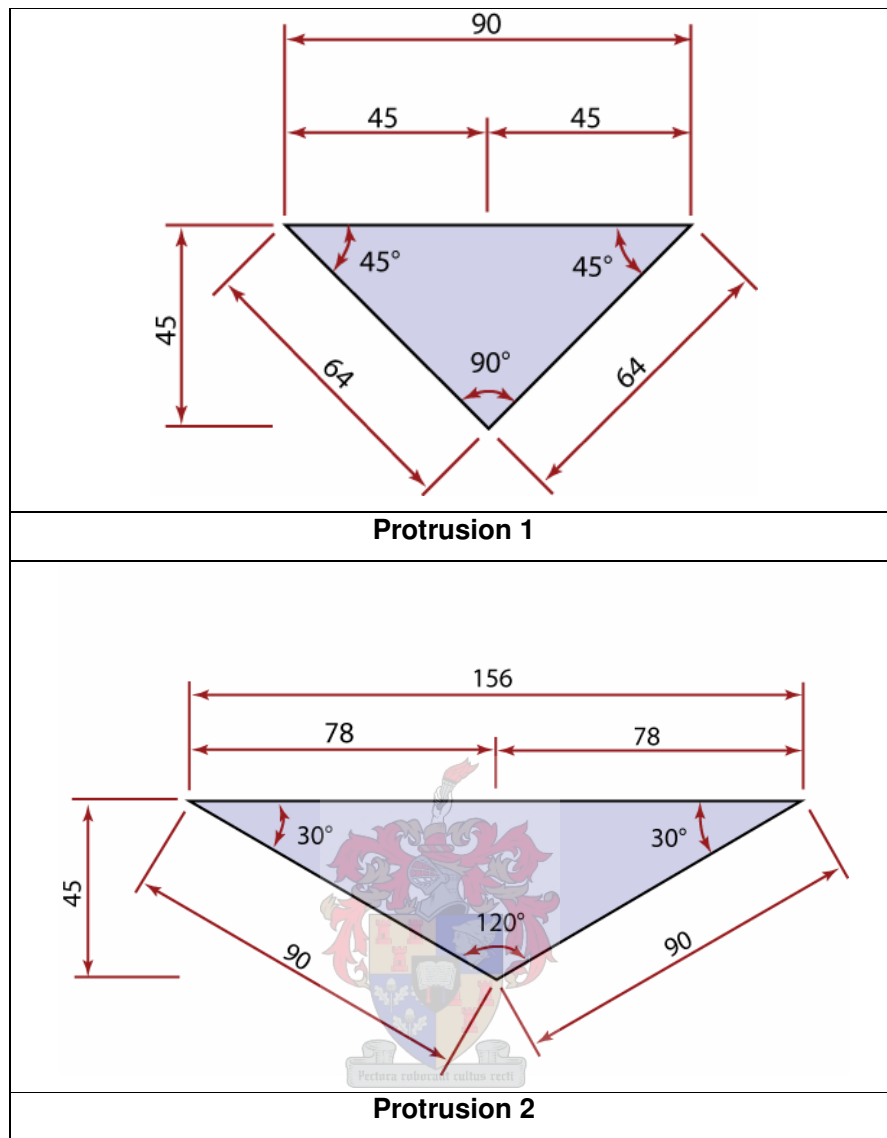


Figure 4.2: Protrusions for the First Model (Scale 1:20)

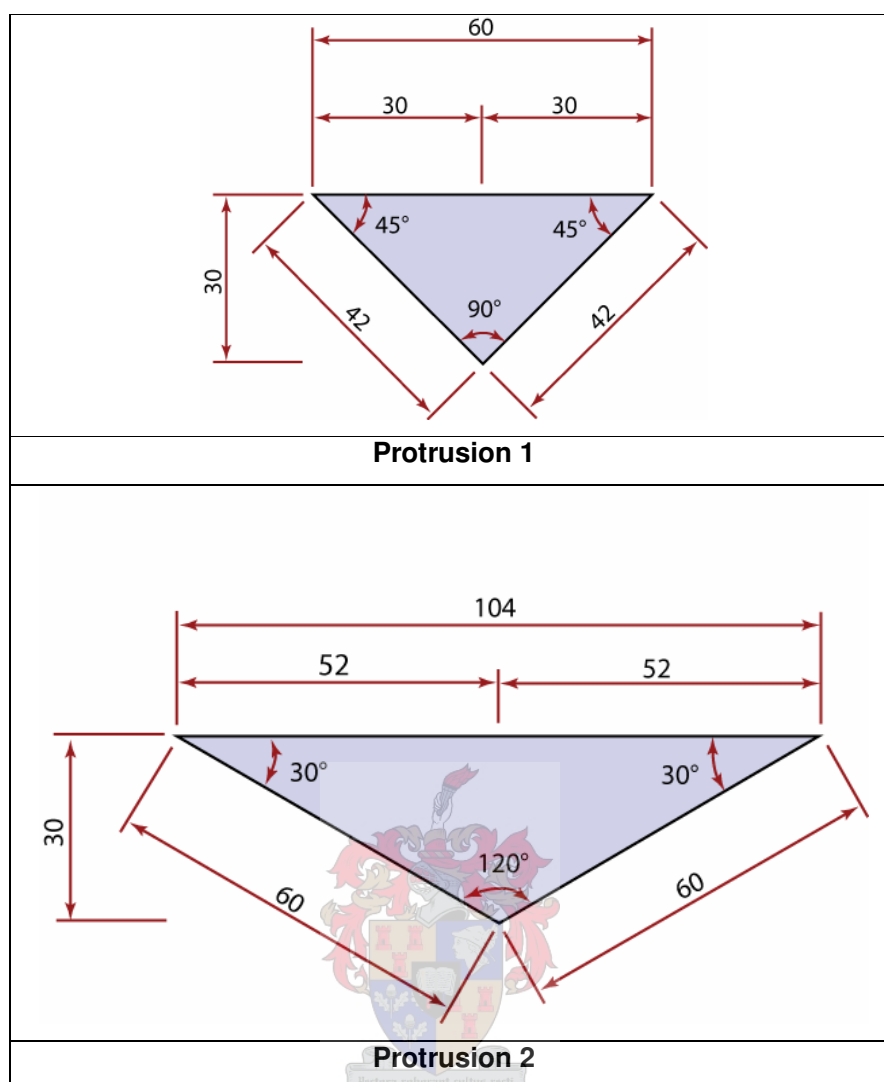


Figure 4.3: Protrusions for the Second Model (Scale 1:30)

4.8 Spacing of Protrusions

The amount of different protrusion spacing is unlimited. Van Deventer (2006) did tests on a 1,2 metre high scale 1:30 model. The width of the model was 1 metre. Van Deventer (2006) tested 4 different protrusion layouts (See Figure 4.4), adding protrusions from the top to the bottom of the downstream slope.

The practicality of the layouts is discussed in Section 7.

The first layout considered protrusions on every step. The second layout considered protrusions alternating in every second successive step. The third layout considered protrusions only every second step. The last layout considered protrusions on every step, but

spaced further apart. Van Deventer (2006) used the average values of the last three layouts to compare the effectiveness of the protrusions compared with a standard spillway. The reason is that the three configurations gave basically the same results. The tread of Van Deventer's (2006) model was 25 mm, with the height of the step equal to 33 mm.

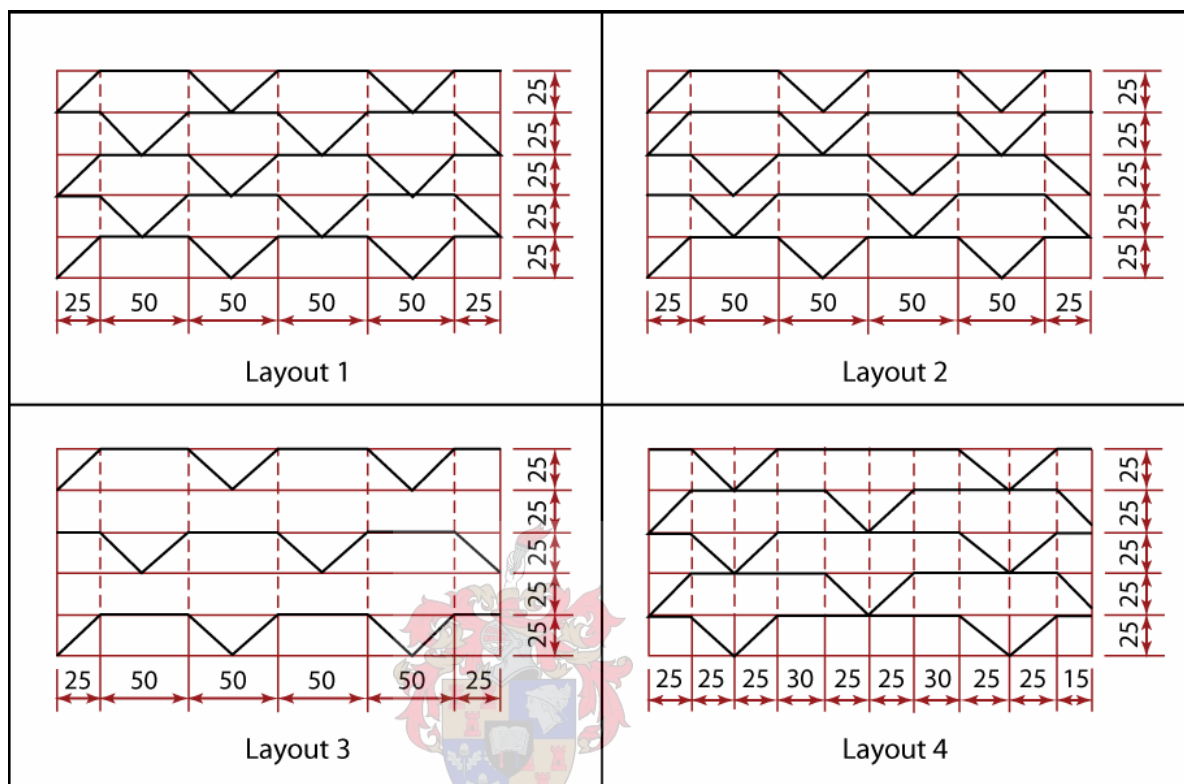


Figure 4.4: Layouts tested by Van Deventer (2006)

4.8.1 Spacing of Protrusions on the First Model (Scale 1:20)

Two different protrusion sizes were tested (Section 4.7). Four different spacings for each protrusion size were tested, with an extra spacing tested for the 1:30 scale model for protrusion 1. This resulted in 8 different layouts for the model, excluding the standard stepped spillway. Nine flows (Section 4.6) were tested with sequent depth measurements taken for each layout. A major constraint of the model was the width of 0,45 metres, allowing limited options for spacing over the width of the model. Protrusions were added from the second step of the ogee cap.

Protrusion 1**a) Layout 1**

The layout is shown in Figure 4.5. Only full sized protrusions could be used and would have fitted into the 0,45 metre width of the model, but protrusions were deliberately placed at the edges of the model to measure the effect of protrusions at the edges. This layout used the width of 2 times the tread (90 mm) of the steps. The protrusions were added on every second step of the model. This was based on a recommendation by Van Deventer (2006). It would also be time consuming to add protrusions on every step.

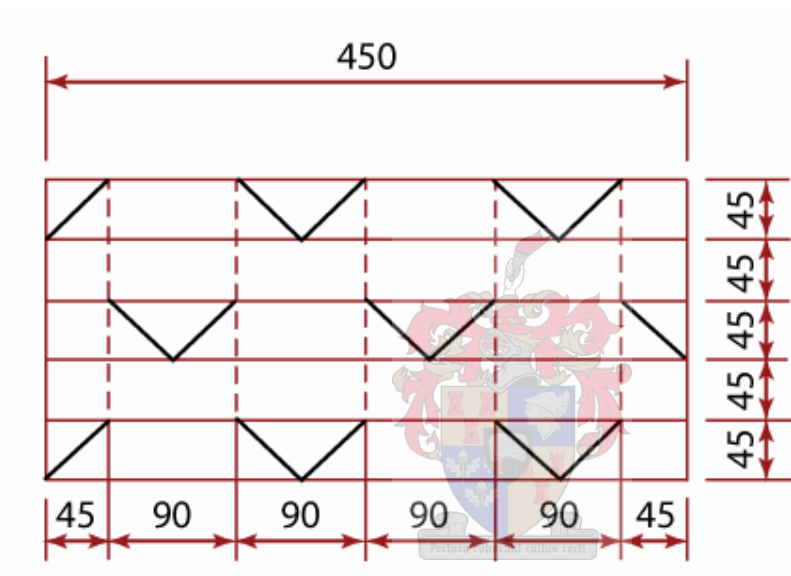
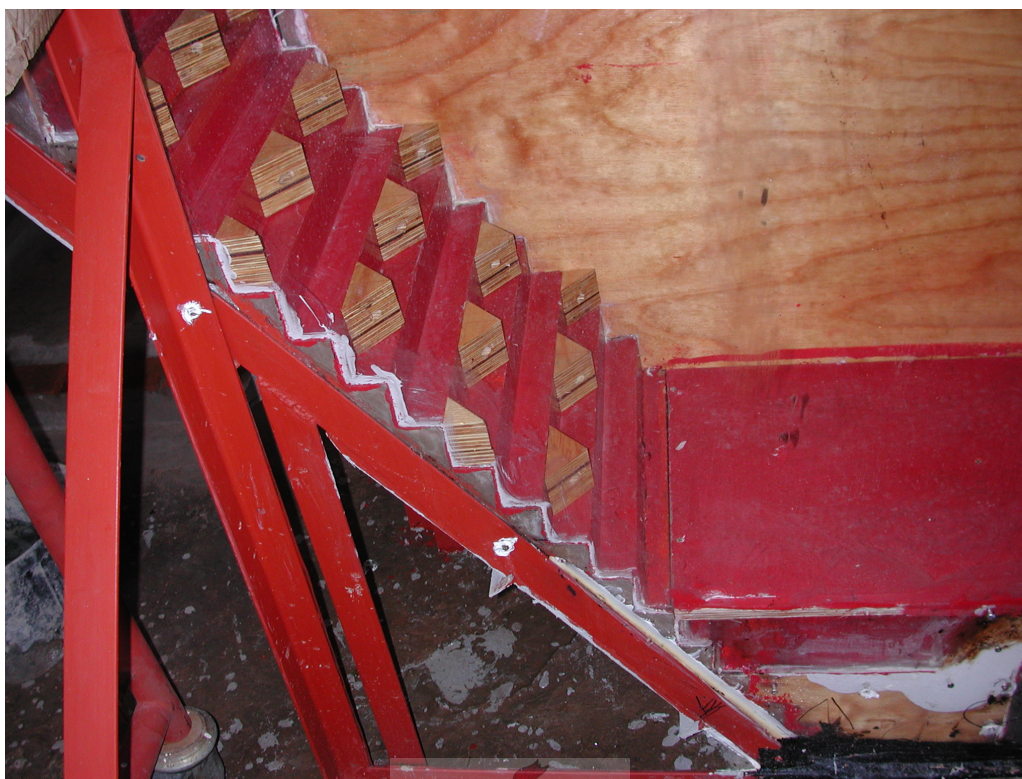


Figure 4.5: Plan of layout of Protrusion 1 Layout 1 (Scale 1:20)



Photograph 4.8: Protrusion 1 Layout 1 (Scale 1:20)

b) Layout 2

The layout is shown in Figure 4.6. Protrusions were added on every second step. They were spaced further apart than Layout 1. This was done to determine the sensitivity of the lateral spacing of the protrusions. This effect was however studied further with the 1:30 scale model.

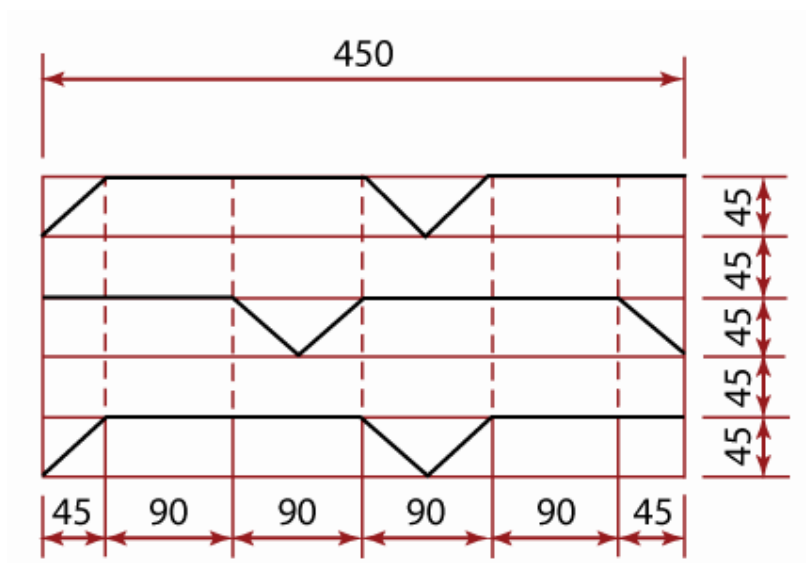
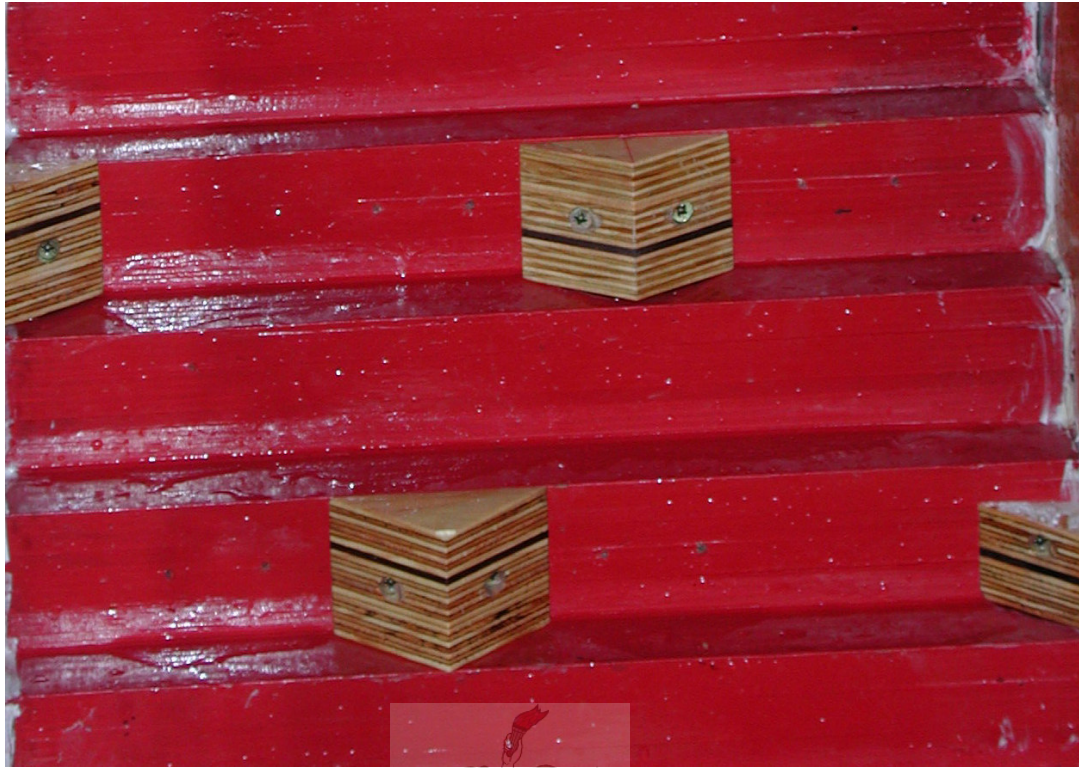


Figure 4.6: Plan of layout of Protrusion 1 Layout 2 (Scale 1:20)



Photograph 4.9: Protrusion 1 Layout 2 (Scale 1:20)

c) Layout 3

The layout is shown in Figure 4.7. Protrusions were added on every fourth step. They were spaced at the same intervals as Layout 1. This was done to determine the sensitivity of the spacing of the protrusions down the steps.

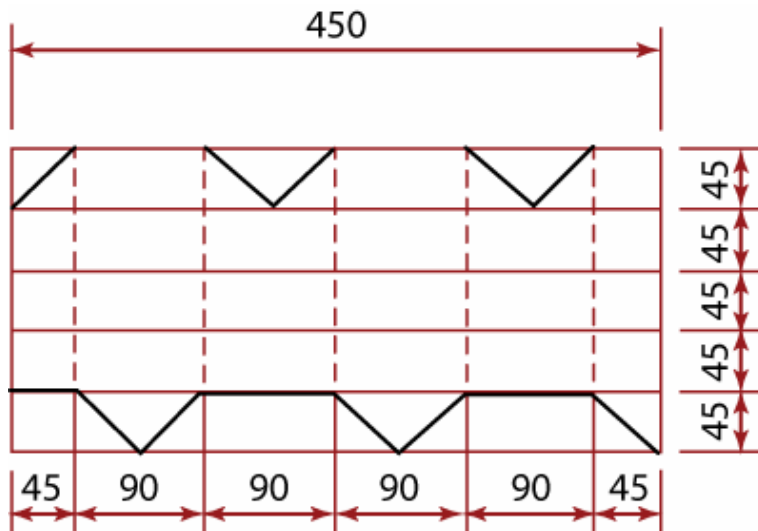


Figure 4.7: Plan of layout of Protrusion 1 Layout 3 (Scale 1:20)

d) Layout 4

The layout is shown in Figure 4.8. Protrusions were added on every step for the first third of the dam height. They were spaced at the same intervals as Layout 1. This was done to determine how early air entrainment is possible. The effect on the roughness of the whole downstream slope will be discussed in Section 5.

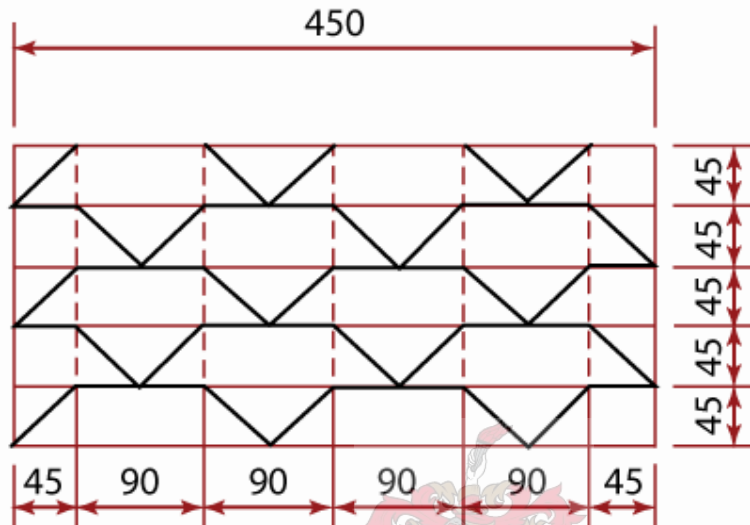


Figure 4.8: Plan of layout of Protrusion 1 Layout 4 (Scale 1:20)



Photograph 4.10: Protrusion 1 Layout 4 (view 1) (Scale 1:20)



Photograph 4.11: Protrusion 1 Layout 4 (view 2) (Scale 1:20)

Protrusion 2

a) Layout 1

The layout is shown in Figure 4.9. Again protrusions were deliberately placed at the edges of the model to measure the effect of protrusions at the edges. The protrusions were added on every second step of the model.

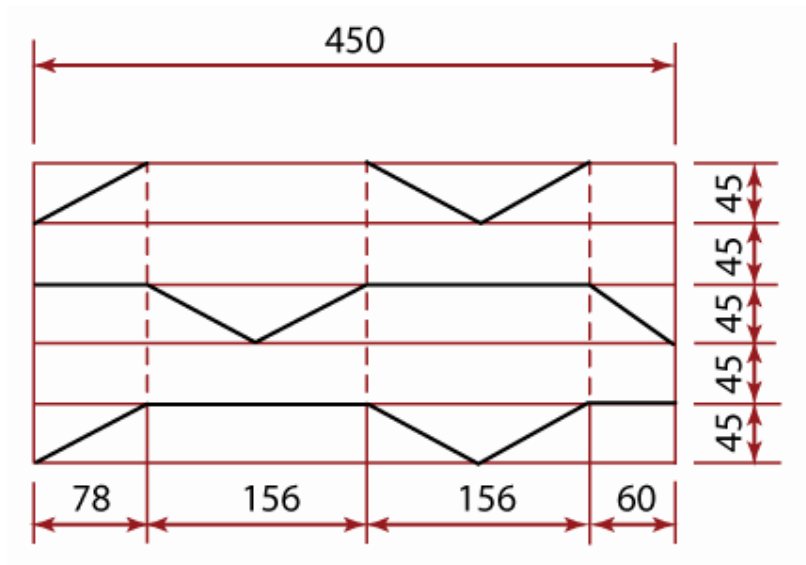


Figure 4.9: Plan of layout of Protrusion 2 Layout 1 (Scale 1:20)



Photograph 4.12: Protrusion 2 Layout 1 (Scale 1:20)

b) Layout 2

The layout is shown in Figure 4.10. Protrusions were added on every step for the first third of the dam height (at the bottom). They were spaced at the same intervals as Layout 1. This was done to determine how early air entrainment is possible. The effect on the roughness of the whole downstream slope will be discussed in Chapter 5.

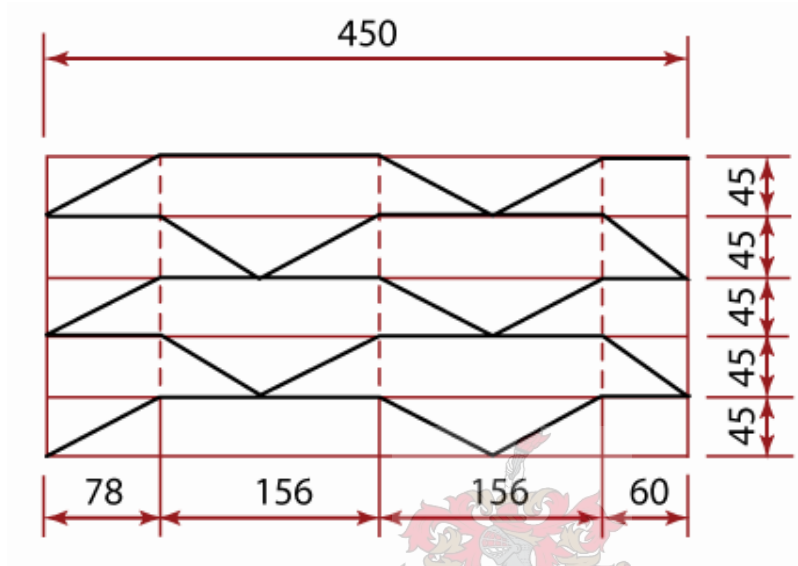


Figure 4.10: Plan of layout of Protrusion 2 Layout 2 (Scale 1:20)



Photograph 4.13: Protrusion 2 Layout 2 (Scale 1:20)

c) Layout 3

The layout is shown in Figure 4.11. Protrusions were added on every fourth step. They were spaced at the same intervals as Layout 1. This was done to determine the sensitivity of the spacing of the protrusions down the steps.

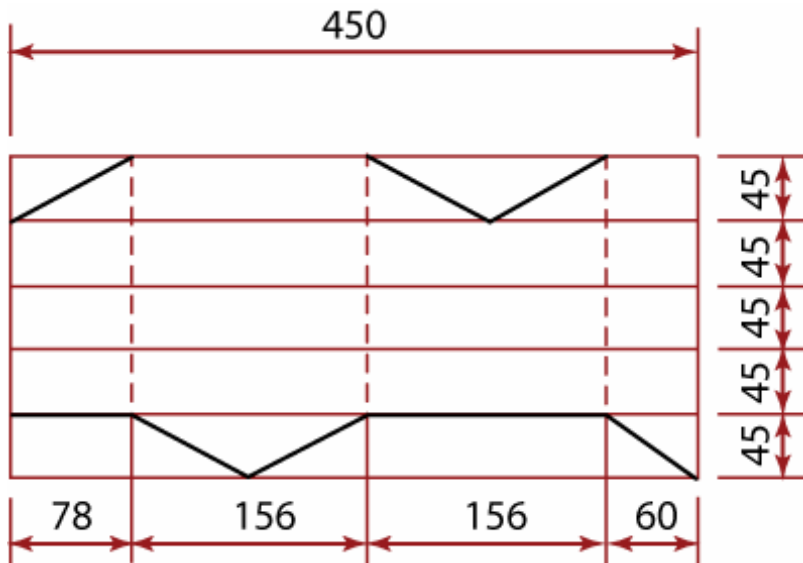


Figure 4.11: Plan of layout of Protrusion 2 Layout 3 (Scale 1:20)

d) Layout 4

The layout is shown in Figure 4.12. Protrusions were added on every step for the last third of the dam height. They were spaced at the same intervals as Layout 1. The effect on the roughness of the whole downstream slope will be discussed in Chapter 5.

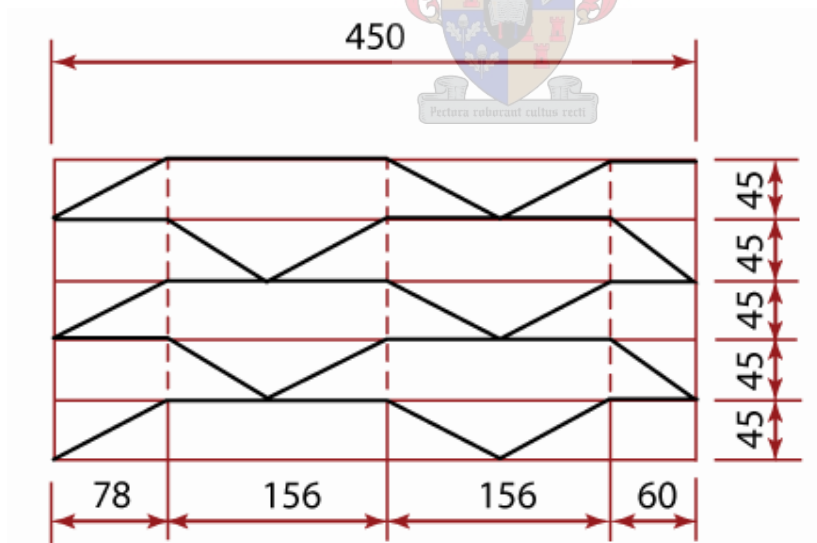


Figure 4.12: Plan of layout of Protrusion 2 Layout 4 (Scale 1:20)



Photograph 4.14: Protrusion 2 Layout 4 (Scale 1:20)

4.8.2 Spacing of Protrusions on the Second Model (Scale 1:30)

Protrusion 1

a) Layout 1

The layout is shown in Figure 4.13. Protrusions were deliberately placed at the edges of the model to measure the effect of protrusions at the edges. This layout used the width of 2 times the tread (60 mm) of the steps. The protrusions were added on every second step of the model.

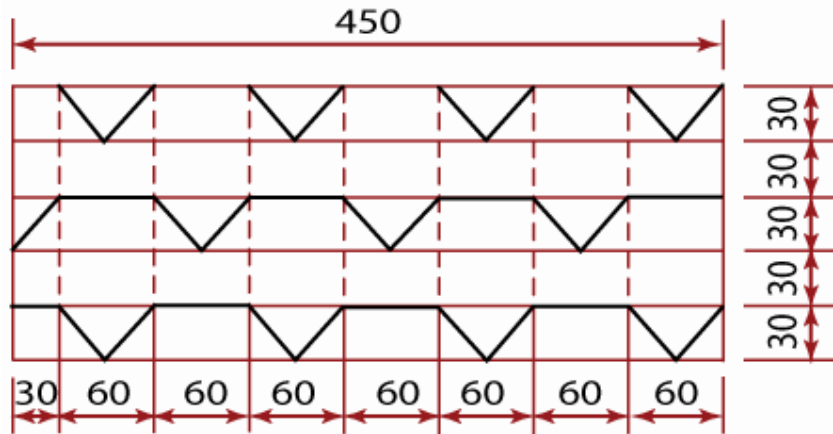


Figure 4.13: Plan of layout of Protrusion 1 Layout 1 (Scale 1:30)



Photograph 4.15: Protrusion 1 Layout 1 (Scale 1:30)

b) Layout 2

The layout is shown in Figure 4.14. Protrusions were added on every second step. They were spaced further apart than Layout 1. This was done to determine the sensitivity of the lateral spacing of the protrusions.

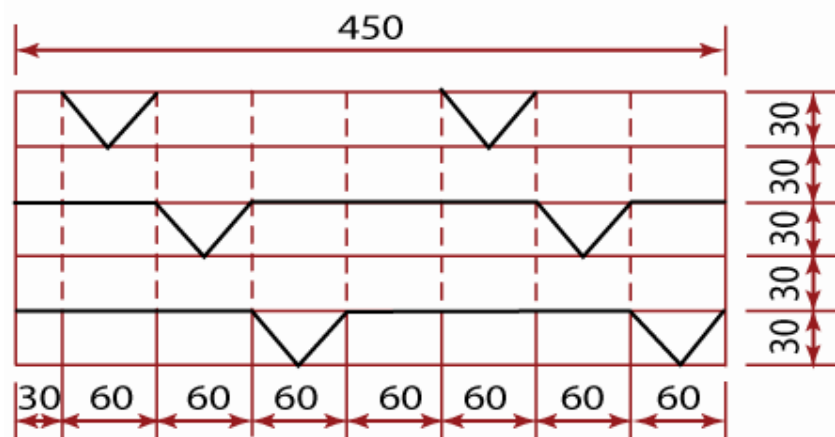


Figure 4.14: Protrusion 1 Layout 2 (Scale 1:30)



Photograph 4.16: Protrusion 1 Layout 2 (Scale 1:30)

c) Layout 3

The layout is shown in Figure 4.15. Protrusions were added on every fourth step. They were spaced at the same intervals as Layout 1. This was done to determine the sensitivity of the spacing of the protrusions down the steps.

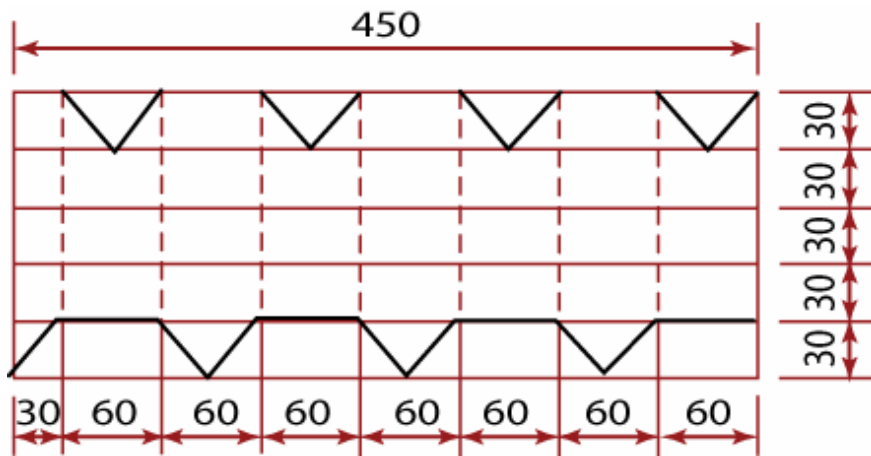


Figure 4.15: Plan of layout of Protrusion 1 Layout 3 (Scale 1:30)



Photograph 4.17: Protrusion 1 Layout 3 (Scale 1:30)

d) Layout 4

The layout is shown in Figure 4.16. Protrusions were added on every step for the first third of the dam height. They were spaced at the same intervals as Layout 1. This was done to determine how early air entrainment is possible. The effect on the roughness of the whole downstream slope will be discussed in Section 5.

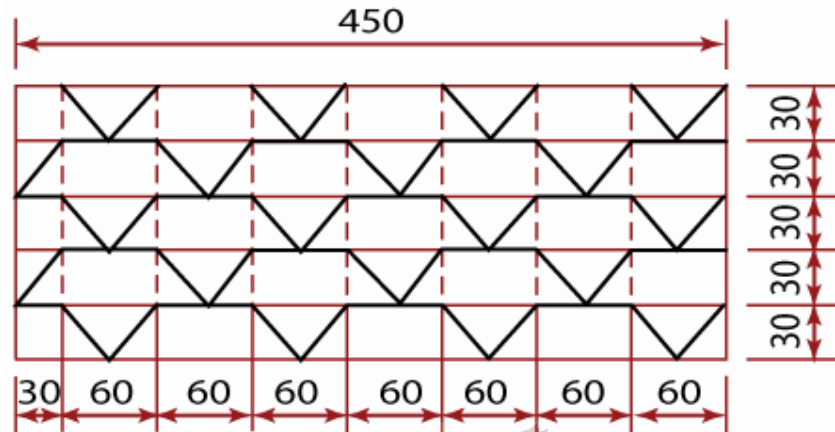
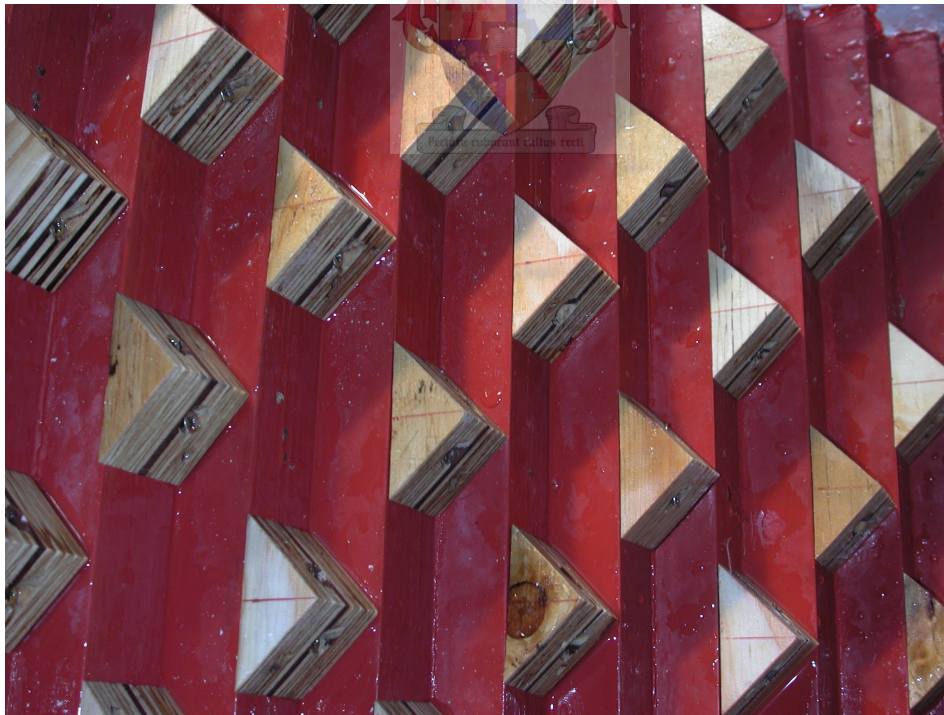


Figure 4.16: Plan of layout of Protrusion 1 Layout 4 (Scale 1:30)



Photograph 4.18: Protrusion 1 Layout 4 (Scale 1:30)

e) Layout 5

The layout is shown in Figure 4.17. Protrusions were added on every second step. They were spaced further apart than Layout 1 but closer than Layout 2. This was done to determine the sensitivity of the lateral spacing of the protrusions.

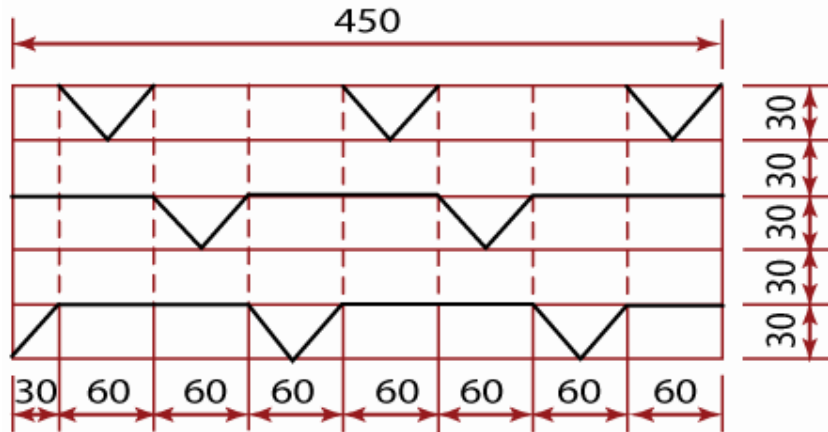


Figure 4.17: Plan of layout of Protrusion 1 Layout 5 (Scale 1:30)

Protrusion 2

a) Layout 1

The layout is shown in Figure 4.18. Again protrusions were deliberately placed at the edges of the model to measure the effect of protrusions at the edges. The protrusions were added on every second step of the model.

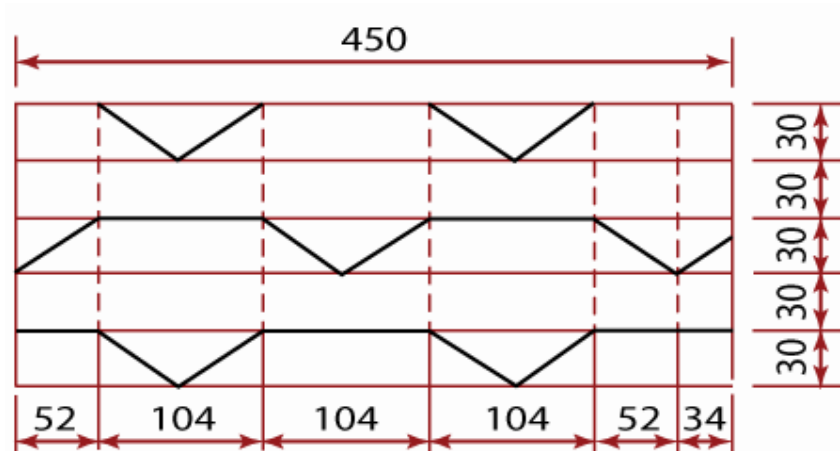


Figure 4.18: Plan of layout of Protrusion 2 Layout 1 (Scale 1:30)



Photograph 4.19: Protrusion 2 Layout 1 (Scale 1:30)

b) Layout 2

The layout is shown in Figure 4.19. Protrusions were added on every second step. They were spaced further apart than Layout 1. This was done to determine the sensitivity of the lateral spacing of the protrusions down the steps.

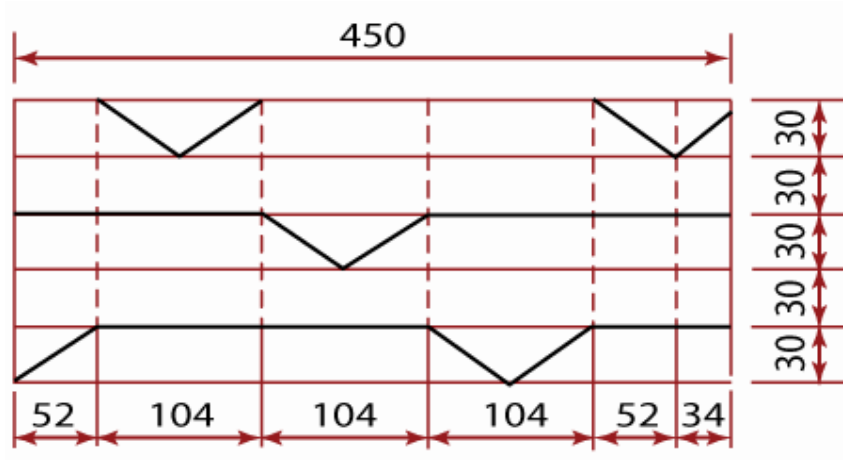


Figure 4.19: Plan of layout of Protrusion 2 Layout 2 (Scale 1:30)



Photograph 4.20 Protrusion 2 Layout 2 (Scale 1:30)

c) Layout 3

The layout is shown in Figure 4.20. Protrusions were added on every fourth step. They were spaced at the same intervals as Layout 1.

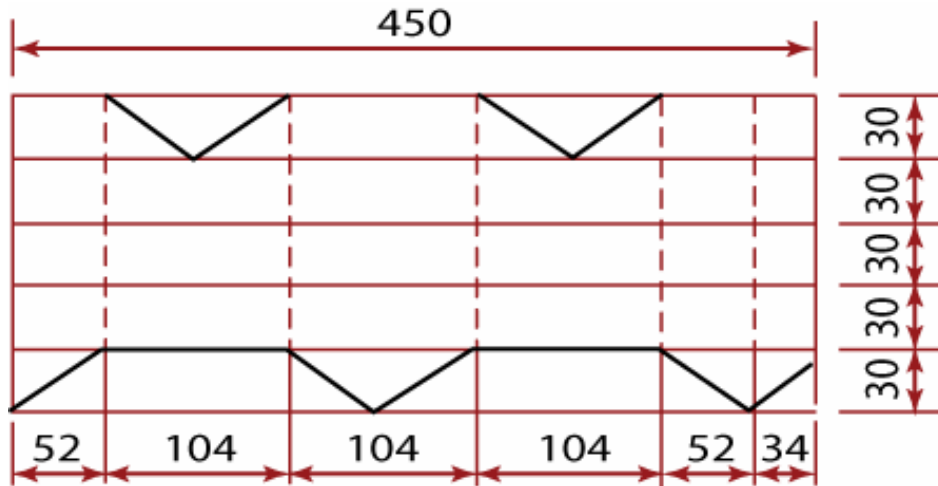
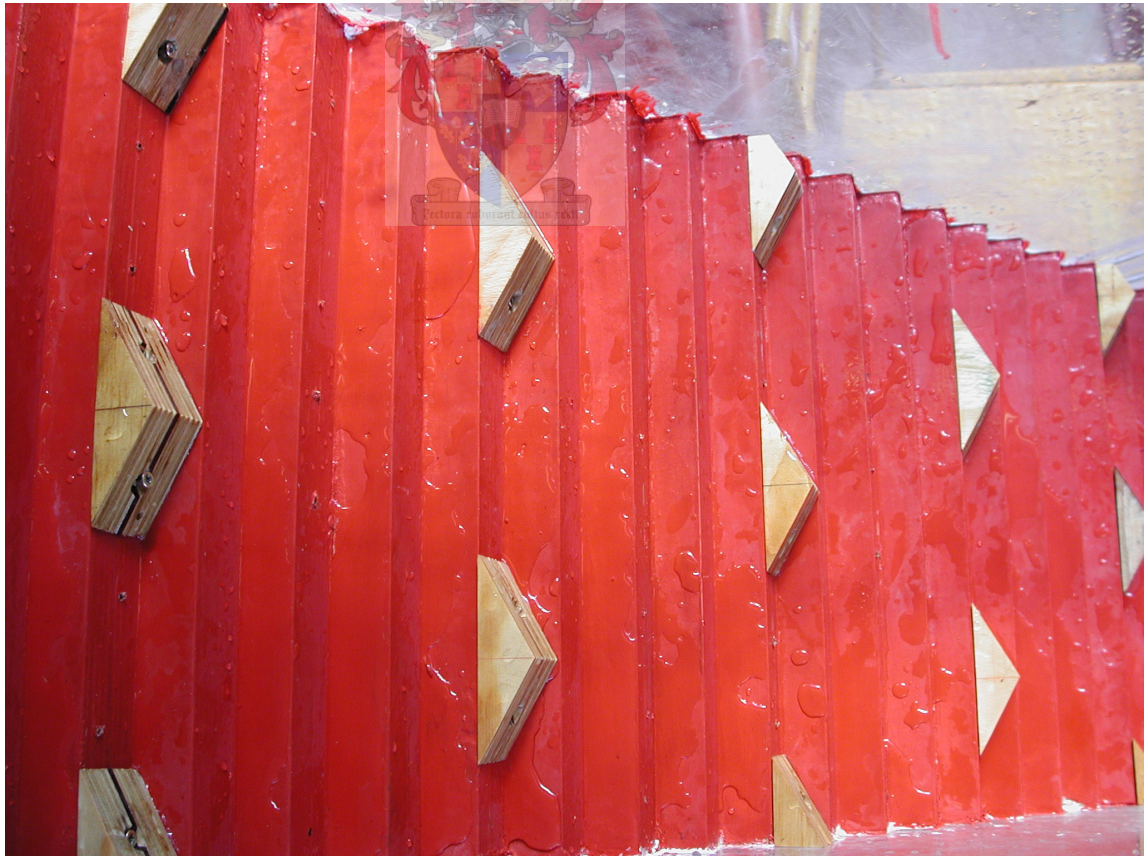


Figure 4.20: Plan of layout of Protrusion 2 Layout 3 (Scale 1:30)



Photograph 4.21: Protrusion 2 Layout 3 (Scale 1:30)

d) Layout 4

The layout is shown in Figure 4.21. Protrusions were added on every step for the first third of the dam height. They were spaced at the same intervals as Layout 1. This was done to determine how early air entrainment is possible. The effect on the roughness of the whole downstream slope will be discussed in Chapter 5.

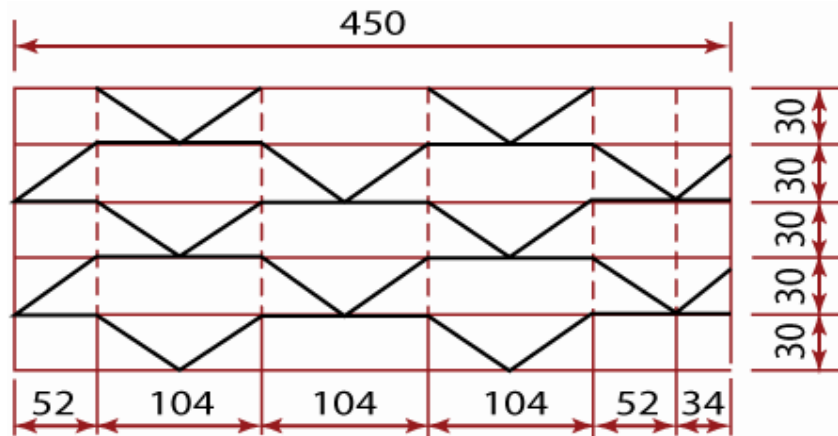


Figure 4.21: Plan of layout of Protrusion 2 Layout 4 (Scale 1:30)



Photograph 4.22: Protrusion 2 Layout 4 (Scale 1:30)

4.9 Ratio between the Area of Protrusions

From the layouts described in Section 4.8 a protrusion density was determined. The formula uses 60 tested steps, thus the full dam height (in this case 75 m in the prototype) to calculate the protrusion density. The protrusion density for a standard stepped spillway is 1, with the protrusion density with the mentioned protrusion configurations ranging from 1,0 to 1,13. The following formula is proposed:

$$\text{Protrusion Density} = \frac{A_{\text{Total}} (\text{over 60 steps}) + A_{\text{Triangle}} (\text{over 60 steps})}{A_{\text{Total}} (\text{over 60 steps})}$$

with:

$$\begin{aligned} A_{\text{Total}} &= \text{The total area of the steps in plan} \\ &= \text{Total width} \times \text{tread of step} \times \text{number of steps (60)} \\ A_{\text{Triangle}} &= \text{The total area of the triangles on the steps in plan} \end{aligned}$$

The ratio will always be equal or more than 1,0.

4.9.1 Model 1 (Scale 1:20)

From Figure 4.2 for Protrusion 1:

$$\begin{aligned} A_{\text{Protrusion}} &= 0,5 \times 0,09 \times 0,045 = 0,00202 \text{ m}^2 \text{ for one protrusion} \\ A_{0,5 \text{ Protrusion}} &= 0,5 \times 0,09 \times 0,045 / 2 = 0,00101 \text{ m}^2 \text{ for a half protrusion} \end{aligned}$$

From Figure 4.2 for Protrusion 2:

$$\begin{aligned} A_{\text{Protrusion}} &= 0,5 \times 0,156 \times 0,045 = 0,00351 \text{ m}^2 \text{ for one protrusion} \\ A_{0,5 \text{ Protrusion}} &= 0,5 \times 0,156 \times 0,045 / 2 = 0,00175 \text{ m}^2 \text{ for a half protrusion} \end{aligned}$$

From Figures 4.5 to 4.12:

$$A_{\text{Total}} = 0,045 \times 60 \times 0,45 = 1,215 \text{ m}^2 \text{ over 60 steps}$$

The protrusion density (PD) is summarised in Table 4.1.

Table 4.1: Protrusion Density for Model 1 (Scale 1:20)

Protrusion Configuration	Protrusion Density (PD)
P 1(1)	1,125
P 1(2)	1,075
P 1(3)	1,062
P 1(4)	1,083
P 2(1)	1,130
P 2(2)	1,087
P 2(3)	1,065
P 2(4)	1,087

4.9.2 Model 2 (Scale 1:30)

From Figure 4.3 for Protrusion 1:

$$A_{\text{Protrusion}} = 0,5 \times 0,06 \times 0,03 = 0,00090 \text{ m}^2 \text{ for one protrusion}$$

$$A_{0,5 \text{ Protrusion}} = 0,5 \times 0,06 \times 0,03 / 2 = 0,00045 \text{ m}^2 \text{ for a half protrusion}$$

From Figure 4.3 for Protrusion 2:

$$A_{\text{Protrusion}} = 0,5 \times 0,104 \times 0,03 = 0,00156 \text{ m}^2 \text{ for one protrusion}$$

$$A_{0,5 \text{ Protrusion}} = 0,5 \times 0,104 \times 0,03 / 2 = 0,00078 \text{ m}^2 \text{ for a half protrusion}$$

$$A_{0,7 \text{ Protrusion}} = 0,5 \times 0,052 \times 0,03 + 0,5 \times (0,01 + 0,03) \times 0,34 = 0,00146 \text{ m}^2 \text{ for a } 7/10^{\text{th}} \text{ protrusion}$$

From Figures 4.13 to 4.21:

$$A_{\text{Total}} = 0,03 \times 60 \times 0,45 = 0,810 \text{ m}^2 \text{ over 60 steps}$$

Table 4.2: Protrusion Density for Model 2 (Scale 1:30)

Protrusion Configuration	Protrusion Density (PD)
P 1(1)	1,125
P 1(2)	1,067
P 1(3)	1,063
P 1(4)	1,083
P 1(5)	1,083
P 2(1)	1,128
P 2(2)	1,085
P 2(3)	1,085
P 2(4)	1,085

4.10 Hydraulic Jump Calculation and Flow Profile Calculation

The flow velocity at the toe of the spillway was determined by the momentum conservation principle through the hydraulic jump. Figure 4.22 shows the measuring point (Section 2 -2) and the point where the velocity was calculated (Section 1 - 1). The sequent depth of the stable hydraulic jump was taken at the measuring point.

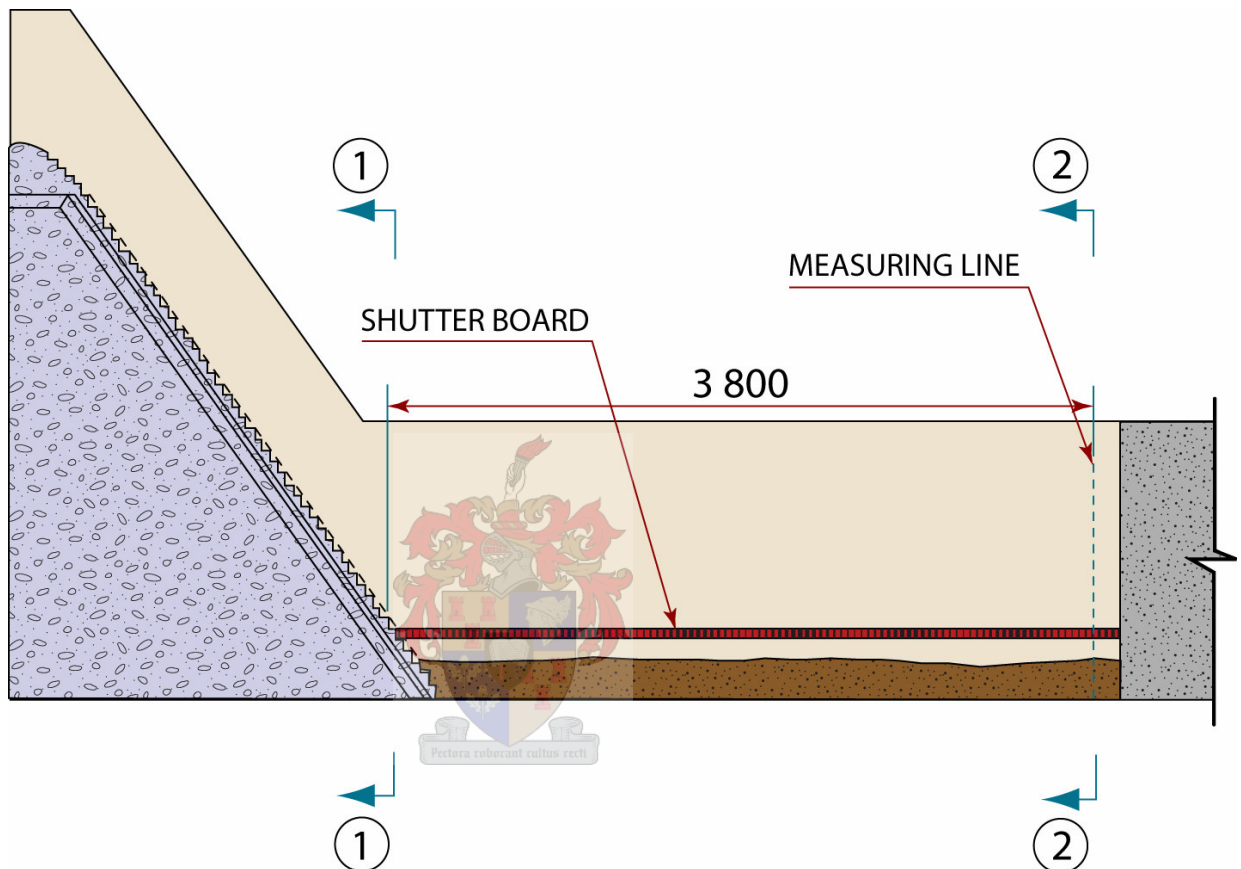


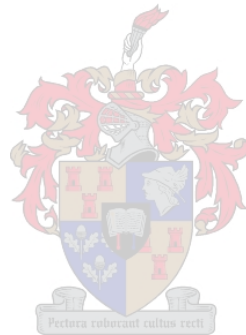
Figure 4.22: Measuring line on model

With the sequent depth (Y_2) measured at the measuring line and the flow rate (Q) known, the friction factor f could be calculated. The flow rate (Q in m^3/s) was converted to a unit flow rate (q in $\text{m}^3/\text{s}\cdot\text{m}$). The velocity (v) at the sequent depth could then be calculated. The Froude number was also calculated at the measuring point. The Froude number and sequent depth were then used to calculate the depth at Section 1–1. The depth was then converted to a velocity. With all the parameters known, the Darcy Friction Loss Equation was used to obtain a value for the friction factor f . The equation used is:

$$f = 8 g \sin \theta q / v^3$$

No secondary losses were assumed.

- 1 INTRODUCTION**
- 2 LITERATURE STUDY**
- 3 REVIEW OF LITERAURE**
- 4 EXPERIMENTAL WORK/PHYSICAL MODELING**



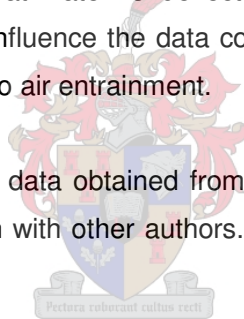
5 HYDRAULIC MODEL TEST RESULTS

Data was obtained by measuring the water surface 3,8 m downstream of the spillway toe. The fluctuation of the water level was small enough to obtain a reliable average value. Individual readings differed by 5 mm or less. This is acceptable in the scope of the thesis. The sluice gate and gate valve were adjusted to keep the upstream point of the hydraulic jump at the toe of the spillway. Several gate and valve adjustments were required to obtain a “stable” water level to record the average level.

As stated in Section 4, no scoop was utilised at the toe of the spillway, with no losses assumed. Van Deventer (2006) did a sensitivity analysis on the use of a scoop and found a 10 % difference in measurements. This formed the basis of not using a scoop for this study.

Data was plotted after the measurements were taken in order to check for deficiencies. This could be used to determine if it was necessary to redo the test. At low flows with protrusions on the steps it was found that water is deflected away from the spillway surface. It is concluded that this does not influence the data considerably. When the flow rate increased, no deflection is observed due to air entrainment.

Appendix G shows the typical data obtained from model testing, together with reworking of the data to enable comparison with other authors. Appendix C shows selective photographs taken during modeling.



5.1 Standard Steps

5.1.1 Water Levels

Figure 5.1 shows the data for both models. From this first graph can be seen that the data for the various layouts does not deviate considerably. A further breakdown of the data will show the difference between the standard steps for both models.

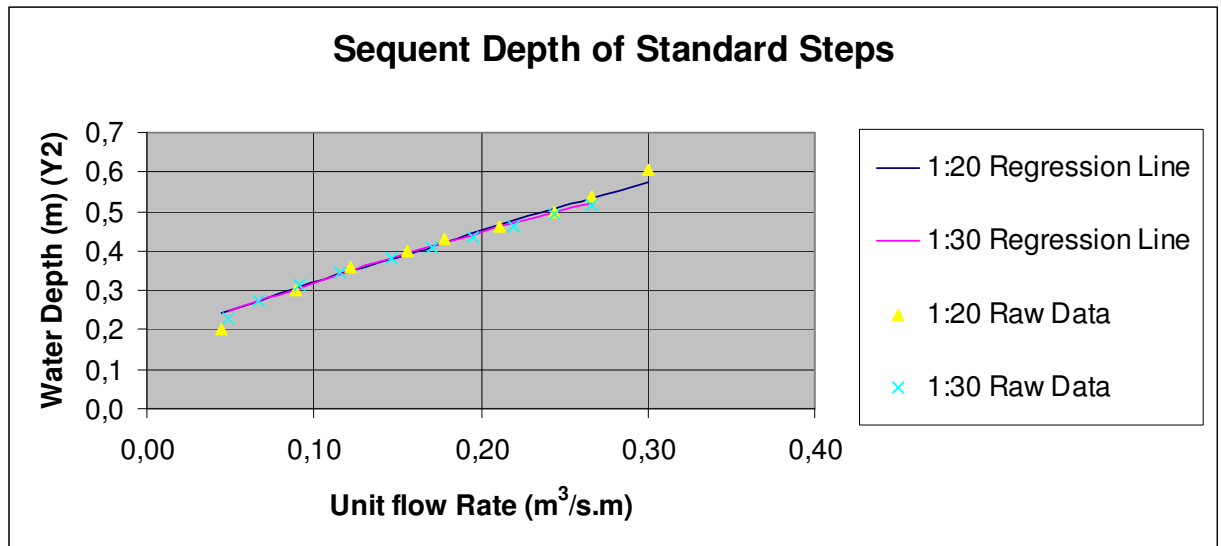


Figure 5.1: Sequent depth measurements for both models

5.1.2 Roughness

Figure 5.2 and Table 5.1 show the roughness as determined for both models. It is evident that some form of scale effect exists. This will be discussed in Chapter 6. An interesting observation is that the roughness values achieved are less than that published by Tozzi, etc.

Table 5.1: Roughness values for the standard steps for both models

Scale 1:20		Scale 1:30	
Unit Flow Rate (m ³ /s.m)	Roughness f	Unit Flow Rate (m ³ /s.m)	Roughness f
0,04	0,012	0,05	0,016
0,09	0,045	0,07	0,029
0,12	0,068	0,09	0,048
0,16	0,088	0,12	0,065
0,18	0,096	0,15	0,083
0,21	0,105	0,17	0,095
0,24	0,112	0,20	0,106
0,27	0,116	0,22	0,116
0,30	0,118	0,24	0,125
		0,27	0,133

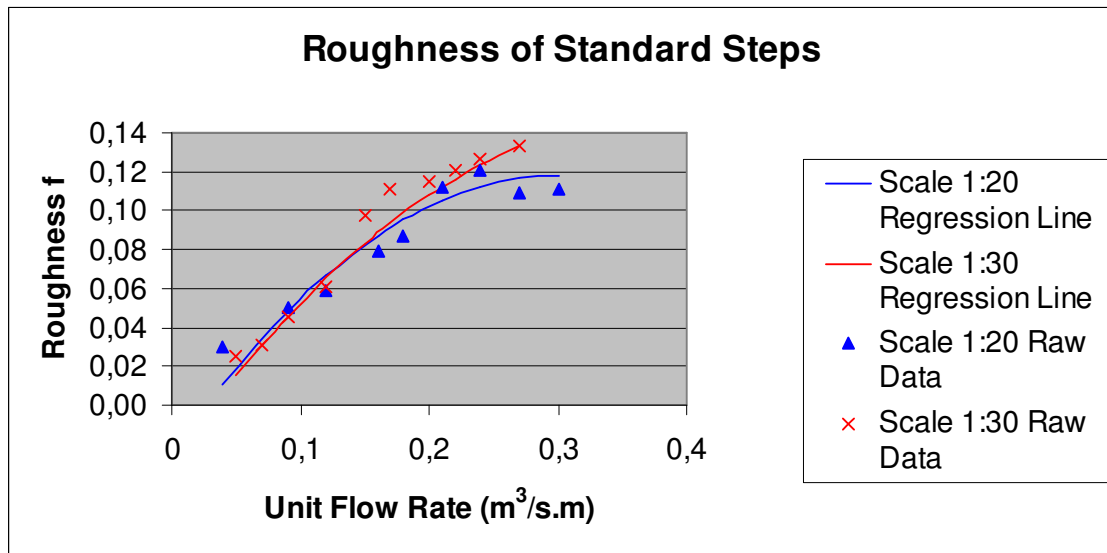


Figure 5.2: Roughness of standard steps for both models obtained from modeling

From Figure 3.3 the following equations for the roughness value in terms of Y_c and k can be derived for the equations of Tozzi (1994), Chamani et al (1999) and Boes & Minor (2002):

- Tozzi (1994): $f = 0,3029 (Y_c / k)^{-0,3429}$ (5.1)

with: $R^2 = 1,0$

when $Y_c/k < 6,1$ the friction factor stays constant at $f = 0,163$

- Chamani et al (1999): $k = 72 \text{ mm: } f = 0,1419 (Y_c / k)^{1,0351}$ (5.2)

with: $R^2 = 0,75$

- $k = 36 \text{ mm: } f = 0,0641 (Y_c / k)^{0,9280}$ (5.3)

with: $R^2 = 0,95$

- $k = 18 \text{ mm: } f = 0,0814 (Y_c / k)^{0,3995}$ (5.4)

with: $R^2 = 0,15$

- Boes & Minor (2002): $f = 0,0926 (Y_c / k)^{-0,1637}$ (5.5)

With: $R^2 = 0,99$

The above equations are shown on Figure 5.3, with the data obtained for the standard steps obtained from the physical modeling as described in Chapter 4. A large scatter of data was obtained from the reworked data from Chamani et al (1999), thus resulting in equations that do not show a good correlation. These equations by Chamani et al (1999) however give an indication of the range obtained relative to Tozzi (1994) and Boes & Minor (2002). Note that

the power of the equations of Tozzi (1994) and Boes & Minor (2002) is negative, whilst the power of the equations by Chamani et al (1999) is positive.

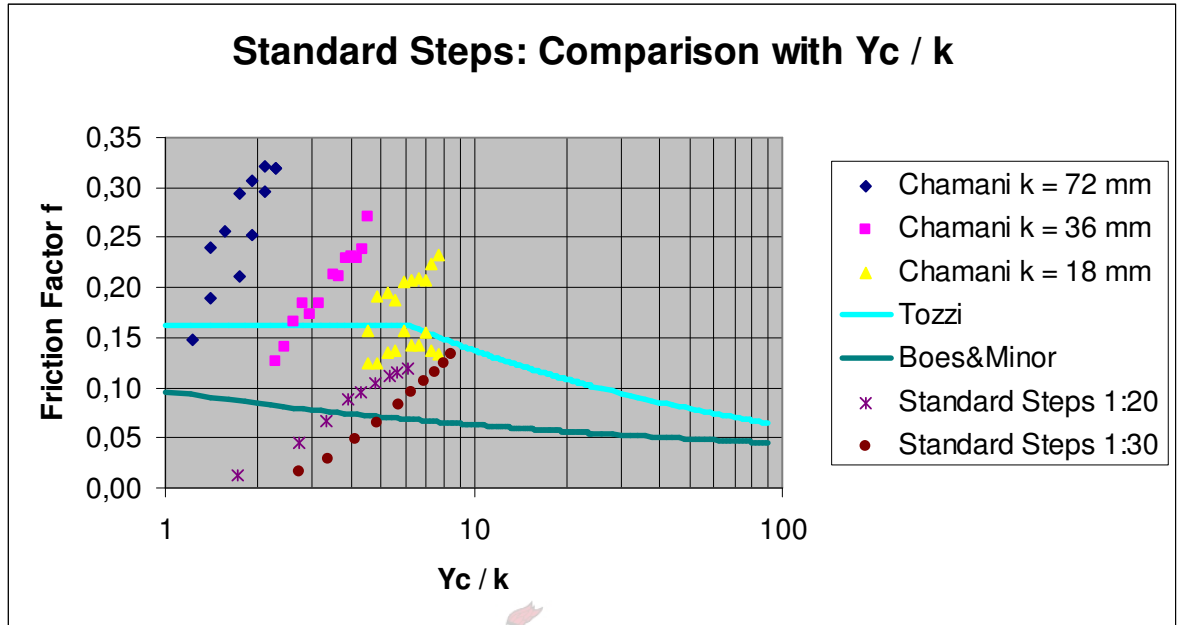


Figure 5.3: Data of roughness of standard steps compared with Tozzi (1994), Chamani et al (1999) and Boes & Minor (2002)

The data for Model 1 and Model 2 were used (from Figure 5.3) and the following equations for the roughness for the standard steps were obtained:

- Model 1: $f = 0,0066 (Y_c / k)^{1,7341}$ (5.6)
with: $R^2 = 0,92$

- Model 2: $f = 0,0033 (Y_c / k)^{1,7919}$ (5.7)
with: $R^2 = 0,97$

Both data sets were combined and the following equation for the roughness for the standard steps was obtained:

$$f = 0,0073 (Y_c / k)^{1,4678} \dots\dots\dots (5.8)$$

with: $R^2 = 0,80$

5.1.3 Point of Inception (PI)

Figure 5.4 shows the inception length L_i measured from the top of the crest, while Table 5.2 shows the values of the inception length L_i (refer to Figures 2.4 and 2.9). Some form of scale effect exists. This will be discussed in Chapter 6.

Table 5.2: Inception length L_i for the standard steps for both models

1:20 Model		1:30 Model	
Unit flow rate ($\text{m}^3/\text{s.m}$)	Inception Length (L_i) (m)	Unit flow rate ($\text{m}^3/\text{s.m}$)	Inception Length (L_i) (m)
0,04	0,693	0,05	0,671
0,09	1,110	0,07	0,853
0,12	1,388	0,09	1,079
0,16	1,638	0,12	1,276
0,18	1,788	0,15	1,487
0,21	1,990	0,17	1,619
0,24	2,163	0,20	1,724
0,27	2,263	0,22	1,800
0,30	2,388	0,24	1,848
		0,27	1,866

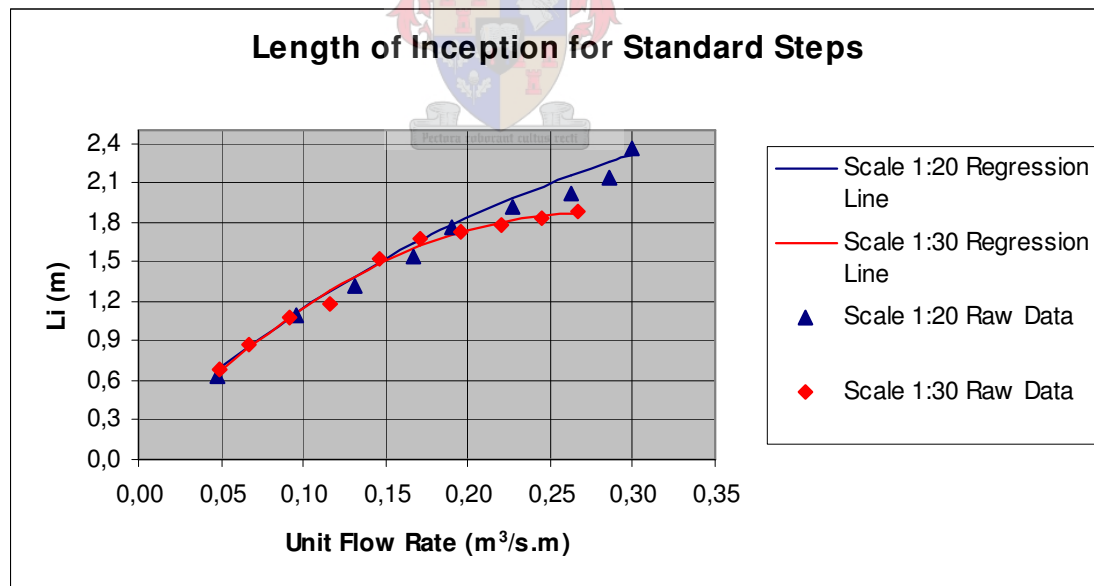


Figure 5.4: Inception Length for both models obtained from modeling

From Figure 3.5 the following power equations for the length of inception in terms of L_i , Y_c and k can be derived for the equations of Boes & Minor (2002), Chanson (1994) and Matos (2000):

- Boes & Minor (2002): $L_i / Y_c = 10,350 (Y_c / k)^{0,0693}$ (5.9)
with: $R^2 = 0,99$
- Chanson (1994): $L_i / Y_c = 7,298 (Y_c / K)^{0,2002}$ (5.10)
with: $R^2 = 0,98$
- Matos (1999): $L_i / Y_c = 6,828 (Y_c / k)^{0,1011}$ (5.11)
with: $R^2 = 0,99$
- Matos et al (2000): $L_i / Y_c = 8,656 (Y_c / k)^{0,1205}$ (5.12)
with: $R^2 = 0,98$

The above equations are shown on Figure 5.5, with the data obtained for the standard steps obtained from the physical modeling as described in Chapter 4.

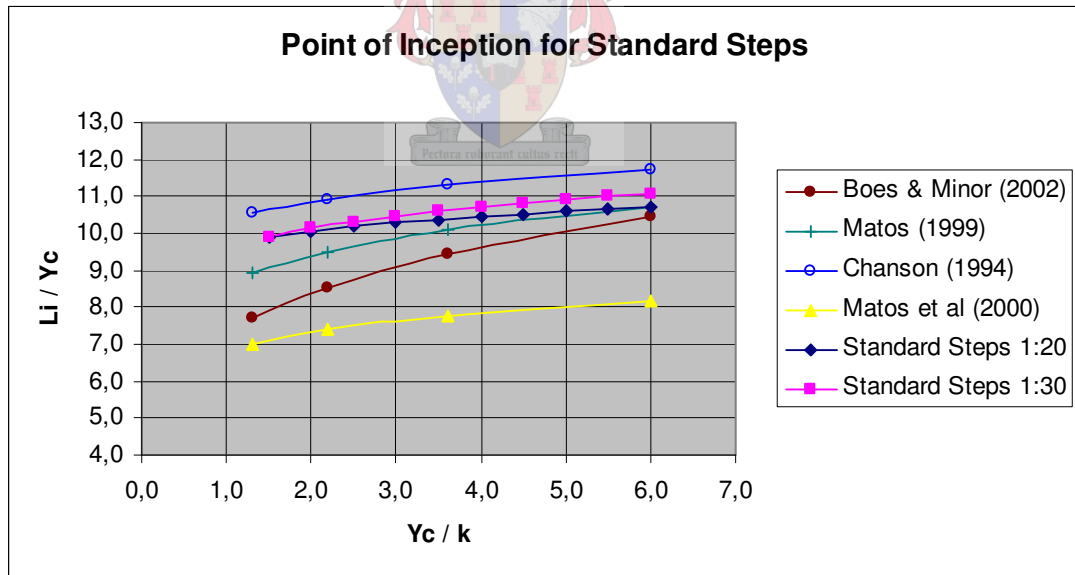


Figure 5.5: Length of inception of standard steps for both models compared with Boes & Minor (2002), Chanson (1994), Matos (1999) and Matos et al (2000)

The data for Model 1 (Scale 1:20) and Model 2 (Scale 1:30) were used (from Figure 5.5) and the following equations for the length of inception for the standard steps were obtained:

- Model 1: $L_i / Y_c = 9,5911 (Y_c / k)^{0,0802}$ (5.13)
with: $R^2 = 0,99$

- Model 2: $L_i / Y_c = 9,6924 (Y_c / k)^{0,0548}$ (5.14)
with: $R^2 = 0,98$

Both data sets were combined (See Figure 5.6) and the following equation for the length of inception for the standard steps was obtained:

$$L_i / Y_c = 9,6416 (Y_c / k)^{0,0675} \text{ (5.15)}$$

with: $R^2 = 0,91$

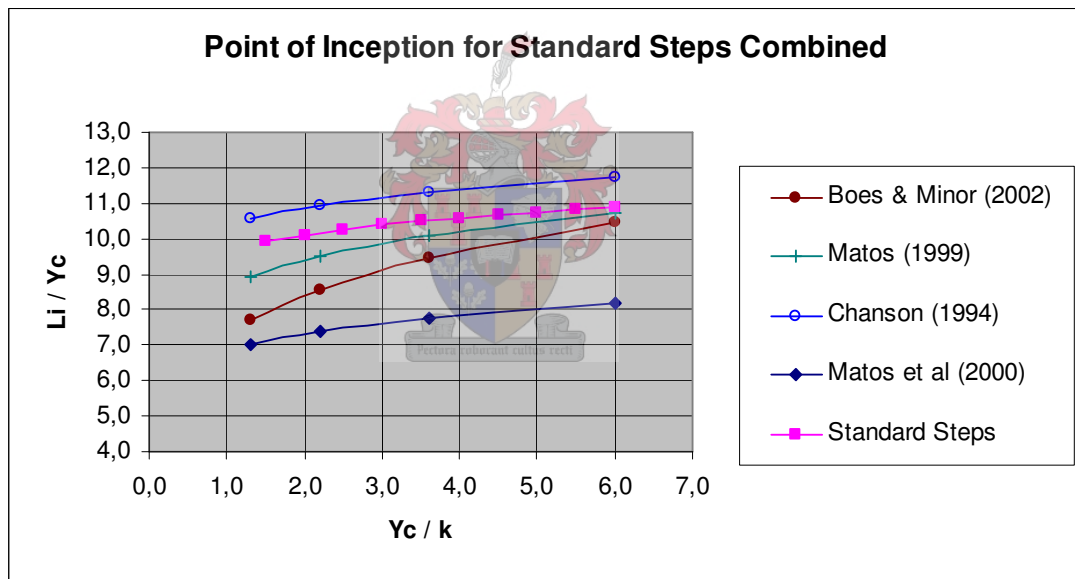


Figure 5.6: Length of inception of standard steps combined for both models compared with Boes & Minor (2002), Chanson (1994), Matos (1999) and Matos et al (2000)

5.1.4 Scour

As mentioned in Section 4, a 1:60 scale 3D model was constructed of the whole De Hoop Dam spillway configuration. Only the standard steps were tested at flows corresponding to the RDF, RMF and SEF. No protrusions were added on this model. Scour surveys were done with the aid of a tachymeter and photographic equipment. Both these methods corresponded very well. Scour depths of 2,0 metres for the RMF ($q = 28 \text{ m}^3/\text{s.m}$) and 3,5 metres for the SEF ($q = 40 \text{ m}^3/\text{s.m}$) were obtained. Figure 5.7 shows the schematic layout of scour measurements. Table 5.3 shows the comparison of the scour depths for the three models (scales 1:20, 1:30 and 1:60). Appendix D shows relevant scour drawings.

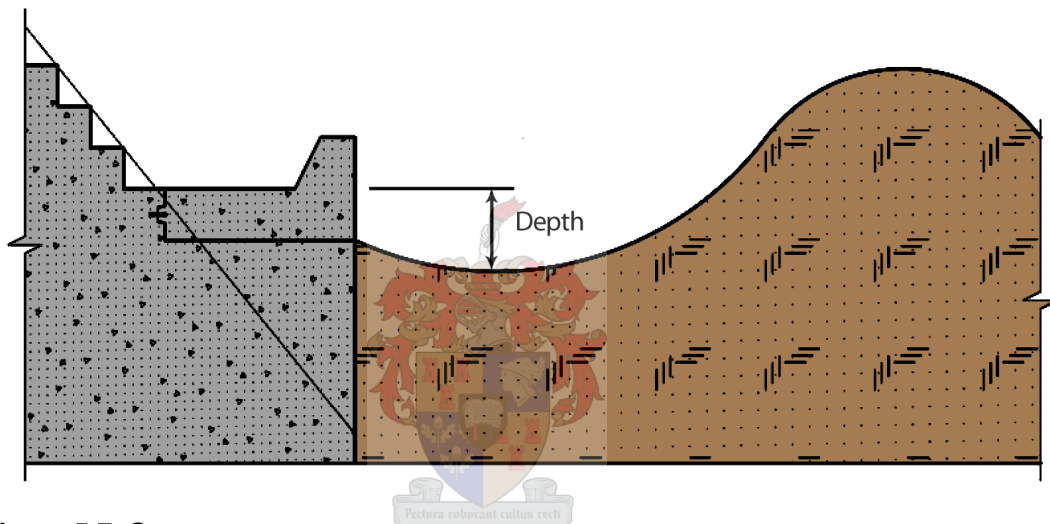


Figure 5.7: Scour measurements

Table 5.3: Scour depths for the standard steps for three models

Flood	Prototype Flow (q in $\text{m}^3/\text{s.m}$)	Prototype		
		Scale 1:20 Scour Depth (m)	Scale 1:30 Scour Depth (m)	Scale 1:60 Scour Depth (m)
RDF	10	0,0	0,0	0,0
RMF	26	1,8	1,8	2,0
SEF	37	Could not be tested	3,7	3,5

5.2 The First Model (Scale 1:20)

5.2.1 Water Levels

Figures 5.8 and 5.9 show the data for the 1:20 scale model. From this first graphs can be seen that the data for the various protrusion layouts does not deviate considerably. At this early stage there is however a difference between the standard stepped spillway and the stepped spillway with protrusions.

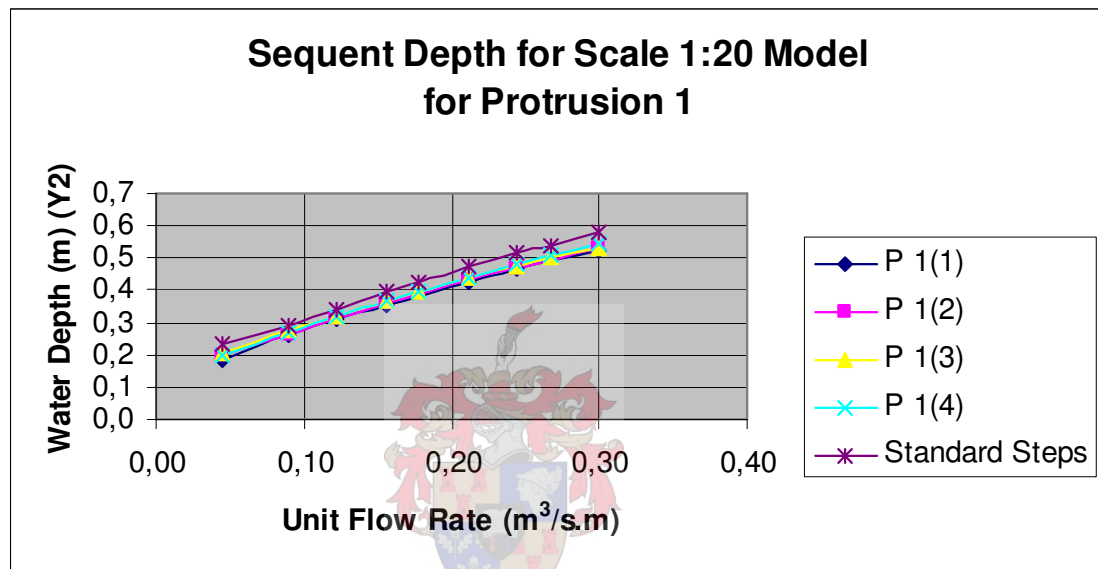


Figure 5.8: Sequent depth measurements for Model 1 Protrusion 1 (Scale 1:20)

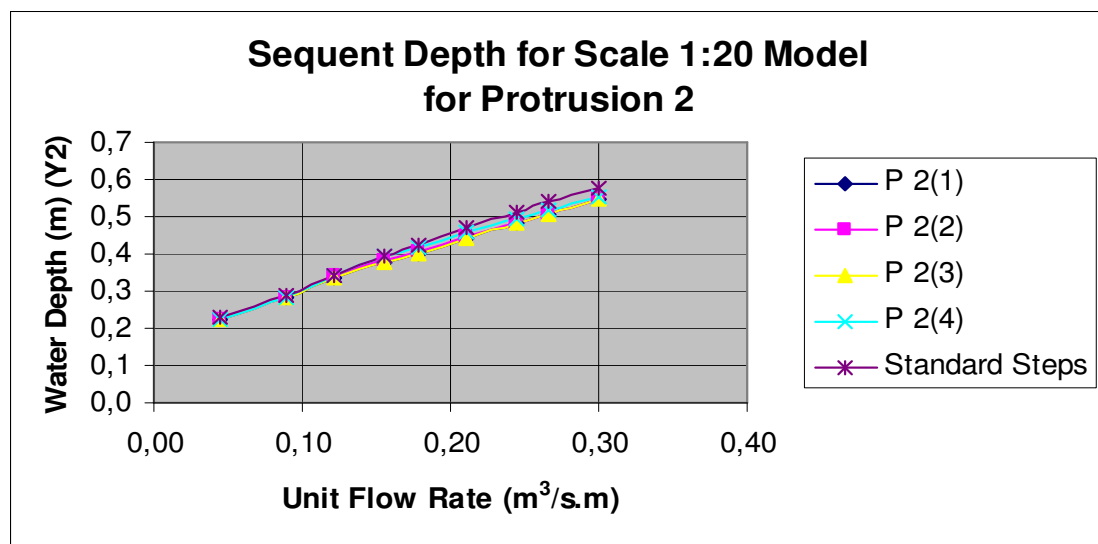


Figure 5.9: Sequent depth measurements for Model 1 Protrusion 2 (Scale 1:20)

5.2.2 Roughness

Figure 5.10 shows the roughness as determined for Protrusion 1. From this graph can be seen that there is a definite increase in roughness for steps with protrusions over the standard steps. It is clear that the more protrusions are added, the higher the roughness value.

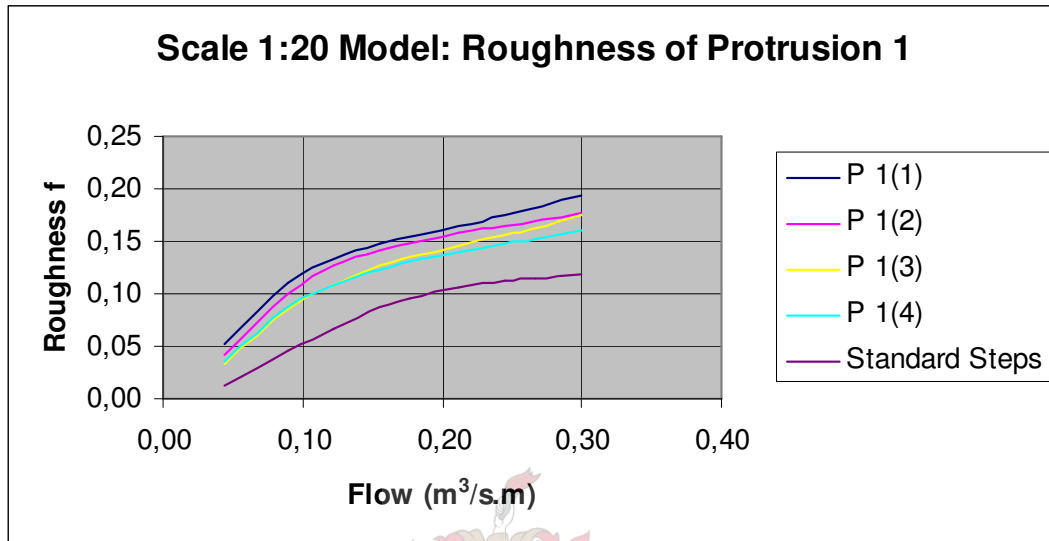


Figure 5.10: Roughness of Model 1 Protrusion 1 (Scale 1:20) obtained from modeling

Figure 5.11 shows the roughness as determined for Protrusion 2. From this graph can be seen that there is an increase in roughness for steps with protrusions over the standard steps. It is also clear that the more protrusions are added, the higher the roughness value. The roughness values for this protrusion shape are however lower than for Protrusion 1.

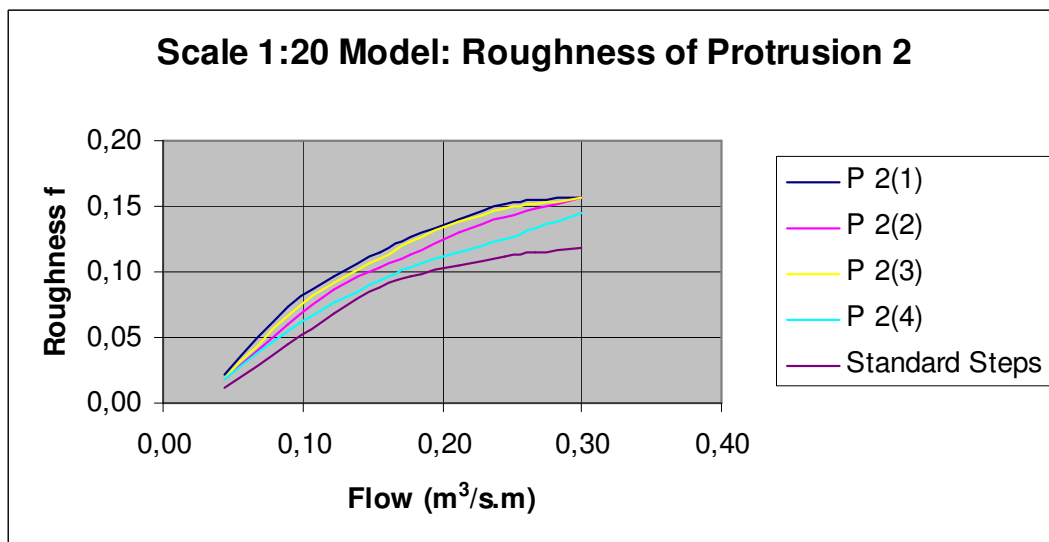


Figure 5.11 Roughness of Model 1 Protrusion 2 (Scale 1:20) obtained from modeling

Figure 5.12 compares the model data with the reworked data from Tozzi (1994) and Pegram et al (1999). Note that only the values of $P 1(1)$, $P 2(1)$ and the standard steps are shown. It can be seen that two intervals exist, where Y_c is smaller than 0,1 and where $0,1 < Y_c < 0,2$. The values from the model are lower than those obtained by Pegram et al (1999) for the standard steps.

From Figure 5.12 can be seen that if the values of the data are extrapolated, it is expected the values will not converge at some point. This indicates no flattening of the roughness value f . Chanson et al (2000) indicated that a value of 0,2 can be used as a practical value for f for prototypes. However, the comparison with data from Tozzi (19994) and Pegram et al (1999) give enough indication that a value for f of 0,2 is reasonable to use, as explained in Section 3.2.

The roughness values for the protrusions are higher than the compared standard steps. The trends are also similar.

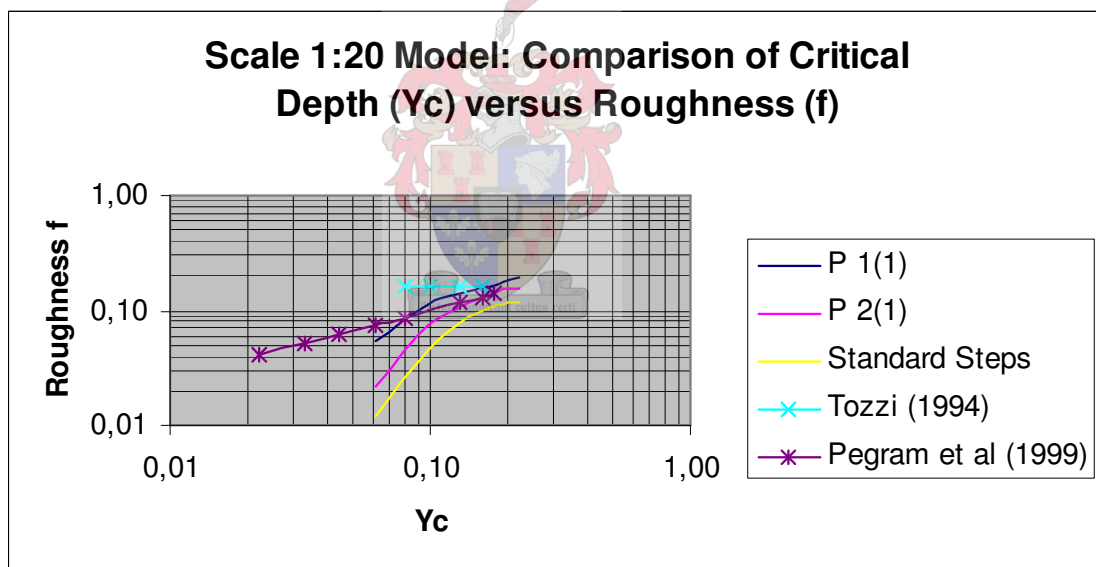


Figure 5.12: Model data for Model 1 (Scale 1:20) compared with Tozzi (1994) and Pegram et al (1999)

From Figures 5.10 and 5.11 the unit flow rate was reworked into a flow depth (Y_c) and step roughness (k). This was then compared with the reworked data as shown in Figure 3.3. Due to a large scatter in data, the correlation between the data is not too good.

Figures 5.13 and 5.14 show the relationship between the friction factor and Y_c/k for the different protrusion configurations for Protrusion 1 and Protrusion 2 compared to Tozzi (1994), Boes & Minor (2002) and Chamani et al (1999).

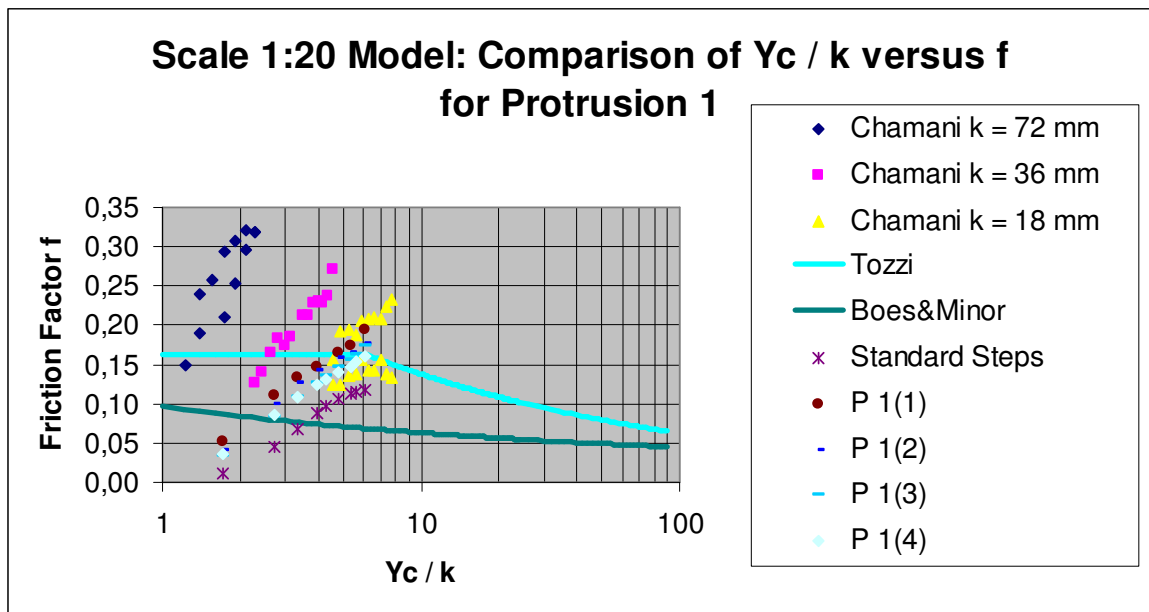


Figure 5.13: Comparison of observed roughness data for Model 1 Protrusion 1 (Scale 1:20) with Tozzi (1994), Chamani et al (2000) and Boes & Minor (2002)

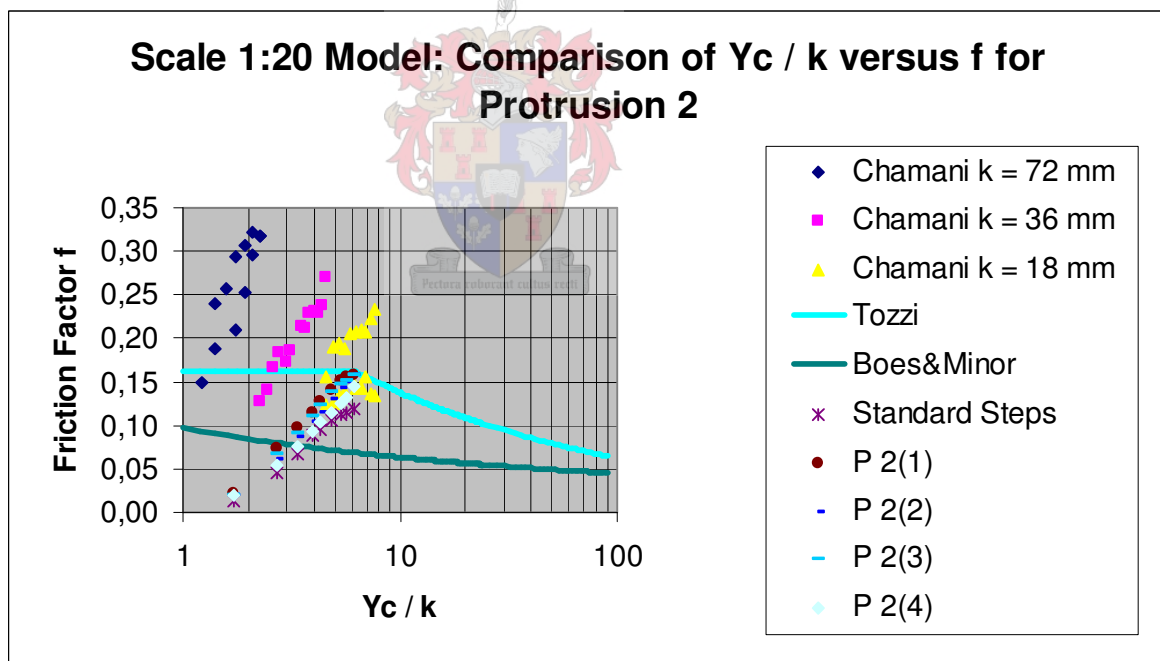


Figure 5.14: Comparison of observed roughness data for Model 1 Protrusion 2 (Scale 1:20) with Tozzi (1994), Chamani et al (2000) and Boes & Minor (2002)

Linear regression of all the data for the 1:20 Model was done. The data was combined (shown in Figure 5.15) and the following equation for the roughness is obtained:

- Standard steps: $f = 0,0066 (Y_c / k)^{1,7341}$ (5.16)
with: $R^2 = 0,92$

- Protrusions: $f = 0,01751 (Y_c / k)^{1,3142}$ (5.17)
with: $R^2 = 0,83$

Using the protrusion density as described in Section 4.9, the following equation for roughness is obtained after linear regression of the data:

$$f = 0,0157 (Y_c / k)^{1,3153} (PD)^{1,2179} \text{ (5.18)}$$

with: $R^2 = 0,83$

where: PD = Protrusion Density (see Section 4.9)

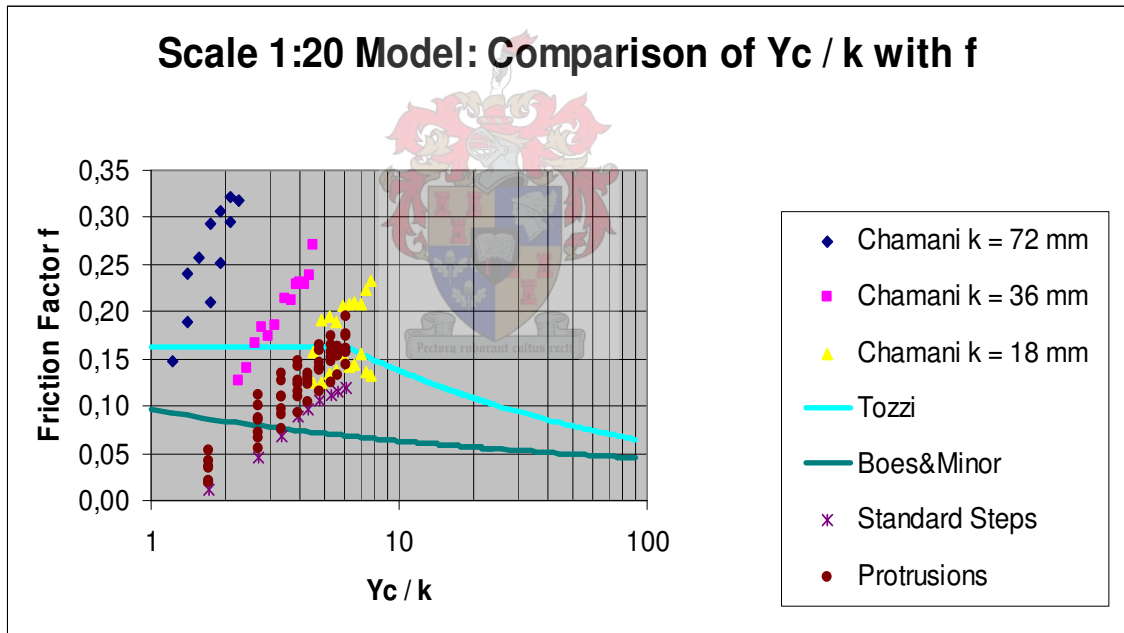


Figure 5.15: Comparison of combined observed roughness data for protrusions with Tozzi (1994), Chamani et al (1999) and Boes & Minor (2002) for 1:20 Scale Model

A large scatter of data can be seen on the above graphs. It is thus understandable that the correlation coefficient is not as high as ideally wanted.

5.2.3 Point of Inception (PI)

Figure 5.16 and Table 5.4 show the inception length L_i measured from the top of the crest (refer to Figures 2.4 and 2.9). As anticipated, L_i for the standard steps are considerably longer than for any of the protrusions. Note that for Figure 5.16 P 1(1) and P 1(2) are exactly the same. It is also evident that where the protrusions are spaced on every row for the first third of the height of the dam, L_i values are smaller. If early air entrainment is the objective of the spillway designer, then this is the optimum spacing.

Table 5.4: Inception Length (L_i) for Protrusion 1 for Scale 1:20 Model

Unit Flow Rate ($\text{m}^3/\text{s.m}$)	P 1(1)	P 1(2)	P 1(3)	P 1(4)	Standard Steps
	Inception Length (L_i)				
	(m)	(m)	(m)	(m)	(m)
0,04	0,375	0,375	0,628	0,308	0,693
0,09	0,596	0,596	0,859	0,452	1,110
0,12	0,748	0,748	1,016	0,574	1,388
0,16	0,888	0,888	1,157	0,707	1,638
0,18	0,943	0,943	1,244	0,803	1,788
0,21	1,098	1,098	1,360	0,956	1,990
0,24	1,208	1,208	1,462	1,122	2,163
0,27	1,255	1,255	1,522	1,238	2,263
0,30	1,366	1,366	1,599	1,423	2,388

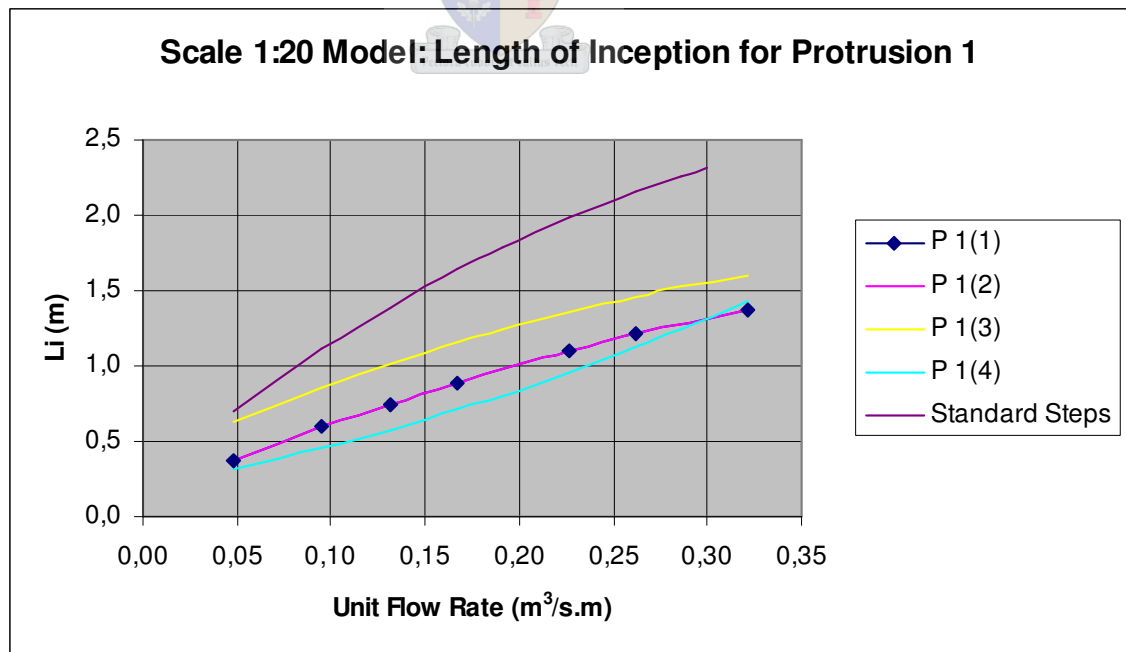


Figure 5.16: Length of inception for Scale 1:20 Model for Protrusion 1

From Figure 5.17 and Table 5.5 can also be seen that the addition of protrusions shortens the length of inception. It is also evident that where the protrusions are spaced on every row for the first third of the height of the dam, L_i are smaller. If early air entrainment is the objective of the spillway designer, then this spacing is the optimum. Configuration P 2(3), where the protrusions are added on every step for the last third of the dam height (refer to Figure 4.12), behaves the same as standard steps with no protrusions added.

Table 5.5: Inception Length (L_i) for Protrusion 2 for Scale 1:20 Model

Unit Flow Rate ($\text{m}^3/\text{s.m}$)	Configuration				
	P 2(1)	P 2(2)	P 2(3)	P 2(4)	Standard Steps
	Inception Length (L_i) (m)				
0,04	0,357	0,378	0,696	0,284	0,693
0,09	0,589	0,664	1,066	0,456	1,110
0,12	0,699	0,862	1,328	0,620	1,388
0,16	0,814	1,045	1,576	0,780	1,638
0,18	0,893	1,159	1,734	0,884	1,788
0,21	1,016	1,318	1,960	1,038	1,990
0,24	1,142	1,463	2,171	1,189	2,163
0,27	1,229	1,552	2,183	1,287	2,263
0,30	1,364	1,672	2,315	1,431	2,388

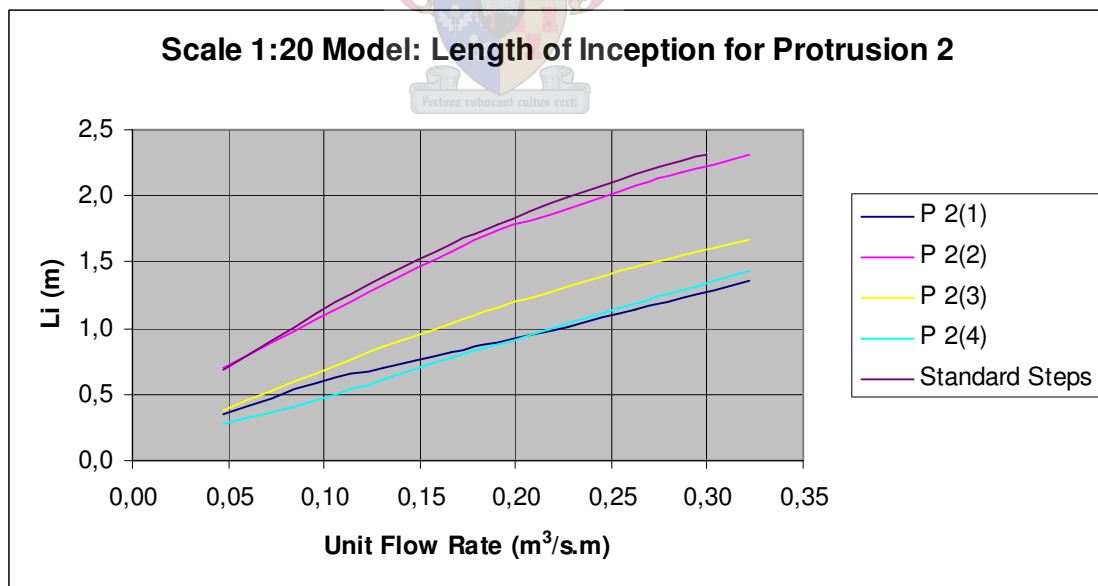


Figure 5.17: Length of inception for Scale 1:20 Model for Protrusion 2

If the equations of Matos et al (2000) (Equation 2.15), Matos (1999), Chanson (1994) and Boes & Minor (2002) (Equation 2.21) are used to determine a length of inception (L_i) and compared to the results obtained from the model, some observations can be made. From Figures 5.18 and 5.19 can be seen that L_i for the protrusion are lower than the L_i calculated from all the authors' equations. $P_1(1)$ and $P_1(2)$ are in this case exactly the same. L_i obtained from the model data for the standard steps and $P_2(2)$ are however higher than L_i calculated from the Boes & Minor (2002), Matos (1999) and Matos et al (2000) equations, but lower than the Chanson (1994) Equation.

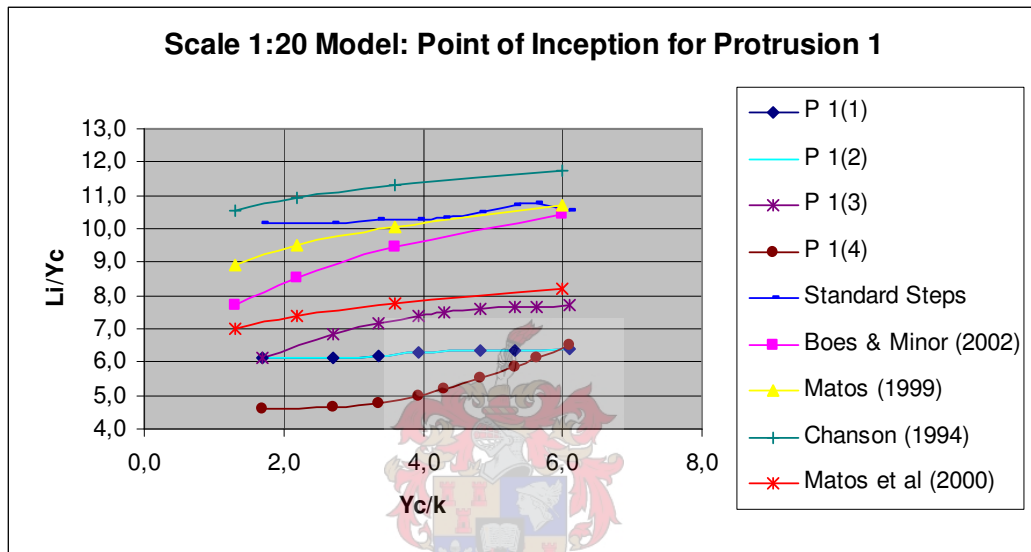


Figure 5.18: Comparison of model data for Protrusion 1 (Scale 1:20) with Boes & Minor (2002), Chanson (1994), Matos et al (2000) and Matos (1999) for L_i

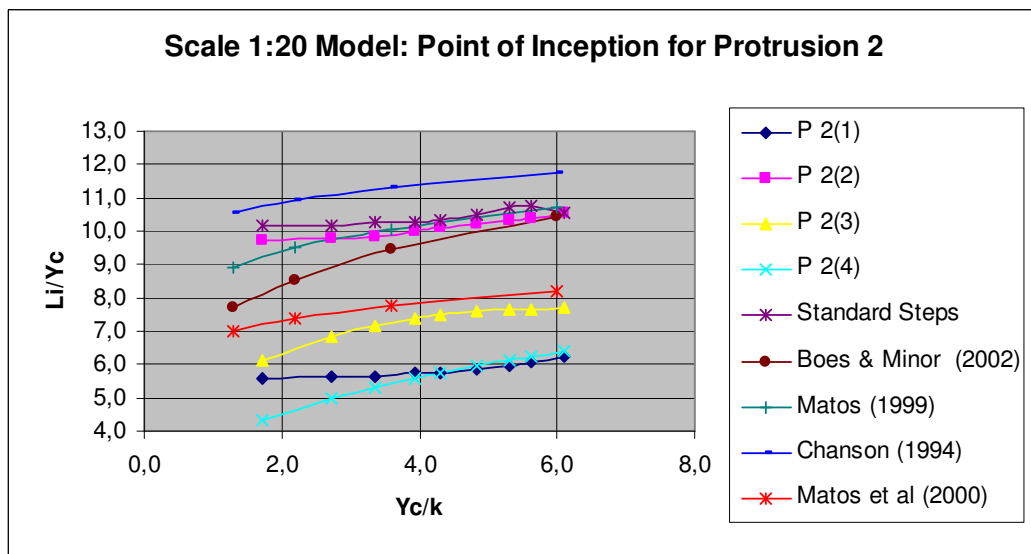


Figure 5.19: Comparison of model data for Protrusion 2 and (Scale 1:20) with Boes & Minor (2002), Chanson (1994), Matos et al (2000) and Matos (1999) for L_i

From Figures 5.18 and 5.19 it is difficult to determine a formula which is accurate for all protrusion configurations. The following equations are proposed for the two (and in some cases three) lowest lengths of inception per protrusion, as obtained from the physical modeling.

For Protrusion 1 the following equations for the length of inception are obtained:

- P 1(1) and P 1(2):

$$L_i / Y_c = 5,9315 (Y_c / k)^{0,0403} \quad \dots\dots\dots (5.19)$$

with: $R^2 = 0,90$

- P 1(4):

$$L_i / Y_c = 3,6523 (Y_c / k)^{0,2730} \quad \dots\dots\dots (5.20)$$

with: $R^2 = 0,80$

For Protrusion 2 the following equations for the length of inception are obtained:

- P 2(1):

$$L_i / Y_c = 5,2568 (Y_c / k)^{0,0757} \quad \dots\dots\dots (5.21)$$

with: $R^2 = 0,74$

- P 2(4):

$$L_i / Y_c = 3,7068 (Y_c / k)^{0,3004} \quad \dots\dots\dots (5.22)$$

with: $R^2 = 0,99$

Combining all the above equations results in the following formula, as shown in Figure 5.20:

$$L_i / Y_c = 5,1958 (Y_c / k)^{0,1151} \quad \dots\dots\dots (5.23)$$

with: $R^2 = 0,99$

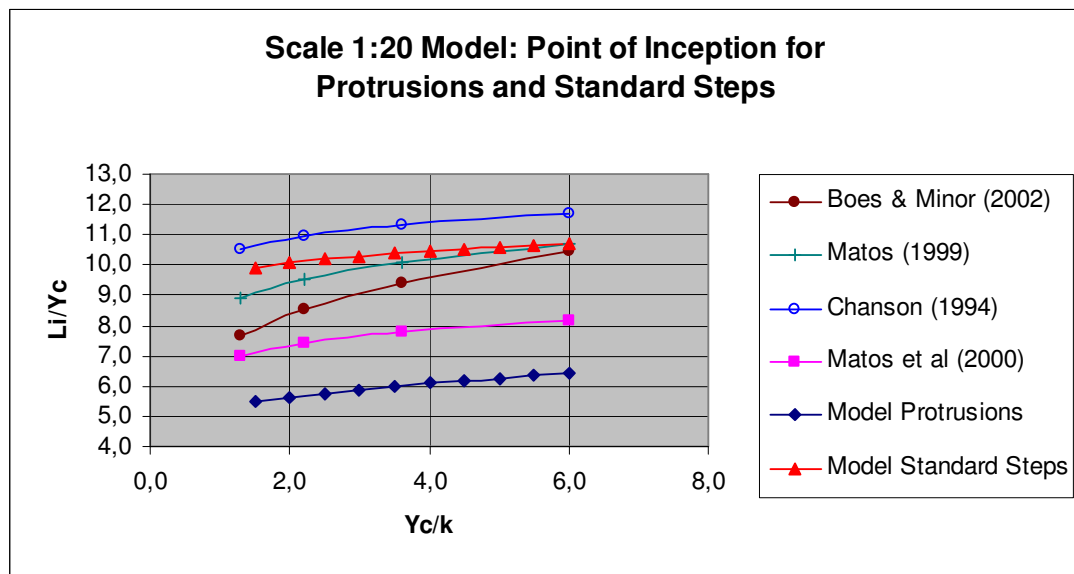


Figure 5.20: Combined Point of Inception for Model 1 (Scale 1:20) compared with Boes & Minor (2002), Chanson (1994), Matos et al (2000) and Matos (1999) for L_i

5.3 The Second Model (Scale 1:30)

5.3.1 Water Levels

Figures 5.21 and 5.22 show the data for the 1:30 scale model. From this first graphs can be seen that the data for the various layouts does not deviate considerably. At this early stage there is however not a material difference between the standard stepped spillway and the stepped spillway with protrusions. A further breakdown of the data will show the difference between the standard steps and protrusions.

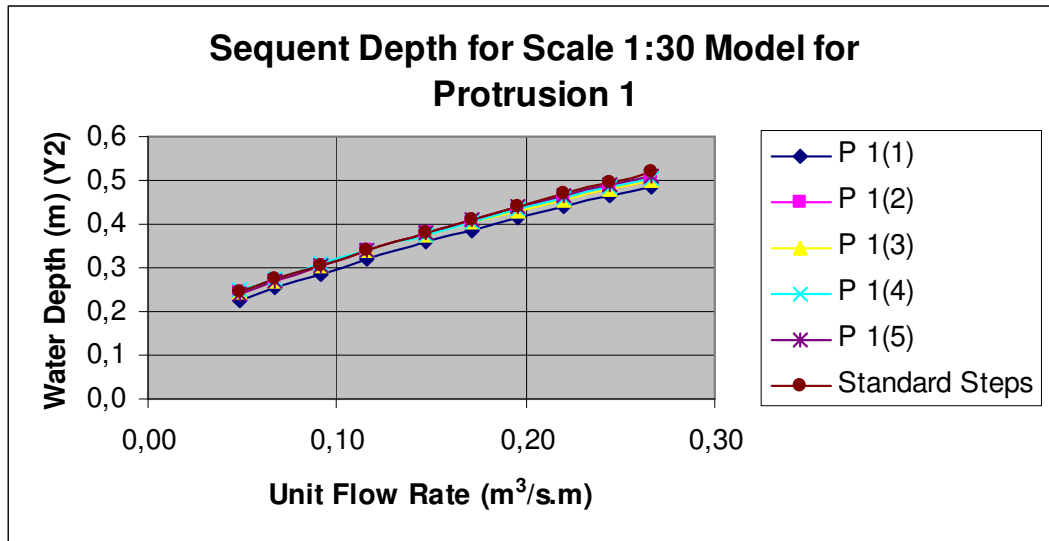


Figure 5.21: Sequent depth measurements for Model 2 Protrusion 1 (Scale 1:30)

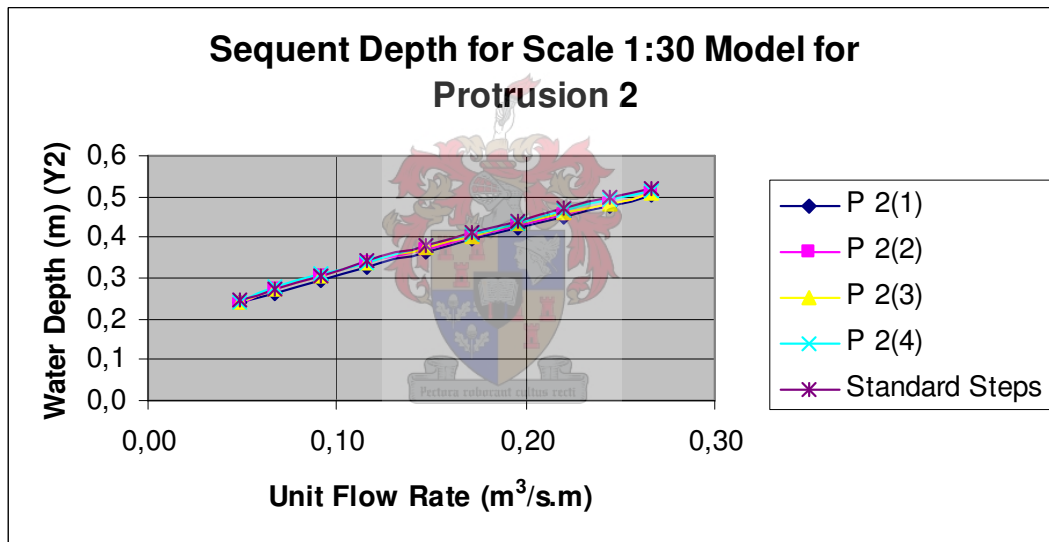


Figure 5.22: Sequent depth measurements for Model 2 Protrusion 2 (Scale 1:30)

5.3.2 Roughness

Figure 5.23 shows the roughness as determined for Protrusion 1. From this graph can be seen that there is a definite increase in roughness for steps with protrusions over the standard steps. It is clear that the more protrusions are added, the higher the roughness value.

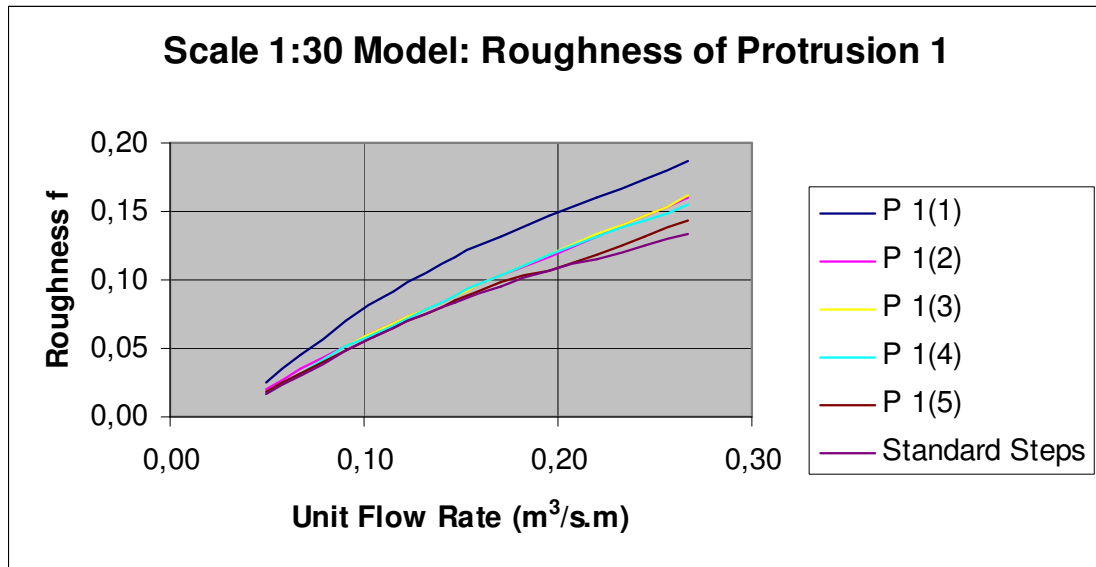


Figure 5.23: Roughness of Model 2 Protrusion 1 (Scale 1:30) obtained from modeling

Figure 5.24 shows the roughness as determined for Protrusion 2. From this graph can be seen that there is a definite increase in roughness for steps with protrusions over the standard steps. It is also clear that the more protrusions are added, the higher the roughness value. The roughness values for this protrusion shape are however lower than for Protrusion 1.

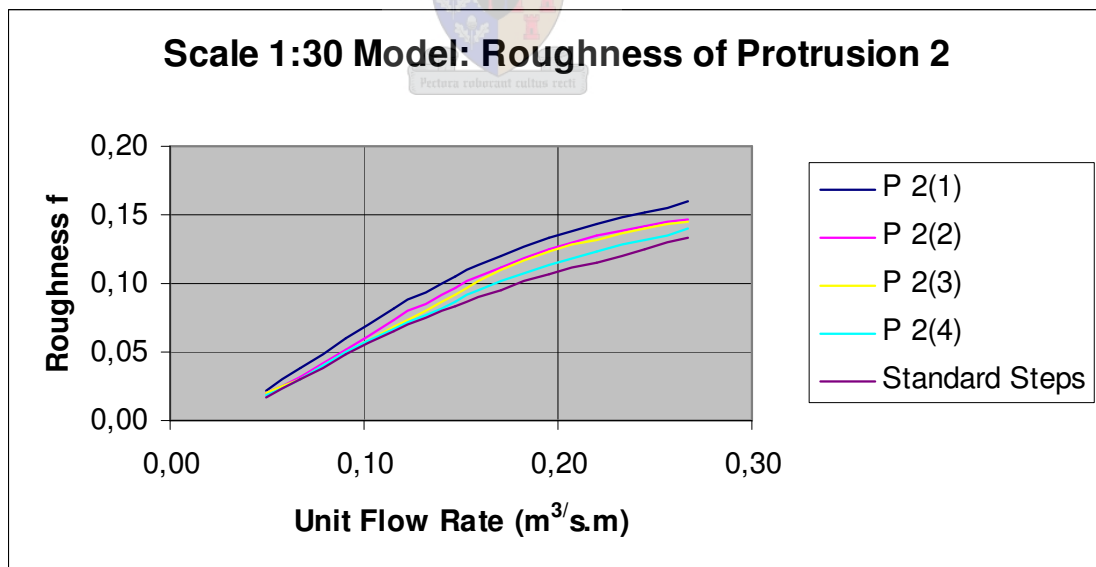


Figure 5.24: Roughness of Model 2 Protrusion 2 (Scale 1:30) obtained from modeling

Figure 5.25 compares the model data with the reworked data from Tozzi (1994) and Pegram et al (1999). Note that only the values of $P 1(1)$, $P 2(1)$ and the standard steps are shown. It can be seen that two intervals exist, where Y_c is smaller than 0,12 and where $0,12 < Y_c < 0,2$. The values from the model are lower than those obtained by Pegram et al (1999) for the standard steps.

From Figure 5.25 can be seen that if the values of the data are extrapolated, it is expected the values will not converge at some point. This indicates no flattening of the roughness value f . Chanson et al (2000) indicated that a value of 0,2 can be used as a practical value for f for prototypes. However, the comparison with data from Tozzi (1994) and Pegram et al (1999) give enough indication that a value for f of 0,2 is reasonable to use, as explained in Section 3.2.

The roughness values for the protrusions are higher than the compared standard steps. The trends are also similar.

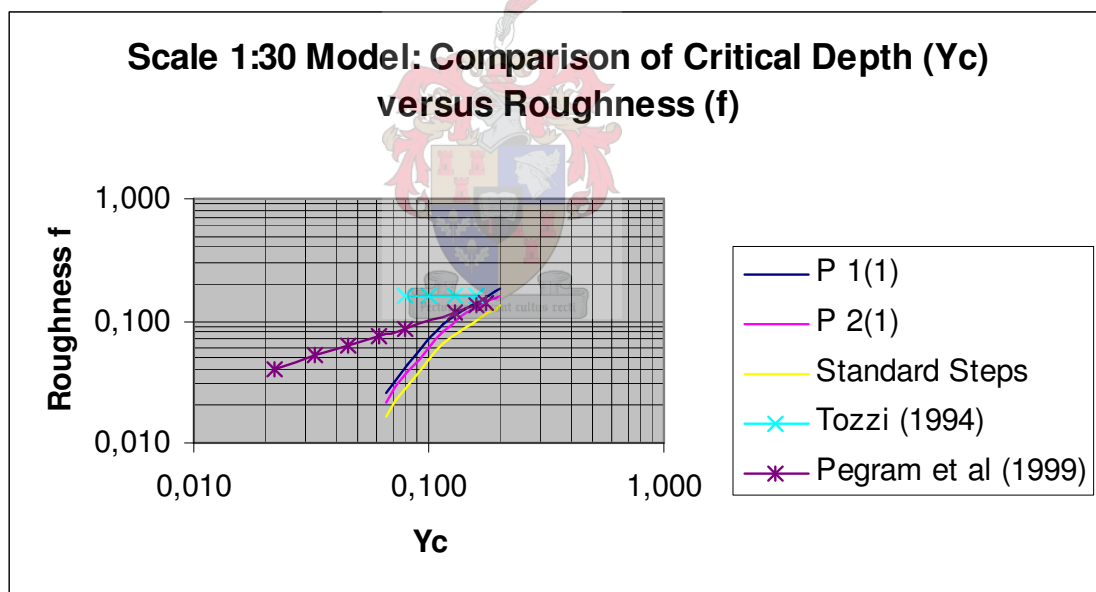


Figure 5.25: Model data for Model 2 (Scale 1:30) compared with Tozzi (1994) and Pegram et al (1999)

From Figures 5.23 and 5.24 the unit flow rate was reworked into a flow depth (Y_c) and step roughness (k). This was then compared with the reworked data as shown in Figure 3.3. Due to a large scatter in data, the correlation between the data is not too good.

Figures 5.26 and 5.27 shows the relationship between friction factor and Y_c / k for the different protrusion configurations for Protrusion 1 and Protrusion 2 compared to Tozzi (1994), Boes & Minor (2002) and Chamani et al (1999).

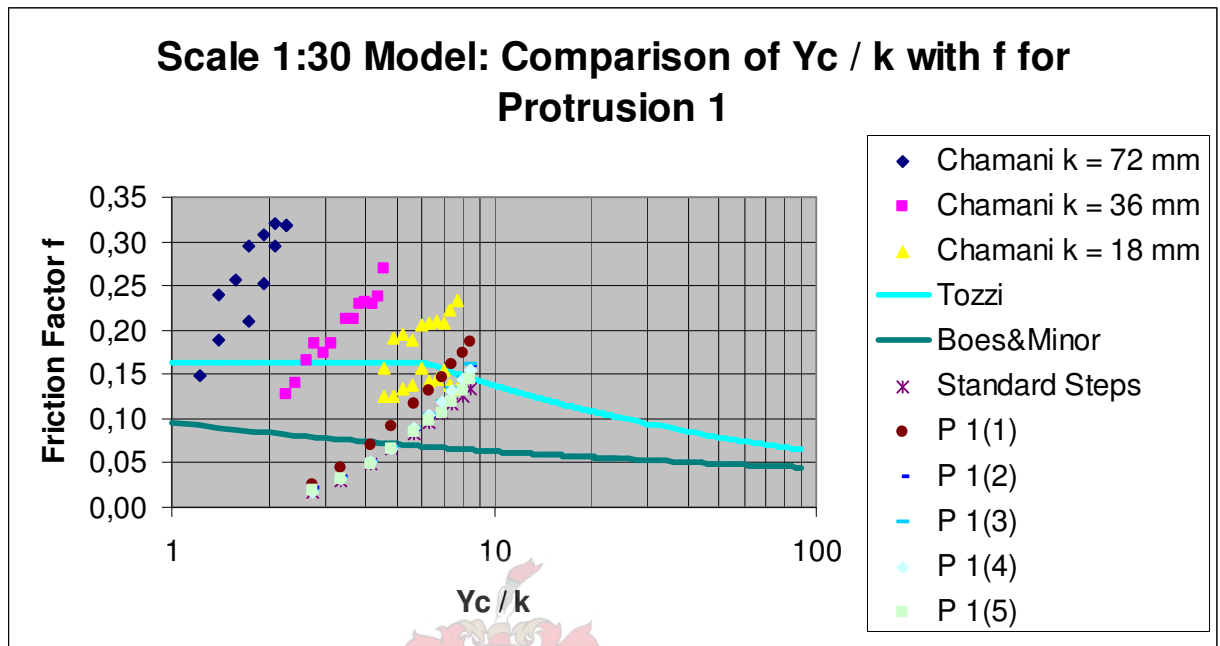


Figure 5.26: Comparison of observed roughness data for Model 2 Protrusion 1 (Scale 1:30) with Tozzi (1994), Chamani et al (2000) and Boes & Minor (2002)

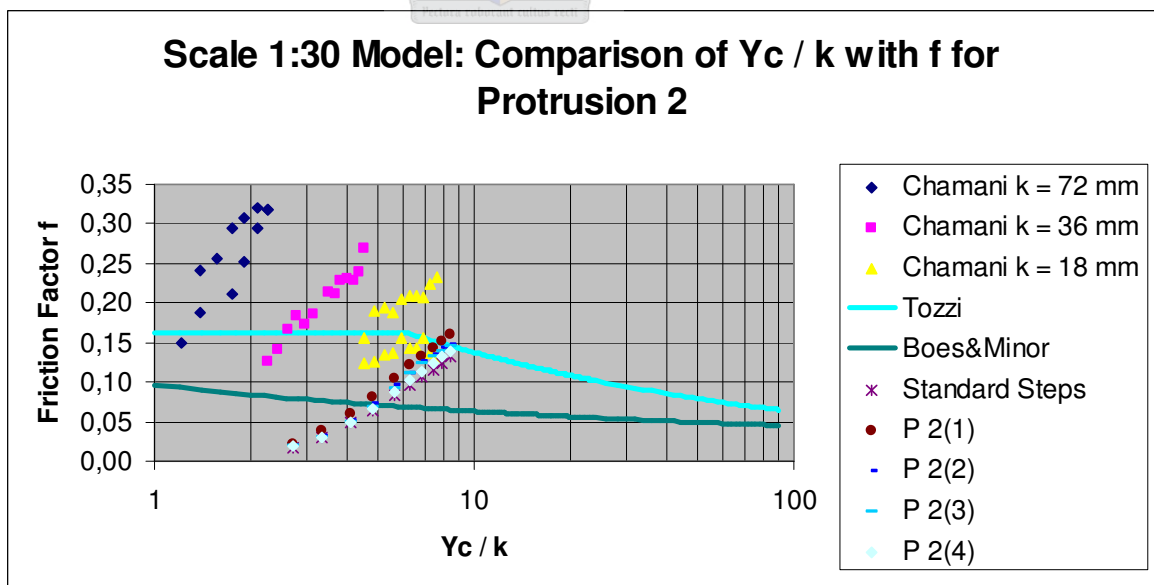


Figure 5.27: Comparison of observed data for Model 2 Protrusion 2 with Tozzi (1994), Chamani et al (1999) and Boes & Minor (2002)

Linear regression of all the data for the 1:30 Model was done. The data was combined (shown in Figure 5.28) and the following equation for the roughness is obtained:

- Standard steps: $f = 0,0033 (Y_c / k)^{1,7919}$ (5.24)
with: $R^2 = 0,97$

- Protrusions: $f = 0,038 (Y_c / k)^{1,7882}$ (5.25)
with: $R^2 = 0,96$

Using the protrusion density as described in Section 4.9, the following equation for roughness is obtained after linear regression of the data:

$$f = 0,00275 (Y_c / k)^{1,7881} (PD)^{3,837} \text{ (5.26)}$$

with: $R^2 = 0,97$

where: PD = Protrusion Density (see Section 4.9)

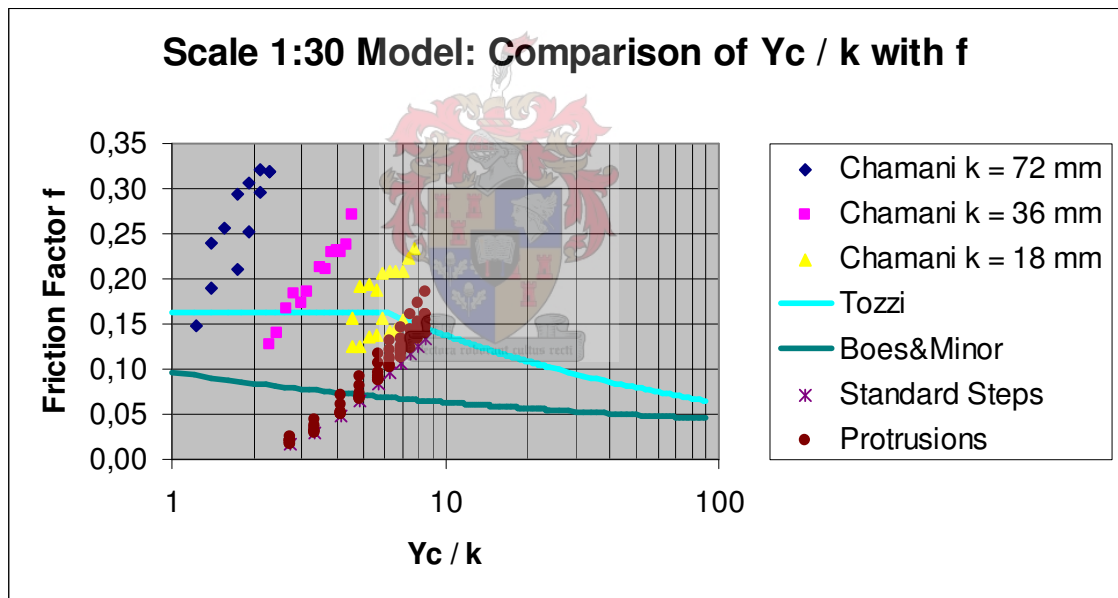


Figure 5.28: Comparison of combined observed roughness data for protrusions with Tozzi (1994), Chamani et al (1999) and Boes & Minor (2002) for Scale 1:30 Model

A large scatter of data can be seen on the above graphs. It is thus understandable that the correlation coefficient is not as high as ideally wanted.

5.3.3 Point of Inception (PI)

Figure 5.29 and Table 5.6 show the inception length L_i measured from the top of the crest (refer to Figures 2.4 and 2.9). As anticipated, L_i for the standard steps are considerably longer than for any of the protrusions. As for the 1:20 model, protrusions spaced on every row for the first third of the height of the dam, L_i is the smallest.

Table 5.6: Inception Length (L_i) for Protrusion 1 for Scale 1:30 Model

Unit Flow Rate ($\text{m}^3/\text{s.m}$)	Configuration					Standard Steps Inception Length (L_i) (m)
	P 1(1) Inception Length (L_i) (m)	P 1(2) Inception Length (L_i) (m)	P 1(3) Inception Length (L_i) (m)	P 1(4) Inception Length (L_i) (m)	P 1(5) Inception Length (L_i) (m)	
0,05	0,290	0,336	0,363	0,308	0,380	0,671
0,07	0,396	0,439	0,474	0,397	0,447	0,853
0,09	0,539	0,580	0,625	0,518	0,539	1,079
0,12	0,679	0,722	0,774	0,640	0,679	1,276
0,15	0,852	0,903	0,959	0,796	0,852	1,487
0,17	0,985	1,046	1,102	0,919	0,985	1,619
0,20	1,114	1,188	1,242	1,042	1,114	1,724
0,22	1,239	1,331	1,380	1,165	1,238	1,800
0,24	1,362	1,474	1,515	1,289	1,399	1,848
0,27	1,470	1,604	1,635	1,402	1,554	1,866

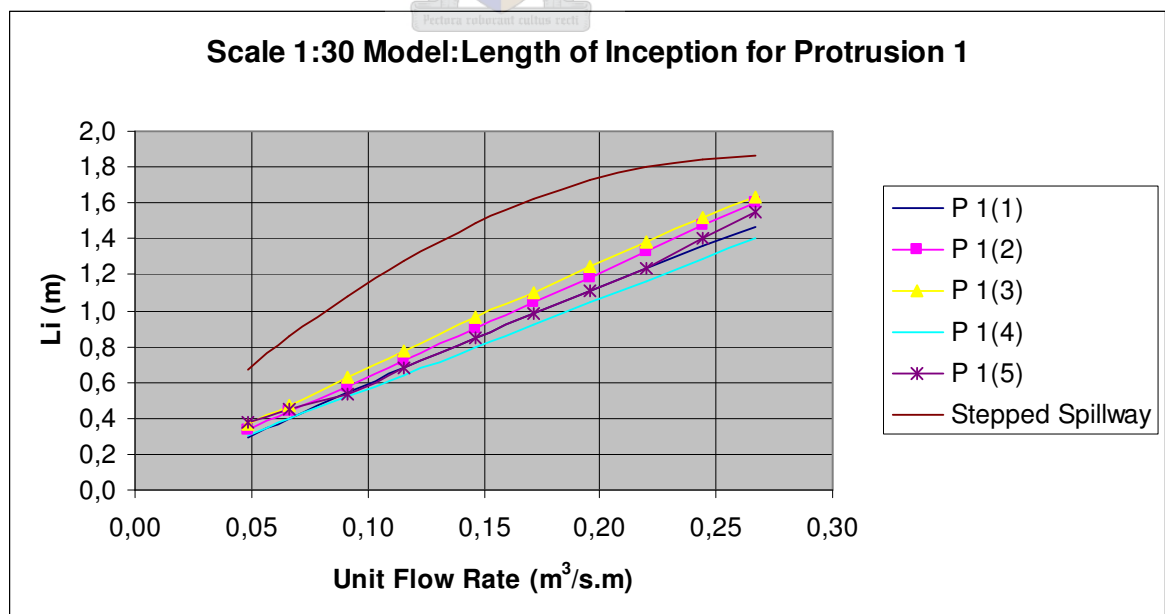


Figure 5.29: Length of inception for Scale 1:30 Model for Protrusion 1

From Figure 5.30 and Table 5.7 it can also be seen that the addition of protrusions shortens the length of inception. It is also evident that where the protrusions are spaced on every row for the first third of the height of the dam, L_i is smaller. It can be noted that Protrusion 2 leads to shorter inception lengths than Protrusion 1. If early air entrainment is the objective of the spillway designer, then this is the optimum spacing.

Table 5.7: Inception Length (L_i) for Protrusion 2 for Scale 1:30 Model

Unit Flow Rate ($m^3/s.m$)	Configuration				
	P 2(1) Inception Length (L_i) (m)	P 2(2) Inception Length (L_i) (m)	P 2(3) Inception Length (L_i) (m)	P 2(4) Inception Length (L_i) (m)	Standard Steps Inception Length (L_i) (m)
0,05	0,333	0,309	0,375	0,333	0,671
0,07	0,496	0,389	0,466	0,496	0,853
0,09	0,570	0,502	0,588	0,570	1,079
0,12	0,653	0,618	0,707	0,653	1,276
0,15	0,772	0,772	0,855	0,772	1,487
0,17	0,877	0,896	0,967	0,983	1,619
0,20	0,991	1,025	1,076	1,072	1,724
0,22	1,114	1,157	1,182	1,155	1,800
0,24	1,247	1,292	1,284	1,233	1,848
0,27	1,376	1,418	1,375	1,298	1,866

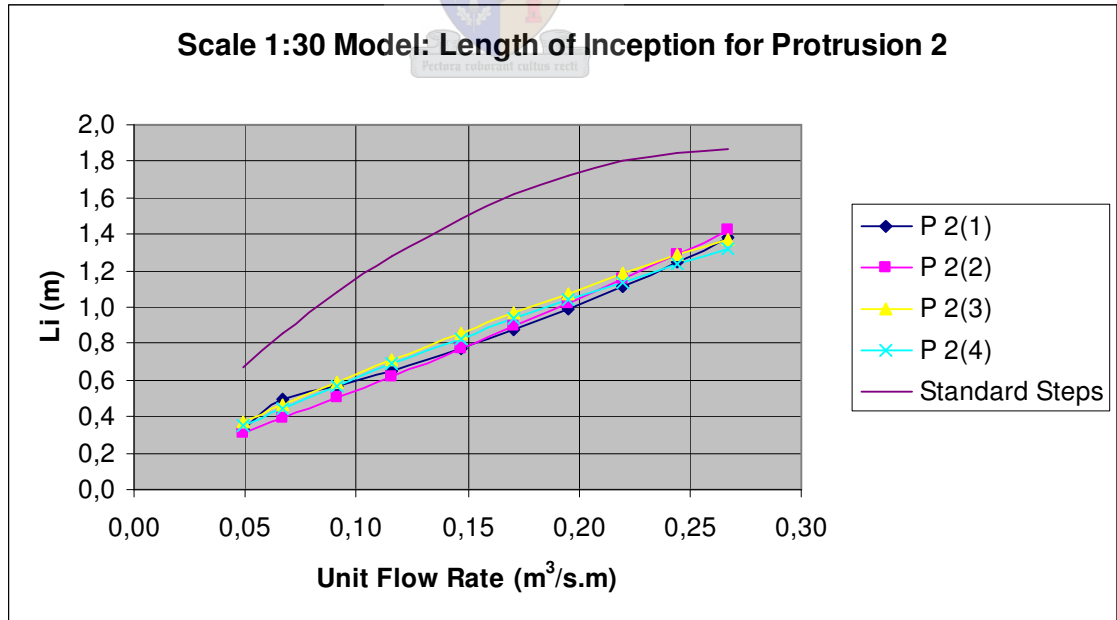


Figure 5.30: Length of inception for Scale 1:30 Model for Protrusion 2

If the equations of Matos et al (2000) (Equation 2.15), Matos (1999), Chanson (1994) (Equation 2.19) and Boes & Minor (2002) (Equation 2.21) are used to determine a length of inception (L_i) and compared to the results obtained from the model, some observations can be made. From Figures 5.31 and 5.32 can be seen that L_i for the protrusions are lower than the L_i calculated from all the authors' equations. L_i obtained from the model data for the standard steps are however higher than L_i calculated from the Boes & Minor (2002), Matos (1999) and Matos et al (2000) equation, but lower than the Chanson (1994) Equation.

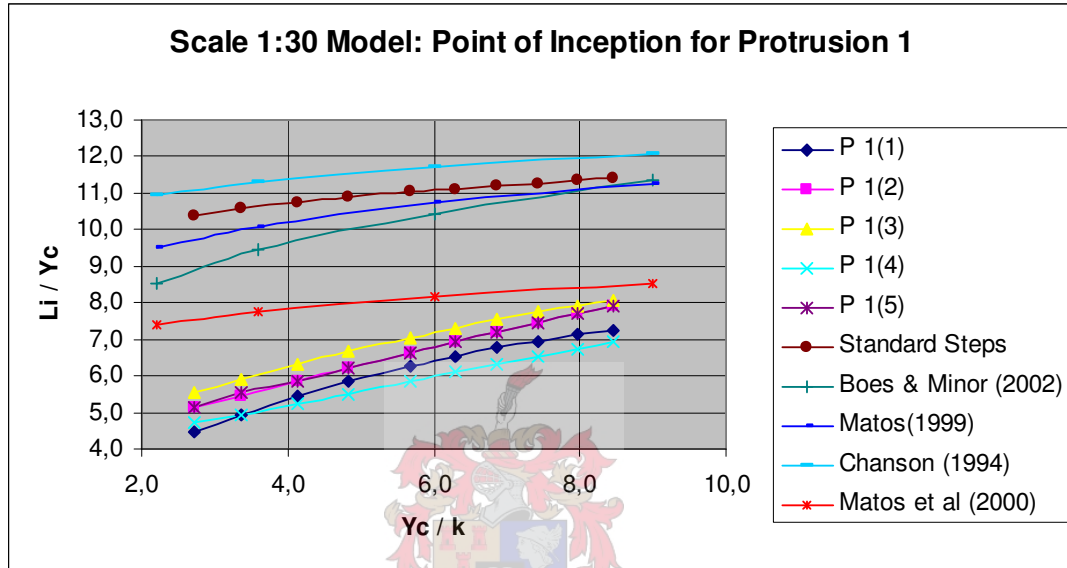


Figure 5.31: Comparison of model data for Protrusion 1 (Scale 1:30) with Boes & Minor (2002), Chanson (1994), Matos et al (2000) and Matos (1999) for L_i

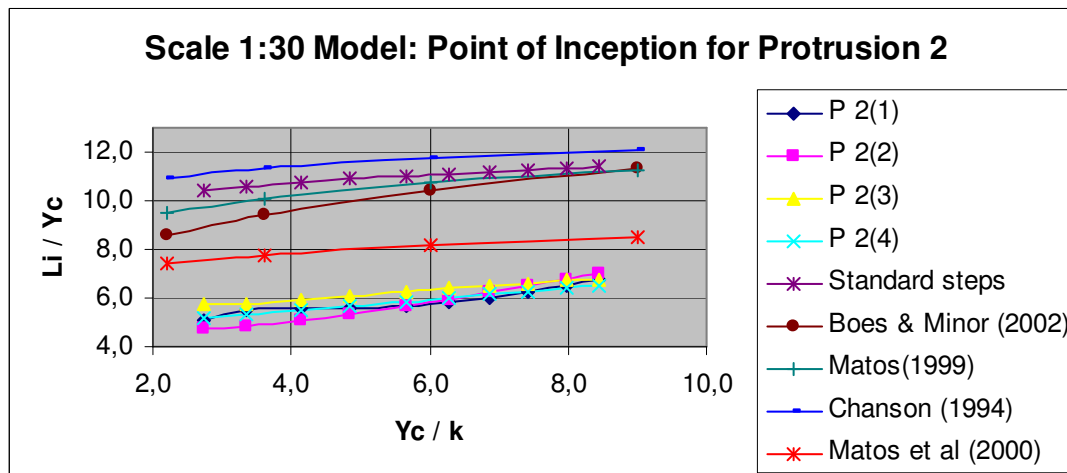


Figure 5.32: Comparison of model data for Protrusion 2 (Scale 1:30) with Boes & Minor (2002), Chanson (1994), Matos et al (2000) and Matos (1999) for L_i

From Figures 5.31 and 5.32 it is difficult to determine a formula which is accurate for all protrusion configurations. The following equations are proposed for the two (and in some cases three) best configurations per protrusion, as obtained from the physical modeling.

For Protrusion 1 the following equations for the length of inception are obtained:

• P 1(1):

$$L_i / Y_c = 2,9213 (Y_c / k)^{0,4328} \dots\dots\dots (5.27)$$
 with: $R^2 = 0,99$

• P 1(4):

$$L_i / Y_c = 3,2475 (Y_c / k)^{0,3463} \dots\dots\dots (5.28)$$
 with: $R^2 = 0,98$

For Protrusion 2 the following equations for the length of inception are obtained:

• P 2(1):

$$L_i / Y_c = 4,1261 (Y_c / k)^{0,2078} \dots\dots\dots (5.29)$$
 with: $R^2 = 0,86$

• P 2(4):

$$L_i / Y_c = 4,1653 (Y_c / k)^{0,2023} \dots\dots\dots (5.30)$$
 with: $R^2 = 0,98$

Combining all the above equations results in the following formula, as shown in Figure 5.33:

$$L_i / Y_c = 3,5734 (Y_c / k)^{0,2975} \dots\dots\dots (5.31)$$

with: $R^2 = 0,89$

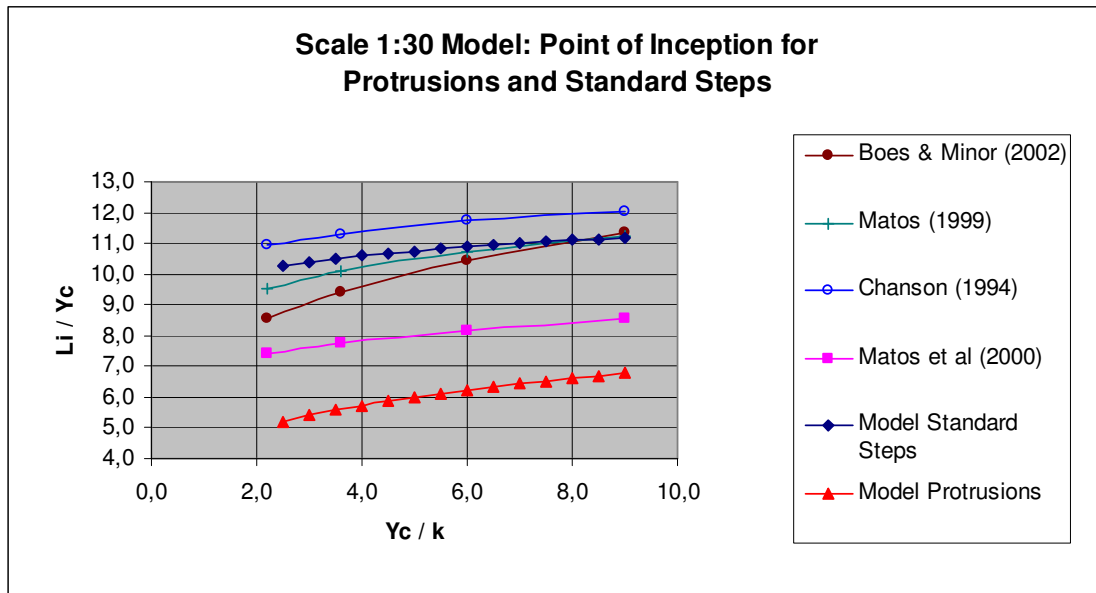


Figure 5.33: Combined Point of Inception for Model 2 (Scale 1:30) compared with Boes & Minor (2002), Chanson (1994), Matos (1999) and Matos et al (2000) for L_i

5.4 Combined Roughness of both Models

Combining data of both models the following equation can be obtained (See Figure 5.34):

- Standard steps:

$$f = 0,0073 (Y_c / k)^{1,4678} \dots\dots\dots (5.32)$$

with: $R^2 = 0,80$

- Protrusions:

$$f = 0,00144 (Y_c / k)^{1,1744} \dots\dots\dots (5.33)$$

with: $R^2 = 0,57$

The correlation is not good due to the large scatter of data.

Using the protrusion density as described in Section 4.9, the following equation for roughness is obtained after linear regression of the data:

$$f = 0,0111 (Y_c / k)^{1,205} (PD)^{2,536} \dots\dots\dots (5.34)$$

with: $R^2 = 0,60$
 where: PD = Protrusion Density (see Section 4.9)

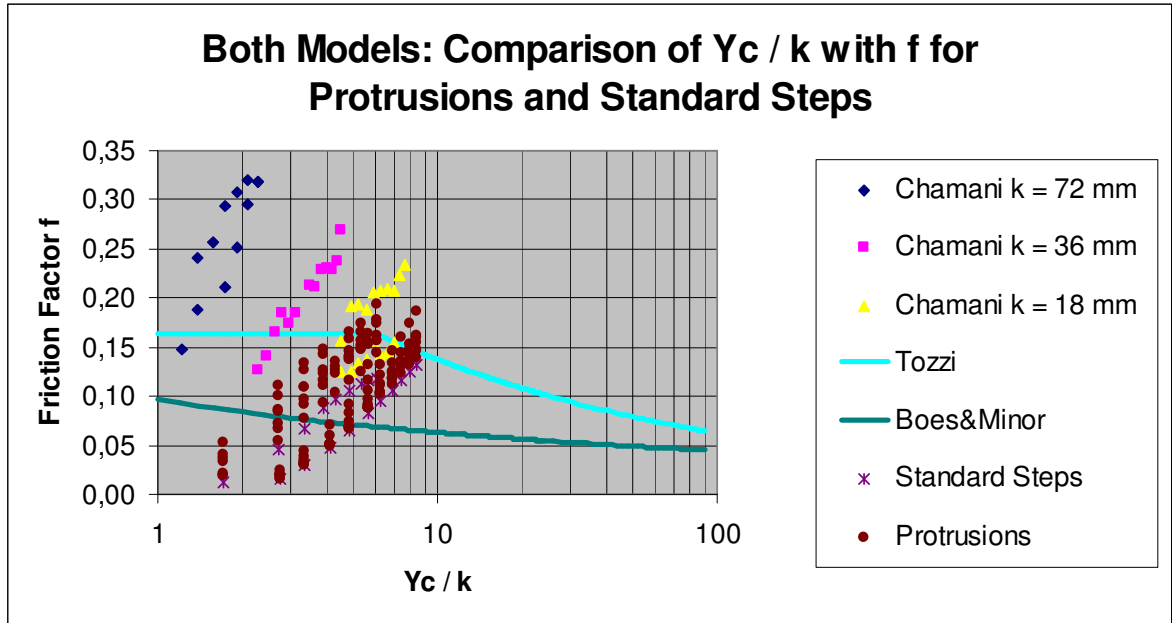
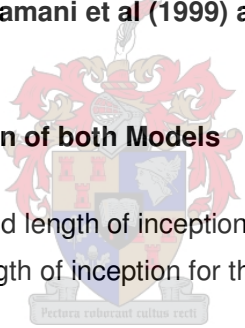


Figure 5.34: Comparison of observed data for protrusions and standard steps with Tozzi (1994), Chamani et al (1999) and Boes & Minor (2002)

5.5 Combined Length of Inception of both Models

Figure 5.35 shows the combined length of inception for the standard steps for the two models together with the combined length of inception for the protrusions for Model 1 and Model 2.



The formula for the length of inception for the standards steps is:

$$L_i / Y_c = 9,6416 (Y_c / k)^{0,0675} \dots\dots\dots (5.35)$$

with: $R^2 = 0,91$

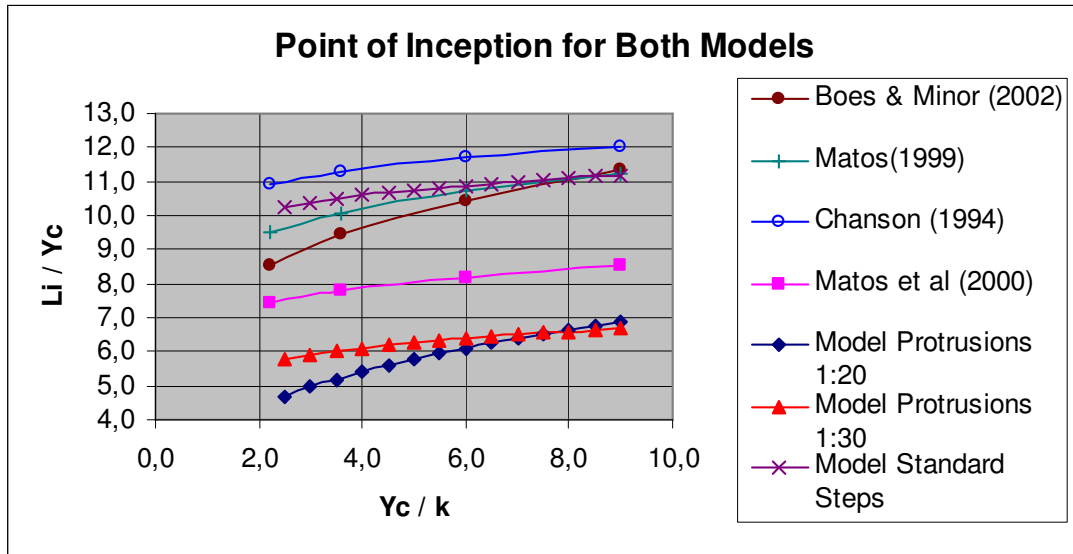


Figure 5.35: Point of Inception for both models compared with Boes & Minor (2002), Matos (1999), Matos et al (2000) and Chanson (1994)

Combining the above equations for the protrusions for Models 1 and 2 results in the following formula for the protrusions:

- $$L_i / Y_c = 4,3089 (Y_c / k)^{0,2063} \dots\dots\dots (5.36)$$

with: $R^2 = 0,98$

The formula is shown in Figure 5.36, together with the length of inception as determined for the standard steps and by Boes & Minor (2002), Chanson (1994), Matos (1999) and Matos et al (2000).

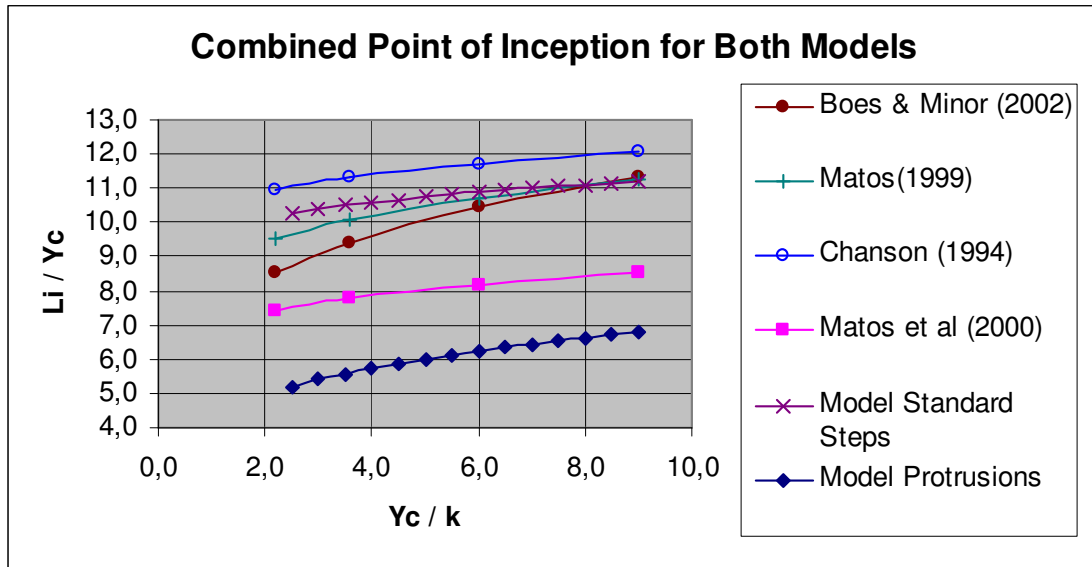


Figure 5.36: Combined Point of Inception for both models compared with Boes & Minor (2002), Matos (1999), Matos et al (2000) and Chanson (1994)

5.6 Scouring at Both Models

Figure 5.7 shows the schematic layout of scour measurements. Table 5.8 shows the comparison of the scour depths for the two 2D models (scales 1:20 and 1:30). Figure 5.37 shows the scour depths for a prototype flow of 25 m³/s.m. These depths were obtained by using the apron configuration as discussed in Section 4 and shown in Appendix B. Appendix D shows scour drawings.

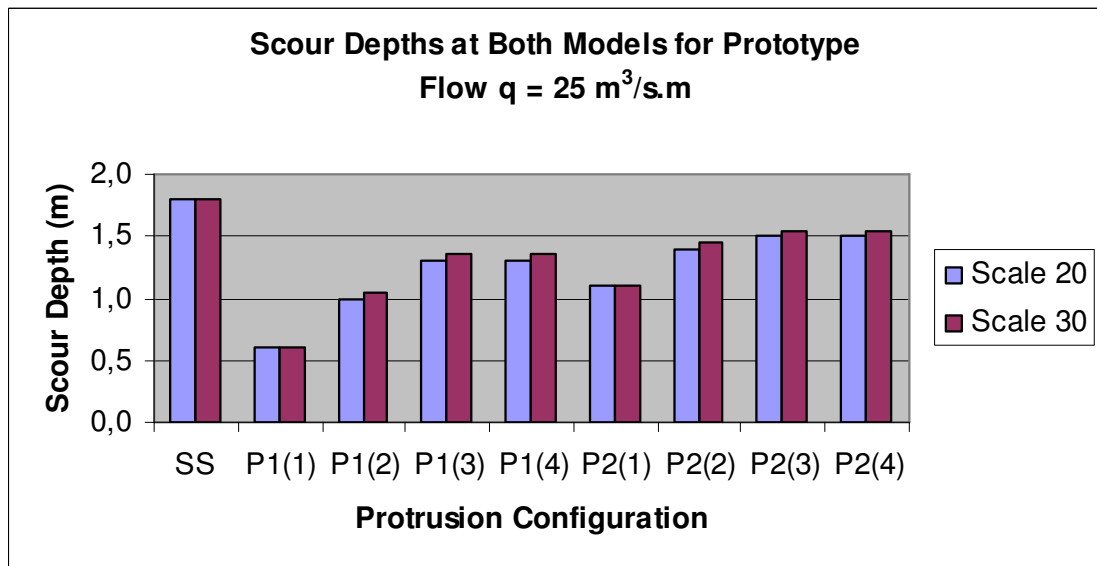


Figure 5.37: Scour depths obtained for triangular protrusions and standard steps for both models at a prototype unit discharge of $q = 25 \text{ m}^3/\text{s.m}$ (RMF)

Table 5.8: Scour Measurements at both models

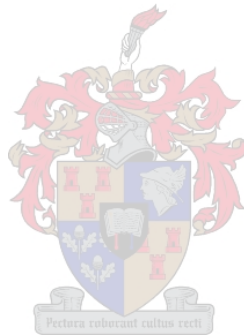
Flood	Prototype Flow (q in m ³ /s.m)	Prototype		
		Protrusion Configuration	Scale 1:20 Scour Depth (m)	Scale 1:30 Scour Depth (m)
RDF	10	Standard Steps	0,00	0,00
RMF	26		1,80	1,80
SEF	40		-	3,50
RDF	10	P 1(1)	0,00	0,00
RMF	26		0,60	0,60
SEF	40		-	4,00*
RDF	10	P 1(2)	0,00	0,00
RMF	26		1,00	1,05
SEF	40		-	Not tested
RDF	10	P 1(3)	0,00	0,00
RMF	26		1,30	1,35
SEF	40		-	Not tested
RDF	10	P 1(4)	0,00	0,00
RMF	26		1,30	1,35
SEF	40		-	Not tested
RDF	10	P 2(1)	0,00	0,00
RMF	26		1,10	1,10
SEF	40		-	4,00 *
RDF	10	P 2(2)	0,00	0,00
RMF	26		1,40	1,45
SEF	40		-	Not tested
RDF	10	P 2(3)	0,00	0,00
RMF	26		1,50	1,55
SEF	40		-	Not tested
RDF	10	P 2(4)	0,00	0,00
RMF	26		1,50	1,55
SEF	40		-	Not tested

* See explanation in Chapter 6

From the above table can be seen that only limited scour measurements were done with the 1:30 scale model. The main reason was the limited time that was available to conduct these tests. More effort was put into the determination of the roughness value and the location of the point of inception. From the table it must be noted that the amount of scour for the SEF with the protrusions added is more than for the standard steps. This will be discussed in Chapter 6.

From the scour depths observed and the roughness values obtained for a specific unit discharge, a correlation between these two quantitative measurements can be obtained. The results will be discussed in Chapter 6.

- 1 INTRODUCTION**
- 2 LITERATURE STUDY**
- 3 REIEW OF LITERATURE**
- 4 EMPERIMENTAL WORK**
- 5 RESULTS**



6 DISCUSSION OF RESULTS

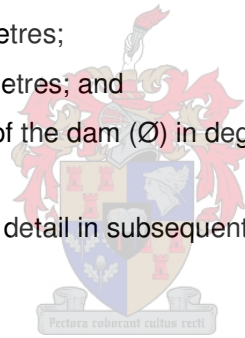
The results from the tests described in Chapter 5 are discussed, with particular attention given to the parameters influencing the effectiveness of the protrusions. The parameters influencing the roughness, the point of inception and the amount of scour downstream of the spillway toe influence the effectiveness of the protrusions. The benefits of the protrusions are reported on relative to the standard steps. Construction aspects, cost, conclusions and recommendations are made in subsequent sections.

6.1 Variables

As mentioned in Section 2, the following parameters have an influence on the energy dissipation of stepped spillways:

- Unit discharge (q) in cubic metres per second per metre ($\text{m}^3/\text{s}\cdot\text{m}$);
- Flow depth (y) in metres;
- Step height (h) in metres;
- Dam height (H) in metres; and
- Downstream slope of the dam (θ) in degrees ($^\circ$).

This will be discussed in more detail in subsequent paragraphs.



6.1.1 The Effect of Unit Discharge on the Effectivity of the Triangular Protrusions

For low discharges nappe flow occurs, while for larger discharges skim flow occurs (see Section 2.1 for definitions). As mentioned, skim flow is of importance for this thesis. Unit discharges of up to $42 \text{ m}^3/\text{s}\cdot\text{m}$ for prototypes were modeled during this study. Skim flow starts at unit discharges of $8 \text{ m}^3/\text{s}\cdot\text{m}$. The higher the discharge becomes, the more the effectivity of the steps becomes less due to the flow that moves down the steps without “touching” the steps (as if there were no steps present, just like the spillway of a normal conventional concrete dam with a smooth downstream face).

As with standard stepped spillways, once the flow increases up to $25 \text{ m}^3/\text{s}\cdot\text{m}$, the effectivity of the steps decreases dramatically. Many authors state that stepped spillways are only effective for unit discharges smaller than $25 \text{ m}^3/\text{s}\cdot\text{m}$ (Boes & Minor, 2002). From the results presented in Section 5, it is concluded that the protrusions are effective for unit discharges up to $35 \text{ m}^3/\text{s}\cdot\text{m}$ for a certain apron configuration. The figures plotting the unit discharge versus the roughness values indicate that the roughness still increases with increasing unit

discharge, although the scour measurements suggest that the effectivity of the protrusions lessen with increasing discharge for a certain apron configuration. The effect of the apron configuration will be discussed in Section 6.2.2.

6.1.2 The Effect of Flow Depth on the Effectivity of the Triangular Protrusions

The flow depth is dependent on the unit discharge ($q = v/Y$ or $q = \sqrt{9,81 \times Y_c^3}$ or $Q = v Y$). The same conclusion from Section 6.1.1 applies.

Researchers generally used the parameter Y/k to predict the roughness value (f). Logarithmic equations are used to plot data over ranges of Y/k . This study used the Y_c/k parameter to determine the value of the roughness (f).

The data of Pegram et al (1999) proposed that the roughness (f) is independent of Y/k . Thus their data are independent of Y_c/k . Tozzi's (1994) data shows that the roughness of the steps are equal to 0,163 for $Y/k < 1,8$. This can be reworked to $Y_c/k < 6,1$. For values of Y_c/k up to 6,1, the roughness of the steps (f) largely depends on the value of k . The value of k is dependent on the downstream slope of the dam (\emptyset) and the step height (h), $k = h \text{ Cos } \emptyset$.

6.1.3 The Effect of Step Height on the Effectivity of the Triangular Protrusions

Some authors reported that after a certain step height is reached, the effectivity of the stepped spillway does not increase. This study only used two different step heights, which were too close to each other. More step heights should have been tested to obtain the "real" influence of the step height on the roughness value. As mentioned in Sectioned 6.1.2, the step height influences the roughness of the steps (k), which in turn influences the roughness value (f).

6.1.4 The Effect of Dam Height on the Effectivity of the Triangular Protrusions

Only one dam height (75 metres) was tested in this thesis. The higher the dam, the more energy needs to be dissipated. From this study the influence of dam height cannot be commented on.

6.1.5 The Effect of the Downstream Slope on the Effectivity of the Triangular Protrusions

From Section 6.1.2 the downstream slope influences the roughness of the steps (k), which in turn influences the roughness value (f). Only one downstream slope was modeled during this research, resulting in insufficient data to comment on the influence of the downstream slope on the roughness value.

6.2 Protrusion Spacing

From the results presented in Chapter 5 it is clear that the protrusion spacing has an influence on the roughness values, the amount of scouring at the downstream toe of the dam and the location of the point of inception. The effect of the protrusion spacing will be discussed in subsequent sections.

6.2.1 The Effect of Protrusion Spacing on the Roughness Value f

From Figures 5.10 and 5.11 it is clear that the more dense the protrusions are spaced, the higher the roughness f of the spillway. It is also evident that the protrusion with width equal to twice the tread of the step (Protrusion 1, refer to Figures 4.2 and 4.3) is more effective than the protrusion 3,46 times the tread of the step. Table 6.1 presents the roughness ratio of the steps with protrusions to the standard steps for various discharges and protrusion spacings. From Tables 6.1, 4.1 and 4.2 it is evident that the denser the protrusions are spaced, the higher the roughness f of the steps. The relative increase in roughness over the standard stepped spillway is between 20% and 30%.

It is concluded that if the roughness value f is the factor governing the effectiveness of the protrusions, protrusions can be used for all unit discharges, spaced at every second row.

Table 6.1: Relative Roughness of the Triangular Protrusions

Unit Flow (q in m ³ /s.m)	Protrusion Configuration	Model	
		Scale 1:20	Scale 1:30
		f_p / f_{ss}	f_p / f_{ss}
0,12	P 1(1)	1,980	1,420
0,21		1,564	1,384
0,27		1,602	1,404
0,12	P 1(2)	1,620	1,059
0,21		1,404	1,120
0,27		1,442	1,205
0,12	P 1(3)	1,620	1,044
0,21		1,404	1,132
0,27		1,413	1,216
0,12	P 1(4)	1,400	1,026
0,21		1,319	1,122
0,27		1,320	1,166
0,12	P 1(5)	-	1,023
0,21		-	1,026
0,27		-	1,027
0,12	P 2(1)	1,440	1,262
0,21		1,326	1,248
0,27		1,337	1,202
0,12	P 2(2)	1,290	1,129
0,21		1,229	1,172
0,27		1,286	1,110
0,12	P 2(3)	1,260	1,042
0,21		1,308	1,129
0,27		1,318	1,096
0,12	P 2(4)	1,130	1,019
0,21		1,096	1,068
0,27		1,148	1,051

Note: f_p = roughness of protrusions

f_{ss} = roughness of standard steps

Figure 6.1 shows the relative roughness of the protrusions for both models.

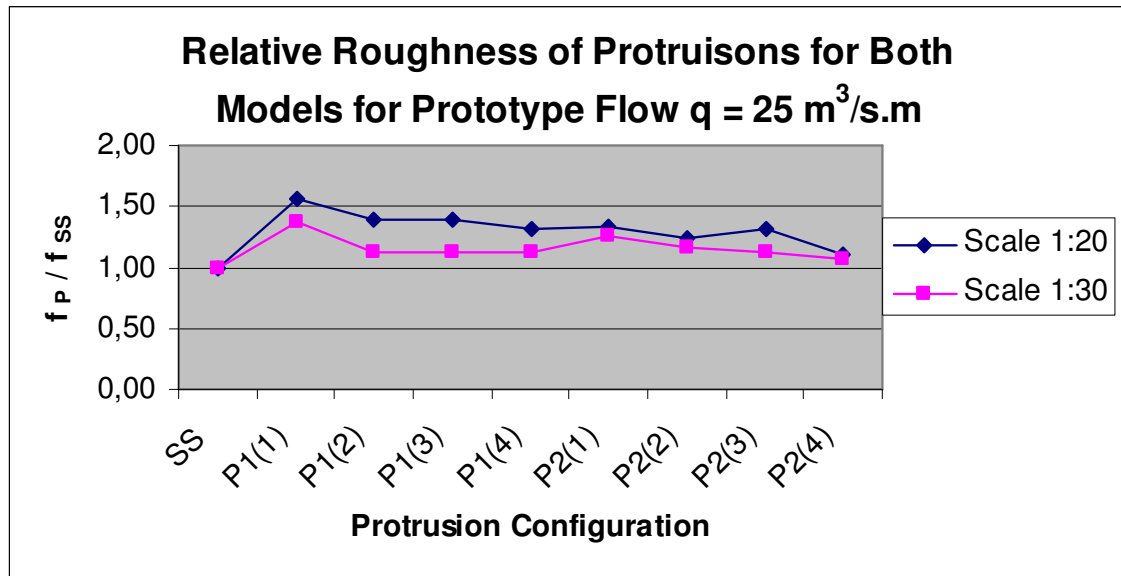


Figure 6.1: Relative roughness of the protrusions for both models

6.2.2 The Effect of Protrusion Spacing on the Scouring

The scour drawings showing the depth of scouring are shown in Appendix D. From the drawings it can be seen that scouring where protrusions are present is in all cases less than scouring for the standard steps, for unit discharges up to $35 \text{ m}^3/\text{s.m}$ and the De Hoop Dam apron configuration. It is also evident that the protrusion with width equal to twice the tread of the step (Protrusion 1, refer to Figures 4.2 and 4.3) is more effective than the protrusion 3,46 times the tread of the step. It can be concluded that the denser the protrusions the less scour will be taking place, up to a unit discharge of $35 \text{ m}^3/\text{s.m}$ for a certain apron configuration.

At discharges higher than $35 \text{ m}^3/\text{s.m}$, as observed from model studies, the scour increased dramatically for the De Hoop Dam apron configuration. At this discharges it seemed that the water was highly aerated, thus the depth of water at the toe of the spillway was 3 times higher than the critical depth (Y_c) at the top of the ogee cap. This resulted in the water “missing” the apron as if there was no apron present. This is schematically shown in Figure 6.3.

It is concluded that if scouring is the factor governing the effectiveness of the protrusions, protrusions can be used for unit discharges up to $35 \text{ m}^3/\text{s.m}$.

Figure 6.2 show the scour depths and relative roughness of the protrusions for both models.

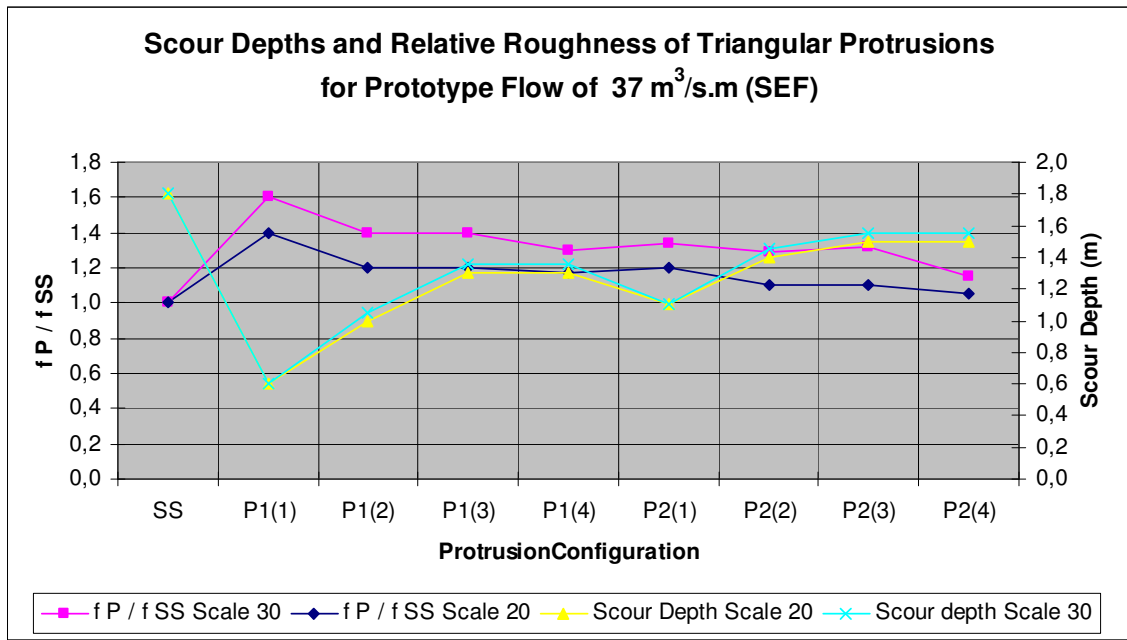


Figure 6.2: Scour depths and relative roughness of triangular protrusions for both models

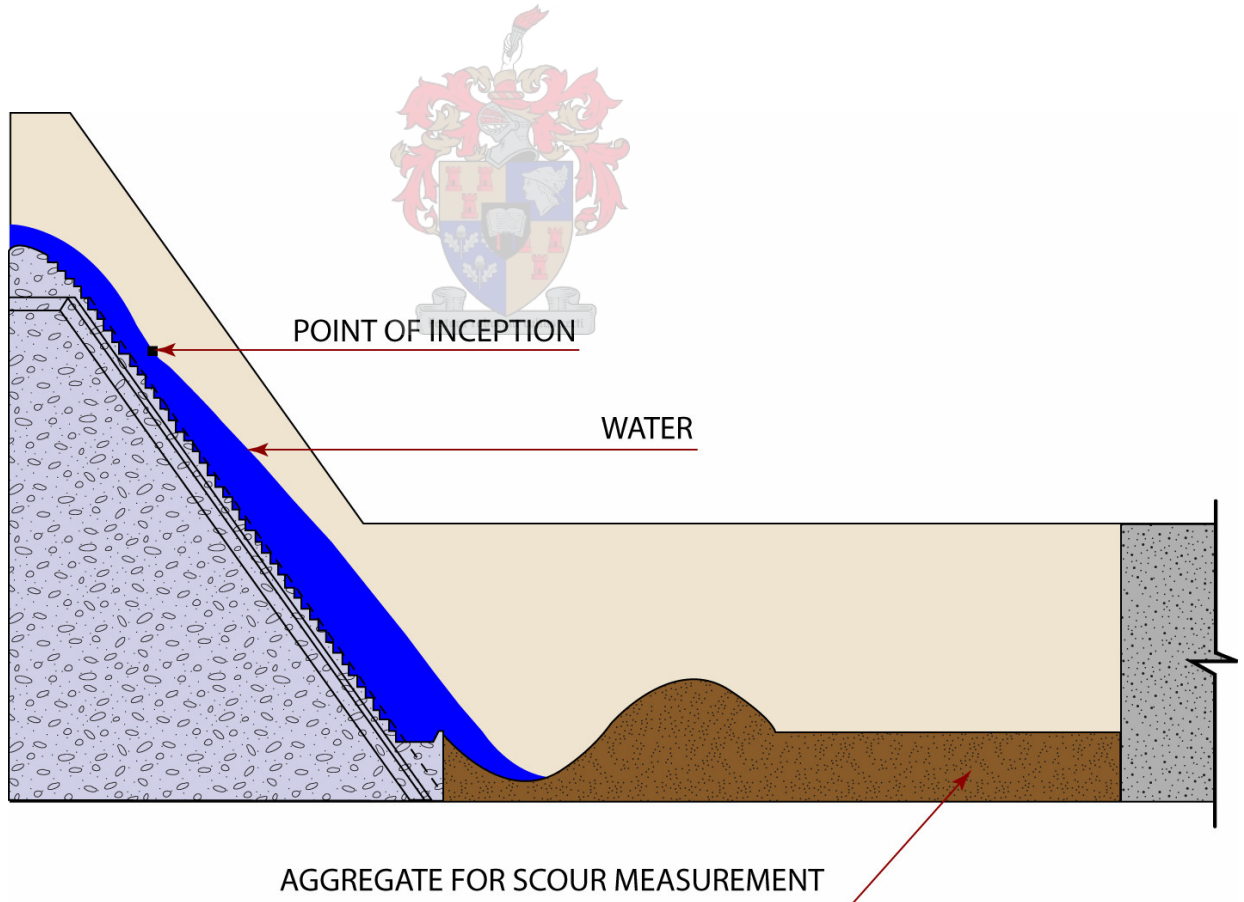


Figure 6.3: Schematical scour effect for unit discharges larger than 35 m³/s.m

6.2.3 The Effect of Protrusion Spacing on the Location of the Point of Inception

From Figures 5.16, 5.17, 5.18, 5.19, 5.20, 5.29, 5.30, 5.31, 5.32, 5.33, 5.35 and 5.36 the effect of the protrusions on the length of inception can be seen. It is also evident that the protrusion with width equal to twice the tread of the step (Protrusion 1, refer to Figures 4.2 and 4.3) is more effective than the protrusion 3,46 times the tread of the step. From the above mentioned figures it can be observed that for the first model (scale 1:20) the shortest length of inception (L_i) is obtained by configuration P 1(4), followed by configuration P 1(1). For the second model (scale 1:30) the shortest length of inception is obtained by configuration P 1(4), followed by configuration P 1(1). Table 6.2 presents the ratio of steps with protrusions to the standard steps for various discharges and protrusion spacings. From the table it is evident that the denser the protrusions are spaced, the shorter the length of inception L_i . The length of inception shortens by about 30% when protrusions are added.

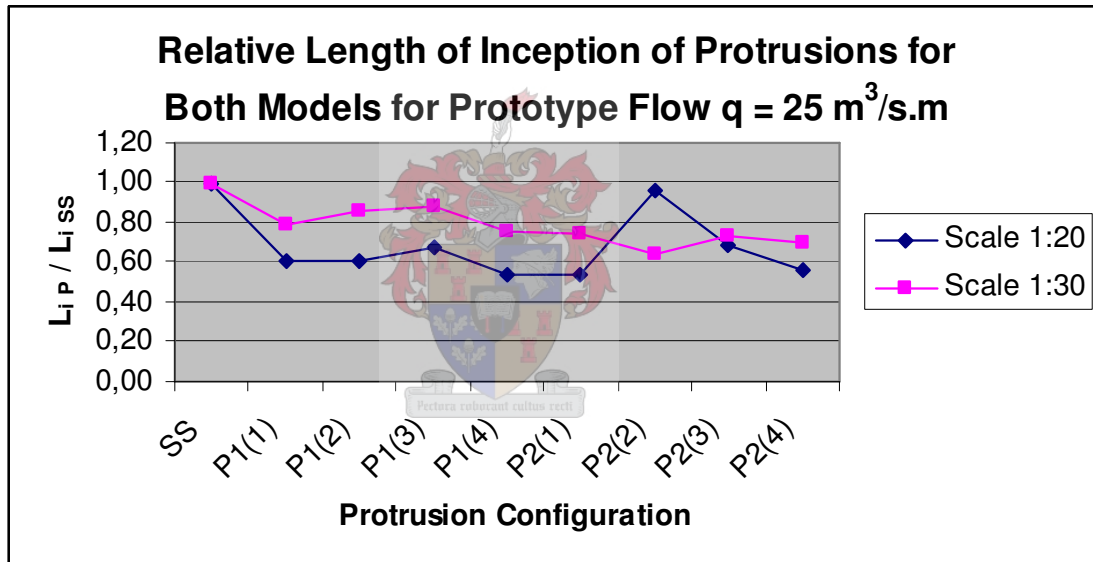


Figure 6.4: Relative length of inception for both models

Table 6.2: Point of Inception of the Triangular Protrusions

Unit Flow (q in m ³ /s.m)	Model		
	Protrusion Configuration	Scale 1:20 L_{iP} / L_{iSS}	Scale 1:30 L_{iP} / L_{iSS}
0,12	P 1(1)	0,539	0,532
0,21		0,614	0,667
0,27		0,607	0,788
0,12	P 1(2)	0,539	0,566
0,21		0,614	0,714
0,27		0,607	0,86
0,12	P 1(3)	0,732	0,606
0,21		0,689	0,744
0,27		0,674	0,876
0,12	P 1(4)	0,684	0,502
0,21		0,465	0,626
0,27		0,533	0,751
0,12	P 1(5)	-	0,532
0,21		-	0,667
0,27		-	0,832
0,12	P 2(1)	0,504	0,511
0,21		0,505	0,597
0,27		0,536	0,738
0,12	P 2(2)	0,957	0,484
0,21		0,962	0,619
0,27		0,961	0,643
0,12	P 2(3)	0,621	0,554
0,21		0,655	0,64
0,27		0,681	0,737
0,12	P 2(4)	0,447	0,511
0,21		0,508	0,632
0,27		0,559	0,696

Note: L_{iP} = length of inception for protrusions

L_{iSS} = length of inception for standard steps

6.2.4 Conclusion on Protrusion Spacing

From the previous sections, it can be concluded that Protrusion 1 (with width equal to twice the thread of the step) should be used at all times. It is proposed that it be spaced as shown in configuration P 1(1). This will ensure optimal roughness, a high point of inception and less scour than for standard steps.

6.3 The Effect of Scale

The results of literature are discussed in Section 2.4.

From the data presented in Section 5 can be seen that some sort of scale effect exist between the two constructed models. This difference could also be due to inaccurate measurements.

It can be concluded that to model dams that need to accommodate large unit flow rates (up to $40 \text{ m}^3/\text{s.m}$) at a scale of 1:10 will require a laboratory with a capacity of at least $1,0 \text{ m}^3/\text{s.m}$. It is proposed to model at the largest possible scale of the laboratory to ensure that results can be extrapolated to prototype values. At this stage, with limited data obtained from physical model studies, it is concluded that values obtained from model studies are a conservative estimate of the prototype roughness values. These values (obtained from model studies) must be used until laboratories that can yield unit flow rates of $1,0 \text{ m}^3/\text{s.m}$ can be used to clarify the roughness values, or measurements from prototypes can be used to determine roughness values.

6.4 The Effect of the Triangular Protrusions on the Spillway Design of the De Hoop Dam

As mentioned earlier, this thesis ran parallel with the optimisation of the spillway for De Hoop Dam. From the results presented, the protrusions works effectively to ensure the early entrainment of air into the water mass. For the chosen apron and end sill configuration more scour than for a standard stepped spillway was observed. Scour downstream of the toe of the dam was the governing factor in determining the optimum spillway layout for De Hoop Dam, thus the use of protrusions was not recommended.

At a later stage during the detail design, concern was raised regarding possible cavitation during extreme floods. The allowable maximum unit discharge of $25 \text{ m}^3/\text{s.m}$ on stepped spillways is based on the allowable velocity of approximately 20 m/s upstream of the point of inception (PI), according to Boes & Minor (2002). Downstream of the PI the aeration is sufficient to allow a unit discharge of $140 \text{ m}^3/\text{s.m}$.

Subsequently, the apron was lengthened by approximately 28% (from $6,75 \text{ m}$ to $8,67 \text{ m}$) by lifting the apron two step heights ($2,4 \text{ m}$) and keeping the same end sill dimensions. The different protrusion configurations as described in Section 4 were tested on the downstream slope, together with the longer apron.

Using the equation from Boes and Minor (2002) for the inception length (L_i) the vertical distance between the crest and the PI (Z_i) for a range of unit discharge was calculated and shown in Figure 6.5.

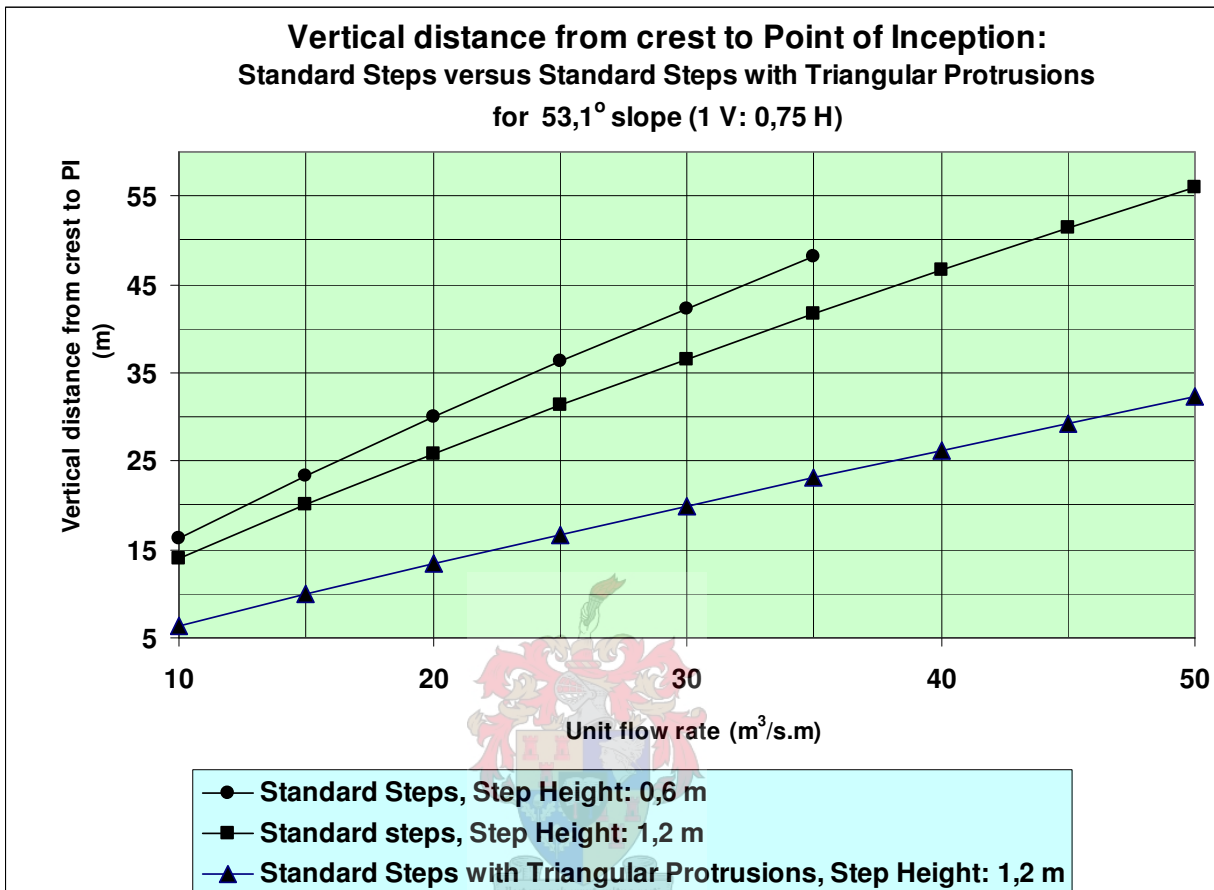


Figure 6.5: Prototype position of point of inception obtained from Model 2 (Scale 1:30)

From Figure 6.5, the PI for standard step spillways with 1,2 m step heights is closer to crest than those for 0,6 m step heights. The potential energy that can be converted to kinetic energy at the PI is thus smaller for 1,2 m step heights. The position of the PI with TP's applied is also indicated on Figure 6.5.

The velocity at the PI is dependent on the relative potential energy head upstream of the crest and the head loss from the crest to the PI. The velocities at the PI, for the various scenarios, are shown in Figure 6.6.

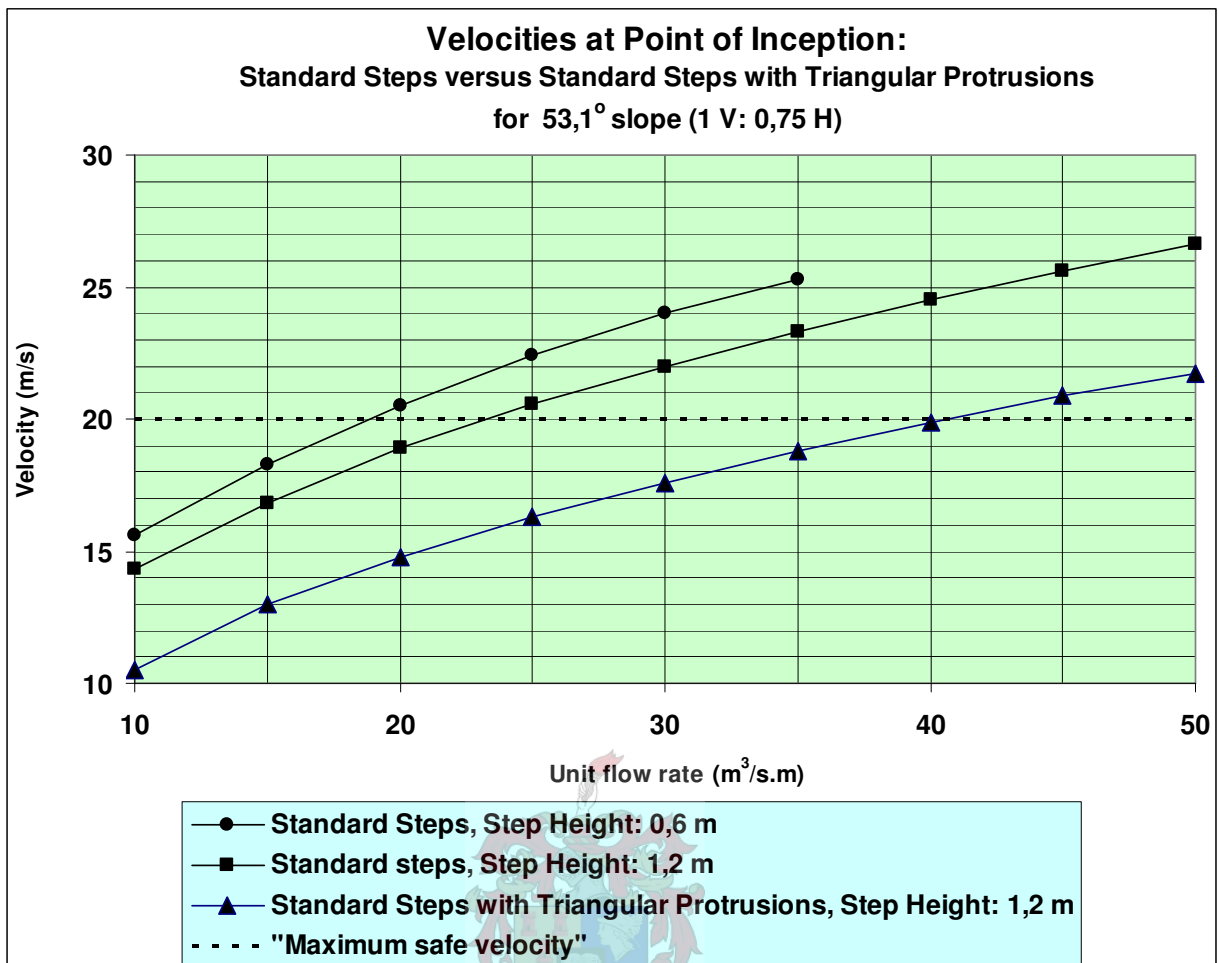


Figure 6.6: Velocities at the point of inception obtained from Model 2 (Scale 1:30)

According to the 20 m/s criteria and data obtained from model studies, a standard step spillway is unsafe at a unit discharge of 25 m³/s.m, whilst a spillway fitted with triangular protrusions will be safe at 40 m³/s.m. The configuration of the triangular protrusions used in Figure 6.6 is that of Protrusion 1 Layout 5 as shown of Figure 4.17.

This additional testing now overrule the previous conclusion that if scouring is the factor governing the effectiveness of the protrusions, protrusions can be used for unit discharges up to 35 m³/s.m. This statement is again subjected to the apron and end sill configuration.

The same criteria and measurements for scour were taken as described in Section 4.6. The depth of scour was measured as demonstrated in Figure 5.7. The same depth of scouring at all tested floods was obtained as for the original apron configuration for the RDD and RMF respectively, but the scour now occurred further away from the spillway toe than was documented for the original configuration. The original apron configuration resulted in the water "missing" the apron (as described in Section 6.2.2) and excessive scour occurred for

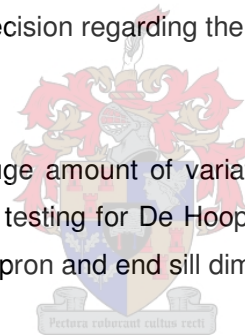
the SED. With the longer apron this phenomenon did not occur, and resulted in 15 % less scour. This reduces the risk of possible undermining of the structure even further.

The following recommendation was made for the design of the spillway for De Hoop Dam (DWAF, 2006):

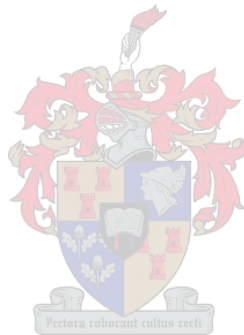
- As the positions of the PI were obtained from model studies, which are conservative in regard to both aeration and friction head loss, it is not a certainty that the prototype spillway with standard steps will be unsafe at $25 \text{ m}^3/\text{s.m}$. However, it is recommended that the results from the model studies are to be accepted as an additional margin of safety.
- If serious erosion of the spillway for the remote probability when the unit flow rate exceeds $25 \text{ m}^3/\text{s.m}$ is not acceptable, the use of triangular protrusions, applied from the crest to a point 25 m vertically downstream, is recommended as an effective measure to avoid this possible erosion.

It is concluded that the final decision regarding the above recommendation must still be made by DWAF.

The thesis did not have a huge amount of variation in terms of apron length and end sill configurations. This additional testing for De Hoop Dam just shows how sensitive the use of protrusions is to the required apron and end sill dimensions.



- 1 INTRODUCTION**
- 2 LITERATURE STUDY**
- 3 REVIEW OF LITERATURE**
- 4 PHYSICAL MODELING**
- 5 RESULTS**
- 6 DISCUSSION OF RESULTS**



7 CONSTRUCTION ASPECTS AND COST

The research will serve little purpose unless a definite improvement in cost can be shown, as most spillways for dams are safe against excessive scour. The constructability of the protrusions must also be easy to avoid time delays for roller compacted concrete (RCC) placement.

7.1 Normal RCC Placement

The manufacturing, transporting, placing, compaction and curing of RCC are described in various publications and specifications. RCC is a combination of fine and coarse sized aggregate, cement, pozzolan and admixtures that are blended with water to a damp consistency that permits hauling and spreading with earth moving equipment and is compacted with a vibratory roller. RCC will exhibit, when set, the same properties of typical conventional mass concrete.

RCC is defined by several characteristics above its strength and structural performance, including the paste/mortar ratio, sand/aggregate ratio and the (modified) Vebe Grade (or time). These parameters influence the density of the RCC, the compaction ratio and the tendency for material segregation.

This chapter will not focus on:

- Mix designs;
- Durability;
- Watertightness;
- Temperature effects (thermomechanical behavior);
- Materials;
- Test sections;
- Cracking; and
- Quality control during construction.

The chapter will focus on the constructability of the protrusions. The process of placing RCC and skin concrete will be briefly described, as this forms the basis for the possible construction of the protrusions.

7.1.1 Types of concrete

a) RCC

RCC consists of Portland cement, fly ash and/or milled slag, or a natural pozzolan, fine aggregate, coarse aggregate and water. All of the materials must be well mixed and brought to proper consistency. Other admixtures can be added to the discretion of the Professional Engineer for a specific project.

The properties of RCC include the following, but it will not be discussed in detail:

- Strength (compressive, tensile, flexural and shear);
- Elastic properties (Modulus of Elasticity, Poisson's ratio);
- Creep;
- Volume change (shrinkage);
- Thermal properties;
- Permeability;
- Density; and
- Durability (abrasion/ erosion resistance, resistance to thawing).

b) Facing/Skin Concrete

Facing or skin concrete is an impermeable conventional mass concrete placed against formwork, or other surface forming the external face of the RCC body, as indicated on the particular drawings or as directed by the Professional Engineer for a specific project. The term skin concrete will be used. The thickness of the skin concrete is normally about 600 mm on the upstream face of the dam, with the thickness varying downstream to ensure overlapping of the downstream steps. Skin concrete normally has a higher cementitious content than RCC, and the maximum coarse aggregate size is usually less than for RCC.

The upstream face of the dam is in contact with the water in the reservoir. To fulfill its protective role, the upstream face must be designed to withstand aggression in the water, in the medium or long term which can “contaminate” the concrete within the dam body. It must be constructed to a high quality standard to ensure durability.

The upstream face is also subjected to temperature and humidity variations, caused mainly by fluctuating reservoir levels. The upstream face must also withstand the impact of any floating debris.

The presence of the skin concrete in the upstream face permits:

- Provision for contraction joints with waterstops;
- Improved watertightening; and
- Improved face appearance.

The downstream face must be designed and constructed to protect the mass concrete against considerable variations in atmospheric conditions (ageing of surface concrete due to freeze cycles, exposure to sunlight, wind, rain, daily and seasonal variations, etc.) and in downstream water levels. The durability of the downstream face is an important design criteria, and a durable surface reduces cavitation of the downstream concrete which can occur due to flooding.

7.1.2 Construction and Compaction of RCC and Skin Concrete

One of the main advantages of the RCC technique is the possibility of constructing massive concrete structures in a short period of time. Rapid dam construction is achieved with plant capable of operating at a fast rate, running in as continuous a manner as possible.

The objective of achieving high construction rates may be restricted by the availability of plant, site characteristics and the project size. The construction rate selected for a particular site is therefore a compromise, and must be optimized taking into account conflicting criteria.

Different conveyance and transporting equipment is available and the use thereof depends on the particular site configuration. To ensure that continuous bonded RCC is achieved, the concrete mixtures must be conveyed from the plant mixers to ensure rapid placement which limit segregation of materials, contamination and surface drying. Possible ways of transporting fresh RCC include the use of conveyors, hoppers, dump trucks and chutes. This will not be discussed in detail, and depends mainly on the specific project. Two typical conveyor systems are shown in Photographs 7.1 and 7.2. Photograph 7.3 shows the installation of waterstop, joint drain and crack initiator.



Photograph 7.1: Conveyor system with self-propelled crawler placer (Courtesy US Corps of Engineers, 2000)



Photograph 7.2: Conveyor system with mobile side discharge belt (Courtesy US Corps of Engineers, 2000)



Photograph 7.3: Installation of waterstop, joint drain and crack initiator (Courtesy US Corps of Engineers, 2000)

RCC is normally compacted by means of a self-propelled smooth drum vibratory roller. Small vibratory rollers, which are capable of operating within 200 – 300 mm of a vertical face are used to compact in areas where large vibratory rollers cannot manoeuvre. These will also be used to compact the interface between the RCC and facing/skin concrete.

All formwork used must ensure that the concrete can be placed and compacted to the required shapes, finishes, positions, levels and dimensions as required for the specific project. The formwork must also be capable of resisting all dead and live loads to which it is subjected. Shutters normally have the height of the step. The shutter system is designed for speed of erection, simplicity and man handled sizes and weights.

The following procedure for RCC placement is normally adopted, after the material has been transported, the shutters have been erected and the receiving surface has been prepared:

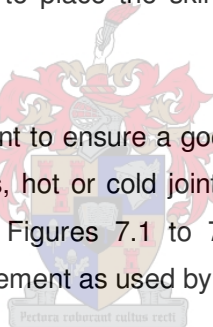
- The RCC is spread over the receiving surface in such a way to prevent segregation. The layer thickness depends on the project, but the compacted thickness is normally between 250 mm and 300 mm.
- The RCC is compacted with a self-propelled vibratory compaction roller. The number of passes to be completed to achieve the target density will be determined during RCC mix trials during construction of the test section.

- During the first pass, which is used to consolidate the layer, no vibration is used. The first pass shall be followed by subsequent passes using vibration until the specified compaction has been achieved.
- Over compaction must be limited.

The following procedure for skin concrete placement is normally adopted, after the material has been transported and shutters have been erected:

- The skin concrete will be placed prior to RCC placement.
- The layer thickness is the same as for the RCC placement.
- The slump of the concrete is important to prevent the concrete to “run away”.
- An immersion vibrator is used to compact the skin concrete to form a 1:1 (V: H) slope at the edge.
- After RCC has been placed against the skin concrete, the contact between the skin concrete and RCC will be vibrated again for final compaction to ensure sufficient bonding between the RCC and skin concrete.
- Care must be taken not to place the skin concrete too far in advance of the RCC placement.

Quality control on site is important to ensure a good end product. Bonding or bedding layers between successive RCC layers, hot or cold joints and the installation of joints, waterstops and drains are not discussed. Figures 7.1 to 7.4 show RCC placement sketches. The procedure adopted for RCC placement as used by DWAF is shown.



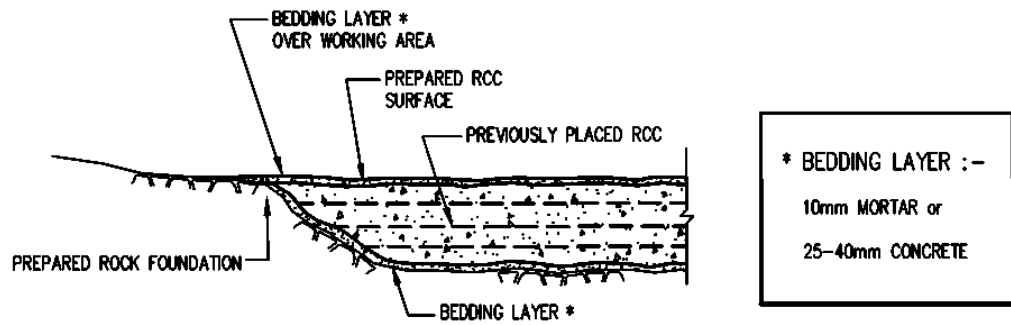


FIGURE 1: PLACING THE BEDDING LAYER

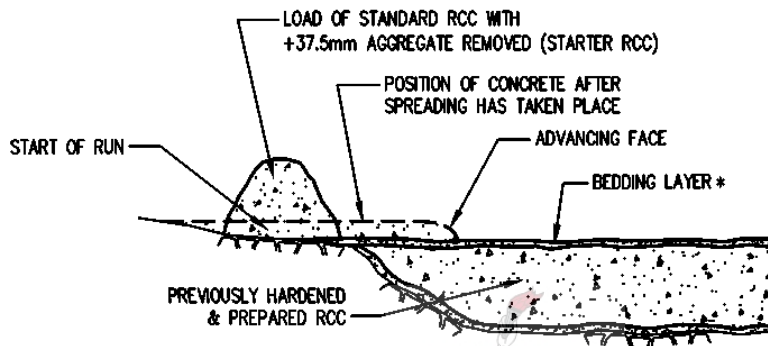


FIGURE 2: PLACING THE RECEIVING BED FOR RCC

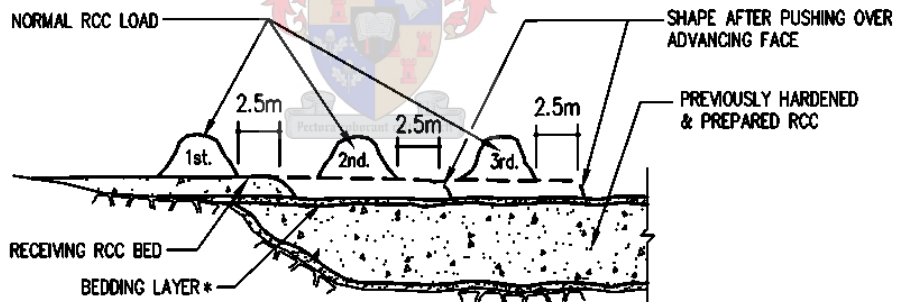


FIGURE 3: PLACING OF A FIRST RCC LAYER

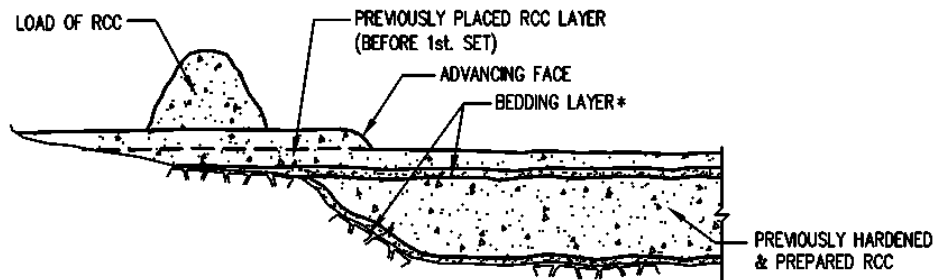


FIGURE 4: PLACING FURTHER RCC LAYERS

Figure 7.1: RCC Placement Procedure (Courtesy DWAF, 2005)

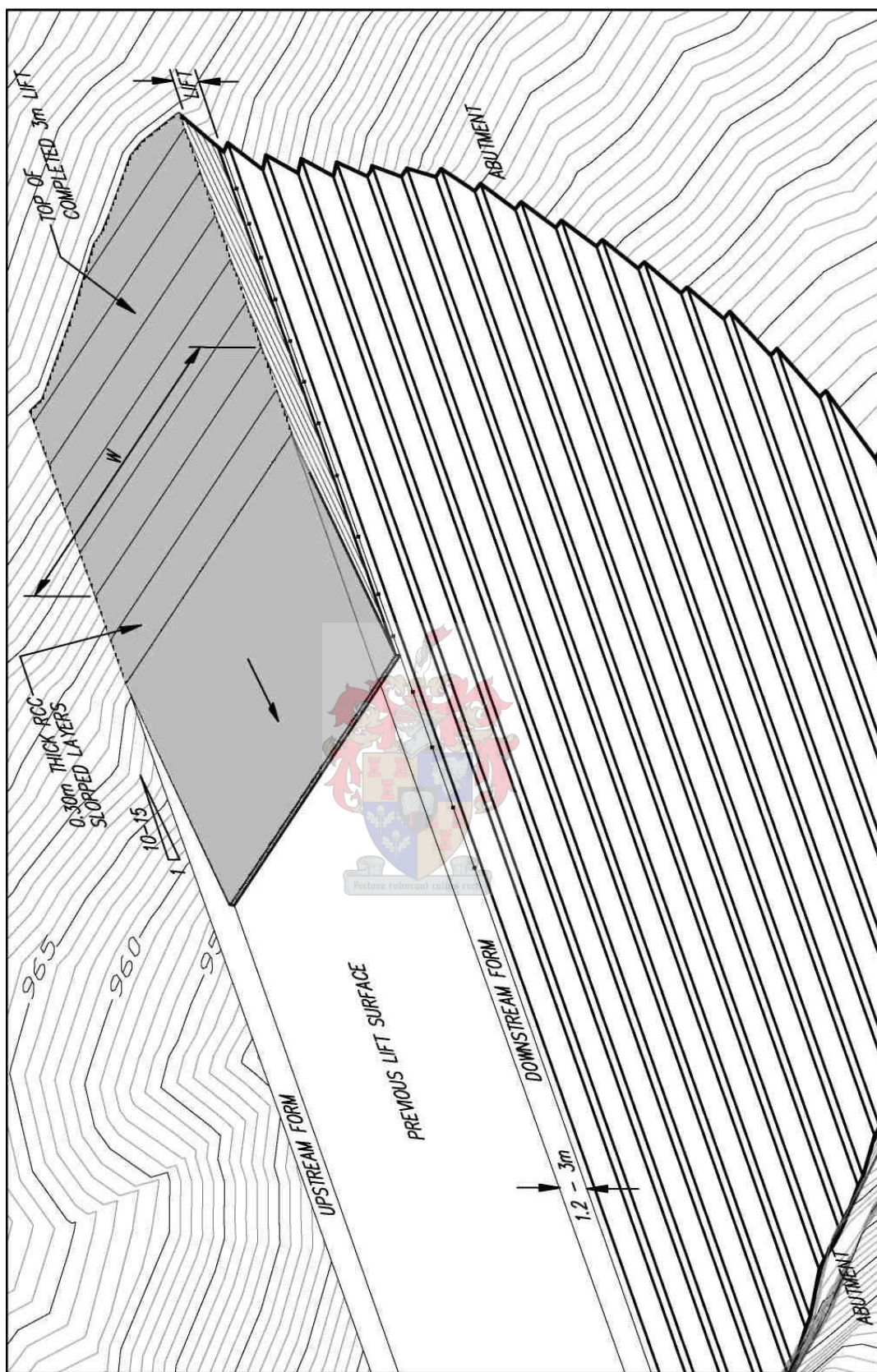


Figure 7.2: Sloped Layer RCC Placement (Courtesy DWAF, 2005)

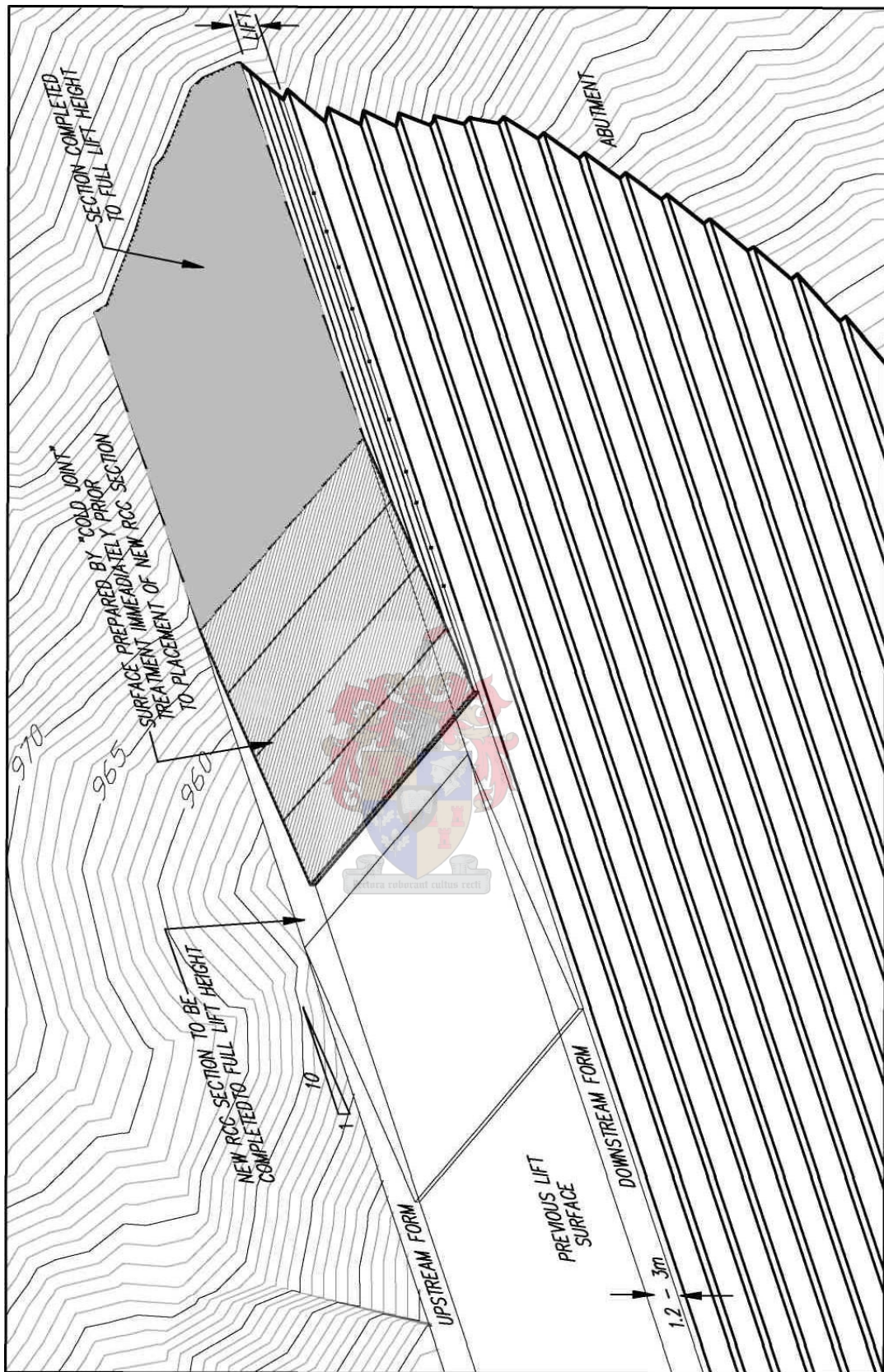


Figure 7.3: Non-continuous RCC Layer Placement (Courtesy DWAF, 2005)

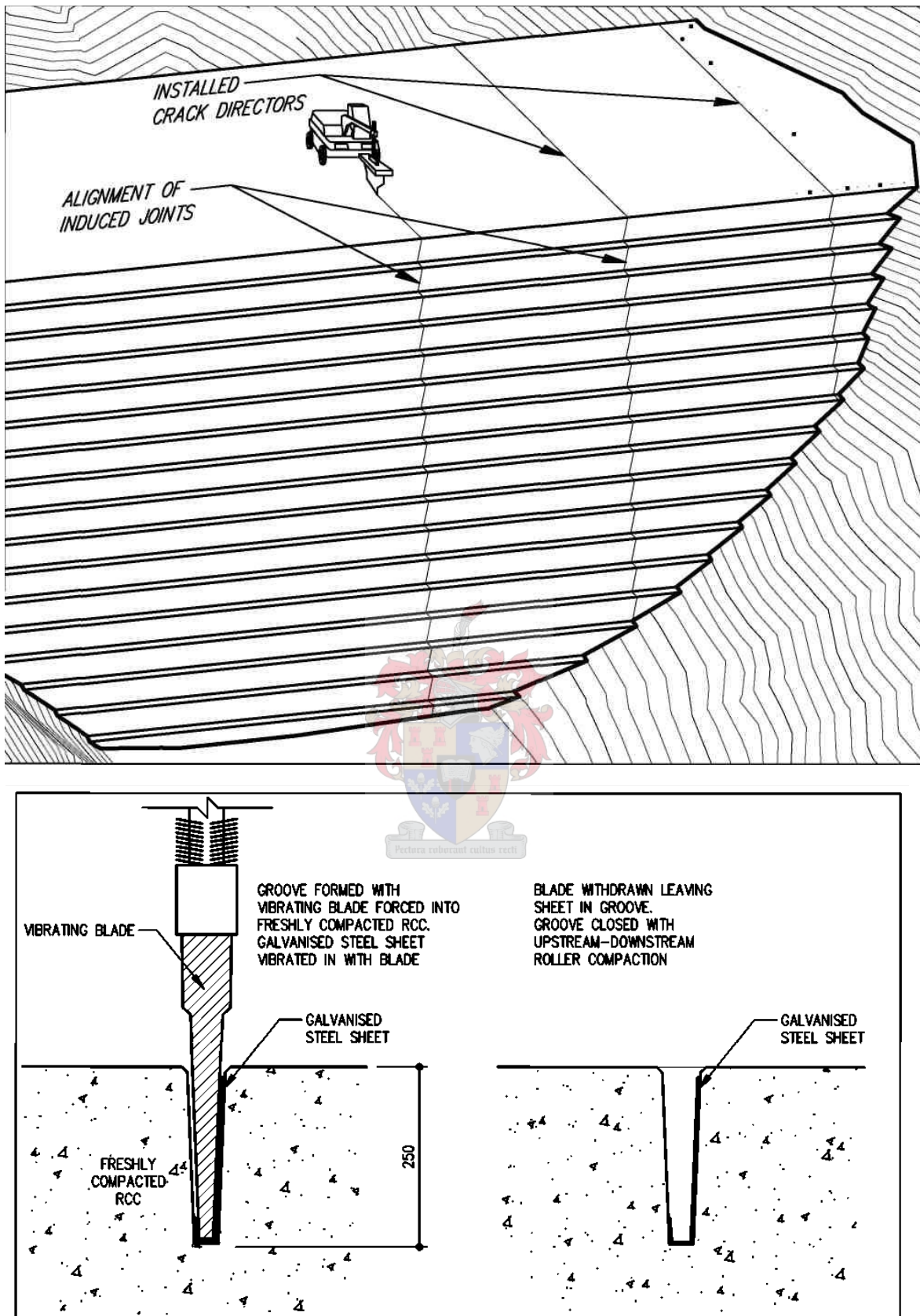


Figure 7.4: Crack Director Installation after RCC Compaction (Courtesy DWAF, 2005)

7.2 Construction Options

After the process of concrete (RCC and skin) placement is known, proposed ways of constructing the protrusions can be described. Much more detail on RCC could have been given in Section 7.1, but the section was included to give the reader a good understanding of construction methods used today.

The following methods to construct these protrusions are proposed:

- Method 1: Develop a special shutter and cast the protrusion with skin concrete together with normal RCC placement.
- Method 2: Precast the protrusion, lift the protrusion with a mobile crane to the desired position, dowel it into the downstream steps and grout the contact.
- Method 3: Precast a mass element that will also be used as “permanent” shutter.

These methods were developed with the help of the Directorate: Construction of DWAF and will be described in detail below.

If protrusion 1 is used, and the dimensions are converted to the De Hoop Dam, the area of the protrusion is $0,92 \text{ m}^2$ and with a height of $1,2 \text{ m}$ the total additional volume of concrete required is $1,10 \text{ m}^3$. If a concrete density of 24 kN/m^3 is assumed, the total weight of one protrusion is $2,7 \text{ ton}$. If protrusion 2 is used, and the dimensions converted, the area of the protrusion is $1,60 \text{ m}^2$ and with a height of $1,2 \text{ m}$ the total volume of concrete required is $1,92 \text{ m}^3$. If a concrete density of 24 kN/m^3 is assumed, the total weight of one protrusion is $4,6 \text{ ton}$. Figure 7.5 shows the converted dimensions of protrusion 1 to the De Hoop Dam dimensions.

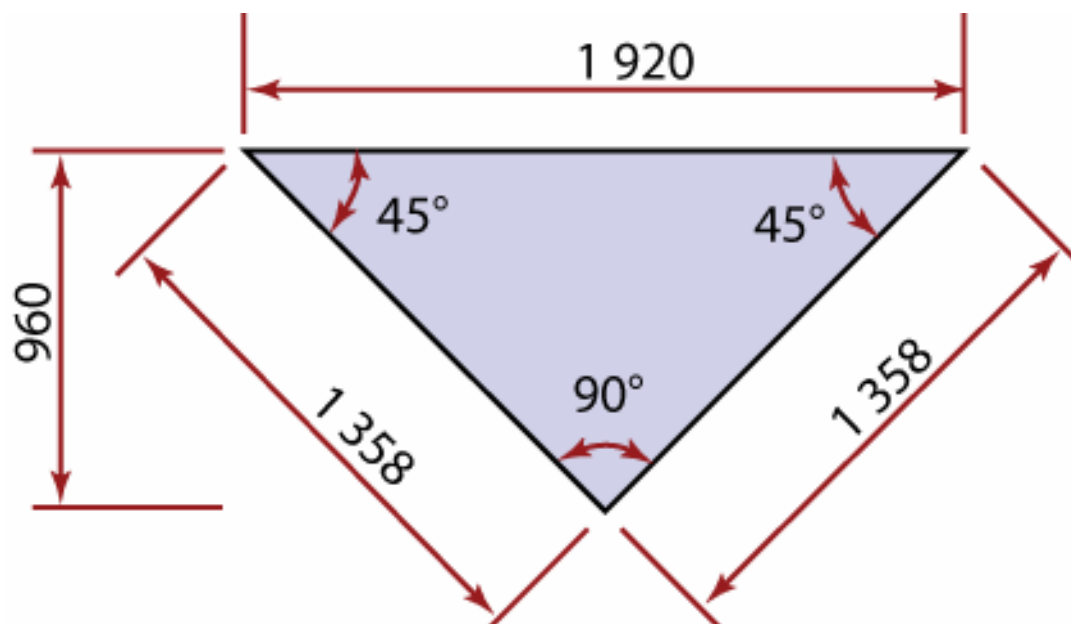


Figure 7.5: Protrusion 1 converted to De Hoop Dam dimensions

7.2.1 Method 1

Method:

Special shutters can be made up to incorporate existing standard shutters with lengths of 2,7 metres. These lengths will however depend on the horizontal distance between the protrusions. Care must also be taken to ensure that a protrusion does not go through a construction joint. The protrusion spacing must be such that this phenomenon does not occur. The protrusions can be cast from only skin concrete or RCC and skin concrete, depending on the type of vibrating equipment that is used on the site.

Advantages:

- There will be little disruption of the normal construction process associated with standard steps.
- The shutter system will be structurally more stable.

Disadvantages:

- The length of shuttering will increase over normal stepped (straight) spillways, which in turn will increase the cost. Special shutters are required.

7.2.2 Method 2

Method:

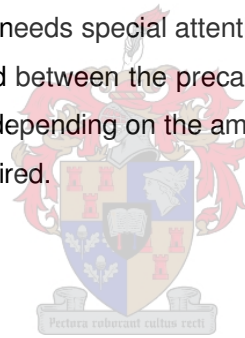
Precast protrusions can be cast on site while normal RCC placement and other activities continue. As stated above, the weight of these protrusions ranges between 2 and 5 tons, depending on the project. Mobile cranes will be required to move these protrusions into the correct positions. The precast protrusions must be reinforced, to ensure durability and to prevent cracking. After the standard step is completed, holes must be drilled into the step to dowel the precast protrusion in. Grouting to seal the contact surface is required. Again, care must be taken to ensure that a protrusion does not go through a construction joint.

Advantages:

- This is a separate activity and protrusions can be added later depending on the construction and impoundment programme.

Disadvantages:

- Doweling and grouting needs special attention during construction.
- The joint sealant added between the precast protrusion and the standard step can be washed out with time, depending on the amount of flooding that occurs.
- Mobile cranes are required.



7.2.3 Method 3

Method:

No shutters and skin concrete will be used. Mass elements consisting of straight sections and protrusions can be precast, with reinforcement if necessary. This will result in very heavy sections, requiring large cranes to put them in the correct position. These elements will be stacked next to each other and on top of each other. The elements will be added directly on the completed step. RCC is then placed directly next to these elements with no skin concrete required. Care must be taken to ensure adequate bonding between the elements and the freshly placed RCC. Adequate bonding between the elements must be ensured.

Advantages:

- No shutters are required.

Disadvantages:

- Large cranes are required to lift the mass elements into position.

7.3 Cost of Adding the Protrusions

Two main cost additions are relevant. It is the extra amount of concrete required and the increase in shutter length, depending which of the above mentioned methods is used. To use configuration P 1(1) on the proposed De Hoop Dam, with a 110 metre long spillway, results in 27,5 protrusions per row. The spillway has 55 steps. Adding the protrusions on every second row, 28 rows will have protrusions. A total of 770 protrusions with a concrete volume of 1,20 m³ each will be required. The total amount of extra concrete is 925 m³. An increase in shutter length of 2,8 m is required per protrusion. The total length of extra shuttering required is 2 200 m. A surface finish of 0,92 m² is required per protrusion. The total surface finish required is 750 m². The unit cost of concrete per m³ is R 550, shuttering per metre length is R 150 and surface finish per m² is R 10. This results in a total cost of R 0,85 million. In terms of the total project cost, this is an approximate increase of 1 %. The precast options will be marginally more expensive due to grouting and doweling operations, and extra cranes that are required. This rough cost estimate shows a small increase in total cost of the spillway. The cost/scour benefit must be quantified to determine if the addition of protrusions is worth the effort. For the proposed De Hoop Dam, a final decision regarding the adding of protrusions must still be taken.

7.4 Cost of Standard Stilling Basins

As previously stated, the hydraulic jump stilling basin is an effective device for dissipating energy, before the flow is returned to the downstream river channel. The hydraulic jump that will occur in a stilling basin has distinctive characteristics and assumes a definite form, depending on the energy of flow that must be dissipated and the depth of the flow. The United States Bureau of Reclamation (USBR) did a comprehensive series of tests to determine the properties of the hydraulic jump. The form of the jump and the flow characteristics can be related to the kinetic flow factor (v^2 / gd), the critical depth of flow (d_c) and the Froude number (v / \sqrt{gd}). Various ranges of the Froude number give different forms of the hydraulic jump.

For this project, a Froude number of higher than 4,5 is assumed. This results in the use of a USBR Type II stilling basin. In this basin, a stable hydraulic jump will occur. The installation of accessory devices such as blocks, baffles, and sills along the floor of the basin produce a stabilizing effect on the hydraulic jump, which can permit the shortening of the basin.

Figure 7.6 shows the typical Type II stilling basin. The Length of the stilling basin, L , can be obtained from the curve on Figure 7.7, but can be approximated as:

$$L = 4,3 \times D_2$$

with:

D_2 = Downstream sequent depth at hydraulic jump (See Figure 7.6 and 7.7).

For this project, the length of a standard Type II stilling basin will be determined for where the protrusions are present and for the standard stepped spillway. The cost of reducing the length of the stilling basin will be calculated.

From the model studies conducted, the sequent depth (Y_2) is known. The depth is used to determine the invert or foundation level for the stilling basin. These values will be converted to prototype values to obtain the length of a standard Type II stilling basin. The cost saving will be reported on. Lowering the foundation level of the stilling basin results in a cost addition due to more excavation being required. The unit rate for excavation is R 125 per m^3 .

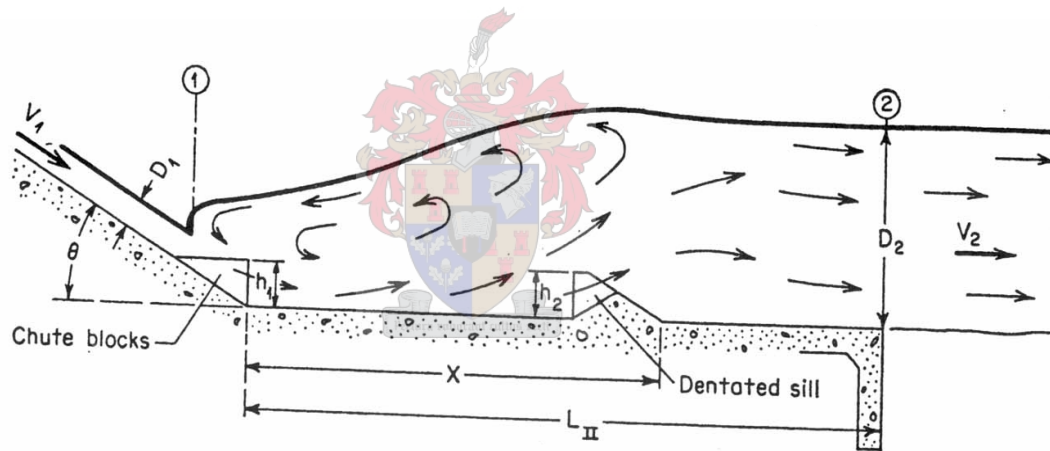


Figure 7.6: USBR Type II Stilling Basin (Courtesy USBR, 1987)

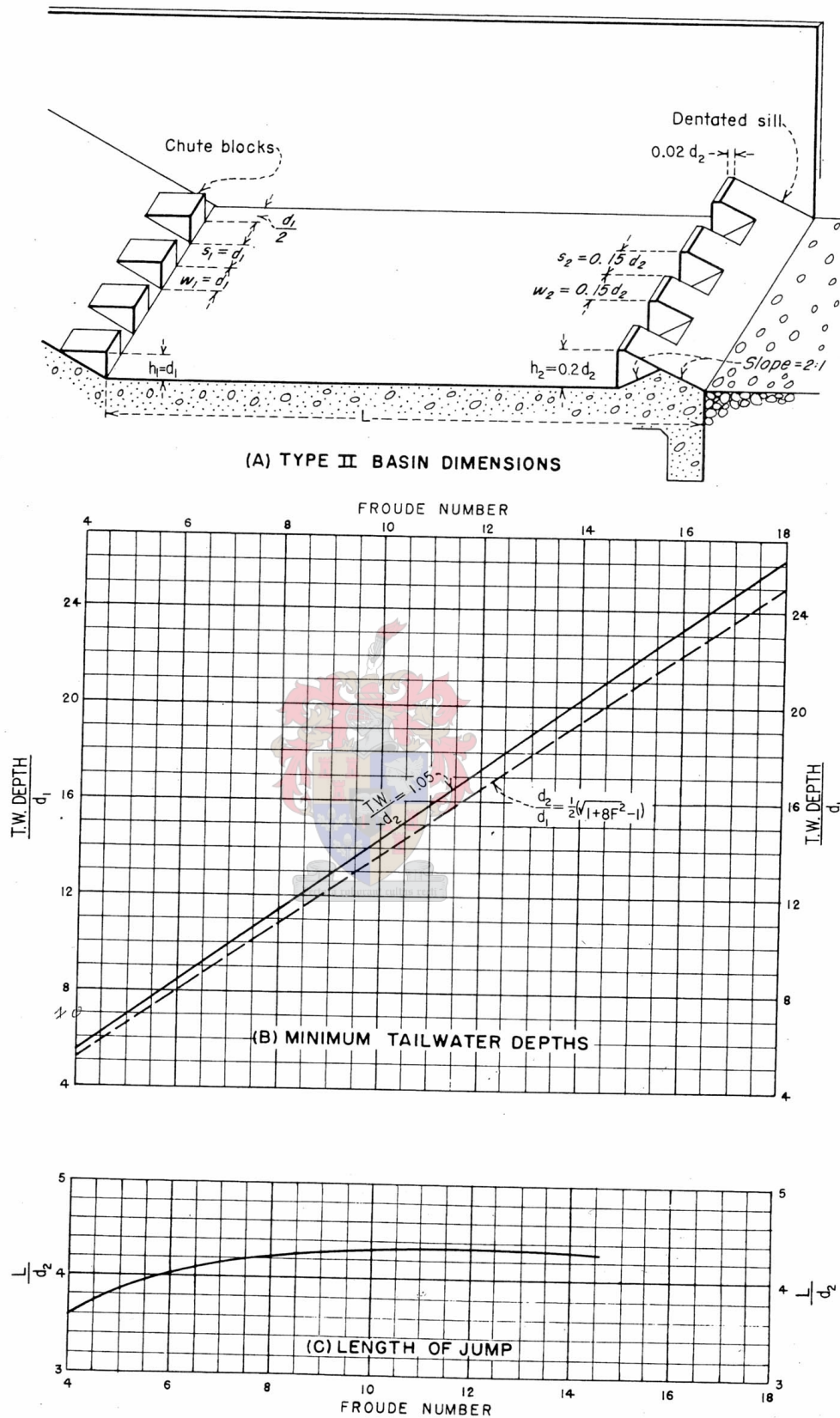


Figure 7.7: Determination of Length of Stilling Basin (Courtesy USBR, 1987)

7.4.1 Converted Sequent Depths

The data of the model test for both models are shown in Table 7.1 for all protrusion configurations. The basin length for Protrusion P 1(1) and the standard steps are shown in Figure 7.8.

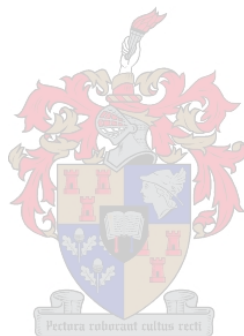


Table 7.1: Sequent depths for all tested protrusion configurations

Model Unit Flow (q in m ³ /s.m)	Protrusion Configuration	Model		Prototype				Type II Basin Length	
		Scale 1:20 Sequent Depth (m)	Scale 1:30 Sequent Depth (m)	Scale 1:20 Unit Flow (q in m ³ /s.m)	Scale 1:30 Unit Flow (q in m ³ /s.m)	Scale 1:20 Sequent Depth (m)	Scale 1:30 Sequent Depth (m)	Scale 1:20 Length (m)	Scale 1:30 Length (m)
0,12	P 1(1)	0,31	0,32	11	19	6,17	9,57	26,55	41,16
0,21		0,43	0,43	19	36	8,53	12,84	36,70	55,20
0,27		0,49	0,49	24	44	9,88	14,61	42,46	62,81
0,12	P 1(2)	0,31	0,34	11	19	6,24	10,11	26,84	43,47
0,21		0,43	0,45	19	36	8,60	13,37	36,99	57,49
0,27		0,50	0,50	24	44	10,02	15,05	43,10	64,72
0,12	P 1(3)	0,32	0,34	11	19	6,42	10,14	27,59	43,59
0,21		0,44	0,44	19	36	8,74	13,34	37,57	57,38
0,27		0,50	0,50	24	44	9,99	15,02	42,97	64,60
0,12	P 1(4)	0,32	0,34	11	19	6,42	10,17	27,61	43,73
0,21		0,44	0,45	19	36	8,82	13,37	37,93	57,48
0,27		0,51	0,50	24	44	10,13	15,15	43,54	65,13
0,12	P 1(5)	-	0,34	11	19	-	10,20	-	43,86
0,21		-	0,45	19	36	-	13,62	-	58,56
0,27		-	0,51	24	44	-	15,37	-	66,09
0,12	P 2(1)	0,33	0,33	11	19	6,56	9,79	28,21	42,08
0,21		0,44	0,44	19	36	8,80	13,10	37,84	56,33
0,27		0,51	0,50	24	44	10,10	15,06	43,43	64,75
0,12	P 2(2)	0,34	0,33	11	19	6,70	9,99	28,81	42,96
0,21		0,45	0,44	19	36	8,94	13,26	38,45	57,01
0,27		0,51	0,51	24	44	10,18	15,29	43,76	65,75
0,12	P 2(3)	0,33	0,34	11	19	6,64	10,14	28,55	43,60
0,21		0,44	0,44	19	36	8,84	13,31	37,99	57,21
0,27		0,51	0,51	24	44	10,13	15,33	43,55	65,92
0,12	P 2(4)	0,34	0,34	11	19	6,86	10,18	29,50	43,78
0,21		0,46	0,45	19	36	9,14	13,49	39,30	58,03
0,27		0,52	0,52	24	44	10,40	15,45	44,73	66,45
0,12	Standard Steps	0,35	0,34	11	19	7,02	10,22	30,19	43,93
0,21		0,47	0,46	19	36	9,30	13,66	39,99	58,76
0,27		0,53	0,52	24	44	10,68	15,60	45,92	67,09

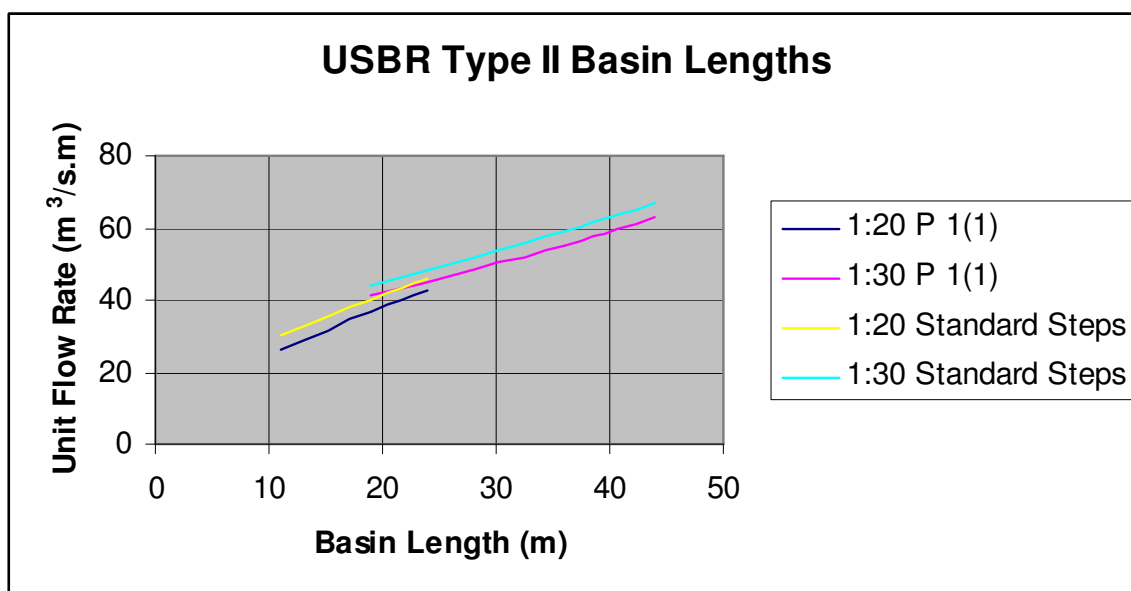


Figure 7.8: Type II Basin Lengths for Protrusion P 1(1)

From Figure 7.8 scale effect can still be seen between the two models. Of importance is the reduction in stilling basin length where protrusions are present as well as the reduction in sequent depth where protrusions are present, as shown in detail in Tables 7.2 and 7.5.

Table 7.2: Reduction of stilling basin length for Scale 1:20 Model

Scale 1:20 Unit Flow (q in $m^3/s.m$)	Type II Basin Length			Basin Length P 1(1) / SS
	P 1(1) Scale 1:20 Length (m)	Standard Steps Scale 1:20 Length (m)	Difference in Length (m)	
11	26,55	30,19	3,64	0,88
19	36,70	39,99	3,29	0,92
24	42,46	45,92	3,46	0,93

Table 7.3: Reduction of stilling basin length for Scale 1:30 Model

Scale 1:30 Unit Flow (q in m ³ /s.m)	Type II Basin Length			Basin Length P 1(1) / SS
	P 1(1) Scale 1:30 Length (m)	Standard Steps Scale 1:30 Length (m)	Difference in Length (m)	
19	41,16	43,93	2,77	0,94
36	55,20	58,76	3,56	0,94
44	62,81	67,09	4,28	0,94

Table 7.4: Reduction in sequent depth and basin depth for Scale 1:20 Model

Scale 1:20 Unit Flow (q in m ³ /s.m)	Sequent Depth			Sequent Depth P 1(1) / SS
	P 1(1) Scale 1:20 Sequent Depth (m)	Standard Steps Scale 1:20 Sequent Depth (m)	Difference in Sequent Depth (m)	
11	6,17	7,02	0,85	0,88
19	8,53	9,30	0,77	0,92
24	9,88	10,68	0,80	0,93

Table 7.5: Reduction in sequent depth and basin depth for Scale 1:30 Model

Scale 1:30 Unit Flow (q in m ³ /s.m)	Sequent Depth			Sequent Depth P 1(1) / SS
	P 1(1) Scale 1:30 Sequent Depth (m)	Standard Steps Scale 1:30 Sequent Depth (m)	Difference in Sequent Depth (m)	
19	9,57	10,22	0,65	0,94
36	12,84	13,66	0,82	0,94
44	14,61	15,60	0,99	0,94

7.4.2 Cost Saving

If the data from the tables in Section 7.4.1 are used, and the unit rates for concrete and excavation as used in Sections 7.3 and 7.4, a cost reduction for the Proposed De Hoop Dam is achieved. A shallower sequent depth requires lower side walls of the stilling basin and less excavation. Depending on which flood is used as the design flood, the saving for the 110 metre long overspill section (plan view) for De Hoop Dam with a thickness of 1,5 metres and two 1,5 m thick side walls is:

- RDF = Shorter stilling basin length + Less excavation + Lower side walls

$$= 3,64 \text{ m} \times 110 \text{ m} \times 1,5 \text{ m} \times \text{R } 550/\text{m}^3 + 0,85 \text{ m} \times 110 \text{ m} \times 3,64 \text{ m} \times \text{R } 125/\text{m}^3$$

$$+ 2 \times 1,5 \text{ m} \times 0,85 \text{ m} \times 3,64 \text{ m} \times \text{R } 550/\text{m}^3$$

$$= \text{R } 380 \text{ 000}$$

- RMF = Shorter stilling basin length + Less excavation + Lower side walls

$$= 3,46 \text{ m} \times 110 \text{ m} \times 1,5 \text{ m} \times \text{R } 550/\text{m}^3 + 0,80 \text{ m} \times 110 \text{ m} \times 3,46 \text{ m} \times \text{R } 125/\text{m}^3$$

$$+ 2 \times 1,5 \text{ m} \times 0,80 \text{ m} \times 3,46 \text{ m} \times \text{R } 550/\text{m}^3$$

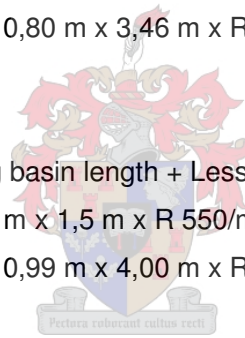
$$= \text{R } 360 \text{ 000}$$

- SED = Shorter stilling basin length + Less excavation + Lower side walls

$$= 4,00 \text{ m} \times 110 \text{ m} \times 1,5 \text{ m} \times \text{R } 550/\text{m}^3 + 0,99 \text{ m} \times 110 \text{ m} \times 4,00 \text{ m} \times \text{R } 125/\text{m}^3$$

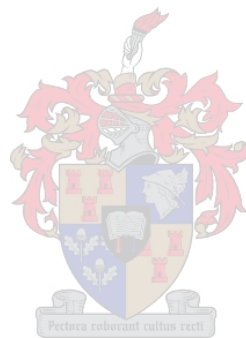
$$+ 2 \times 1,5 \text{ m} \times 0,99 \text{ m} \times 4,00 \text{ m} \times \text{R } 550/\text{m}^3$$

$$= \text{R } 425 \text{ 000}$$



This is not a substantial saving, but in other cases the saving could be more.

- 1 INTRODUCTION**
- 2 LITERATURE STUDY**
- 3 REVIEW OF LITERATURE**
- 4 PHYSICAL MODELING**
- 5 RESULTS**
- 6 DISCUSSION OF RESULTS**
- 7 CONSTRUCTION ASPECTS AND COSTS**



8 CONCLUSIONS

At the start of the research project it was expected that a better understanding could be obtained of standard stepped spillways. The two scale models modeled were however too close to each other, in terms of step height (h) and step roughness (k). Only one downstream slope was modeled, which also limits comparison with published data. The limited capacity of the hydraulic laboratory is also not favouring research in the flow ranges where the most uncertainty lies.

8.1 Scale Effects

As stated in Chapter 2, and is evident from results obtained from the physical modeling, that scale effect exist when constructing models. From Figures 5.12 and 5.25, the value of the roughness f increases as the critical depth (Y_c) increases. From these figures no flattening of the roughness value is indicated, as obtained by some other authors. A larger pump capacity of a hydraulic laboratory was required to investigate possible flattening of the roughness value. It is concluded that scale effects exists on scale models.

8.2 The Effect of the Identified Variables on the Standard Steps

From the studies conducted, the higher the unit discharge (q) becomes, the effectivity of the steps decrease. The unit discharge influences the flow depth, which in turn has an influence on the roughness of the steps.

8.3 Prototype Roughness Values for Stepped Spillways

From the data obtained, no conclusion on prototype values can be made for the roughness value f . It is however expected that prototype roughness values will be higher values than obtained from model data, as stated by some publications due to air entrainment.

8.4 The Effect of the Triangular Protrusions

The model data indicate that the denser the protrusions are spaced, the higher the roughness value f of the spillway becomes. The observed data indicates that the roughness value can increase by up to 40 %, with an average of 20 %. From the obtained data, it is concluded that if the roughness value governs the effectiveness of the protrusions, a dense spacing should be chosen.

The denser protrusions are spaced, the less scour will take place at the downstream toe of the dam. The scour patterns still rely heavily on the apron and stilling basin configuration. Model studies should be used to determine the optimum configuration for specific studies.

The addition of protrusions on the downstream slope of the dam shortens the length of inception (L_i), thus ensuring early air entrainment. The denser the protrusions are spaced, the shorter the length of inception. This can allow higher unit flow rates to be accommodated by stepped spillways. It is concluded that protrusions should be added on the downstream slope of the dam solely for the purpose of early air entrainment.

8.5 Summary

The following remarks are made after scrutiny of the obtained results from the study:

1. The addition of protrusions on the downstream slope of the stepped spillway is an effective way to increase the roughness of the downstream slope.
2. Applying protrusions reduces scour downstream of the toe of the dam.
3. The addition of protrusions ensures earlier entrainment of air into the water mass flowing over the spillway, thus reducing the length of inception.
4. The combination of the increase in roughness value, reduction in scour downstream of the apron or stilling basin and earlier air entrainment results in more effective energy dissipation.
5. A dense protrusion spacing results in more effective energy dissipation.

6. Construction of the protrusions are easy, and it should not significantly influence the cost of a project or cause construction delays.
7. An equation was derived that describes the friction factor (f) for standard steps as well as steps with protrusions, based on both scale models used in this research. The equation is in the format:

$$f = K (Y_c/k)^a (\text{Protrusion Density})^b$$

with:

K = A constant;

Y_c = Critical depth;

k = Roughness of steps;

Protrusion Density = Density as per Section 4.9;

a = A constant; and

b = A constant.

The format yielded the following equation:

$$f = 0,0111 (Y_c / k)^{1,205} (\text{PD})^{2,536} \quad \text{with: } R^2 = 0,60$$

The data of both models were used to cater for unit flow rates up to 40 m³/s.m.

8. An equation was derived that describes the length of inception (L_i) for standard steps as well as steps with protrusions, based on both scale models used in this research. The equation is in the format:

$$L_i/Y_c = A (Y_c / k)^n$$

with:

L_i = Length of inception;

Y_c = Critical depth;

A = A constant;

k = Roughness of steps; and

n = A constant.

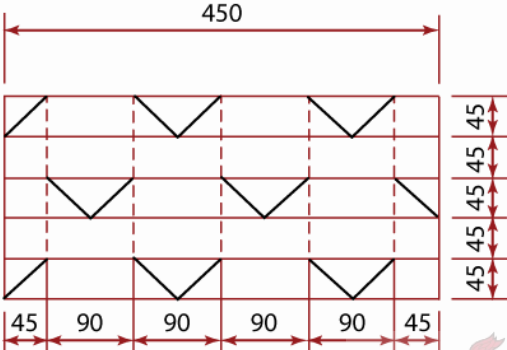
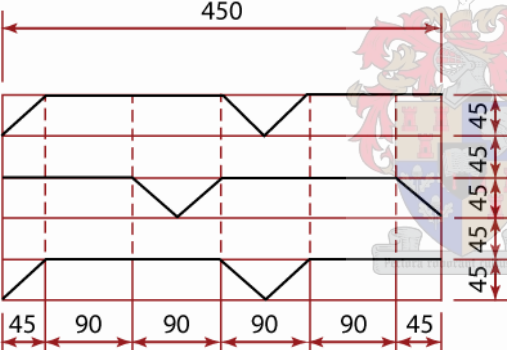
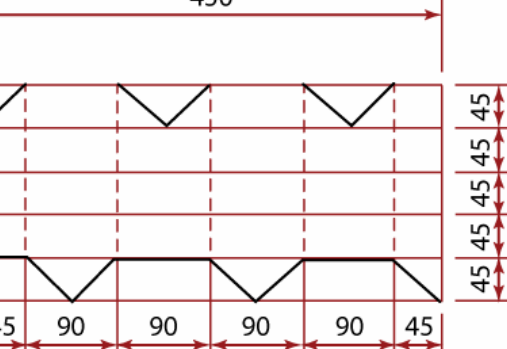
The format yielded the following equation:

$$L_i/Y_c = 9,6416 (Y_c / k)^{0,0675} \quad \text{with: } R^2 = 0,91$$

The data of both models were used to cater for unit flow rates up to 40 m³/s.m.

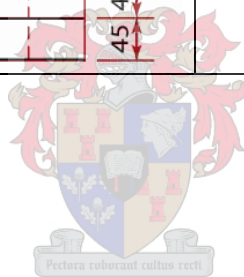
The protrusion density, roughness values ratios of protrusions versus standard steps and length of inception of protrusions versus standard steps for the 1:20 scale model (Model 1) are summarised in Table 8.1.

Table 8.1: Friction, length of inception and protrusion density ratio's for Scale 1:20 Model tests

Name	Protrusion Layout	$f_{\text{protrusions}} / f_{\text{Standard Steps}}$	$L_i^{\text{Protrusions}} / L_i^{\text{Standard Steps}}$	Protrusion Density
P 1(1)		1,60	0,61	1,125
P 1(2)		1,44	0,61	1,075
P 1(3)		1,41	0,67	1,062

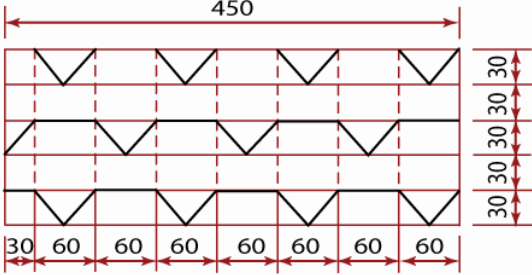
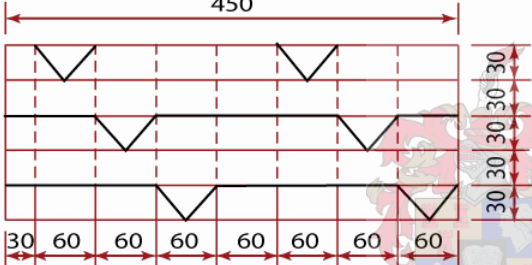
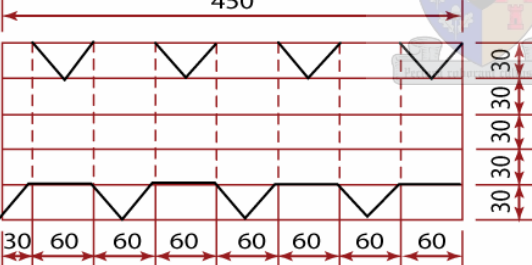
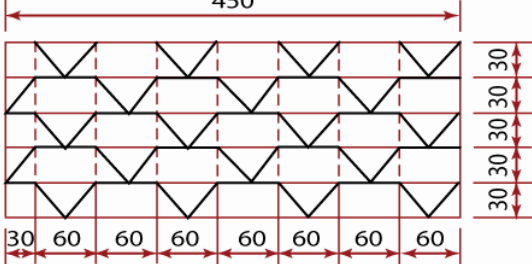
Name	Protrusion Layout	$\frac{f_{\text{protrusions}}}{f_{\text{Standard Steps}}}$	$\frac{L_i \text{ Protrusions}}{L_i \text{ Standard Steps}}$	Protrusion Density
P 1(4)		1,32	0,53	1,083
P 2(1)		1,34	0,54	1,130
P 2(2)		1,29	0,96	1,087
P 2(3)		1,32	0,68	1,065

Name	Protrusion Layout	$f_{\text{protrusions}} / f_{\text{Standard Steps}}$	$L_i_{\text{Protrusions}} / L_i_{\text{Standard Steps}}$	Protrusion Density
P 2(4)		1,15	0,56	1,087
SS		1,00	1,00	1,00

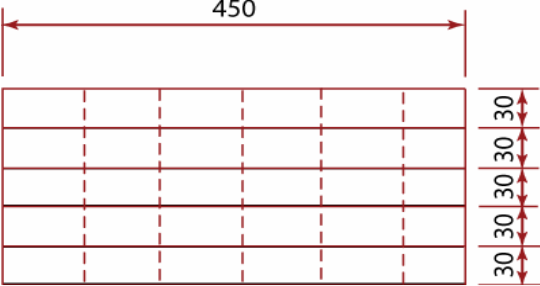


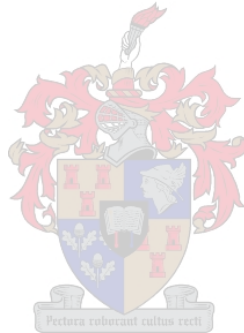
The protrusion density, roughness values ratios of protrusions versus standard steps and length of inception of protrusions versus standard steps for the 1:30 scale model (Model 2) are summarised in Table 8.2.

Table 8.2: Friction, length of inception and protrusion density ratio's for Scale 1:30
Model tests

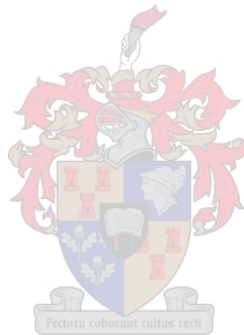
Name	Protrusion Layout	$f_{\text{protrusions}} / f_{\text{Standard Steps}}$	$L_i^{\text{Protrusions}} / L_i^{\text{Standard Steps}}$	Protrusion Density
P 1(1)		1,40	0,61	1,125
P 1(2)		1,21	0,61	1,067
P 1(3)		1,22	0,67	1,063
P 1(4)		1,17	0,79	1,083

Name	Protrusion Layout	$f_{\text{protrusions}} / f_{\text{Standard Steps}}$	$L_i \text{ Protrusions} / L_i \text{ Standard Steps}$	Protrusion Density
P 1(5)		1,03	0,83	1,083
P 2(1)		1,20	0,74	1,128
P 2(2)		1,11	0,64	1,085
P 2(3)		1,10	0,74	1,085
P 2(4)		1,05	0,69	1,085

Name	Protrusion Layout	f protrusions / f Standard Steps	L_i Protrusions / L_i Standard Steps	Protrusion Density
SS		1,00	1,00	1,00



- 1 INTRODUCTION**
- 2 LITERATURE STUDY**
- 3 REVIEW OF LITERATURE**
- 4 PHYSICAL MODELING**
- 5 RESULTS**
- 6 DISCUSSION OF RESULTS**
- 7 CONSTRUCTION ASPECTS AND COSTS**
- 8 CONCLUSIONS**



9 RECOMMENDATIONS

It is concluded that this study is a step in the right direction regarding the use of protrusions on stepped spillways to facilitate better energy dissipation and earlier air entrainment.

The following recommendations can be made regarding the use of triangular protrusions on the downstream slope of a stepped spillway:

1. Triangular protrusions should be added on the downstream slope of the stepped spillway, spaced as dense as possible, but allowing for construction joints.
2. The effectiveness of the protrusions depends on the apron or stilling basin configuration, and this must be optimised with the aid of model studies. The cost saving of the addition of protrusions can be substantial, depending on the project.
3. The addition of protrusions is recommended for a prototype unit discharge of up to $35 \text{ m}^3/\text{s.m}$. Above this unit discharge, a model study should be utilised to refine this value for unit discharge, together with the apron and stilling basin configuration.
4. Scale effects does exist on scale models. Research should be done on larger scale models (bigger than scale 1:20) to clarify the exact influence of scale and the extrapolation of model values to prototype values.
5. Further research is needed to obtain a better understanding of stepped spillways and stepped spillways with triangular protrusions. This should be done in a laboratory capable of yielding a unit discharge of at least $0,5 \text{ m}^3/\text{s.m}$.
6. Alternative energy dissipation measures should also be investigated, including more lateral deflection options.

REFERENCES

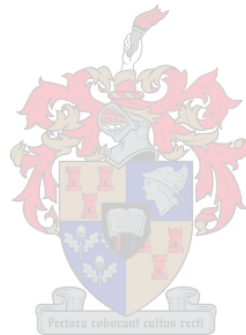
1. Bayat HO: **Stepped spillway feasibility investigation**. Proceedings of 17th ICOLD Congress, Vienna, Austria, 1991.
2. Boes RM and Minor HE: **Hydraulic Design of Stepped Spillways for RCC Dams**. Hydropower and Dams, 2002.
3. Boes RM and Minor HE: **Guidelines for the Hydraulic Design of Stepped Spillways**. Hydraulics of Stepped Spillways, AA Balkema, 2000.
4. Boes RM: **Scale Effects in Monitoring Two-phase Stepped Spillway Flow**. Hydraulics of Stepped Spillways, AA Balkema, 2000.
5. Cain P and Wood IR: **Measurements of Self-Aerated Flow on a Spillway**. Journal of the Hydraulics Division, ASCE, 1981.
6. Chamani MR and Rajaratnam N: **Characteristics of Skimming Flow over Stepped Spillways**. Journal of Hydraulic Engineering, 1999.
7. Chamani MR: **Air Inception in Skimming Flow Regime over Stepped Spillways**. Hydraulics of Stepped Spillways, AA Balkema, 2000.
8. Chanson H: **Hydraulics of Stepped Spillways and Cascades**. AA Balkema, 2002.
9. Chanson H: **State of the Art of the Hydraulic Design of Stepped Chute Spillways**. Hydropower and Dams, 1994.
10. Chanson H, Yasuda Y and Ohtsu I: **Flow Resistance in Skimming Flow: A Critical Review**. Hydraulics of Stepped Spillways, AA Balkema, 2000.
11. Chanson H: **Drag Reduction in Skimming Flow on Stepped Spillways by Aeration**. Journal of Hydraulic Research, 2004.

12. Chanson H: **Hydraulic Design of Stepped Cascades, Channels, Weirs and Spillways**. Pergamon Press, 1994.
13. Chatila JG and Jurdi BR: **Stepped Spillway as an Energy Dissipater**. Canadian Water Resources Journal, 2004.
14. Chemaly, AG; **Principles of Dam Engineering – Spillways**. University of Pretoria, 2001.
15. Chow, VT; **Open-Channel Hydraulics**. McGraw-Hill Incorporated, Singapore, 1959.
16. Christodoulou GC: **Design of Stepped Spillways for Optimal Energy Dissipation**. Hydropower and Dams, 1999.
17. Diez-Cascon J, Blanco JL, Revilla J and Garcia R: **Studies on the Behaviour of Stepped Spillways**. Water Power and Dam Construction, 1991.
18. Druyts FHWM: **Fill Dams**. Applied Geomechanics Course, University of Stellenbosch, 6 – 10 June 2005.
19. DWAF: **Dam Safety Regulations**. Government Notice No 10366, Volume 253. Department of Water Affairs (DWAF). Pretoria, 1986.
20. DWAF: **ORWRDP: De Hoop Dam: Hydraulic Model Study**. Report No 20/2/B400-26/C/1/4-10. Pretoria, 2006.
21. Elviro V and Mateos C: **Spanish Research into Stepped Spillways**. Hydropower and Dams, 1995.
22. Fahlbusch H: **Historical Dams Foundation of the Future Rests on the Achievements of the Past**. International Commission on Irrigation and Drainage, India, 1st Edition, 2001.
23. Ferrando AM and Rico JRR: **On the Incipient Aerated Flow in Chutes and Spillways**. Journal of Hydraulic Research, 2002.
24. Frantino U and Piccinni AF: **Dissipation Efficiency of Stepped Spillways**. Hydraulics of Stepped Spillways, AA Balkema, 2000.

25. French National Research Project BaCaRa; **Roller Compacted Concrete: RCC Dams**. Presses Ponts et Chaussées, Paris, 1997.
26. Geringer JJ; **The Design and Construction of RCC Dams in Southern Africa**. Department of Water Affairs (DWAf). Proceedings of the International Symposium on Roller Compacted Concrete Dams, Volume 3. Santander, Spain, 2 -4 October 1995.
27. Henderson FM: **Open Channel Flow**, MacMillan, New York, 1966.
28. Hollingworth F and Druyts FHWM: **The Development of Rollcrete in South-Africa**. FIP Congress, Hamburg, Germany, May 1990.
29. Keller RJ and Rastogi AK: **Design Chart for Predicting Critical Point on Spillways**. Journal of the Hydraulics Division, 1977.
30. Matos J, Quintela A, Sanchez Juny M and Dolz J: **Air Entrainment and Safety against Cavitation Damage in Stepped Spillways over RCC Dams**. Hydraulics of Stepped Spillways, Balkema, 2000.
31. Matos J: **Emulsionamento de ar e dissipação de energia do escoamento em descarregadores em degraus (“Air entrainment and energy dissipation on stepped spillways”)**. Research Report, IST Lisbon (In Portuguese), 1999.
32. Minor H-E and Hager WH: **Hydraulics of Stepped Spillways**. AA Balkema, Rotterdam, 2000.
33. Ohtsu I, Yasuda Y and Takahashi M: **Flow Characteristics of skimming Flows in Stepped Channels**. Journal of Hydraulic Engineering, 2004.
34. Pegram GGS, Officer AK and Mottram SR: **Hydraulics of Skimming Flow on Modeled Stepped Spillways**. Journal of Hydraulic Engineering, 1999.
35. Pinto NL de S: **Model evaluation of aerators in shooting flow**. Proceedings of IAHR Symposium on Scale Effects in Modeling Hydraulic Structures, Germany, 1984.

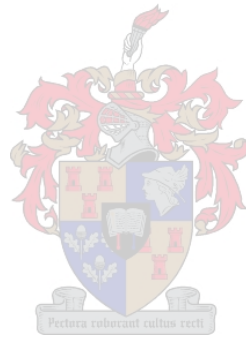
36. Rajaratnam N: **Skimming Flow in Stepped Spillways**. Journal of Hydraulic Engineering, 1990.
37. SANCOLD: **Guidelines on Safety in Relation to Floods**. Report No. 4, Pretoria, 1990.
38. SANCOLD: **Interim Guidelines on Freeboard for Dams**. Report No 3, Pretoria, 1990.
39. Schnitter NJ; **A History of Dams - The Useful Pyramids**. AA Balkema, Rotterdam, 1994.
40. Shand MJ; **Design of Spillways and Outlet Works for Dams**. Planning, Design and Management of Dams Course, University of Stellenbosch, 24 - 26 January 2005.
41. Speerli J: **Strömungsprozesse in Grundablassstollen Flow phenomena in bottom outlets**. Doctoral Dissertation, ETH Zürich, Germany, 1999.
42. Stephenson D: **Energy Dissipation down Stepped Spillways**. Water Power and Dam Construction, 1991.
43. Tozzi MJ: **Residual Energy in Stepped Spillways**. International Water Power and Dam Construction, 1994.
44. USBR: **Design of Small Dams**. Bureau of Reclamation, 1987.
45. US Army Corps of Engineers: **Roller-Compacted Concrete**. Department of the Army, US Army Corps of Engineers, Washington DC, EM 1110-2-2006, 2000.
46. Van Deventer NJ: **Utilizing Lateral Deflection to Improve Energy Dissipation on Stepped Spillways**. M. Eng Thesis, University of Pretoria, 2006.
47. Van Deventer NJ: **Personnel Communication**. 2006.
48. Vischer DL and Hager WH: **Energy Dissipaters**. AA Balkema, Rotterdam, 1995.
49. Wood IR, Ackers P and Loveless J: **General Method for Critical Point on Spillways**. Journal of Hydraulic Engineering, 1983.

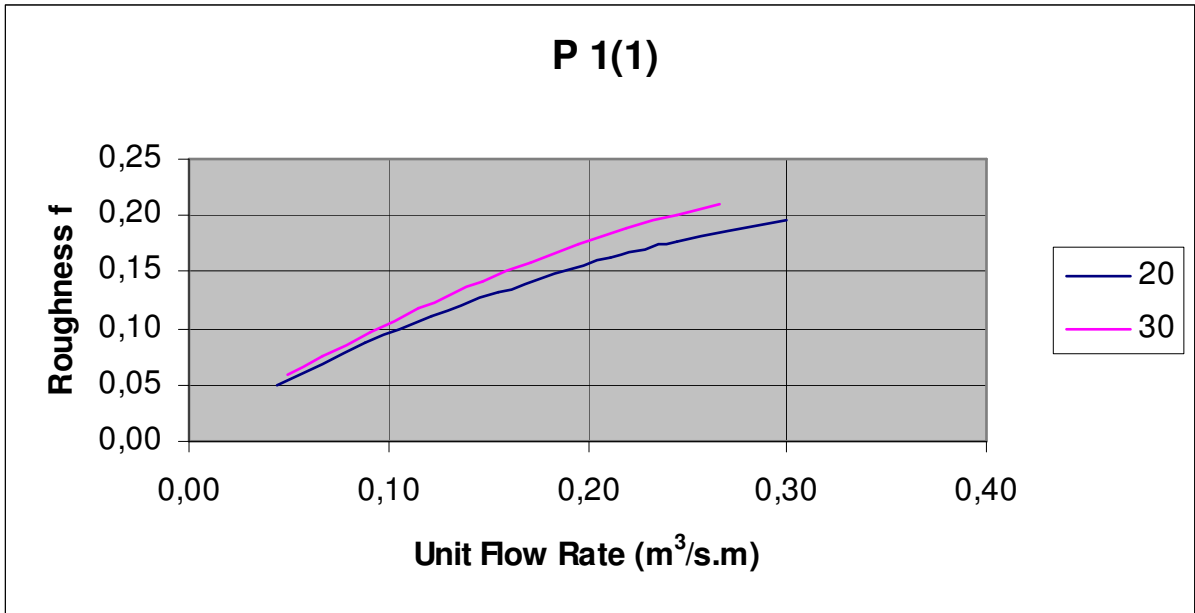
50. Yildiz D and Kas I: **Hydraulic Performance of Stepped Chute Spillways**. Hydropower and Dams, 1998.



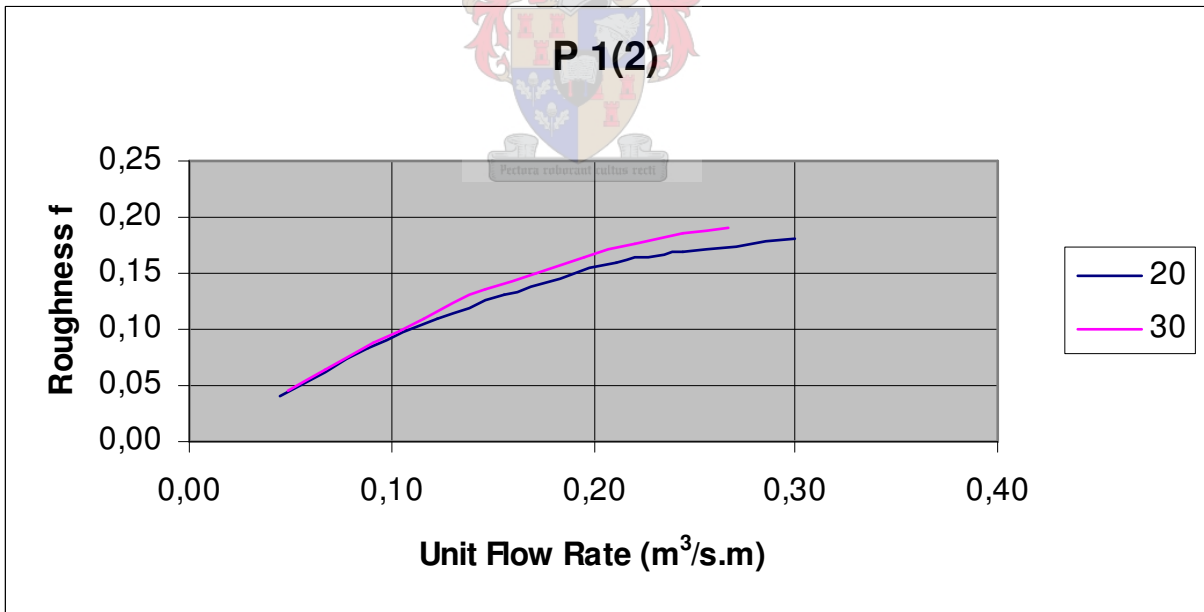
APPENDIX A

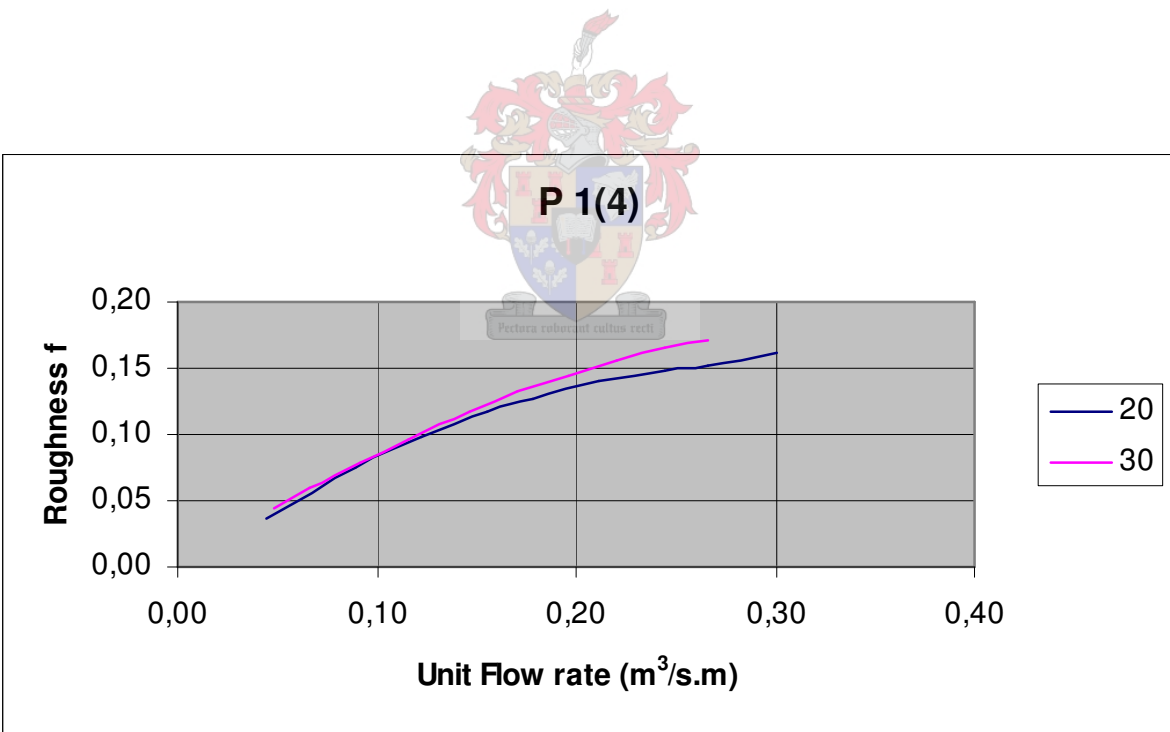
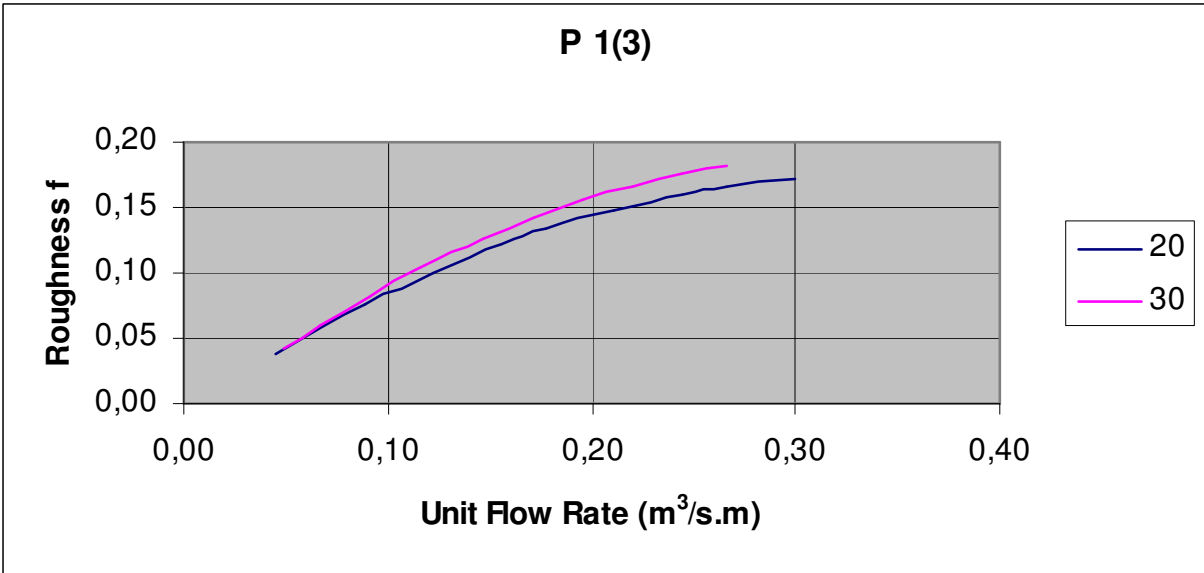
Graphs

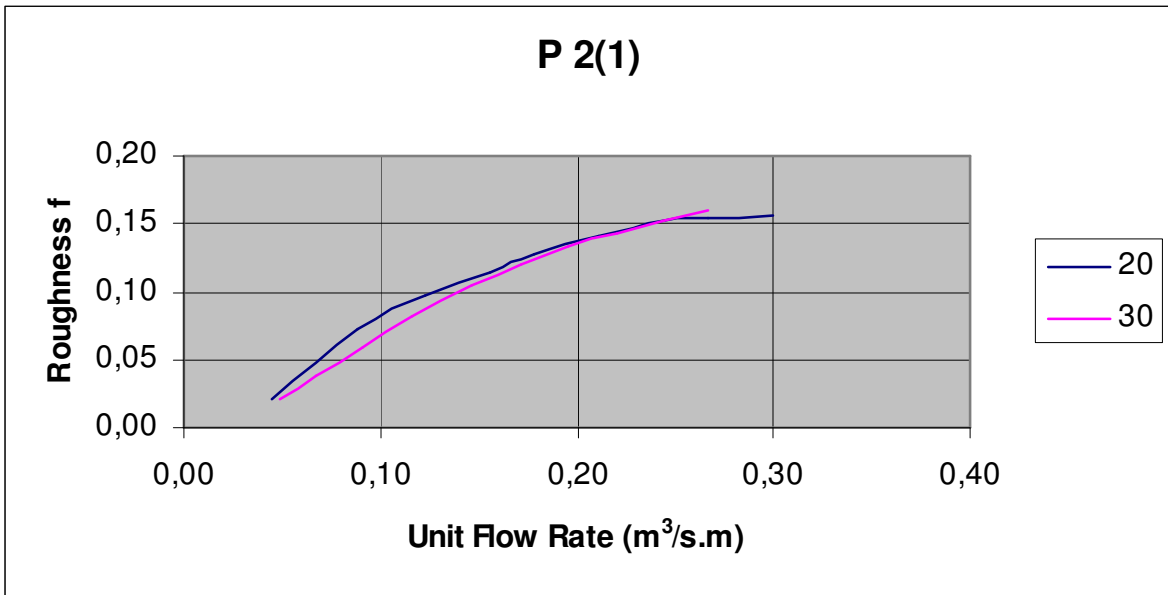




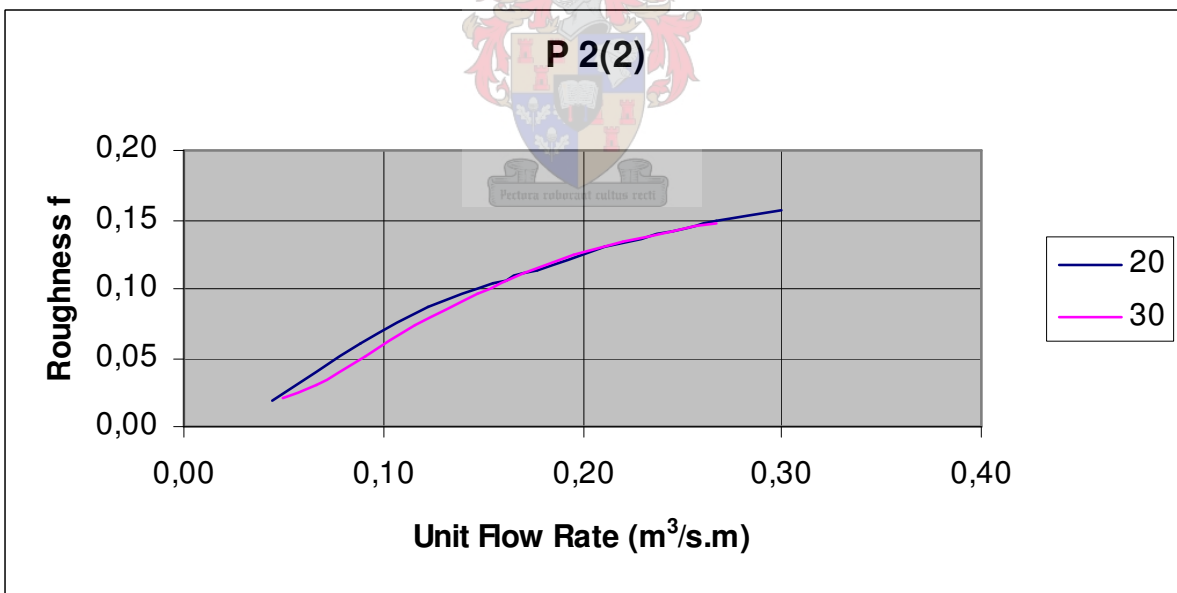
The roughness of these two cannot be compared. Refer to the configurations set out in Chapter 4.



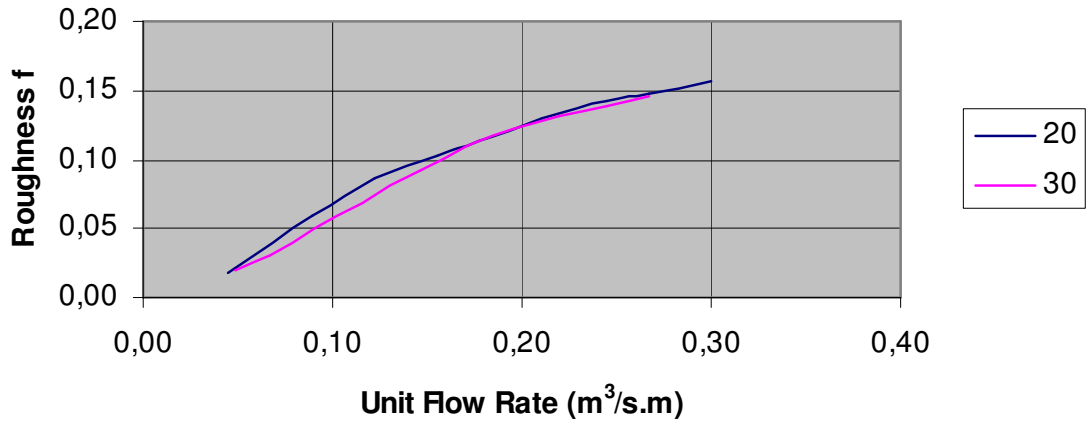




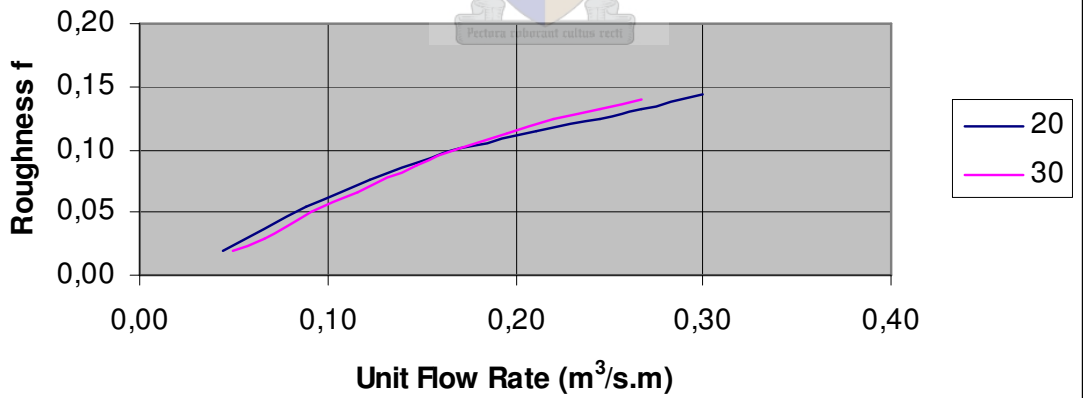
The roughness of these two cannot be compared. Refer to the configurations set out in Chapter 4.

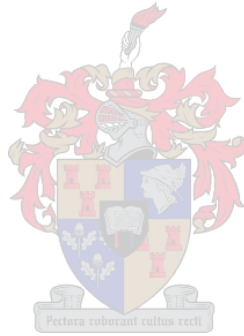
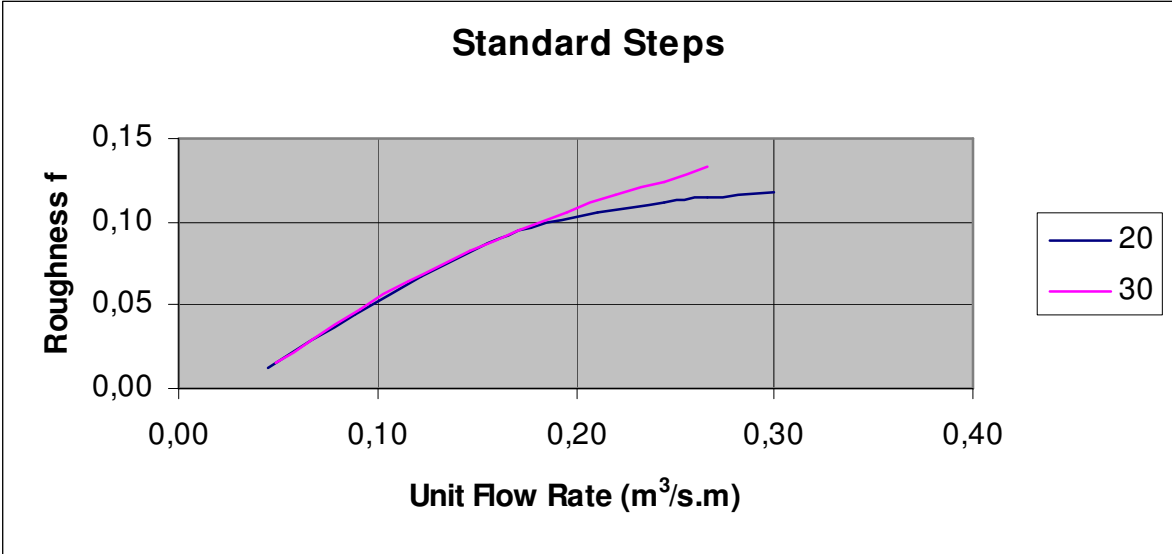


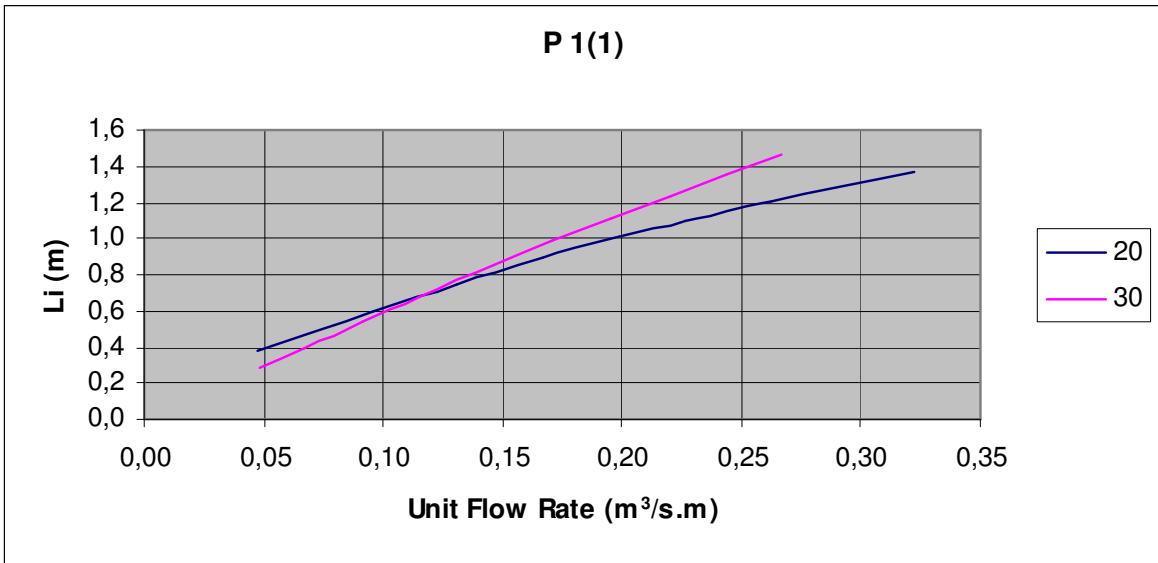
P 2(3)



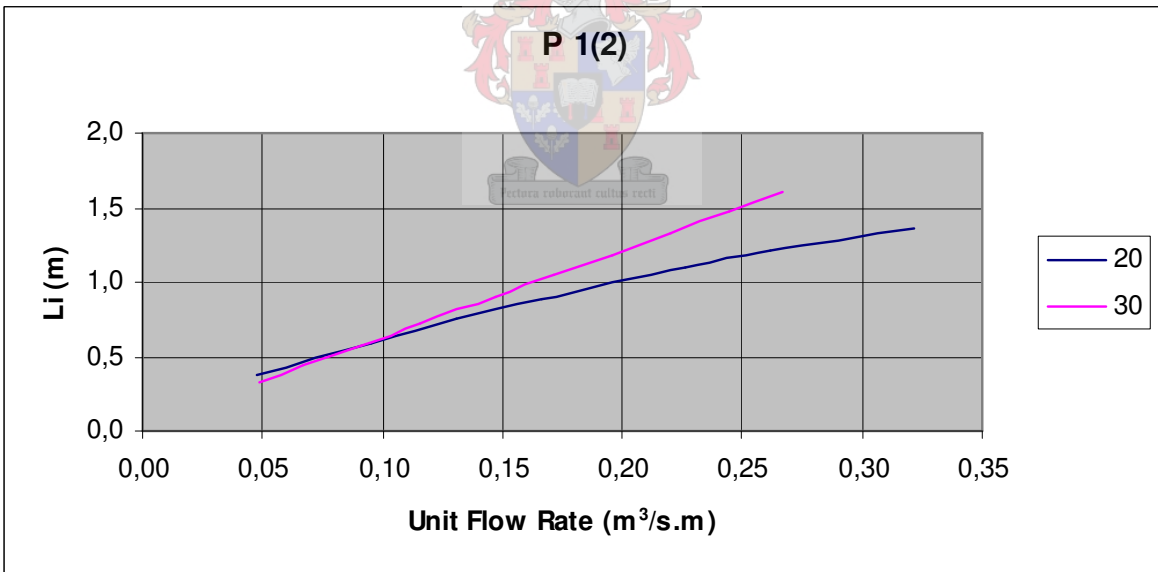
P 2(4)



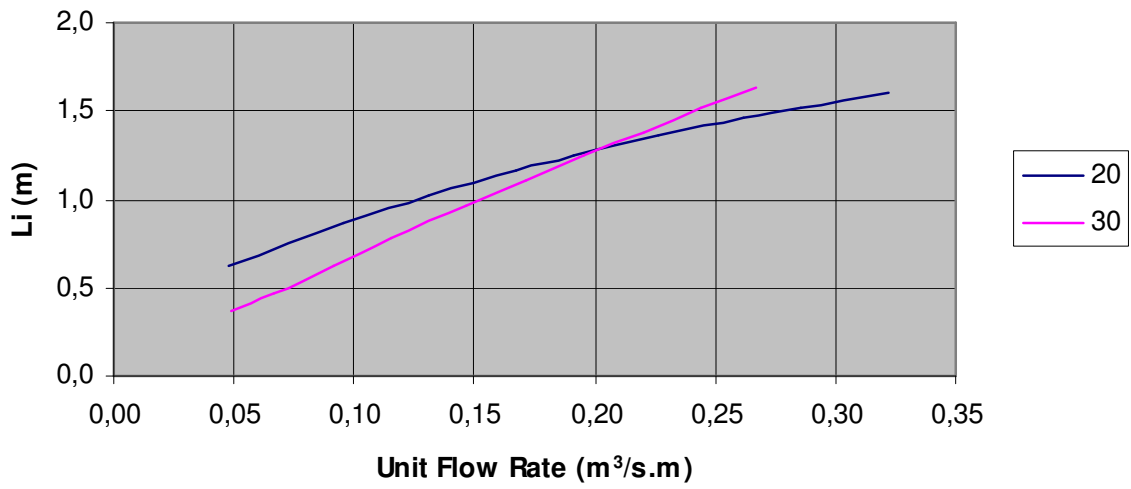




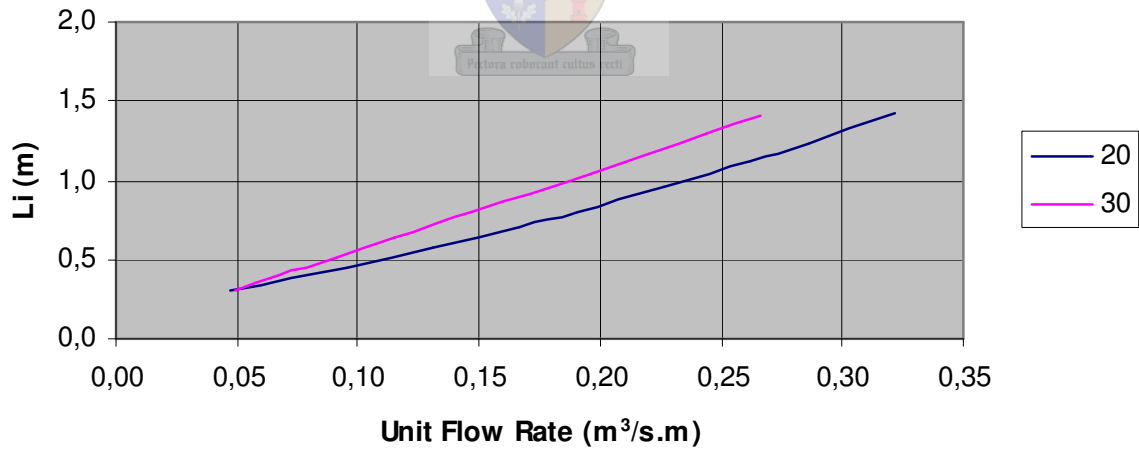
The length of inception of these two cannot be compared. Refer to the configurations set out in Chapter 4.

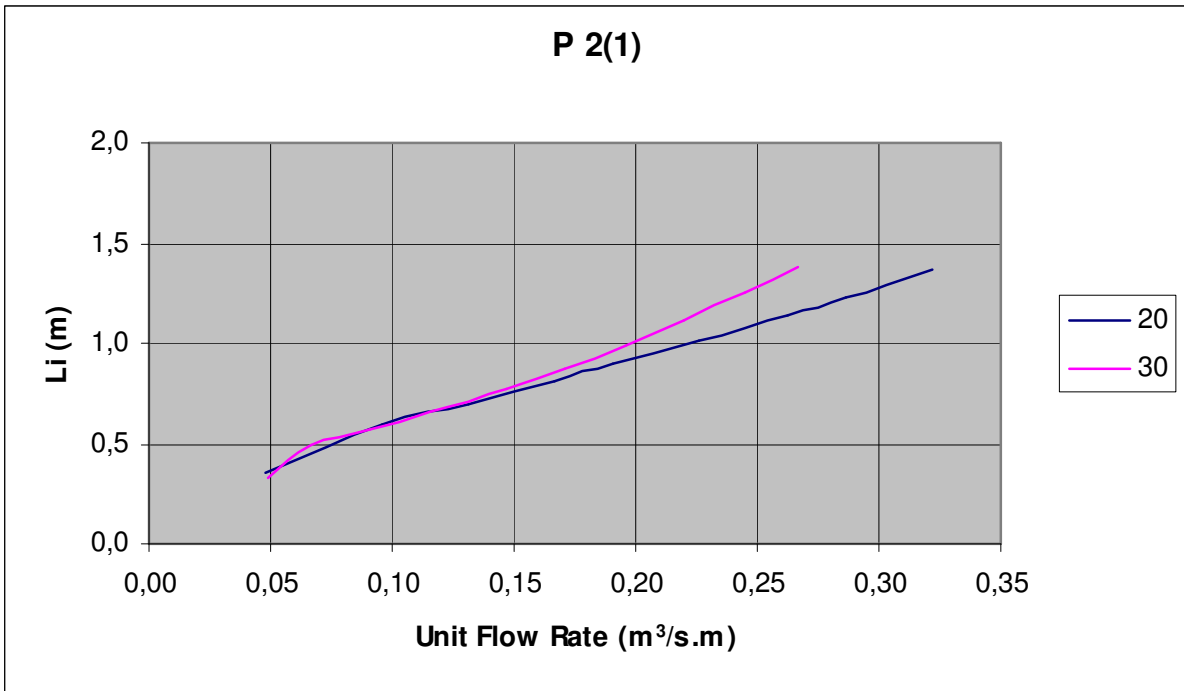


P 1(3)

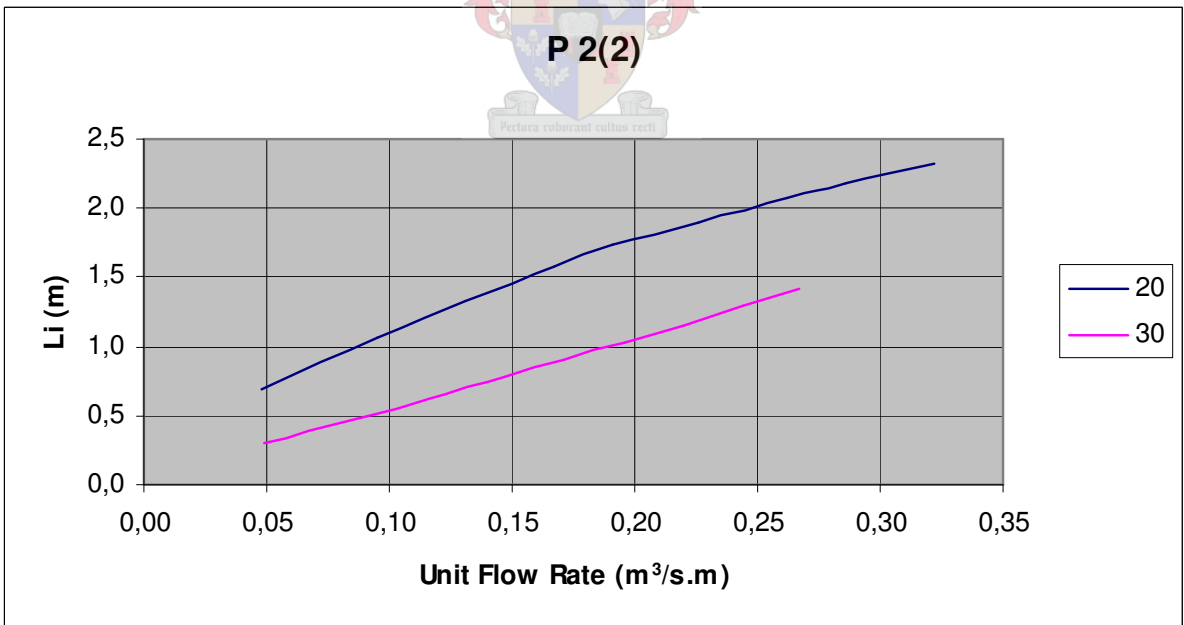


P 1(4)

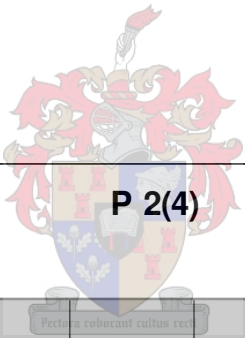
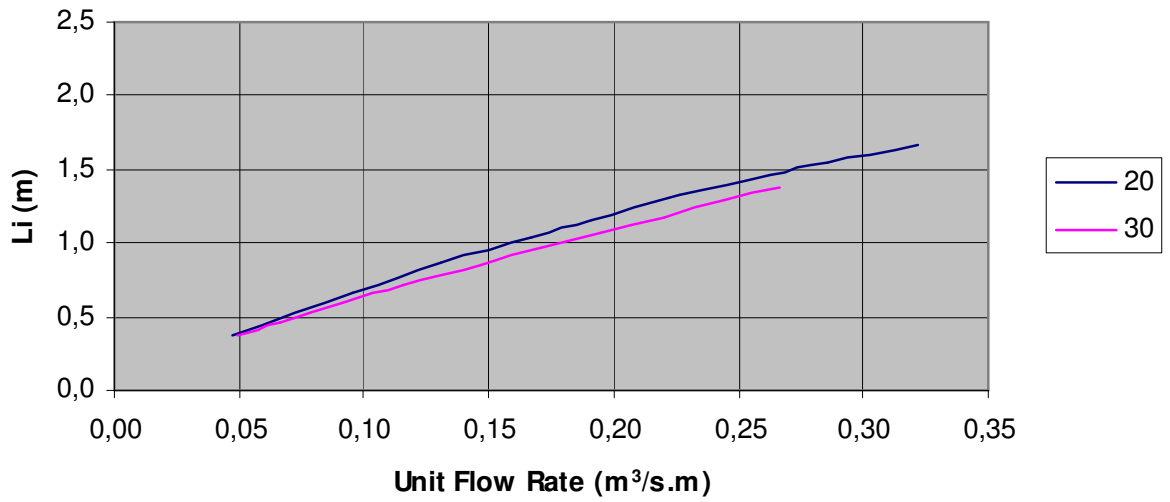




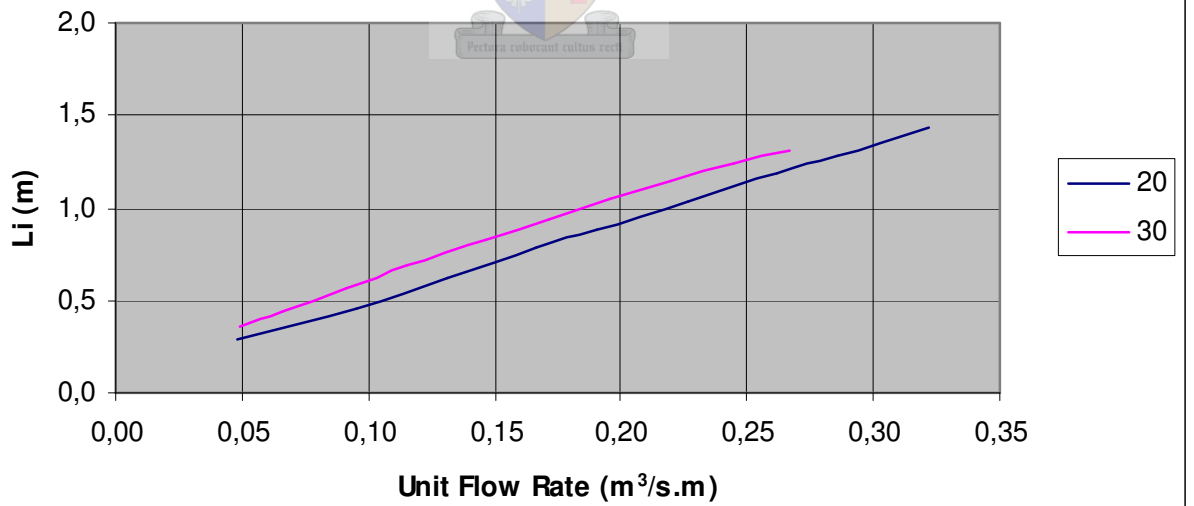
The length of inception of these two cannot be compared. Refer to the configurations set out in Chapter 4.

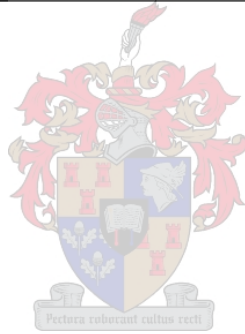
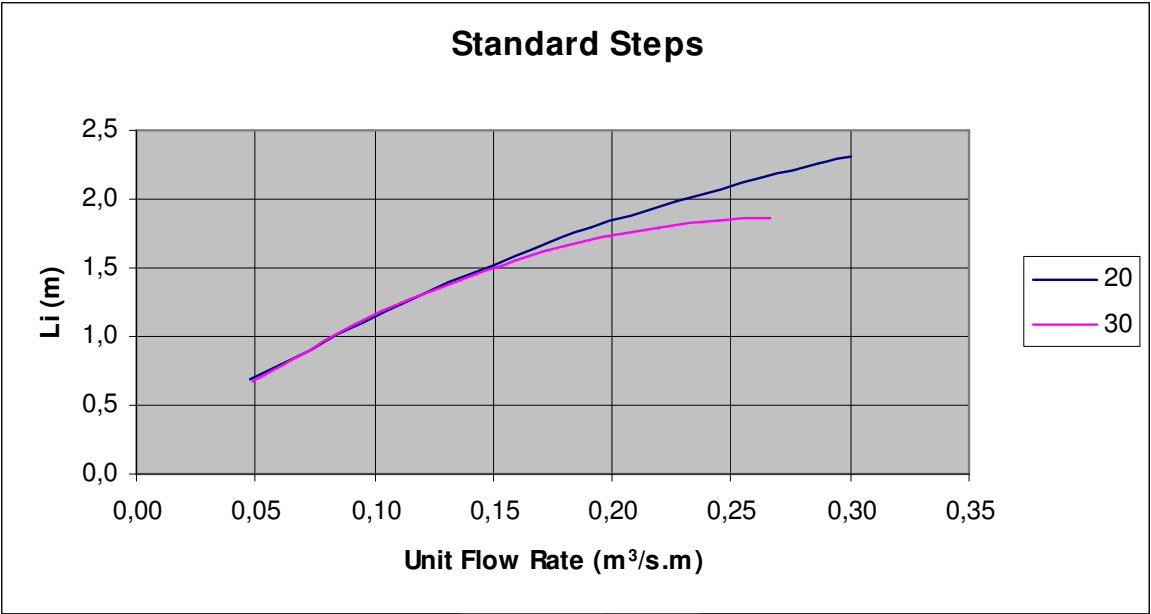


P 2(3)



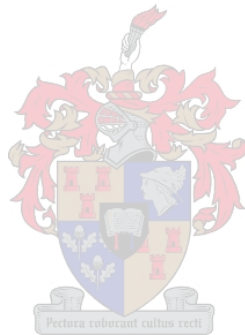
P 2(4)





APPENDIX B

Crest Profile and Apron and End Sill of Proposed De Hoop Dam



Crest profile and apron and end sill of proposed De Hoop Dam

Crest shape:

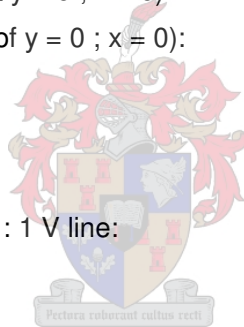
$$X^n = k \times H_d^{n-1} \times y$$

Where:

k and n = constants, whose values depend on the upstream inclination, flow depth and velocity of approach, and H_d = design head.

The profile parameters are (refer to Figure B1):

Design head:	$H_d = 5,0$ m
Constants:	$k = 2,0$ $n = 1,85$
Parabolic curve profile (crest at $y = 0$; $x = 0$):	$Y = 0,127 X^{1,85}$
Parameters (curves upstream of $y = 0$; $x = 0$):	$x_1 = 1,410$ m $x_2 = 0,525$ m $R_1 = 2,500$ m $R_2 = 1,000$ m
Point of intersection with 0,8 H : 1 V line:	$x_a = 7,125$ m $Y_a = 4,815$ m



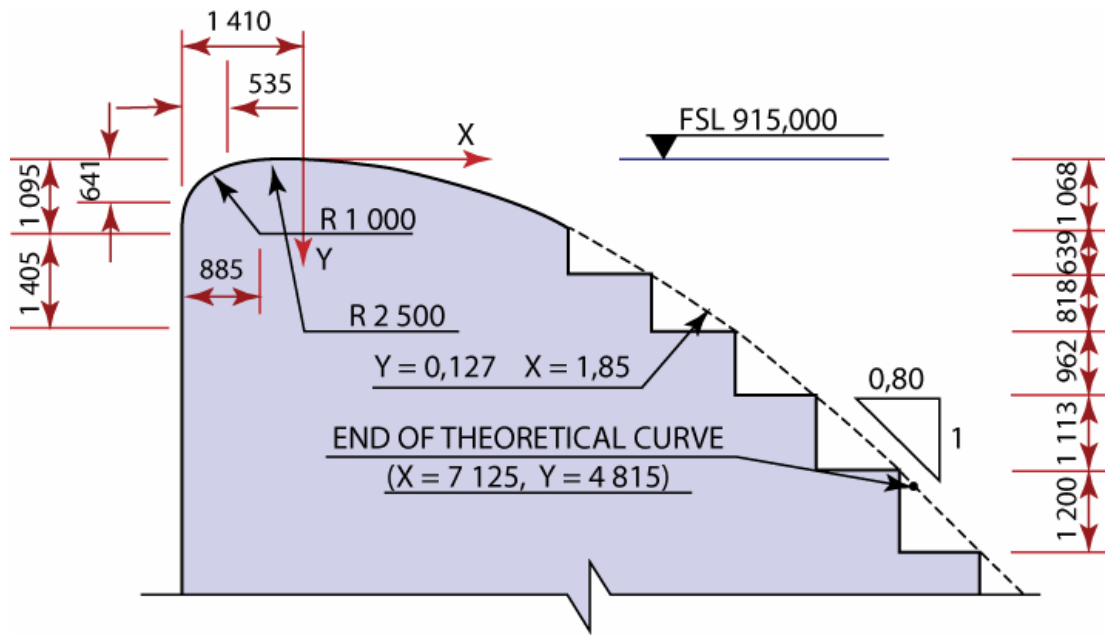
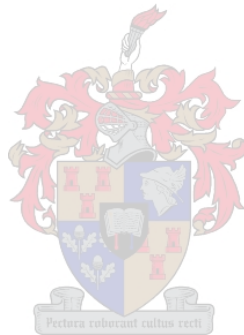


Figure B1: Spillway Crest Profile



The layout of the Apron is shown in Figure B2.

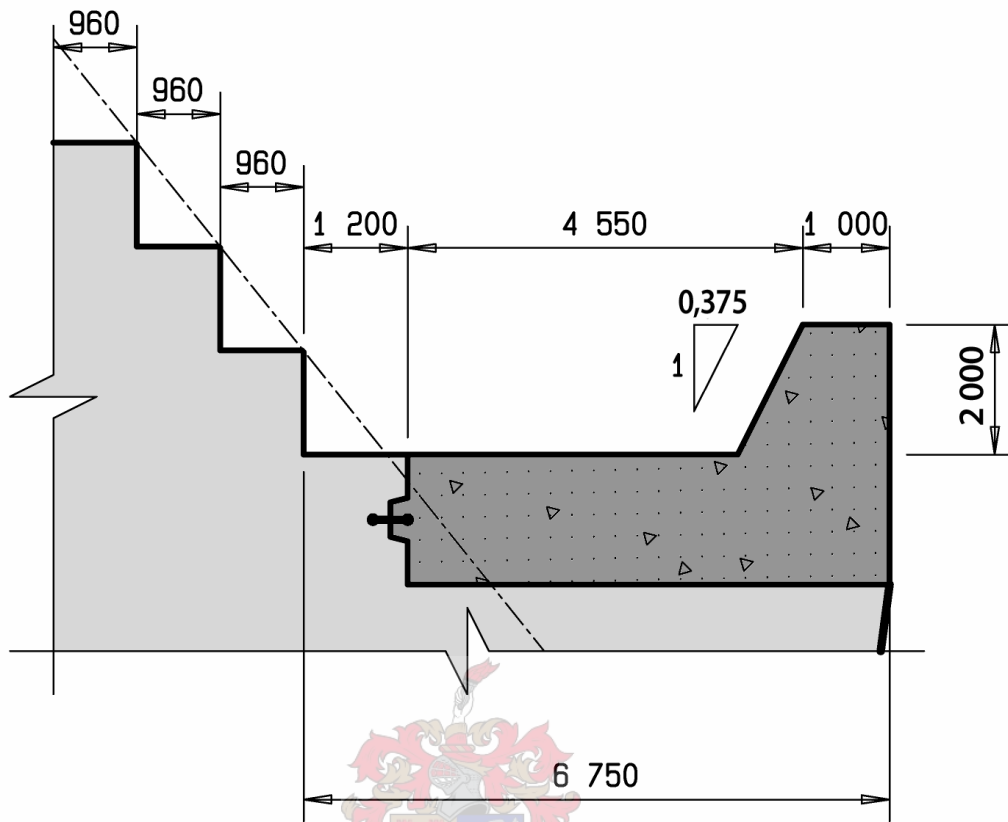
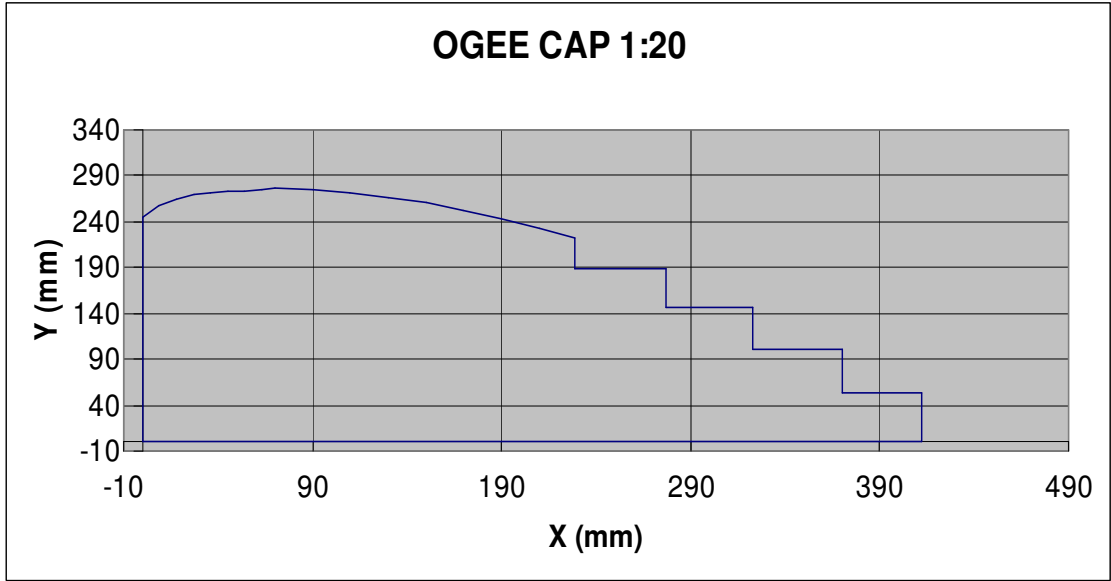
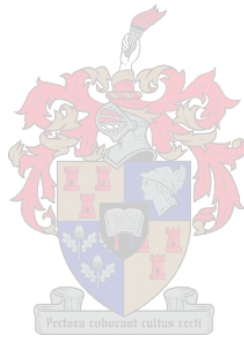


Figure B2: Apron and end sill dimensions

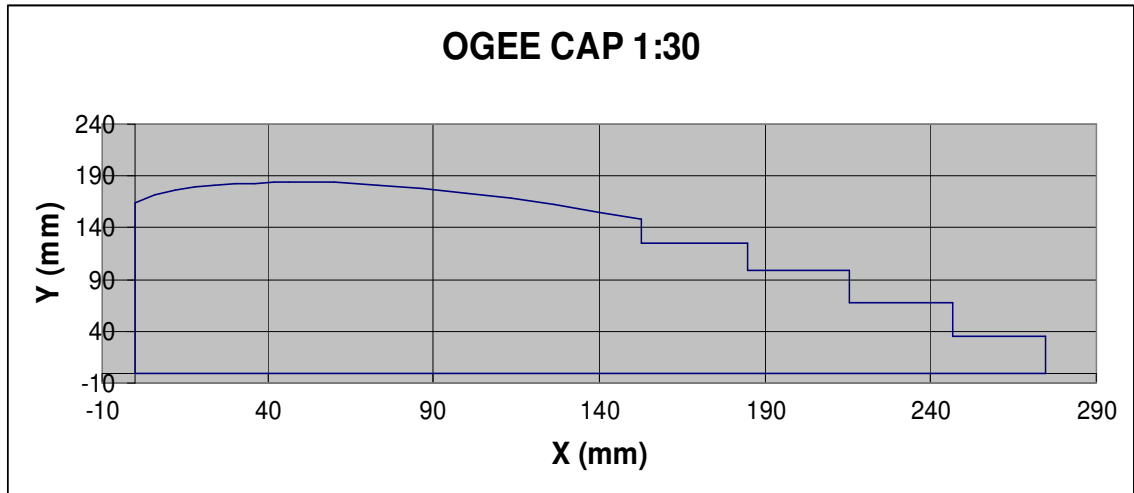
Ogee Cap for 1:20 Scale Model



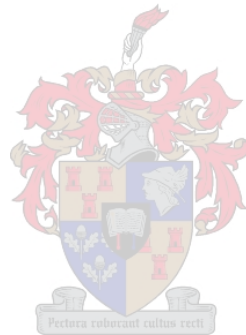
X	Y
0	0
0	245
9	257
18	264
27	269
36	272
45	273
54	274
63	275
70	276
90	275
110	271
130	267
150	260
170	252
190	243
210	232
229	222
229	188
277	188
277	147
323	147
323	101
370	101
370	53
412	53
412	0
0	0



Ogee Cap for 1:30 Scale Model

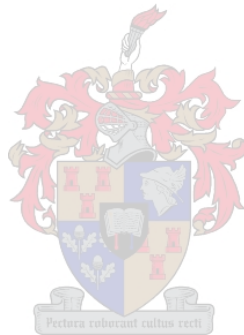


X	Y
0	0
0	163
6	171
12	176
18	179
24	181
30	182
36	183
42	183
47	184
60	183
73	181
87	178
100	173
113	168
127	162
140	155
153	148
153	125
185	125
185	98
215	98
215	67
247	67
247	35
275	35
275	0
0	0



APPENDIX C

Photographs





Scale 1:60 3 Dimensional Model for De Hoop Dam: Spillway and Left Bank Non-overspill Crest



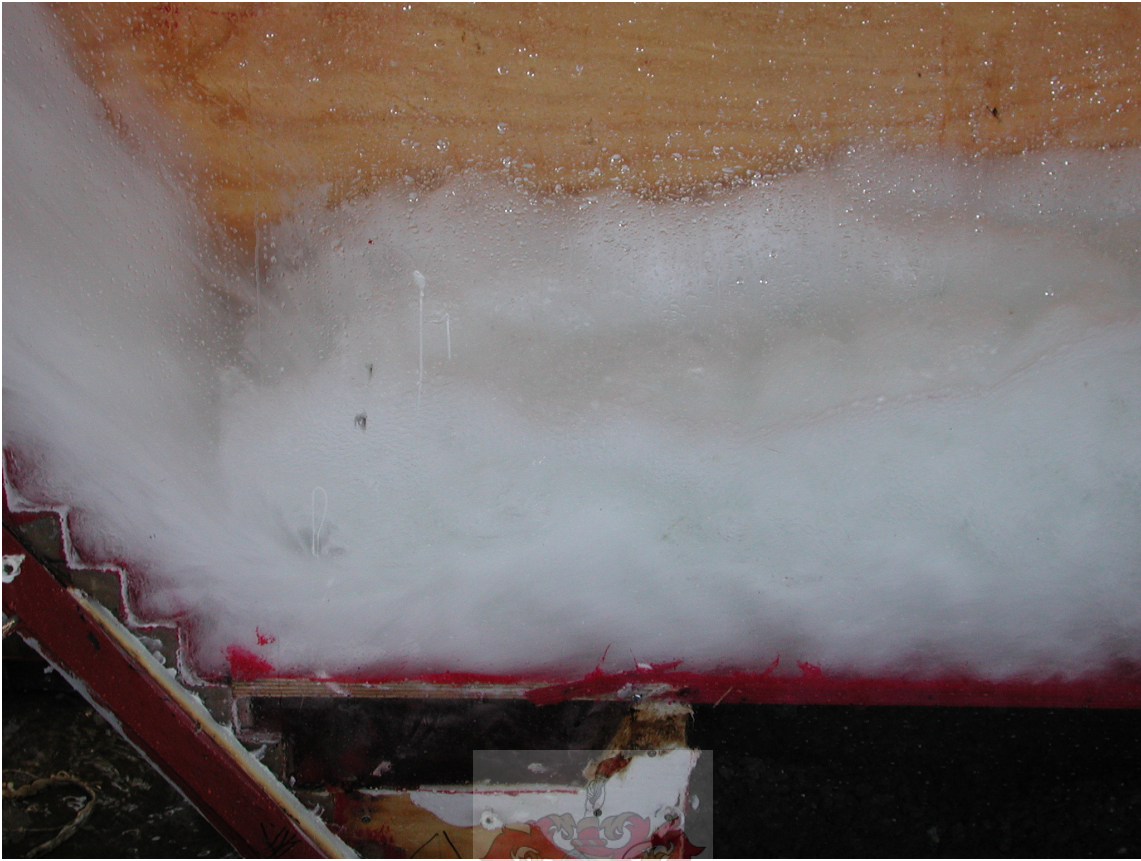
Scale 1:60 3 Dimensional Model for De Hoop Dam: Spillway



Scale 1:20 2 Dimensional Model: Skim flow



1:20 Scale 2 Dimensional Model: Shutter board at model on top of apron



1:20 Scale 2 Dimensional Model: Hydraulic jump



1:20 Scale 2 Dimensional Model: Flow

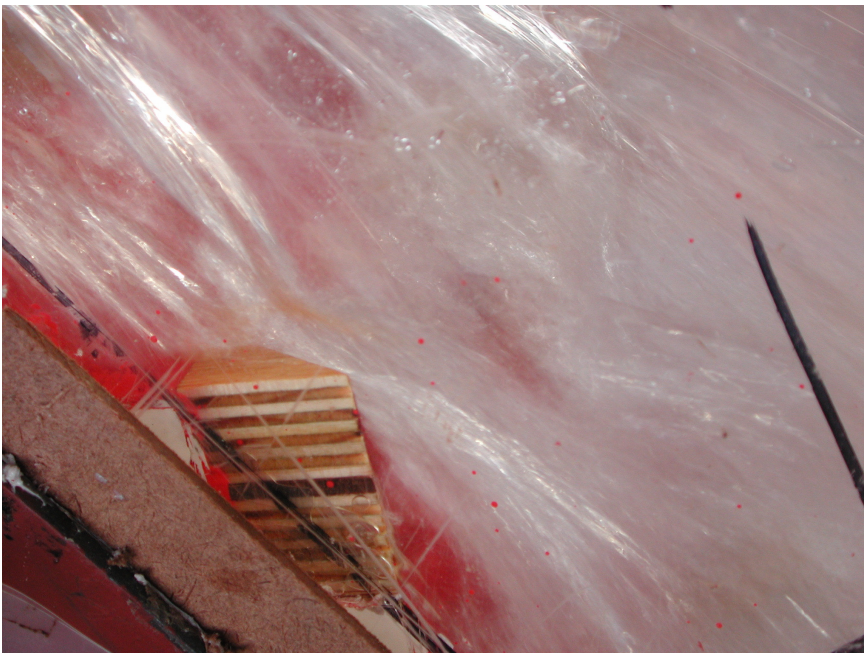


Scale 1:30 2 Dimensional Model: Scour testing with apron and end sill at Recommended Design Flood





1:30 2 Dimensional Scale Model: Low flow (View 1)



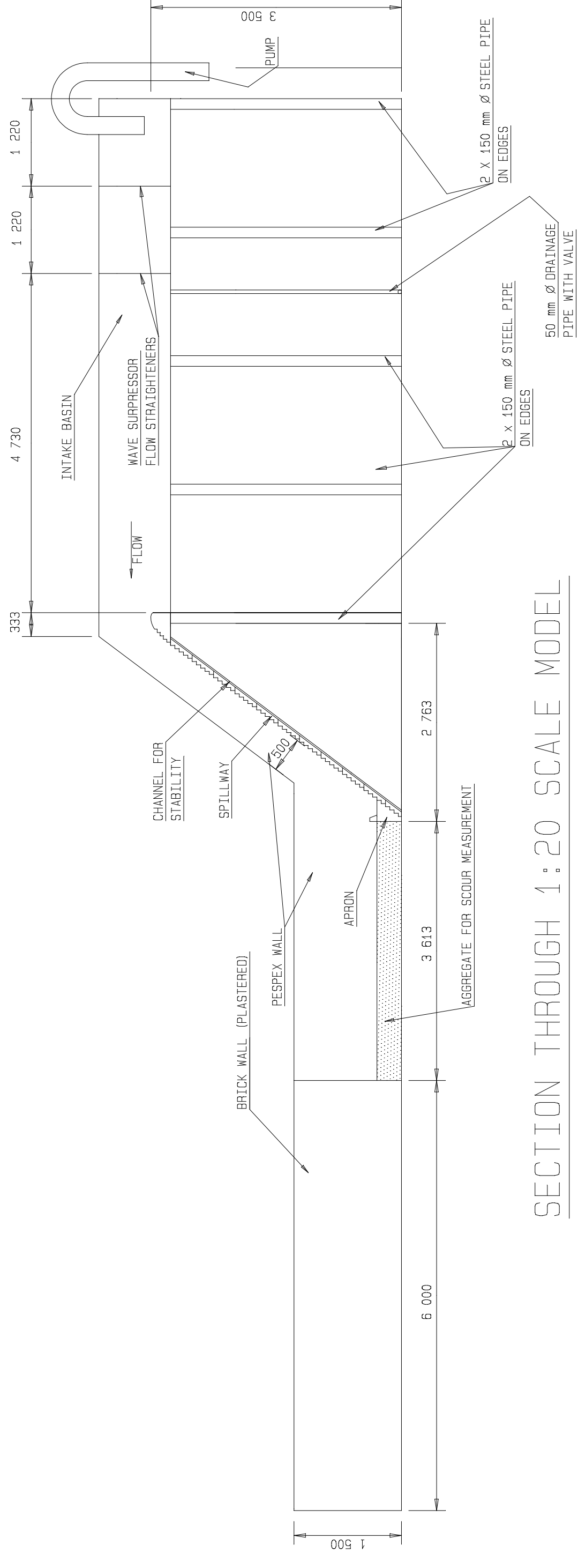
1:30 2 Dimensional Scale Model: Low flow (View 2)



1:30 2 Dimensional Scale Model: Low flows

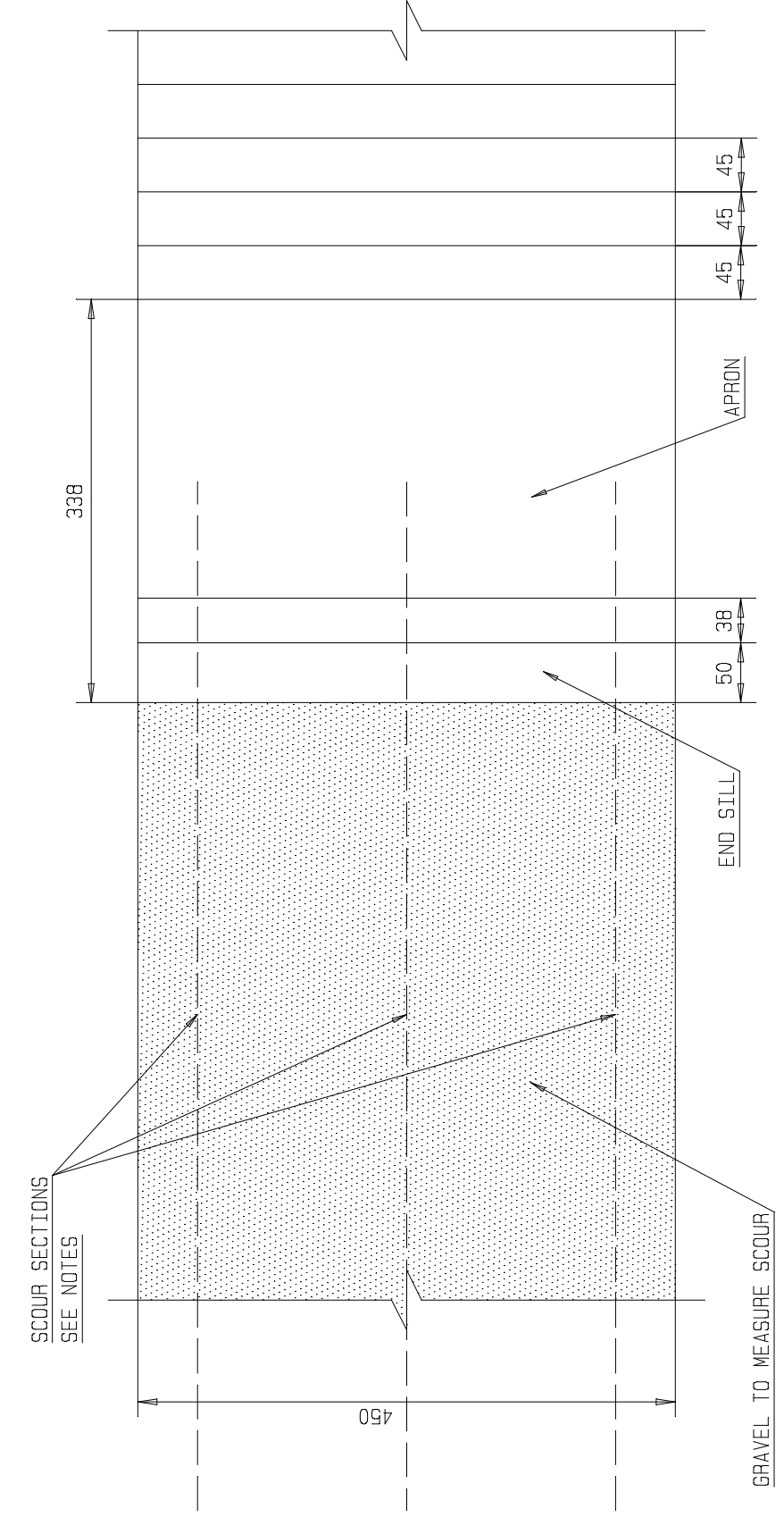


1:30 2 Dimensional Scale Model: Point of Inception



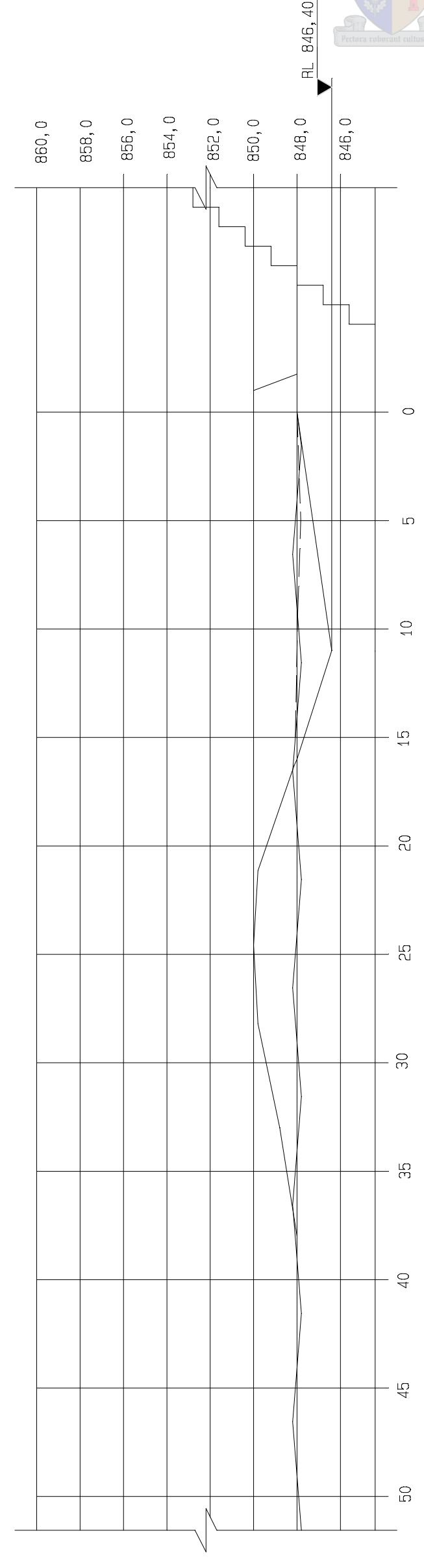
SECTION THROUGH 1:20 SCALE MODEL

SCALE 1:50



PLAN VIEW OF STEPS, APRON AND GRAVEL

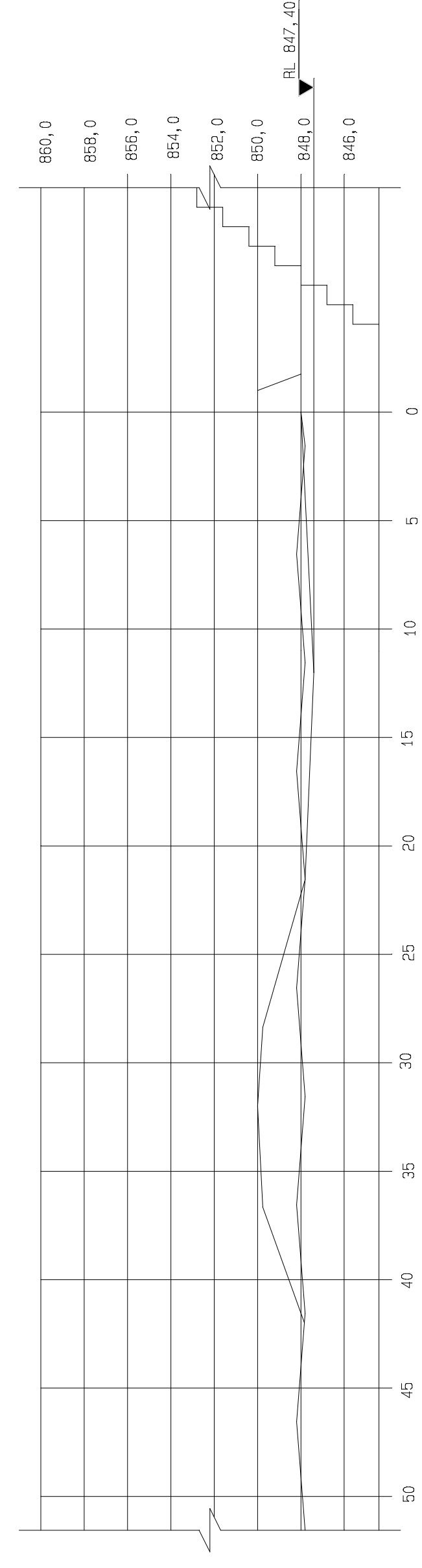
SCALE 1:5



SCOUR

(IND PROTRUSIONS)

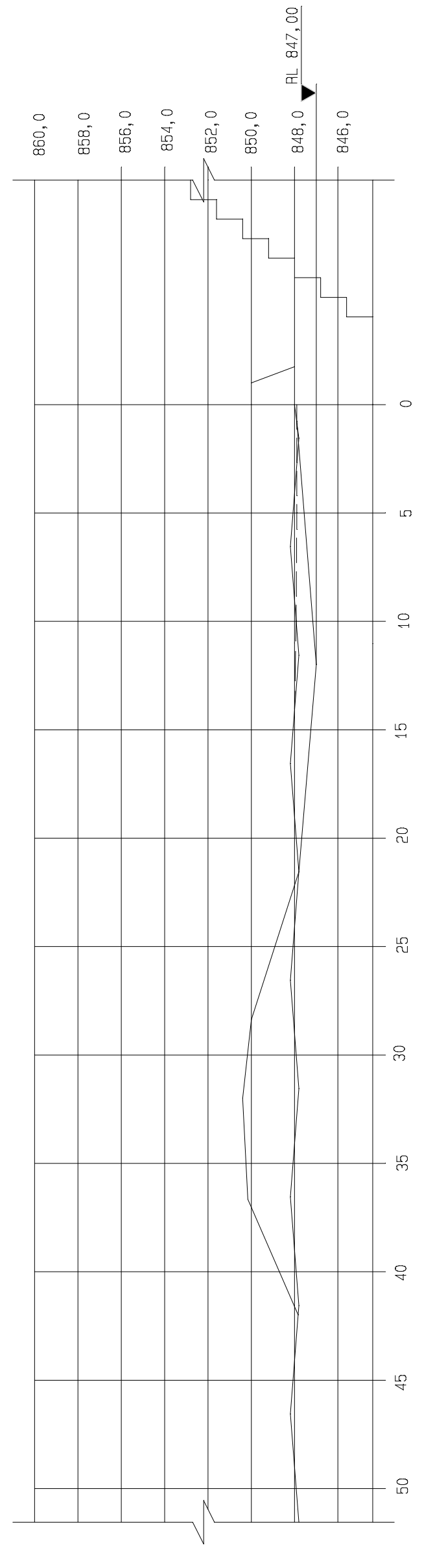
SCALE 1:10



SCOUR

(PROTRUSIONS CONFIGURATION 1)

SCALE 1:10

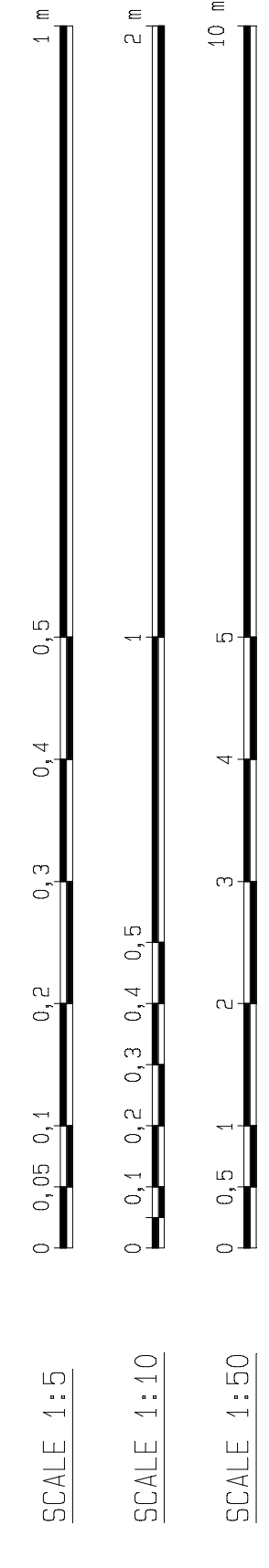
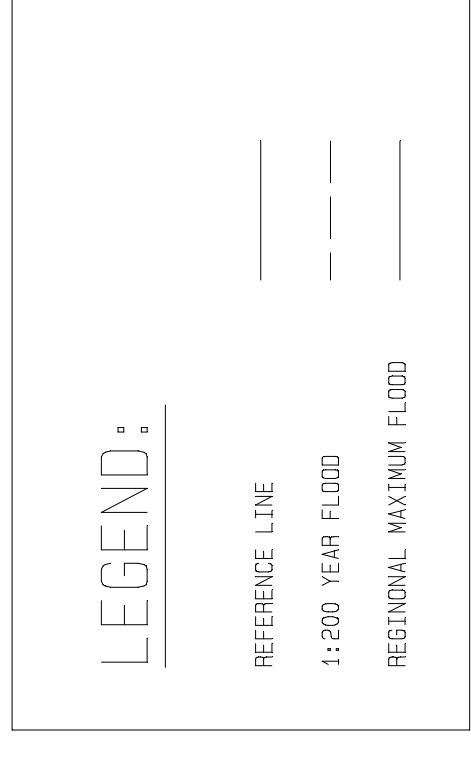


SCOUR

(PROTRUSIONS CONFIGURATION 2)

SCALE 1:10

- NOTES:
1. SEE DRG. REG. NO. X FOR PROTRUSIONS CONFIGURATION.
 2. SEE DRG. REG. NO. X FOR RESULTS OF 1:60 SCALE MODEL.
 3. SEE DRG. REG. NO. X TO FOR RESULTS OF 1:30 SCALE MODEL.
 4. 3 SCOUR SECTIONS WERE MEASURED, WITH THE WORST SCOUR TAKEN AS THE RULING ONE.
 5. MINIMAL SCOUR WAS OBSERVED FOR THE 1:200 YEAR FLOOD.
 6. PROTRUSION 1 CONFIGURATION 1 IS THE OPTIMAL.

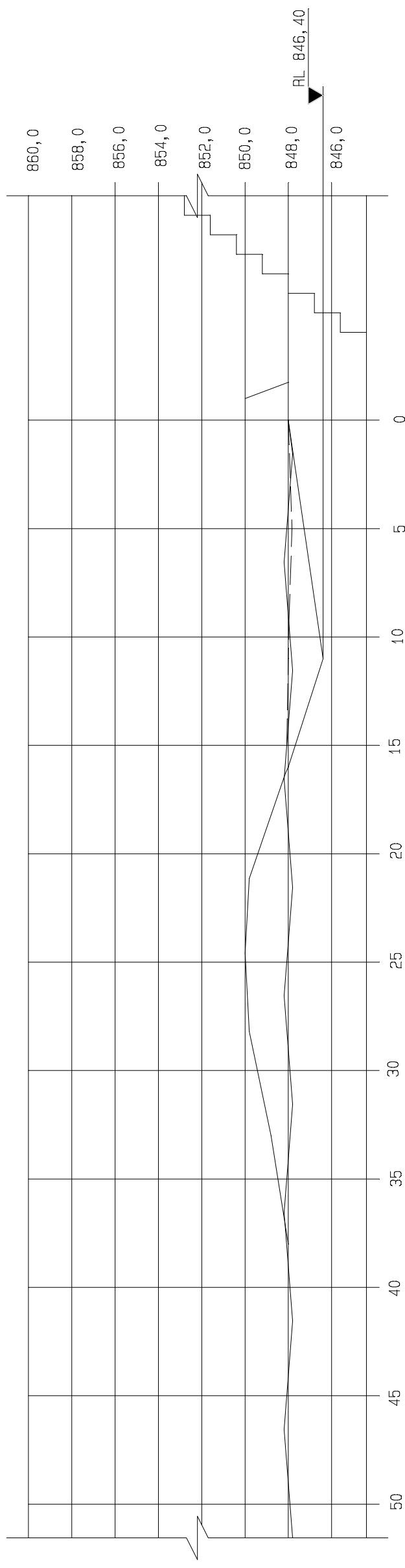


MOD. NO.	DATE	REVISION	DESCRIPTION	FOR	DWA
			PRELIMINARY		

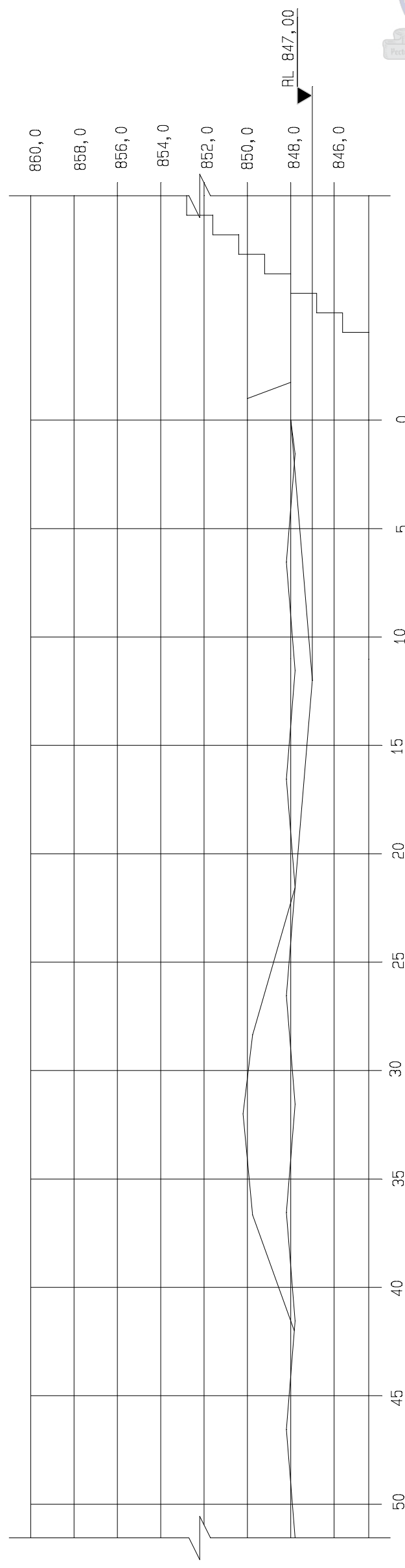
DEPARTMENT OF WATER AFFAIRS AND FORESTRY HEAD OFFICE CIVIL DESIGN PRIVATE BAG X313 PRETORIA 0001		DEPARTMENT OF WATER AFFAIRS AND FORESTRY REPUBLIC OF SOUTH AFRICA OLIFANTS RIVER WATER RESOURCES DEVELOPMENT PROJECT	
DESIGNER: HJ WRIGHT DRAWN: HJ WRIGHT		DE HOOP DAM 2D MODEL STUDY: SCALE 1:20 SCOUR MEASUREMENTS	
CHECKER: HJ WRIGHT ENGINEER: HJ WRIGHT		DISTRICT: SECHUKHUNE TENDER NO.: - CONTRACT NO.: -	
APPROVED: [Signature] RANK: -		PROVINCE: LIMPPOPO DIRECTOR: - CALCULATION FILE: -	
J. STANDANE DIRECTOR GENERAL		SHEET 1 OF 2 REG. NO. X	

2/2	2D MODEL: SCALE 1:20- SCOUR MEASUREMENTS	OTHER NO.	REG. NO.
			X

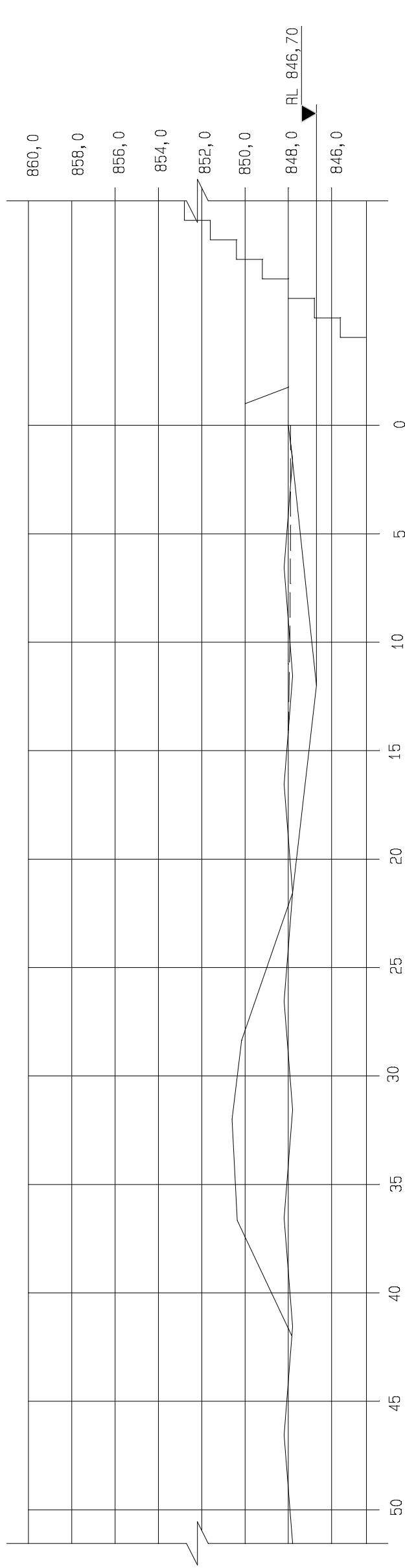
LIST OF DRAWINGS



SCOUR
(NO PROTRUSIONS)
SCALE 1:10



SCOUR
(PROTRUSIONS CONFIGURATION 4)
SCALE 1:10



SCOUR
(PROTRUSIONS CONFIGURATION 3)
SCALE 1:10

LEGEND:

REFERENCE LINE	—
1:200 YEAR FLOOD	—
REGIONAL MAXIMUM FLOOD	—

- NOTES:**
1. SEE DRG. REG. NO. X FOR PROTRUSIONS CONFIGURATION.
 2. SEE DRG. REG. NO. X FOR RESULTS OF 1:60 SCALE MODEL.
 3. SEE DRG. REG. NO. X FOR RESULTS OF 1:30 SCALE MODEL.
 4. 3 SCOUR SECTIONS WERE MEASURED, WITH THE WORST SCOUR TAKEN AS THE RULING ONE.
 5. MINIMAL SCOUR WAS OBSERVED FOR THE 1:200 YEAR FLOOD.
 6. PROTRUSION 1 CONFIGURATION 1 IS THE OPTIMAL.



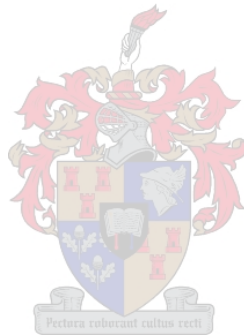
MOD No.	DATE	REVISION DESCRIPTION	FOR	BY
		PRELIMINARY		

DEPARTMENT OF WATER AFFAIRS AND FORESTRY HEAD OFFICE CIVIL DESIGN PRIVATE BAG X313 PRETORIA 0001		DEPARTMENT OF WATER AFFAIRS AND FORESTRY REPUBLIC OF SOUTH AFRICA	
DESIGNER: HJ WRIGHT	TRACER:	PROVINCE: L.M.P.O.F.O	DISTRICT: SECHUKHUNE
DRAWN: HJ WRIGHT	CHECKER:	TELEPHONE No.:	CONTRACT No.:
SIGNATURE	APPROVED	ENGINEER	CHIEF ENGINEER
		RANK	

DEPARTMENT OF WATER AFFAIRS AND FORESTRY REPUBLIC OF SOUTH AFRICA OLIFANTS RIVER WATER RESOURCES DEVELOPMENT PROJECT		DE HOOP DAM 2D MODEL STUDY: SCALE 1:20 SCOUR MEASUREMENTS	
J. STINDANE DIRECTOR GENERAL		DISTRICT: SECHUKHUNE TELEPHONE No.: CALCULATION FILE:	
1/2 SHEET 20 MODEL: SCALE 1:20: SCOUR MEASUREMENTS		LIST OF DRAWINGS SHEET DESCRIPTION OTHER No. REG. No.	
		2 OF 2 REG. No. X	

APPENDIX E

De Hoop Dam Background



OLIFANTS RIVER WATER RESOURCES DEVELOPMENT PROJECT (PHASE 2A):

DE HOOP DAM FACT SHEET

1. LOCALITY

Province: Limpopo
District: Steelpoort
Position:
Latitude: 24° 57' 29" South
Longitude: 29° 57' 25" East
Nearest towns: Steelpoort (40 km)
Roosenekal (38 km)
Nearest railway station: Roosenekal (38 km)
1:50 000 maps: 2429 DD Jane Furse & 2529 BB Roosenekal

2. DAM CLASSIFICATION

Category:
Size class
Hazard potential rating



3. RESERVOIR INFORMATION

Full supply level (FSL): RL 915,00 m
Design overflow flood level (1:200 year flood): RL 917,90 m
Safety evaluation discharge level (SED): RL 921,47 m
Lowest drawdown level (LDDL): RL 875,00 m
Reservoir yield: (domestic, 98% confidence) 80 x 10⁶ m³ / annum

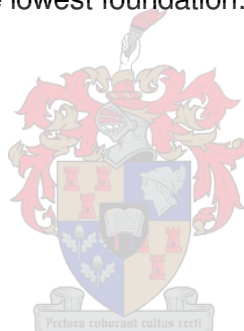
	At FSL	at LDDL
Reservoir capacity	347x10 ⁶ m ³	15x10 ⁶ m ³
Reservoir surface area:	1690 ha	190 ha

4. HYDROLOGY

Drainage region: B400
River: Steelpoort River
Catchment area: 2 865 km²
Mean annual runoff: 116 x 10⁶ m³
Mean annual precipitation: 706 mm

5. STRUCTURAL INFORMATION

Type of dam:	RCC Gravity
Type of spillway:	uncontrolled central ogee
Overall length of wall:	1 015 m
Length of spillway:	110 m
Length of right NOC:	98 m
Length of left NOC:	790 m
Outlet works:	17 m
Crest levels:	
Spillway:	RL 915,00 m
NOC left flank:	RL 921,00 m
NOC right flank:	RL 921,50 m
River bed level:	RL 850,00 m
Lowest foundation level:	RL 840,00 m
Max height of NOC above lowest foundation:	81,5 m
Crest width:	7 m – right flank 6 m – left flank
Upstream slope:	Vertical
Downstream slope:	1 V : 0,8 H



6. VOLUMES

Hard excavation:	145 000 m ³
Soft excavation:	97 000 m ³
RCC:	500 000 m ³
Mass concrete:	200 000 m ³
Structural concrete:	50 000 m ³

7. SPILLWAY

Crest length:	110 m
Total freeboard:	6 m
Design flood discharge:	1 104 m ³ /s
Spillway discharge at NOC:	3 616 m ³ /s
Safety evaluation discharge (SED):	4 463 m ³ /s

8. INFLOW FLOOD PEAKS

Return Period (Years):	Inflow peak (m ³ /s)
2	94
5	206
10	332
20	502
50	804
100	1 100
200	1 460
Safety evaluation flood (SEF)	5 350
Regional maximum flood (RMF)	3 520

9. OUTLET WORKS

Twin stacks of multi-level off-takes
Combined capacity: 20 m³/s
Service outlet valves:
2 x 1 000 mm sleeve valves
2 x 600 mm sleeve valves

10. R555 / P169-1 REALIGNMENT

Length of realignment: 25 km
Design speed: 100 km/h
Road width: 2 x 3,7 m lanes with 3,0 m shoulders
Road reserve width (minimum): 40 m



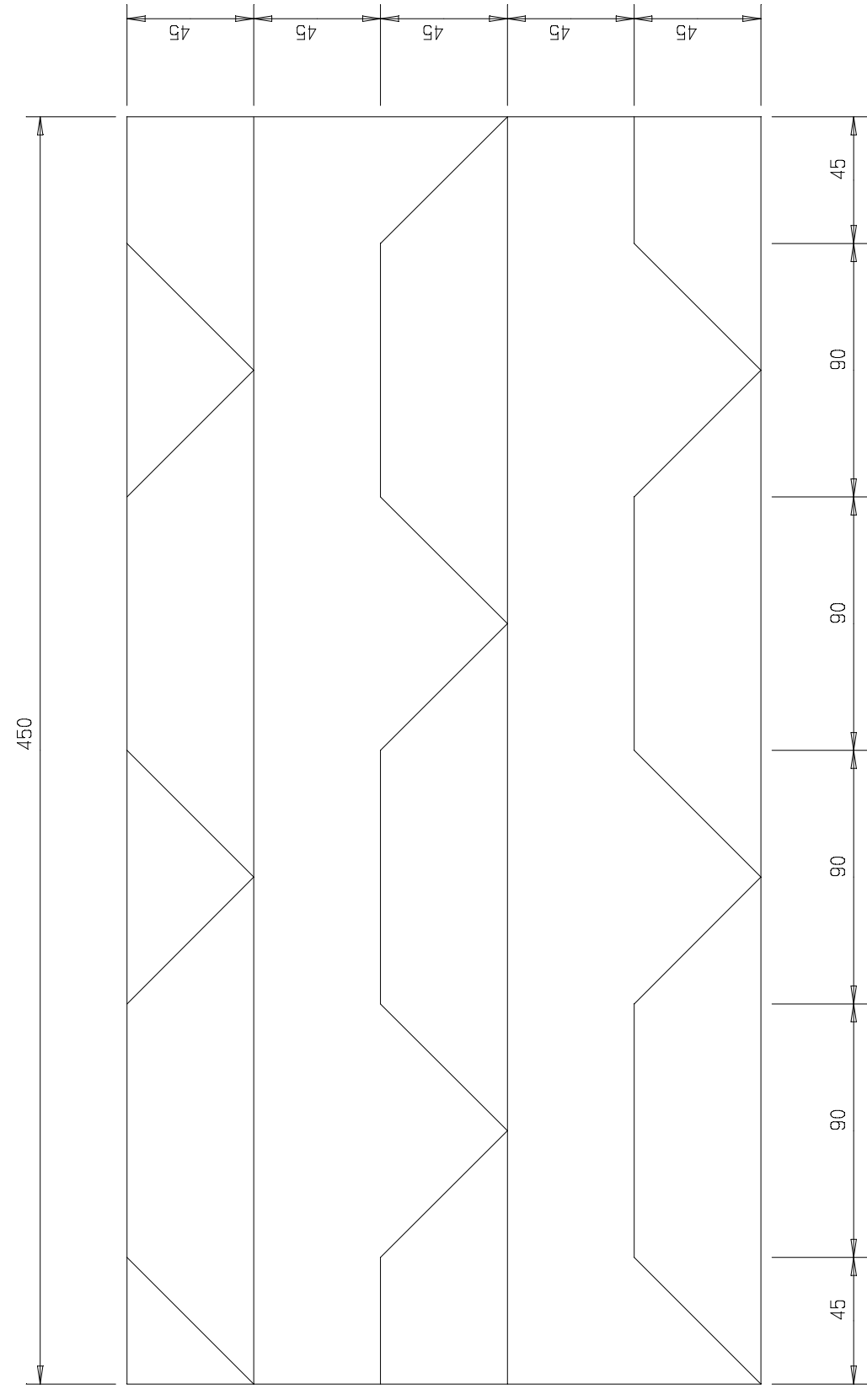
11. ORWRDP PHASING SCHEDULE

<u>Phase</u>	<u>Component</u>	<u>Construction</u>	<u>Commissioning</u>
1:	Raising of Flag Boshielo Dam	2004 – 2006	2006
2A	De Hoop Dam	2006 – 2010	2009
2B	Flag Boshielo to Mokopane pipeline	2008 – 2009	2009
2C	Steelpoort Weir and abstraction works	2008 – 2009	2009
2D	2 nd pipeline from Steelpoort Weir to Mooihoek	2010 – 2011	2011
2E	2 nd pipeline parallel to Lebalelo Scheme	> 2025	
2F	Connect Lebalelo Scheme to Olifantspoort	2012 – 2013	2013
2G	2 nd pipeline from Flag Boshielo to Mokopane	> 2025	
2H	Incorporate Lebalelo Scheme	2008 – 2009	2009

Note: Implementation of Phases 2B to 2H to be regularly reviewed.

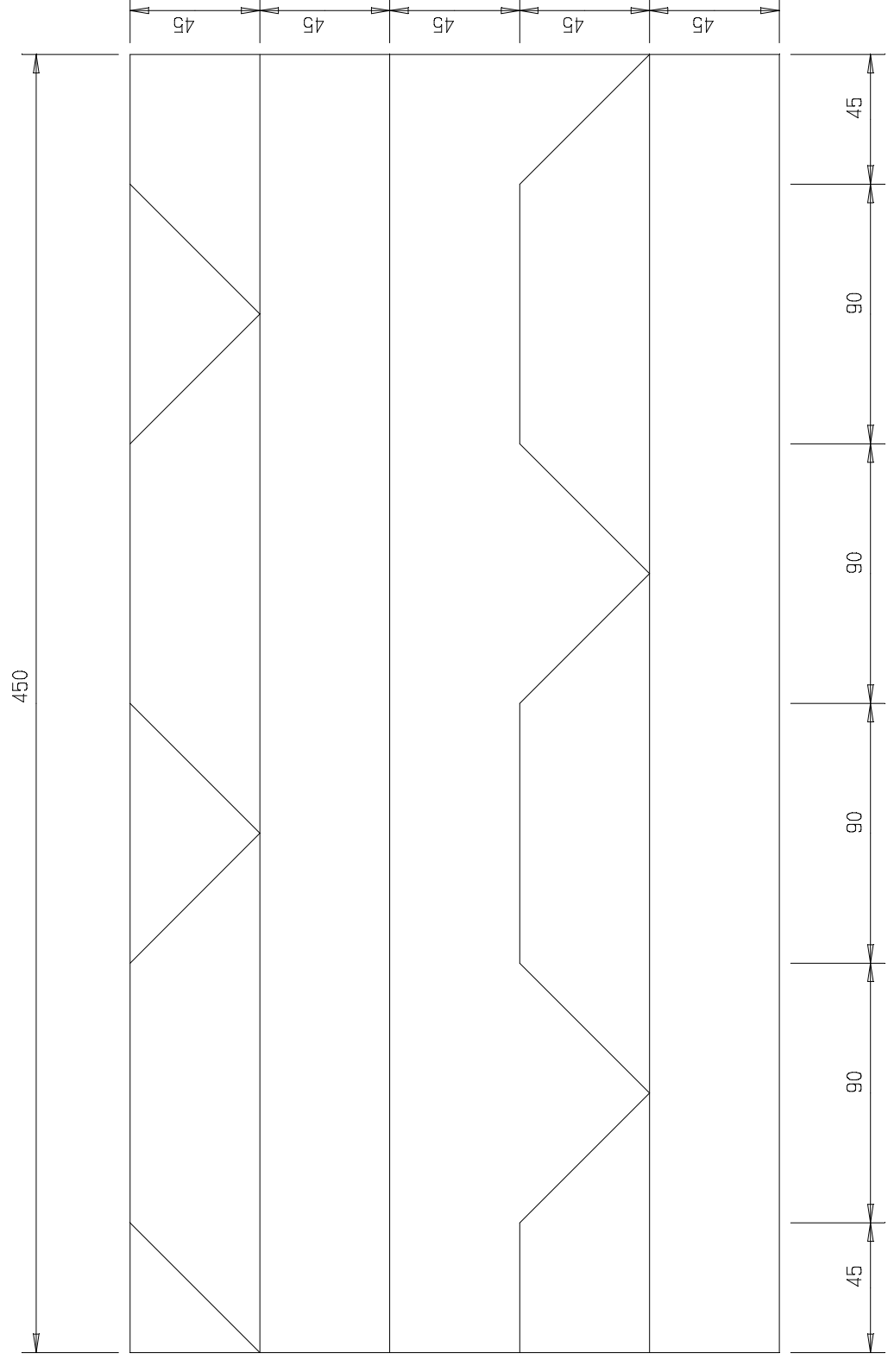


Artist impression of the Proposed De Hoop Dam



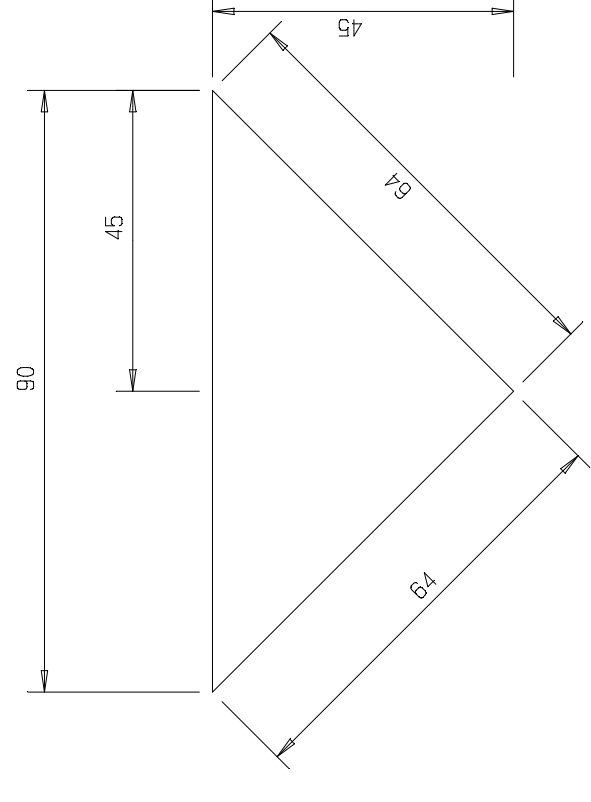
TRIANGLE 1 (1)

SCALE 1:2



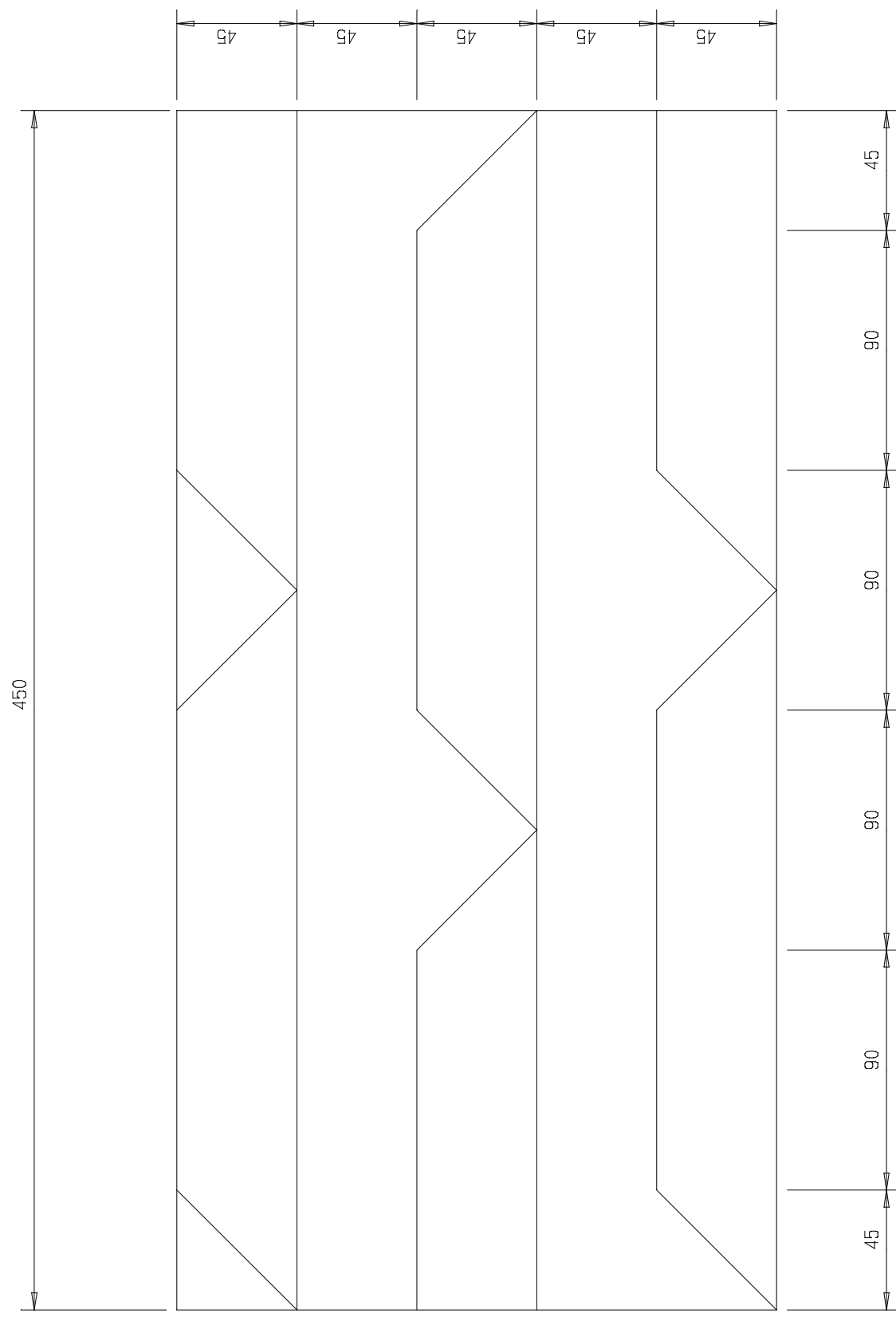
TRIANGLE 1 (3)

SCALE 1:2



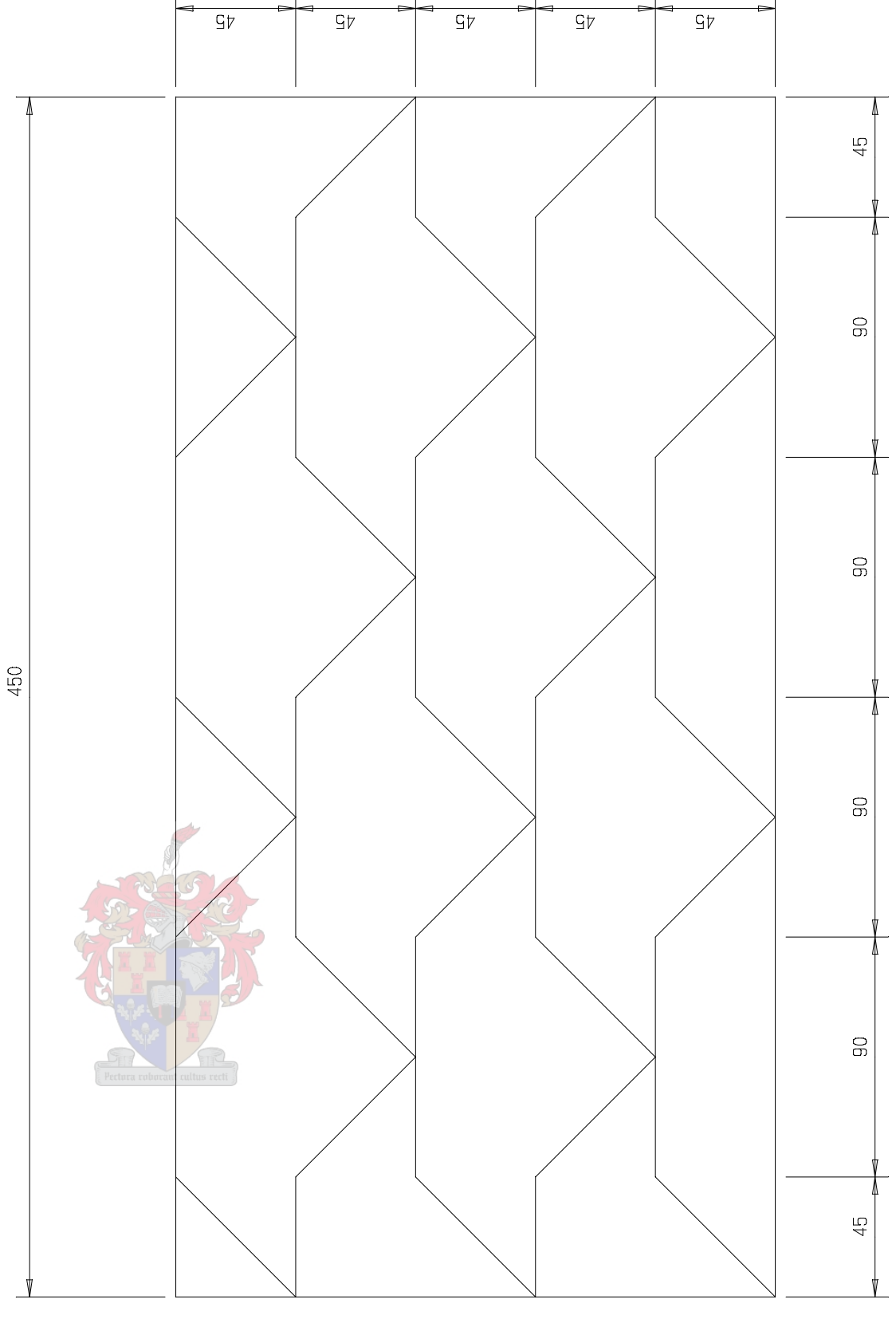
TRIANGLE 1

SCALE 1:1



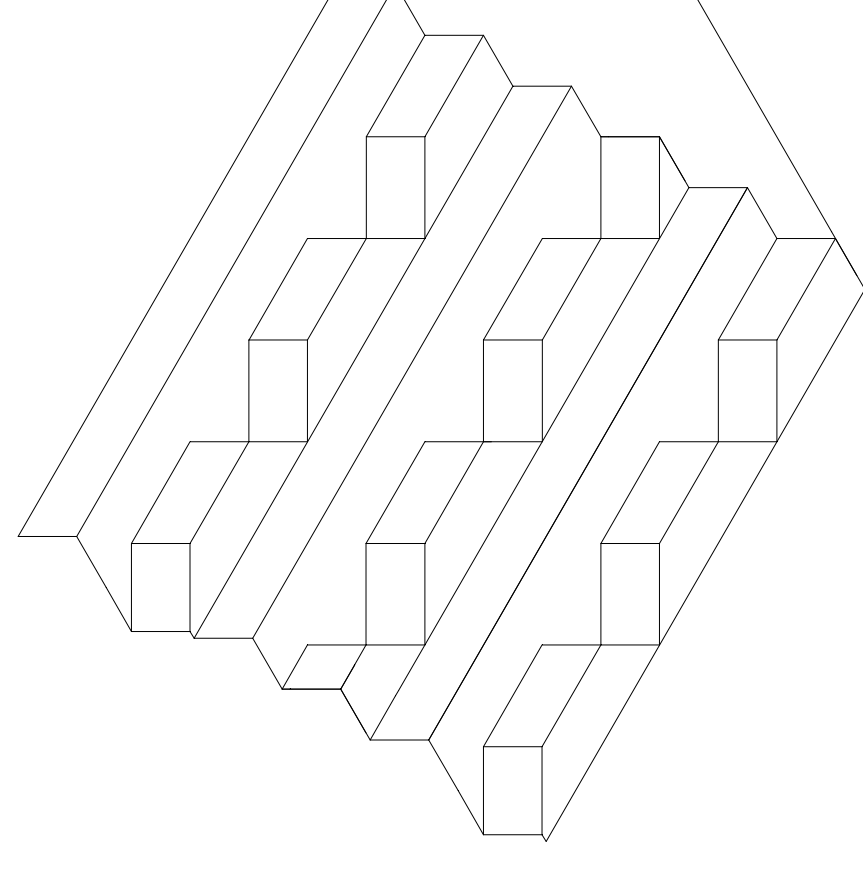
TRIANGLE 1 (2)

SCALE 1:2



TRIANGLE 1 (4)

SCALE 1:2



ISOMETRIC VIEW OF TRIANGLES

SCALE 1:5

ONLY FIRST THIRD OF DAM



SHEET	DESCRIPTION	OTHER NO.	REV. NO.
3/3	2D MODEL: SCALE 1:20 PROTRUSION DETAILS		X
1/3	2D MODEL: SCALE 1:20 GENERAL LAYOUT		X

REV. NO.	DATE	REVISION DESCRIPTION	FOR	DWA
		PRELIMINARY		

DEPARTMENT OF WATER AFFAIRS AND FORESTRY
 CIVIL DESIGN
 PRIVATE BAG X313
 PRETORIA 0001

J. SINDANE
 DIRECTOR GENERAL

DESIGN: HJ WRIGHT
 DRAWN: HJ WRIGHT
 APPROVED: _____
 SIGNATURE

CHECKED: _____
 DESIGNER

ENGINEER

RANK

CHIEF ENGINEER

DEPARTMENT OF WATER AFFAIRS AND FORESTRY
 REPUBLIC OF SOUTH AFRICA

OLIFANTS RIVER WATER RESOURCES DEVELOPMENT PROJECT

DE HOOP DAM

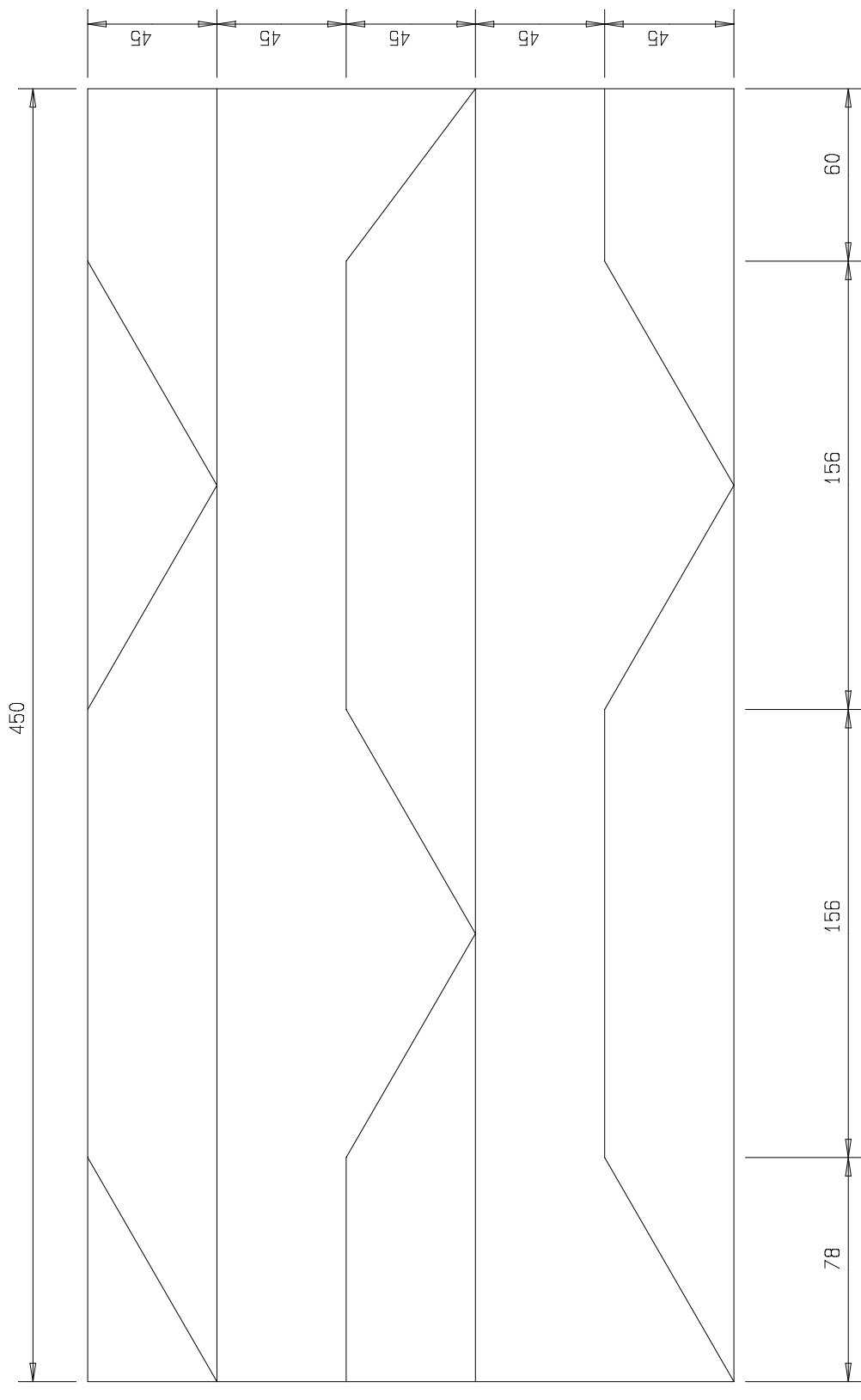
2D MODEL STUDY: SCALE 1:20

PROTRUSION DETAILS

DISTRICT: SEKHUKHUNE
 TENDER No. -
 PROVISIONAL CALCULATION FILE: -

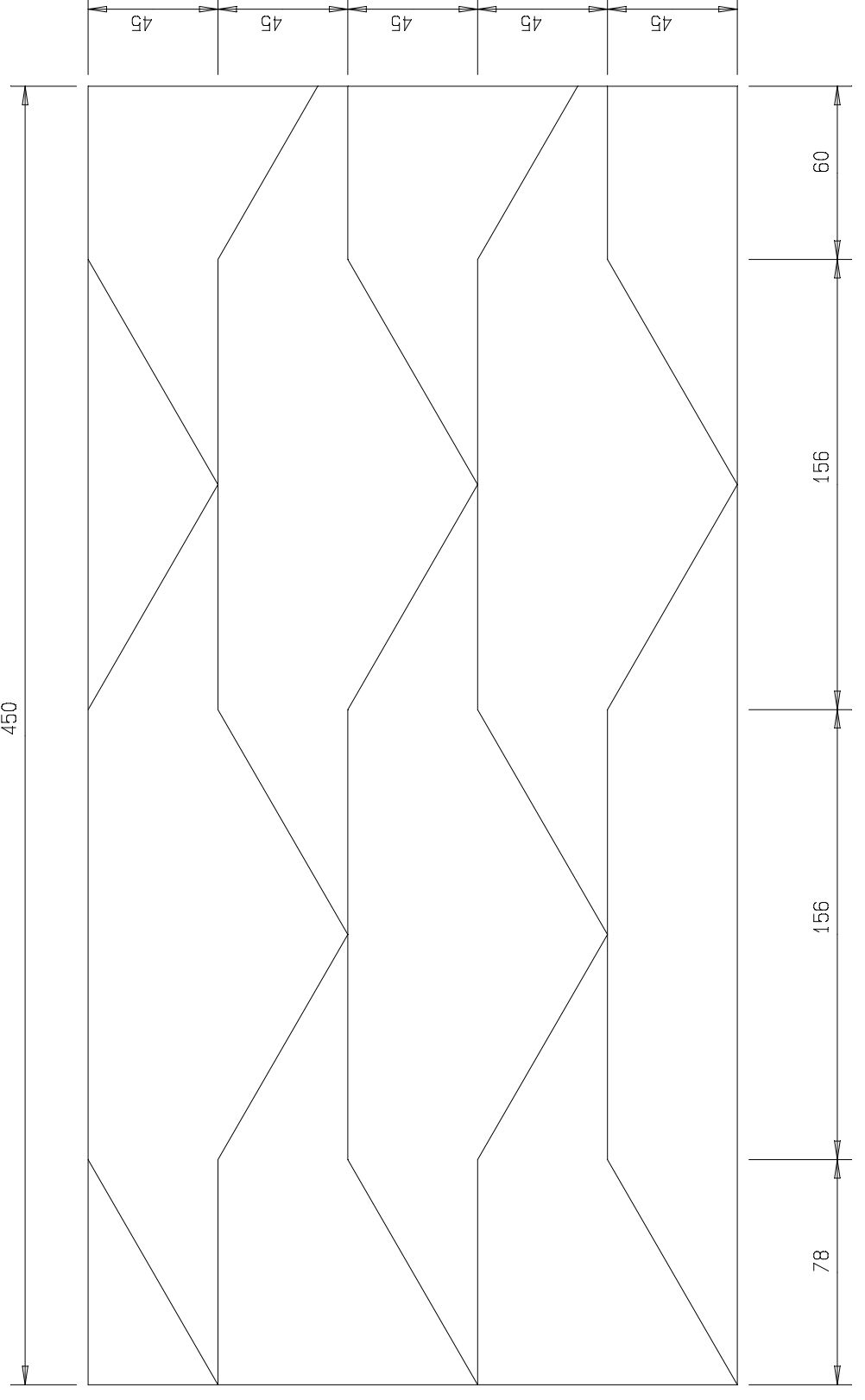
PROVINCE: LIMPOPO
 DISTRICT: SEKHUKHUNE
 TENDER No. -
 PROVISIONAL CALCULATION FILE: -

KEYWORDS: -
 CONTRACT No. -
 SHEET 2 OF 3
 REV. NO. X



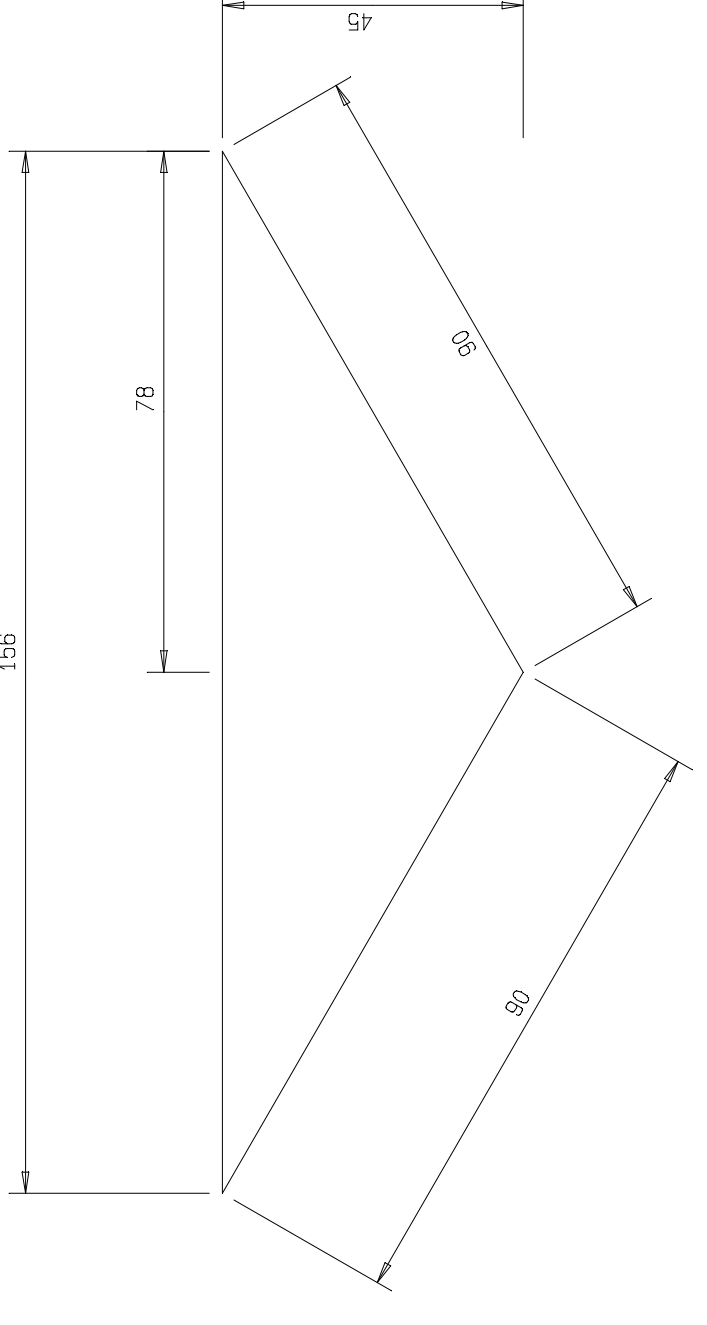
TRIANGLE 2 (1)

SCALE 1:2



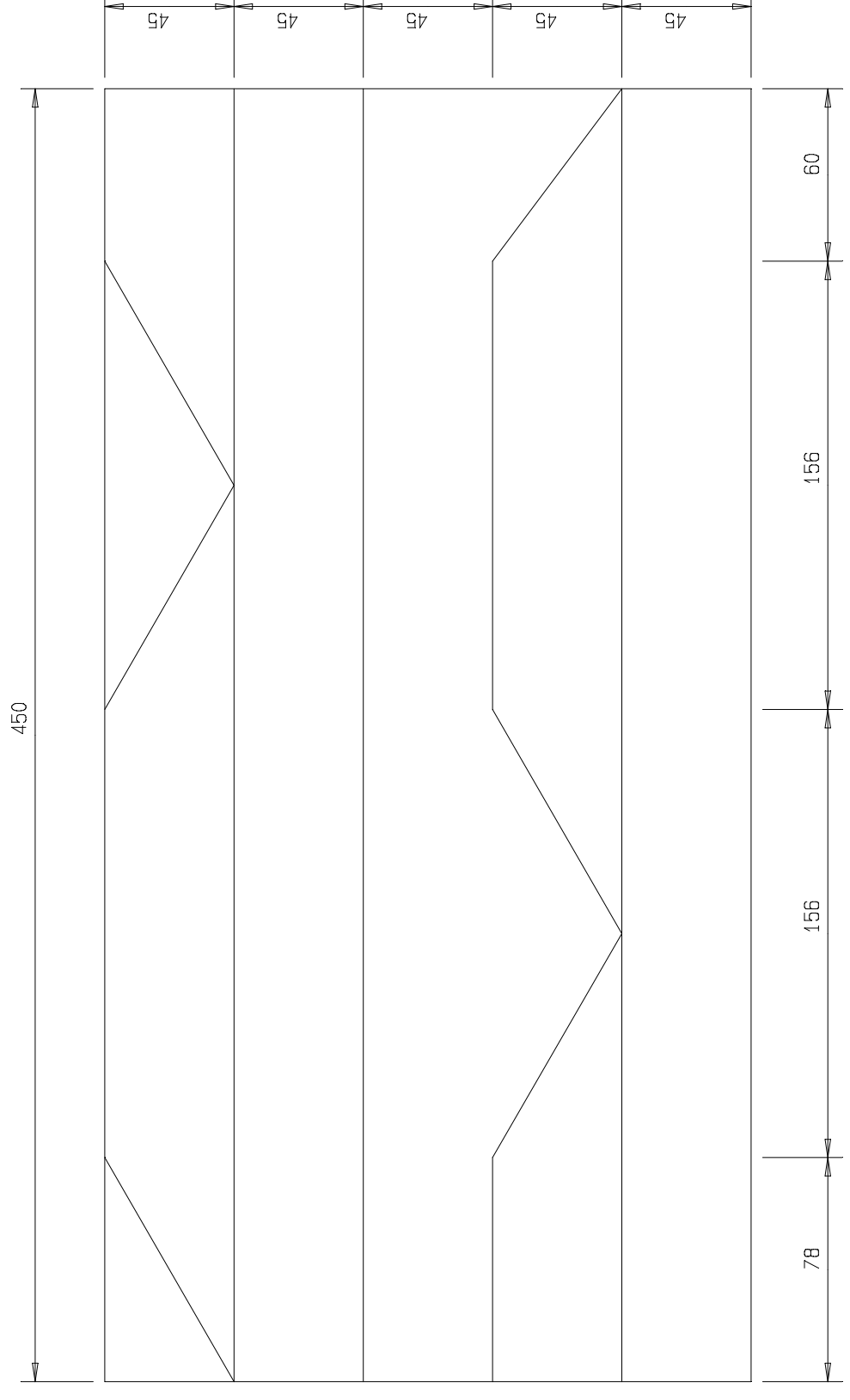
TRIANGLE 2 (3)

SCALE 1:2



TRIANGLE 2

SCALE 1:1



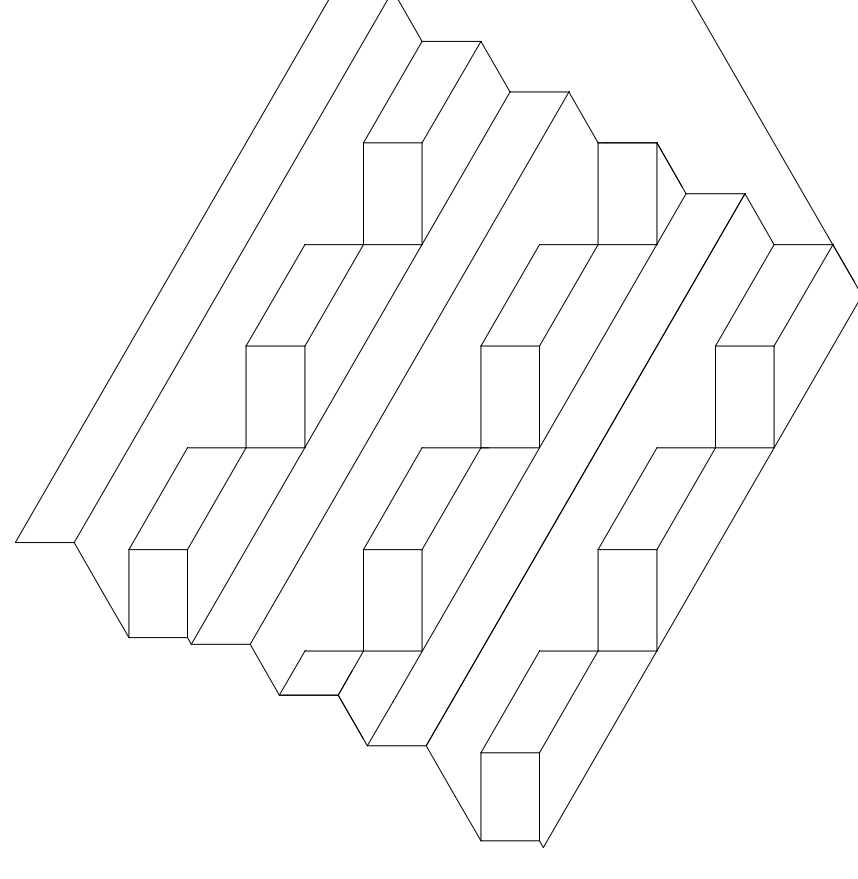
TRIANGLE 2 (2)

SCALE 1:2



TRIANGLE 2 (4)

SCALE 1:2



ISOMETRIC VIEW OF TRIANGLES

SCALE 1:5



REV. NO.	DATE	REVISION DESCRIPTION	FOR	BY	DATE
		PRELIMINARY			

DEPARTMENT OF WATER AFFAIRS AND FORESTRY
 HEAD OFFICE
 CIVIL DESIGN
 PRIVATE BAG X313
 PRETORIA 0001

J. SINDANE
 DIRECTOR GENERAL

DESIGN: HJ WRIGHT
 DRAWN: HJ WRIGHT
 APPROVED: _____
 SIGNATURE

CHECKED: _____
 ENGINEER

PROVINCE: LIMPOPO
 DISTRICT: SEKHUKHUNE
 TENDER No. -
 CALCULATION FILE: -

DEPARTMENT OF WATER AFFAIRS AND FORESTRY
 REPUBLIC OF SOUTH AFRICA

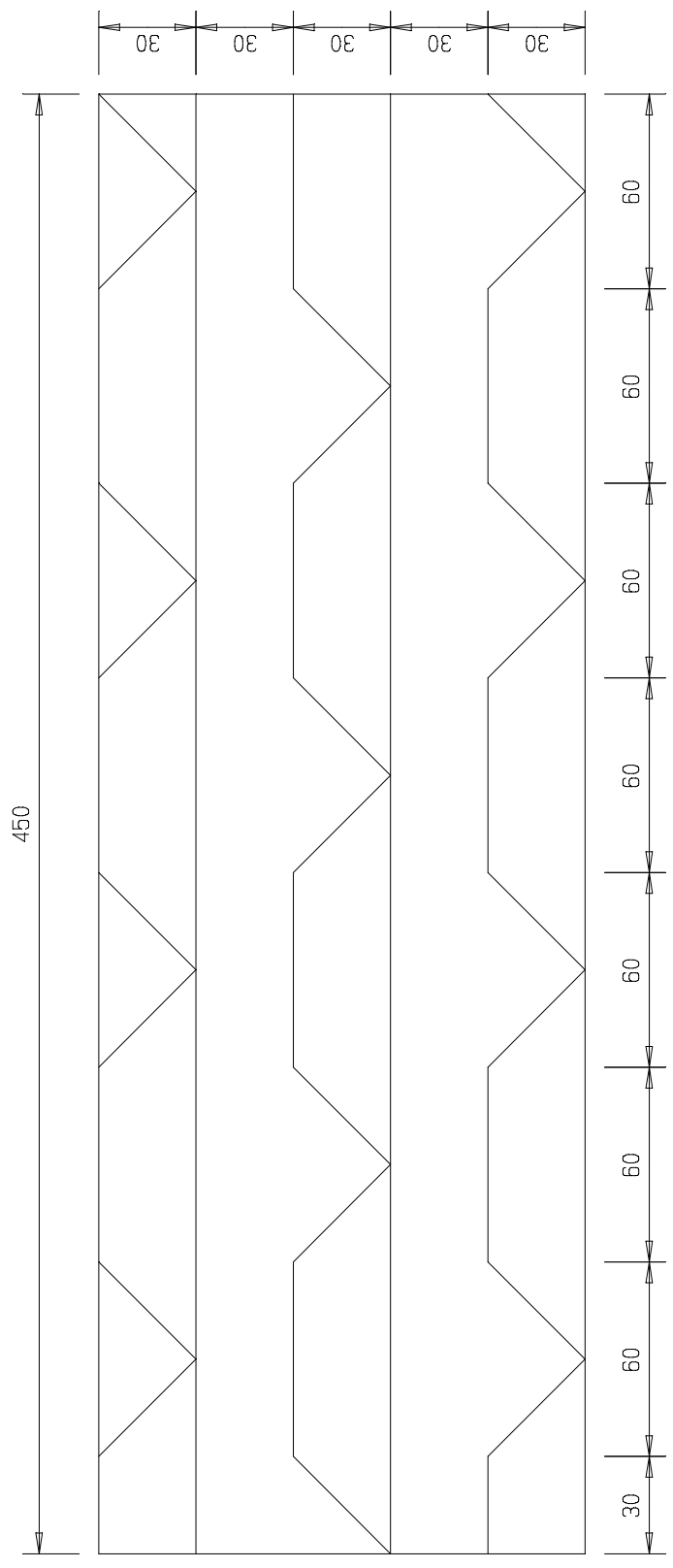
OLIFANTS RIVER WATER RESOURCES DEVELOPMENT PROJECT

DE HOOP DAM
 2D MODEL STUDY: SCALE 1:20

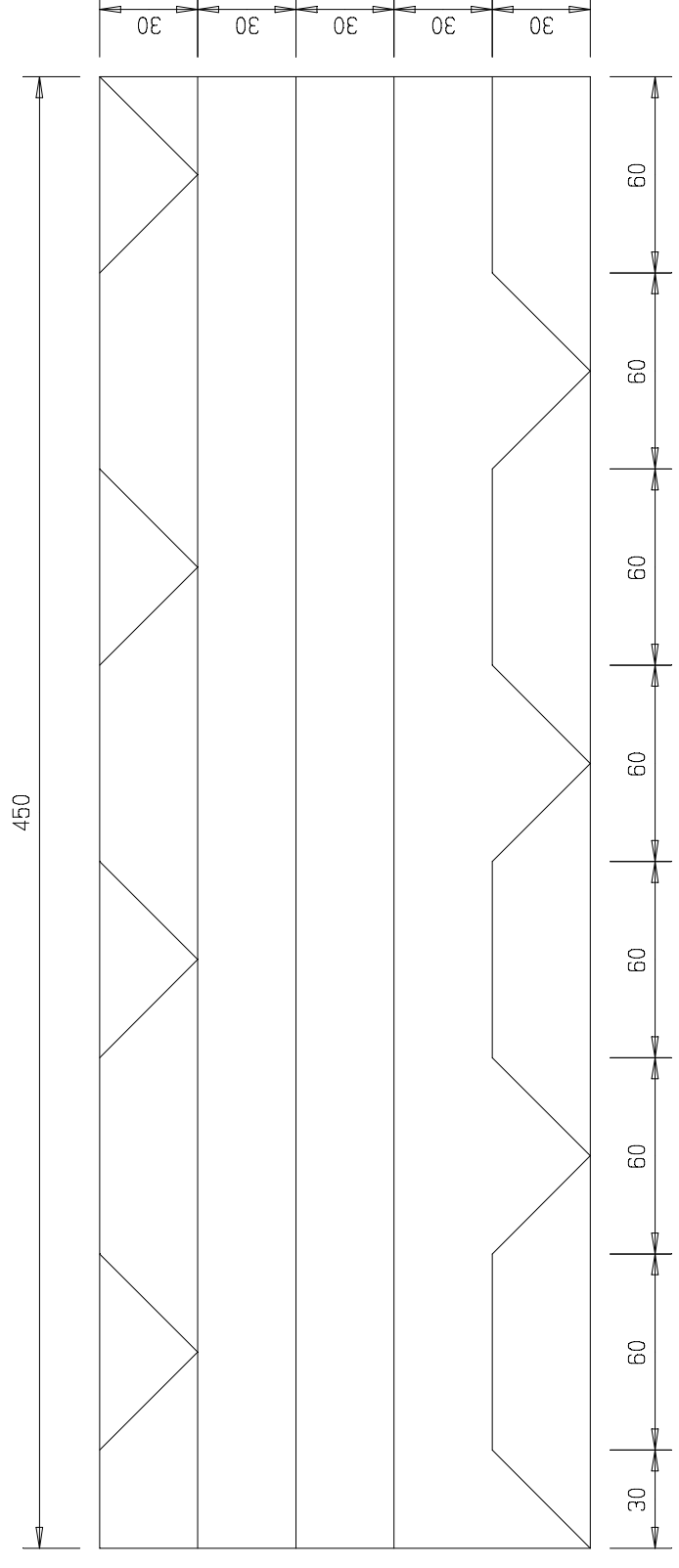
PROTRUSTION DETAILS

KEYWORDS: - - - - -
 CONTRACT No. - - - - -
 SHEET 3 OF 3
 DIR. No. X

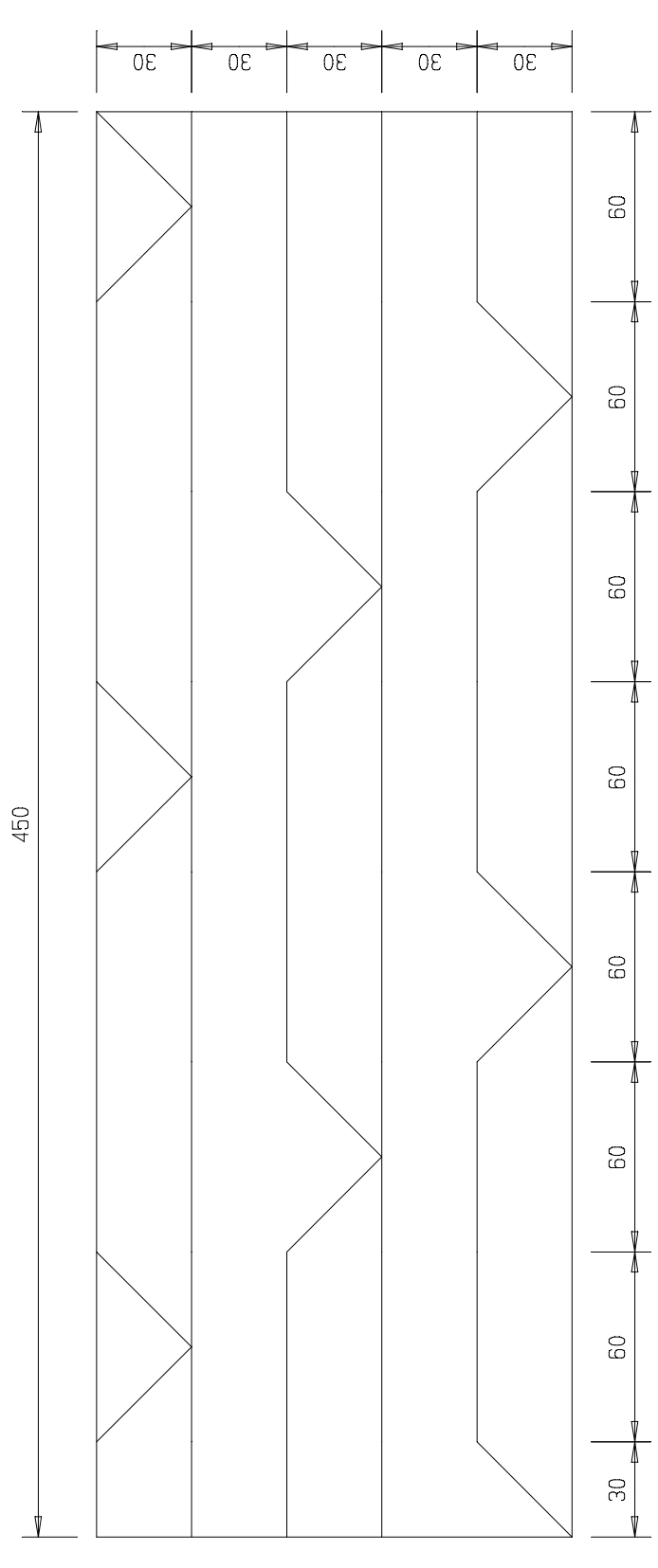
LIST OF DRAWINGS			
NO.	DESCRIPTION	OTHER No.	REV. No.
2/3	2D MODEL: SCALE 1:20 PROTRUSTION DETAILS		X
1/3	2D MODEL: SCALE 1:20 GENERAL LAYOUT		X



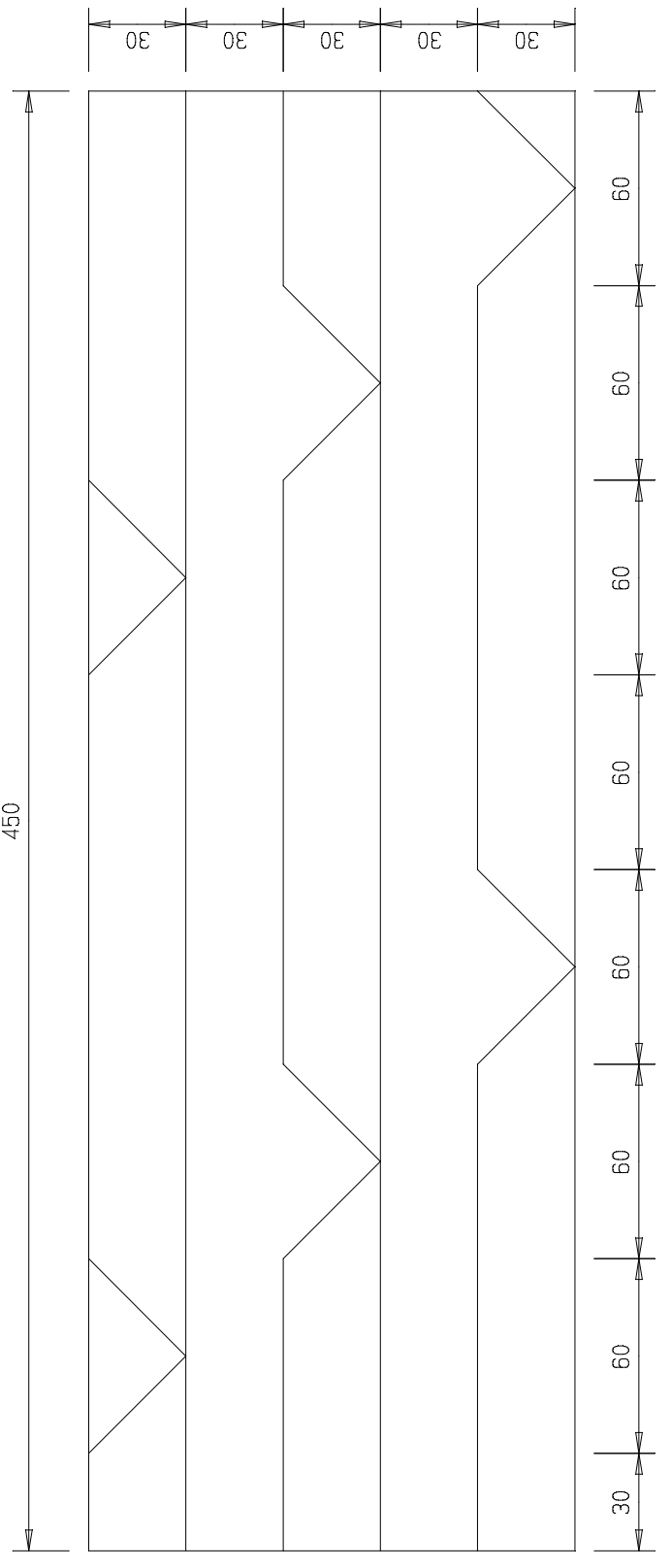
TRIANGLE 1 (1)
SCALE 1:2



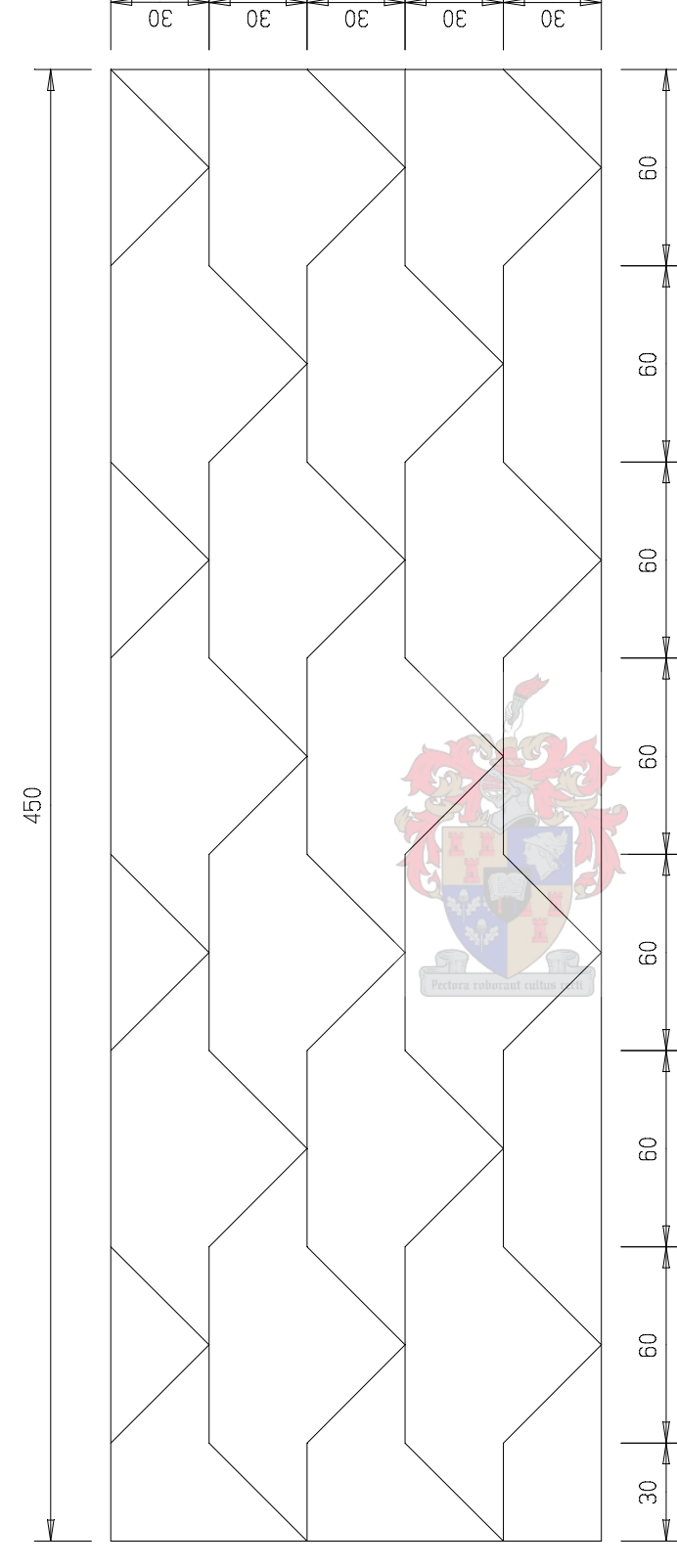
TRIANGLE 1 (3)
SCALE 1:2



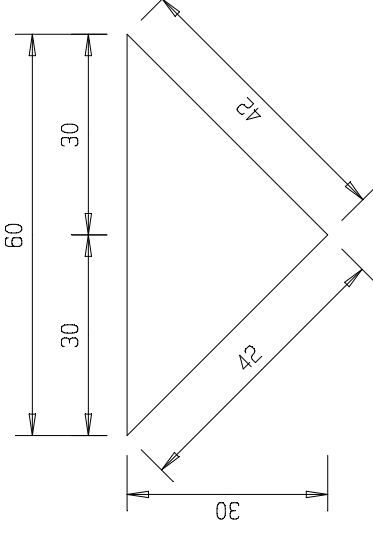
TRIANGLE 1 (5)
SCALE 1:2



TRIANGLE 1 (2)
SCALE 1:2



TRIANGLE 1 (4)
SCALE 1:2



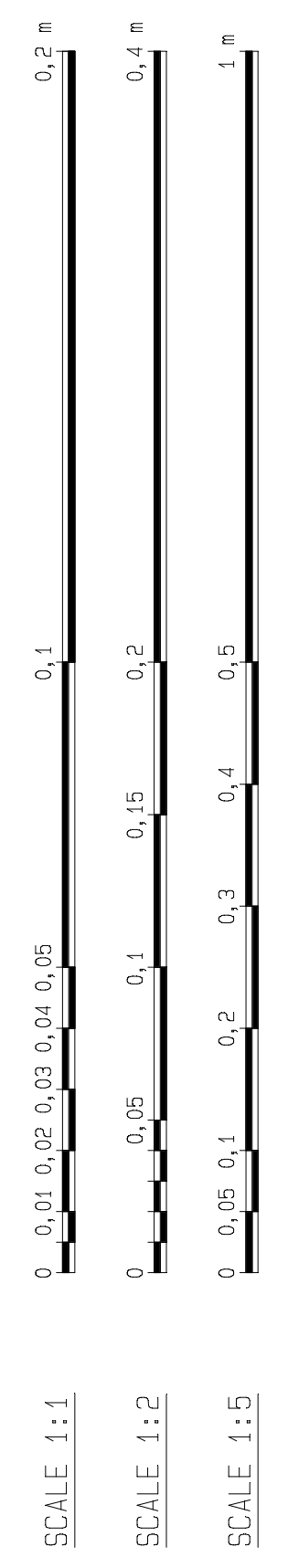
ISOMETRIC VIEW OF TRIANGLES
SCALE 1:5

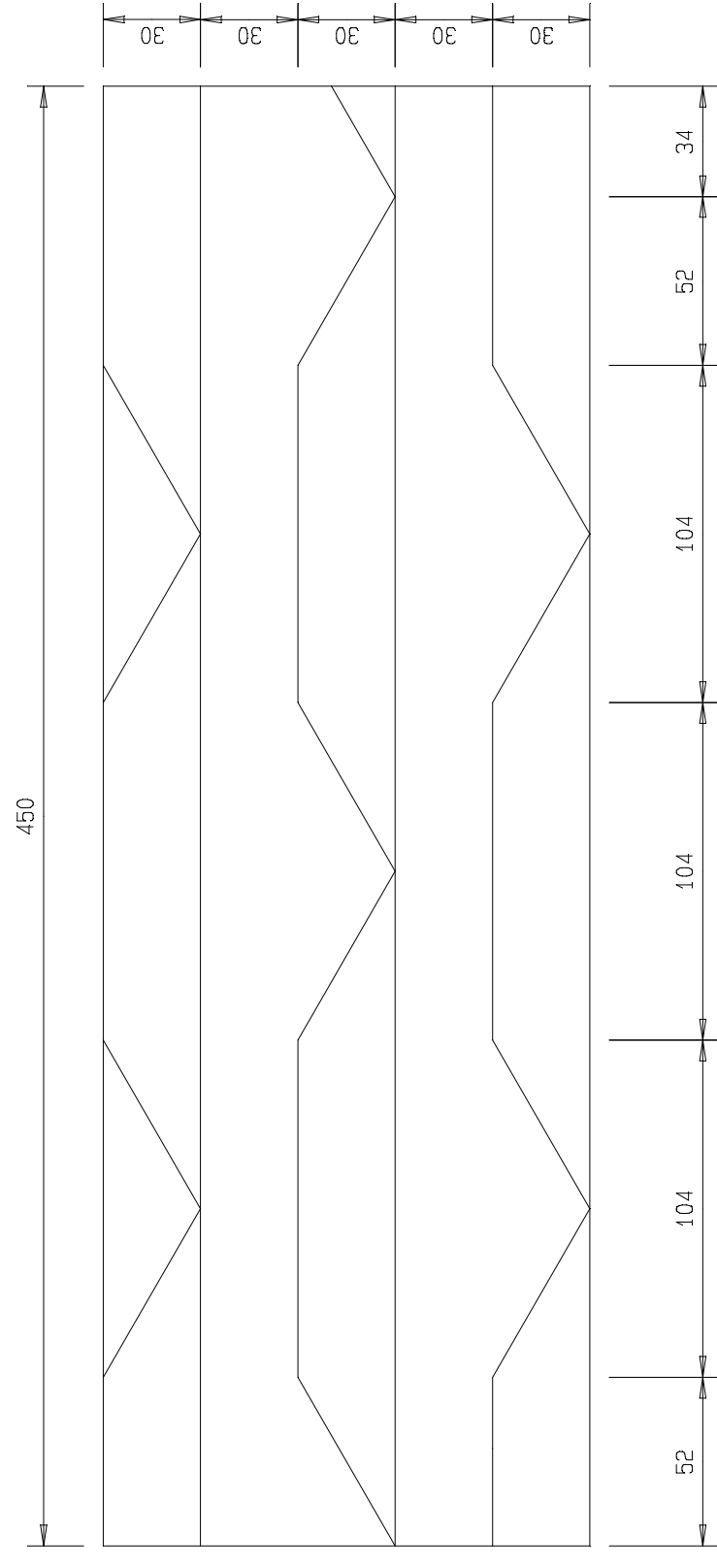
TRIANGLE 1
SCALE 1:1

LIST OF DRAWINGS	
NO.	DESCRIPTION
2/3	2D MODEL: SCALE 1:300; PROVISION DETAIL
1/3	2D MODEL: SCALE 1:300; GENERAL LAYOUT
	OTHER NO.
	REV. NO.

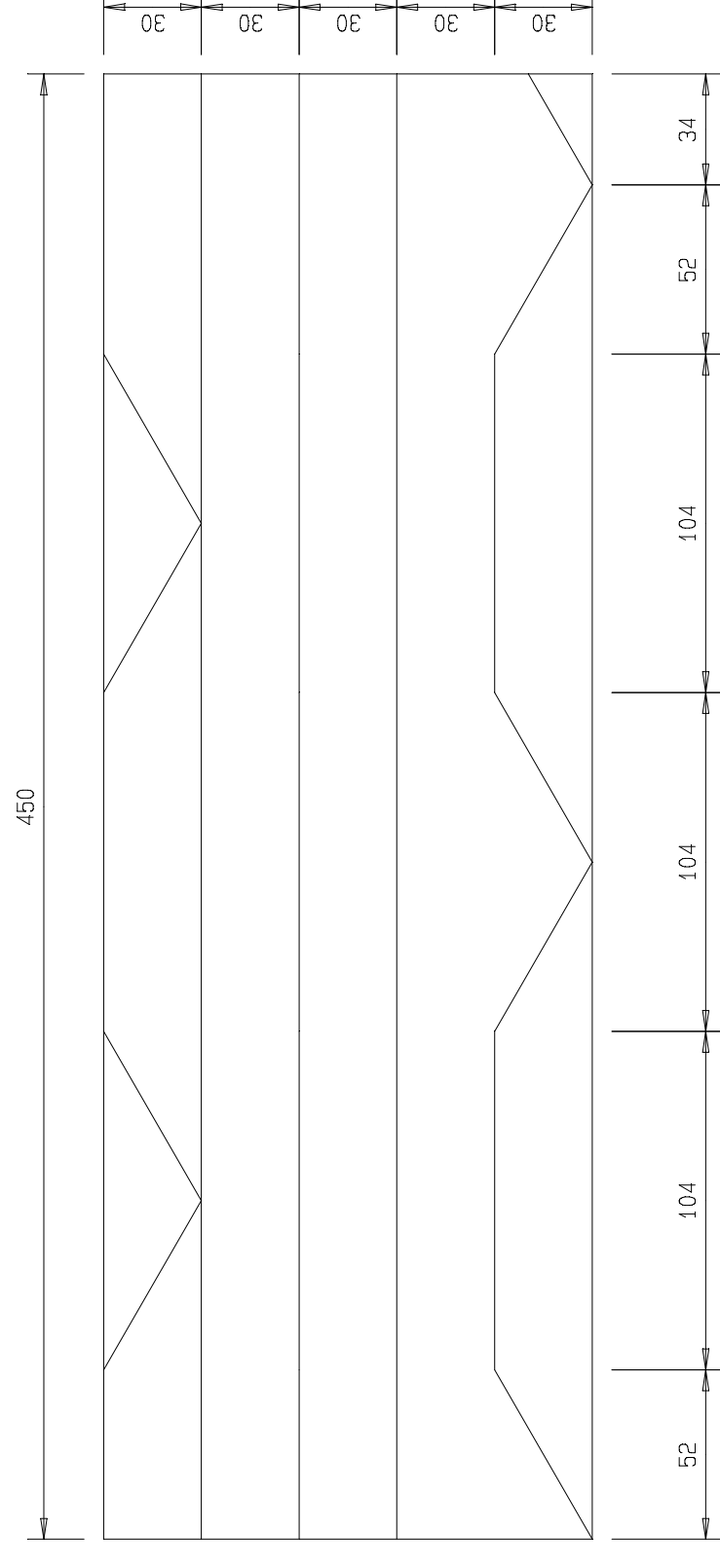
REV. NO.	DATE	REVISION DESCRIPTION	FOR	BY
		PRELIMINARY		

DEPARTMENT OF WATER AFFAIRS AND FORESTRY HEAD OFFICE CIVIL DESIGN PRIVATE BAG X313 PRETORIA 0001		DEPARTMENT OF WATER AFFAIRS AND FORESTRY REPUBLIC OF SOUTH AFRICA OLIFANTS RIVER WATER RESOURCES DEVELOPMENT PROJECT DE HOOP DAM 2D MODEL STUDY: SCALE 1:30 PROVISION DETAILS	
DESIGN: HJ WRIGHT	DESIGN: J. SINDANE	DISTRICT: SEKHUKHUNE	PROV. NO.:
DRAWN: HJ WRIGHT	CHECKER:	TENDER NO.:	CONTRACT NO.:
SIGNATURE	APPROVED	CALCULATION FILE:	REV. NO.:
			2 OF 3
			X

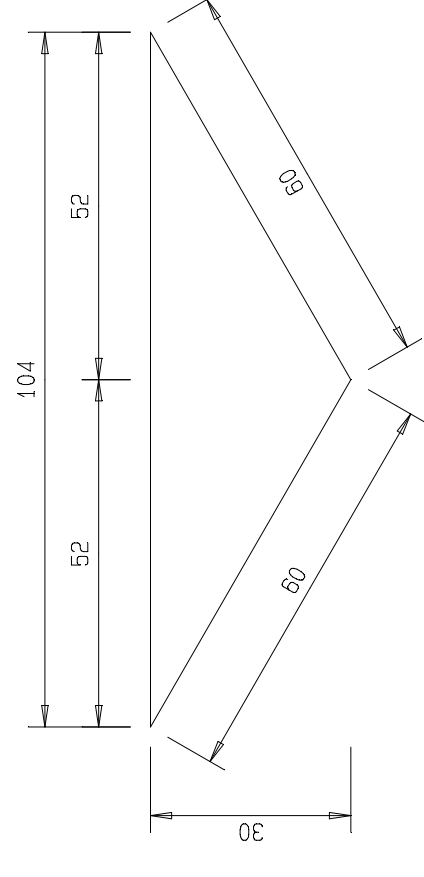




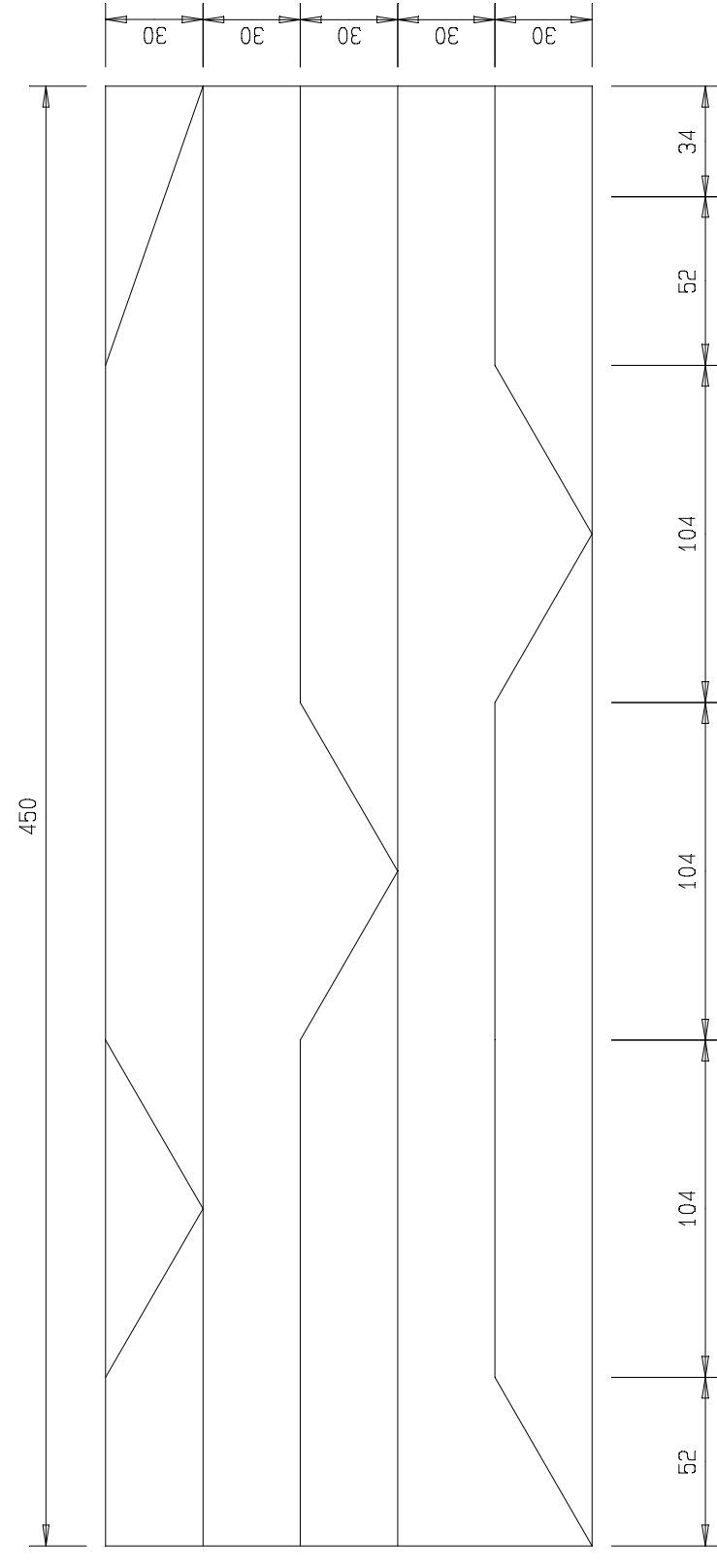
TRIANGLE 2 (1)
SCALE 1:2



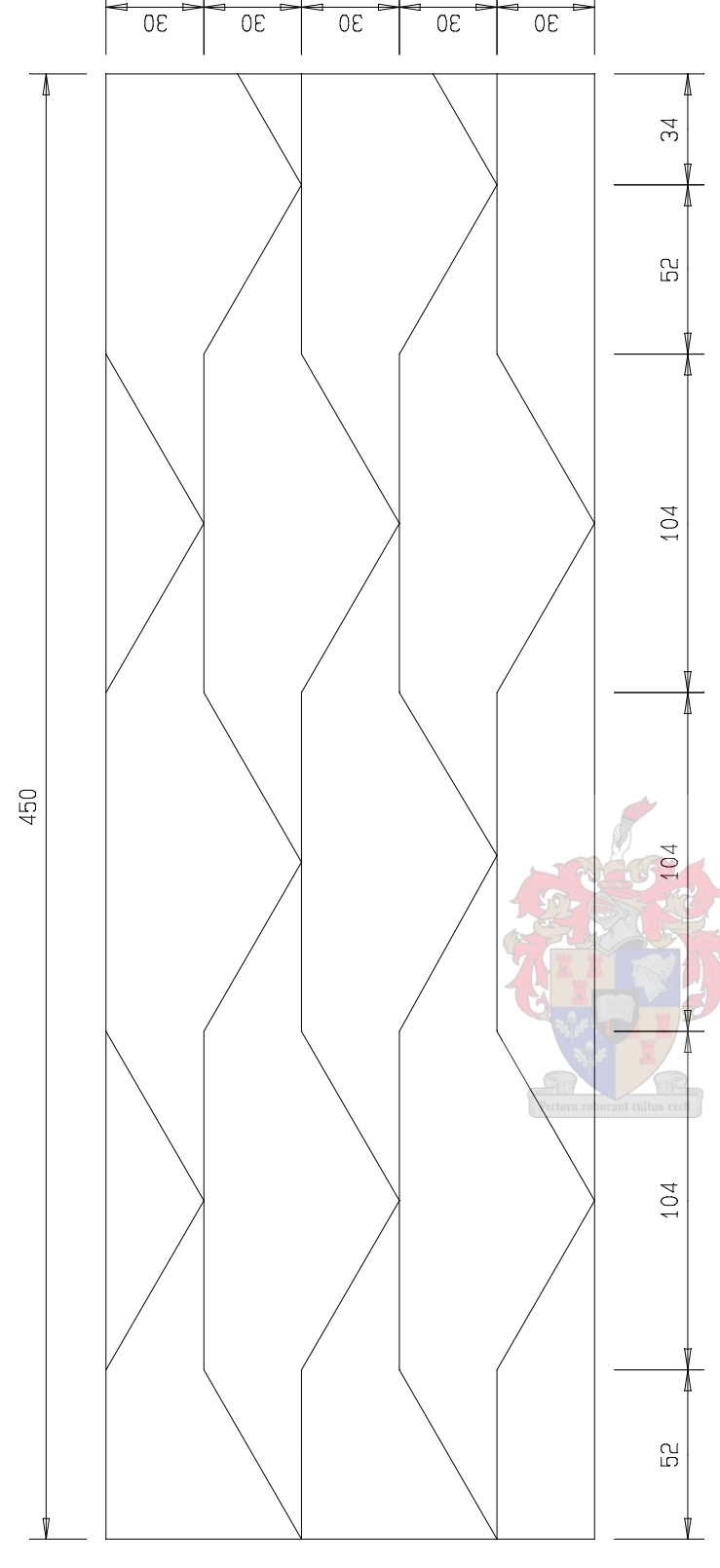
TRIANGLE 2 (3)
SCALE 1:2



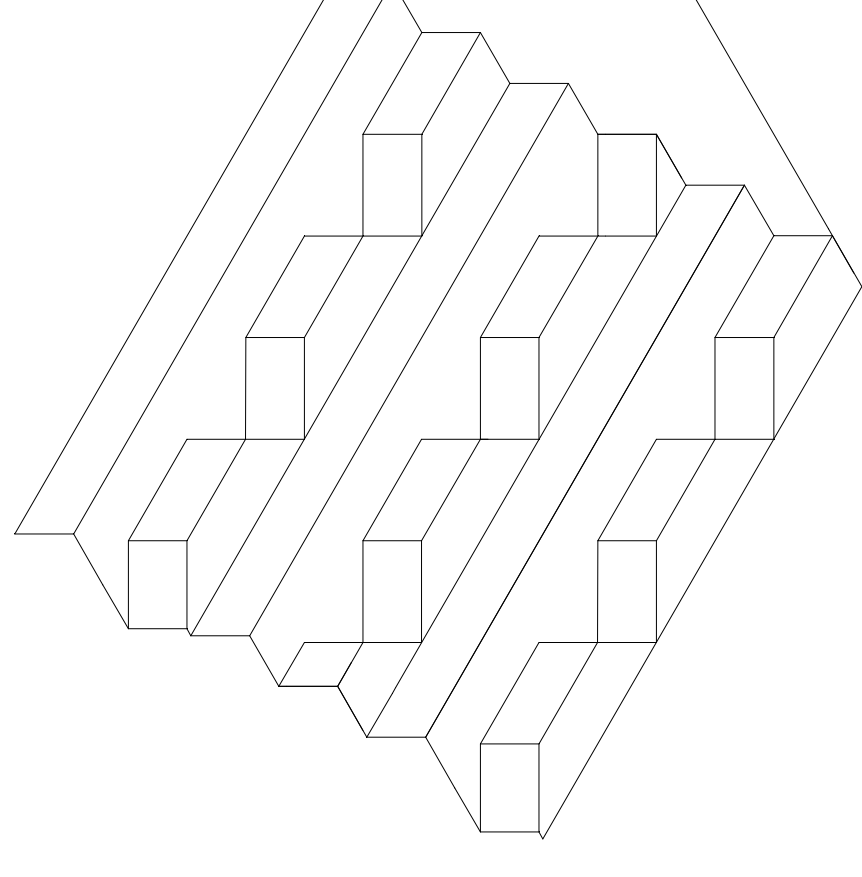
TRIANGLE 2
SCALE 1:1



TRIANGLE 2 (2)
SCALE 1:2



TRIANGLE 2 (4)
SCALE 1:2



ISOMETRIC VIEW OF TRIANGLES
SCALE 1:5



REV. NO.	DATE	REVISION DESCRIPTION	FOR	BY
		PRELIMINARY		

DEPARTMENT OF WATER AFFAIRS AND FORESTRY
 CIVIL DESIGN
 PRIVATE BAG X313
 PRETORIA 0001

DESIGN: HJ WRIGHT
 DRAWN: HJ WRIGHT
 APPROVED: _____
 SIGNATURE

DESIGNER: _____
 CHECKER: _____
 ENGINEER: _____
 RANK: _____

J. SINDANE
 DIRECTOR GENERAL

185 SCHERMAN STREET
 PRETORIA
 (012) 738-7300

DEPARTMENT OF WATER AFFAIRS AND FORESTRY REPUBLIC OF SOUTH AFRICA		LIST OF DRAWINGS	
2/3	2D MODEL: SCALE 1:30: PROTRUSION DETAIL		X
1/3	2D MODEL: SCALE 1:30: GENERAL LAYOUT		X
		DESCRIPTION	OTHER NO.
			REV. NO.
OLIFANTS RIVER WATER RESOURCES DEVELOPMENT PROJECT		DE HOOP DAM	
2D MODEL STUDY: SCALE 1:30		PROTRUSION DETAILS	
PROVINCE: LIMPOPO	DISTRICT: SEKHUKHUNE	KEYWORDS: -	-
TENDER No. -	CONTRACT No. -	SHEET	REV. NO.
CALCULATION FILE: -	DIRECTOR	3	3
		OF	X

RAW DATA**1:20 Model**

Q (l/s)	P 1(1) Depth Y2 (m)	P 1(2) Depth Y2 (m)	P 1(3) Depth Y2 (m)	P 1(4) Depth Y2 (m)	P 2(1) Depth Y2 (m)	P 2(2) Depth Y2 (m)	P 2(3) Depth Y2 (m)	P 2(4) Depth Y2 (m)	SS Depth Y2 (m)
20	0,180	0,190	0,205	0,200	0,200	0,240	0,230	0,230	0,200
40	0,270	0,270	0,270	0,270	0,305	0,310	0,305	0,315	0,300
55	0,320	0,320	0,325	0,320	0,330	0,345	0,340	0,350	0,360
70	0,335	0,340	0,365	0,370	0,355	0,385	0,370	0,395	0,400
80	0,388	0,390	0,395	0,400	0,390	0,405	0,400	0,410	0,430
95	0,420	0,420	0,440	0,440	0,435	0,440	0,430	0,450	0,460
110	0,480	0,480	0,480	0,480	0,470	0,475	0,470	0,480	0,500
120	0,495	0,498	0,500	0,505	0,500	0,500	0,495	0,510	0,540
135	0,520	0,525	0,535	0,545	0,550	0,545	0,545	0,550	0,605

1:30 Model

Q (l/s)	P 1(1) Depth Y2 (m)	P 1(2) Depth Y2 (m)	P 1(3) Depth Y2 (m)	P 1(4) Depth Y2 (m)	P 1(5) Depth Y2 (m)	P 2(1) Depth Y2 (m)	P 2(2) Depth Y2 (m)	P 2(3) Depth Y2 (m)	P 2(4) Depth Y2 (m)	SS Depth Y2 (m)
22	0,210	0,240	0,245	0,245	0,230	0,225	0,235	0,235	0,240	0,210
30	0,265	0,275	0,275	0,280	0,275	0,275	0,285	0,287	0,287	0,270
41	0,295	0,310	0,305	0,315	0,315	0,305	0,310	0,315	0,315	0,310
52	0,330	0,335	0,340	0,340	0,345	0,335	0,335	0,340	0,340	0,345
66	0,350	0,385	0,380	0,380	0,380	0,355	0,370	0,375	0,375	0,370
77	0,380	0,400	0,410	0,400	0,410	0,401	0,395	0,400	0,400	0,400
88	0,410	0,425	0,430	0,435	0,435	0,425	0,430	0,430	0,432	0,435
99	0,440	0,450	0,465	0,465	0,460	0,445	0,450	0,455	0,457	0,460
110	0,470	0,480	0,485	0,490	0,495	0,480	0,485	0,490	0,492	0,495
120	0,490	0,500	0,505	0,510	0,515	0,510	0,510	0,511	0,512	0,520

RAW DATA**1:20 Model**

Q (l/s)	P 1(1) (L _i) (m)	P 1(2) (L _i) (m)	P 1(3) (L _i) (m)	P 1(4) (L _i) (m)	P 2(1) (L _i) (m)	P 2(2) (L _i) (m)	P 2(3) (L _i) (m)	P 2(4) (L _i) (m)	SS (L _i) (m)
20	0,375	0,375	0,628	0,308	0,357	0,696	0,378	0,284	0,693
40	0,596	0,596	0,859	0,452	0,589	1,066	0,664	0,456	1,110
55	0,748	0,748	1,016	0,574	0,699	1,328	0,862	0,620	1,388
70	0,888	0,888	1,157	0,707	0,814	1,576	1,045	0,780	1,638
80	0,967	0,967	1,244	0,803	0,893	1,734	1,159	0,884	1,788
95	1,098	1,098	1,360	0,956	1,016	1,900	1,318	1,038	1,990
110	1,208	1,208	1,462	1,122	1,142	2,070	1,463	1,189	2,163
120	1,276	1,276	1,522	1,238	1,229	2,183	1,552	1,287	2,263
135	1,366	1,366	1,599	1,423	1,364	2,315	1,672	1,431	2,315

1:30 Model

Q (l/s)	P 1(1) (L _i) (m)	P 1(2) (L _i) (m)	P 1(3) (L _i) (m)	P 1(4) (L _i) (m)	P 1(5) (L _i) (m)	P 2(1) (L _i) (m)	P 2(2) (L _i) (m)	P 2(3) (L _i) (m)	P 2(4) (L _i) (m)	SS (L _i) (m)
22	0,290	0,336	0,363	0,308	0,380	0,333	0,309	0,375	0,333	0,333
30	0,396	0,439	0,474	0,397	0,447	0,496	0,389	0,466	0,496	0,496
41	0,539	0,580	0,625	0,518	0,539	0,570	0,502	0,588	0,570	0,570
52	0,679	0,722	0,774	0,640	0,679	0,653	0,618	0,707	0,653	0,653
66	0,852	0,903	0,959	0,796	0,852	0,772	0,772	0,855	0,772	0,772
77	0,985	1,046	1,102	0,919	0,985	0,877	0,896	0,967	0,983	0,983
88	1,114	1,188	1,242	1,042	1,114	0,991	1,025	1,076	1,072	1,072
99	1,239	1,331	1,380	1,165	1,238	1,114	1,157	1,182	1,155	1,155
110	1,362	1,474	1,515	1,289	1,399	1,247	1,292	1,284	1,233	1,233
120	1,470	1,604	1,635	1,402	1,554	1,376	1,418	1,375	1,298	1,298

Scale 1:20 Data

Protrusions 1 (1)

Q (l/s)	Depth Y2 (m)	q (m ³ /s.m)	Velocity v2 (m/s)	Froude 2	Depth Y1 (m)	Velocity v1 (m/s)	f	Y/k	Yc	Yc/k
20	0,187	0,048	0,255	0,188	0,012	3,841	0,053	0,345	0,061	1,706
40	0,259	0,095	0,369	0,231	0,025	3,779	0,111	0,701	0,097	2,708
55	0,309	0,131	0,425	0,244	0,033	3,949	0,134	0,922	0,121	3,349
70	0,356	0,167	0,469	0,251	0,040	4,139	0,148	1,120	0,142	3,933
95	0,427	0,226	0,531	0,259	0,051	4,418	0,165	1,424	0,174	4,821
110	0,465	0,262	0,564	0,264	0,058	4,550	0,175	1,601	0,191	5,316
135	0,522	0,322	0,616	0,272	0,068	4,703	0,194	1,901	0,219	6,094

Protrusions 1 (2)

Q (l/s)	Depth Y2 (m)	q (m ³ /s.m)	Velocity v2 (m/s)	Froude 2	Depth Y1 (m)	Velocity v1 (m/s)	f	Y/k	Yc	Yc/k
20	0,187	0,048	0,255	0,188	0,012	3,841	0,053	0,345	0,061	1,706
40	0,259	0,095	0,369	0,231	0,025	3,779	0,111	0,701	0,097	2,708
55	0,309	0,131	0,425	0,244	0,033	3,949	0,134	0,922	0,121	3,349
70	0,356	0,167	0,469	0,251	0,040	4,139	0,148	1,120	0,142	3,933
95	0,427	0,226	0,531	0,259	0,051	4,418	0,165	1,424	0,174	4,821
110	0,465	0,262	0,564	0,264	0,058	4,550	0,175	1,601	0,191	5,316
135	0,522	0,322	0,616	0,272	0,068	4,703	0,194	1,901	0,219	6,094

Protrusions 1 (3)

Q (l/s)	Depth Y2 (m)	q (m ³ /s.m)	Velocity v2 (m/s)	Froude 2	Depth Y1 (m)	Velocity v1 (m/s)	f	Y/k	Yc	Yc/k
20	0,204	0,048	0,234	0,166	0,011	4,487	0,033	0,295	0,061	1,706
40	0,272	0,095	0,350	0,214	0,023	4,140	0,084	0,640	0,097	2,708
55	0,321	0,131	0,409	0,230	0,031	4,224	0,109	0,862	0,121	3,349
70	0,367	0,167	0,455	0,240	0,038	4,363	0,126	1,062	0,142	3,933
80	0,396	0,191	0,482	0,245	0,043	4,460	0,135	1,188	0,155	4,299
95	0,437	0,226	0,518	0,250	0,049	4,599	0,146	1,368	0,174	4,821
110	0,475	0,262	0,552	0,255	0,056	4,722	0,156	1,543	0,191	5,316
120	0,500	0,286	0,573	0,259	0,060	4,791	0,163	1,658	0,203	5,633
135	0,534	0,322	0,603	0,264	0,066	4,877	0,174	1,833	0,219	6,094

Protrusions 1 (4)

Q (l/s)	Depth Y2 (m)	q (m ³ /s.m)	Velocity v2 (m/s)	Froude 2	Depth Y1 (m)	Velocity v1 (m/s)	f	Y/k	Yc	Yc/k
20	0,200	0,048	0,238	0,170	0,011	4,353	0,036	0,304	0,061	1,706
40	0,271	0,095	0,352	0,216	0,023	4,105	0,087	0,645	0,097	2,708
55	0,321	0,131	0,408	0,230	0,031	4,229	0,109	0,861	0,121	3,349
70	0,368	0,167	0,453	0,238	0,038	4,398	0,123	1,054	0,142	3,933
80	0,398	0,191	0,479	0,242	0,042	4,513	0,130	1,174	0,155	4,299
95	0,441	0,226	0,513	0,247	0,048	4,676	0,139	1,345	0,174	4,821
110	0,481	0,262	0,545	0,251	0,054	4,819	0,147	1,511	0,191	5,316
120	0,506	0,286	0,565	0,254	0,058	4,902	0,152	1,621	0,203	5,633
135	0,542	0,322	0,594	0,258	0,064	5,006	0,161	1,786	0,219	6,094

Protrusions 2 (1)

Q (l/s)	Depth Y2 (m)	q (m ³ /s.m)	Velocity v2 (m/s)	Froude 2	Depth Y1 (m)	Velocity v1 (m/s)	f	Y/k	Yc	Yc/k
20	0,220	0,048	0,217	0,148	0,009	5,188	0,021	0,255	0,061	1,706
40	0,280	0,095	0,341	0,205	0,022	4,349	0,073	0,609	0,097	2,708
55	0,328	0,131	0,400	0,223	0,030	4,391	0,097	0,829	0,121	3,349
70	0,373	0,167	0,447	0,234	0,037	4,497	0,115	1,031	0,142	3,933
80	0,400	0,191	0,477	0,241	0,042	4,547	0,127	1,165	0,155	4,299
95	0,440	0,226	0,515	0,248	0,049	4,657	0,141	1,351	0,174	4,821
110	0,478	0,262	0,549	0,253	0,055	4,766	0,152	1,528	0,191	5,316
120	0,505	0,286	0,566	0,254	0,059	4,880	0,154	1,628	0,203	5,633
135	0,545	0,322	0,591	0,256	0,064	5,049	0,157	1,770	0,219	6,094

Protrusions 2 (2)

Q (l/s)	Depth Y2 (m)	q (m ³ /s.m)	Velocity v2 (m/s)	Froude 2	Depth Y1 (m)	Velocity v1 (m/s)	f	Y/k	Yc	Yc/k
20	0,225	0,048	0,212	0,143	0,009	5,412	0,019	0,245	0,061	1,706
40	0,290	0,095	0,329	0,195	0,021	4,633	0,060	0,572	0,097	2,708
55	0,335	0,131	0,391	0,216	0,029	4,559	0,087	0,799	0,121	3,349
70	0,381	0,167	0,438	0,227	0,036	4,667	0,103	0,993	0,142	3,933
80	0,409	0,191	0,466	0,233	0,040	4,723	0,114	1,122	0,155	4,299
95	0,447	0,226	0,507	0,242	0,047	4,787	0,130	1,314	0,174	4,821
110	0,484	0,262	0,541	0,248	0,054	4,876	0,142	1,494	0,191	5,316
120	0,509	0,286	0,562	0,252	0,058	4,944	0,149	1,607	0,203	5,633
135	0,545	0,322	0,591	0,256	0,064	5,050	0,157	1,770	0,219	6,094

Protrusions 2 (3)

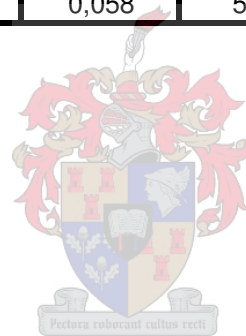
Q (l/s)	Depth Y2 (m)	q (m ³ /s.m)	Velocity v2 (m/s)	Froude 2	Depth Y1 (m)	Velocity v1 (m/s)	f	Y/k	Yc	Yc/k
20	0,225	0,048	0,212	0,143	0,009	5,412	0,019	0,245	0,061	1,706
40	0,285	0,095	0,335	0,200	0,021	4,490	0,066	0,590	0,097	2,708
55	0,332	0,131	0,395	0,219	0,029	4,487	0,091	0,812	0,121	3,349
70	0,376	0,167	0,444	0,231	0,037	4,558	0,111	1,017	0,142	3,933
80	0,402	0,191	0,474	0,239	0,042	4,594	0,123	1,153	0,155	4,299
95	0,442	0,226	0,513	0,246	0,048	4,689	0,138	1,341	0,174	4,821
110	0,481	0,262	0,545	0,251	0,054	4,812	0,148	1,514	0,191	5,316
120	0,506	0,286	0,565	0,253	0,058	4,904	0,152	1,620	0,203	5,633
135	0,545	0,322	0,591	0,256	0,064	5,049	0,157	1,770	0,219	6,094

Protrusions 2 (4)

Q (l/s)	Depth Y2 (m)	q (m ³ /s.m)	Velocity v2 (m/s)	Froude 2	Depth Y1 (m)	Velocity v1 (m/s)	f	Y/k	Yc	Yc/k
20	0,225	0,048	0,212	0,143	0,009	5,412	0,019	0,245	0,061	1,706
40	0,295	0,095	0,323	0,190	0,020	4,779	0,055	0,554	0,097	2,708
55	0,343	0,131	0,382	0,208	0,028	4,755	0,077	0,766	0,121	3,349
70	0,388	0,167	0,430	0,220	0,035	4,820	0,094	0,962	0,142	3,933
80	0,416	0,191	0,458	0,227	0,039	4,870	0,104	1,088	0,155	4,299
95	0,457	0,226	0,496	0,234	0,046	4,974	0,116	1,265	0,174	4,821
110	0,497	0,262	0,528	0,239	0,052	5,092	0,125	1,431	0,191	5,316
120	0,520	0,286	0,550	0,243	0,056	5,135	0,133	1,547	0,203	5,633
135	0,553	0,322	0,581	0,250	0,062	5,192	0,144	1,722	0,219	6,094

Standard Steps

Q (l/s)	Depth Y2 (m)	q (m ³ /s.m)	Velocity v2 (m/s)	Froude 2	Depth Y1 (m)	Velocity v1 (m/s)	f	Y/k	Yc	Yc/k
20	0,243	0,048	0,196	0,127	0,008	6,265	0,012	0,211	0,061	1,706
40	0,306	0,095	0,312	0,180	0,019	5,110	0,045	0,518	0,097	2,708
55	0,351	0,131	0,374	0,201	0,026	4,957	0,068	0,735	0,121	3,349
70	0,393	0,167	0,425	0,217	0,034	4,920	0,088	0,942	0,142	3,933
80	0,422	0,191	0,452	0,222	0,038	4,995	0,096	1,061	0,155	4,299
95	0,465	0,226	0,487	0,228	0,044	5,128	0,105	1,227	0,174	4,821
110	0,507	0,262	0,517	0,232	0,050	5,279	0,112	1,380	0,191	5,316
120	0,534	0,286	0,536	0,234	0,053	5,377	0,116	1,478	0,203	5,633
135	0,575	0,322	0,560	0,236	0,058	5,548	0,118	1,611	0,219	6,094



Scale 1:30 Data

Protrusions 1 (1)

Q (l/s)	Depth Y2 (m)	q (m ³ /s.m)	Velocity v2 (m/s)	Froude 2	Depth Y1 (m)	Velocity v1 (m/s)	f	Y/k	Yc	Yc/k
22	0,227	0,052	0,231	0,154	0,010	5,057	0,025	0,432	0,065	2,727
30	0,253	0,072	0,283	0,180	0,015	4,653	0,045	0,640	0,080	3,353
41	0,287	0,098	0,341	0,203	0,022	4,442	0,070	0,917	0,099	4,130
52	0,319	0,124	0,388	0,220	0,028	4,386	0,092	1,178	0,116	4,839
66	0,358	0,157	0,439	0,234	0,036	4,399	0,116	1,490	0,136	5,672
77	0,387	0,184	0,474	0,243	0,041	4,435	0,132	1,724	0,151	6,286
88	0,415	0,210	0,506	0,251	0,047	4,478	0,147	1,952	0,165	6,872
99	0,441	0,236	0,535	0,257	0,052	4,521	0,160	2,175	0,178	7,433
110	0,466	0,262	0,563	0,263	0,058	4,558	0,174	2,397	0,191	7,974
120	0,487	0,286	0,587	0,269	0,062	4,586	0,186	2,599	0,203	8,450

Protrusions 1 (2)

Q (l/s)	Depth Y2 (m)	q (m ³ /s.m)	Velocity v2 (m/s)	Froude 2	Depth Y1 (m)	Velocity v1 (m/s)	f	Y/k	Yc	Yc/k
22	0,237	0,052	0,221	0,145	0,010	5,466	0,020	0,400	0,065	2,727
30	0,265	0,072	0,270	0,167	0,014	5,073	0,034	0,587	0,080	3,353
41	0,303	0,098	0,323	0,187	0,020	4,910	0,052	0,829	0,099	4,130
52	0,337	0,124	0,368	0,202	0,026	4,836	0,069	1,068	0,116	4,839
66	0,378	0,157	0,417	0,216	0,033	4,829	0,088	1,358	0,136	5,672
77	0,406	0,184	0,452	0,226	0,038	4,822	0,103	1,586	0,151	6,286
88	0,433	0,210	0,484	0,235	0,043	4,826	0,117	1,811	0,165	6,872
99	0,458	0,236	0,515	0,243	0,049	4,831	0,131	2,036	0,178	7,433
110	0,482	0,262	0,544	0,250	0,054	4,831	0,146	2,261	0,191	7,974
120	0,502	0,286	0,570	0,257	0,059	4,826	0,160	2,470	0,203	8,450

Protrusions 1 (3)

Q (l/s)	Depth Y2 (m)	q (m ³ /s.m)	Velocity v2 (m/s)	Froude 2	Depth Y1 (m)	Velocity v1 (m/s)	f	Y/k	Yc	Yc/k
22	0,245	0,052	0,214	0,138	0,009	5,839	0,017	0,374	0,065	2,727
30	0,270	0,072	0,265	0,163	0,014	5,252	0,031	0,567	0,080	3,353
41	0,304	0,098	0,321	0,186	0,020	4,940	0,051	0,824	0,099	4,130
52	0,338	0,124	0,367	0,202	0,026	4,858	0,068	1,063	0,116	4,839
66	0,377	0,157	0,418	0,217	0,033	4,809	0,089	1,363	0,136	5,672
77	0,405	0,184	0,453	0,227	0,038	4,804	0,104	1,592	0,151	6,286
88	0,432	0,210	0,485	0,236	0,044	4,808	0,118	1,818	0,165	6,872
99	0,457	0,236	0,516	0,244	0,049	4,814	0,133	2,042	0,178	7,433
110	0,481	0,262	0,545	0,251	0,054	4,816	0,147	2,269	0,191	7,974
120	0,501	0,286	0,571	0,258	0,059	4,811	0,161	2,477	0,203	8,450

Protrusions 1 (4)

Q (l/s)	Depth Y2 (m)	q (m ³ /s.m)	Velocity v2 (m/s)	Froude 2	Depth Y1 (m)	Velocity v1 (m/s)	f	Y/k	Yc	Yc/k
22	0,245	0,052	0,214	0,138	0,009	5,821	0,017	0,375	0,065	2,727
30	0,270	0,072	0,265	0,163	0,014	5,252	0,031	0,567	0,080	3,353
41	0,304	0,098	0,321	0,186	0,020	4,940	0,051	0,824	0,099	4,130
52	0,339	0,124	0,366	0,201	0,025	4,887	0,067	1,057	0,116	4,839
66	0,377	0,157	0,417	0,217	0,033	4,813	0,089	1,362	0,136	5,672
77	0,405	0,184	0,453	0,227	0,038	4,805	0,104	1,592	0,151	6,286
88	0,433	0,210	0,485	0,235	0,044	4,816	0,118	1,815	0,165	6,872
99	0,459	0,236	0,515	0,243	0,049	4,836	0,131	2,033	0,178	7,433
110	0,483	0,262	0,542	0,249	0,054	4,859	0,143	2,248	0,191	7,974
120	0,505	0,286	0,567	0,255	0,059	4,879	0,155	2,443	0,203	8,450

Protrusions 1 (5)

Q (l/s)	Depth Y2 (m)	q (m ³ /s.m)	Velocity v2 (m/s)	Froude 2	Depth Y1 (m)	Velocity v1 (m/s)	f	Y/k	Yc	Yc/k
22	0,241	0,052	0,217	0,141	0,009	5,661	0,018	0,386	0,065	2,727
30	0,269	0,072	0,266	0,163	0,014	5,227	0,031	0,570	0,080	3,353
41	0,306	0,098	0,319	0,184	0,020	4,998	0,049	0,815	0,099	4,130
52	0,340	0,124	0,365	0,200	0,025	4,914	0,066	1,051	0,116	4,839
66	0,380	0,157	0,414	0,214	0,032	4,884	0,085	1,342	0,136	5,672
77	0,410	0,184	0,448	0,223	0,037	4,902	0,098	1,560	0,151	6,286
88	0,441	0,210	0,476	0,229	0,042	4,977	0,107	1,756	0,165	6,872
99	0,467	0,236	0,505	0,236	0,047	4,995	0,119	1,968	0,178	7,433
110	0,492	0,262	0,533	0,243	0,052	5,004	0,131	2,183	0,191	7,974
120	0,512	0,286	0,558	0,249	0,057	5,003	0,143	2,383	0,203	8,450

Protrusions 2 (1)

Q (l/s)	Depth Y2 (m)	q (m ³ /s.m)	Velocity v2 (m/s)	Froude 2	Depth Y1 (m)	Velocity v1 (m/s)	f	Y/k	Yc	Yc/k
22	0,235	0,052	0,223	0,147	0,010	5,373	0,021	0,407	0,065	2,727
30	0,260	0,072	0,275	0,172	0,015	4,897	0,038	0,608	0,080	3,353
41	0,295	0,098	0,331	0,195	0,021	4,681	0,060	0,870	0,099	4,130
52	0,326	0,124	0,380	0,212	0,027	4,561	0,082	1,132	0,116	4,839
66	0,365	0,157	0,431	0,228	0,035	4,539	0,106	1,444	0,136	5,672
77	0,394	0,184	0,466	0,237	0,040	4,571	0,121	1,673	0,151	6,286
88	0,423	0,210	0,496	0,244	0,045	4,625	0,133	1,890	0,165	6,872
99	0,451	0,236	0,524	0,249	0,050	4,691	0,144	2,096	0,178	7,433
110	0,478	0,262	0,549	0,253	0,055	4,763	0,152	2,294	0,191	7,974
120	0,502	0,286	0,570	0,257	0,059	4,829	0,159	2,468	0,203	8,450

Protrusions 2 (2)

Q (l/s)	Depth Y2 (m)	q (m ³ /s.m)	Velocity v2 (m/s)	Froude 2	Depth Y1 (m)	Velocity v1 (m/s)	f	Y/k	Yc	Yc/k
22	0,237	0,052	0,221	0,145	0,010	5,466	0,020	0,400	0,065	2,727
30	0,270	0,072	0,265	0,163	0,014	5,252	0,031	0,567	0,080	3,353
41	0,303	0,098	0,323	0,187	0,020	4,910	0,052	0,829	0,099	4,130
52	0,333	0,124	0,372	0,206	0,026	4,733	0,073	1,091	0,116	4,839
66	0,371	0,157	0,424	0,222	0,034	4,687	0,096	1,399	0,136	5,672
77	0,400	0,184	0,459	0,232	0,039	4,686	0,112	1,632	0,151	6,286
88	0,428	0,210	0,490	0,239	0,044	4,725	0,125	1,850	0,165	6,872
99	0,456	0,236	0,517	0,245	0,049	4,790	0,135	2,053	0,178	7,433
110	0,484	0,262	0,542	0,248	0,054	4,873	0,142	2,242	0,191	7,974
120	0,510	0,286	0,561	0,251	0,058	4,959	0,147	2,403	0,203	8,450

Protrusions 2 (3)

Q (l/s)	Depth Y2 (m)	q (m ³ /s.m)	Velocity v2 (m/s)	Froude 2	Depth Y1 (m)	Velocity v1 (m/s)	f	Y/k	Yc	Yc/k
22	0,238	0,052	0,220	0,144	0,010	5,510	0,020	0,397	0,065	2,727
30	0,272	0,072	0,263	0,161	0,013	5,325	0,030	0,560	0,080	3,353
41	0,305	0,098	0,320	0,185	0,020	4,970	0,050	0,819	0,099	4,130
52	0,338	0,124	0,367	0,201	0,025	4,862	0,068	1,062	0,116	4,839
66	0,375	0,157	0,420	0,219	0,033	4,770	0,091	1,374	0,136	5,672
77	0,401	0,184	0,458	0,231	0,039	4,714	0,110	1,622	0,151	6,286
88	0,429	0,210	0,489	0,238	0,044	4,747	0,123	1,841	0,165	6,872
99	0,458	0,236	0,515	0,243	0,049	4,825	0,132	2,038	0,178	7,433
110	0,486	0,262	0,540	0,247	0,053	4,904	0,140	2,228	0,191	7,974
120	0,511	0,286	0,560	0,250	0,057	4,981	0,145	2,393	0,203	8,450

Protrusions 2 (4)

Q (l/s)	Depth Y2 (m)	q (m ³ /s.m)	Velocity v2 (m/s)	Froude 2	Depth Y1 (m)	Velocity v1 (m/s)	f	Y/k	Yc	Yc/k
22	0,240	0,052	0,219	0,142	0,009	5,598	0,019	0,390	0,065	2,727
30	0,272	0,072	0,263	0,161	0,013	5,325	0,030	0,560	0,080	3,353
41	0,305	0,098	0,320	0,185	0,020	4,970	0,050	0,819	0,099	4,130
52	0,339	0,124	0,365	0,200	0,025	4,898	0,066	1,055	0,116	4,839
66	0,378	0,157	0,416	0,216	0,033	4,834	0,087	1,356	0,136	5,672
77	0,407	0,184	0,451	0,226	0,038	4,844	0,101	1,579	0,151	6,286
88	0,436	0,210	0,481	0,233	0,043	4,880	0,113	1,791	0,165	6,872
99	0,464	0,236	0,509	0,239	0,048	4,932	0,123	1,994	0,178	7,433
110	0,491	0,262	0,534	0,243	0,053	4,992	0,132	2,189	0,191	7,974
120	0,515	0,286	0,555	0,247	0,057	5,050	0,139	2,360	0,203	8,450

Standard Steps

Q (l/s)	Depth Y2 (m)	q (m ³ /s.m)	Velocity v2 (m/s)	Froude 2	Depth Y1 (m)	Velocity v1 (m/s)	f	Y/k	Yc	Yc/k
22	0,247	0,052	0,213	0,137	0,009	5,897	0,016	0,371	0,065	2,727
30	0,273	0,072	0,262	0,160	0,013	5,347	0,029	0,557	0,080	3,353
41	0,307	0,098	0,318	0,183	0,019	5,035	0,048	0,809	0,099	4,130
52	0,341	0,124	0,364	0,199	0,025	4,929	0,065	1,048	0,116	4,839
66	0,381	0,157	0,413	0,213	0,032	4,914	0,083	1,334	0,136	5,672
77	0,412	0,184	0,446	0,222	0,037	4,944	0,095	1,547	0,151	6,286
88	0,441	0,210	0,475	0,228	0,042	4,989	0,106	1,752	0,165	6,872
99	0,470	0,236	0,503	0,234	0,047	5,040	0,116	1,951	0,178	7,433
110	0,497	0,262	0,528	0,239	0,052	5,092	0,125	2,146	0,191	7,974
120	0,520	0,286	0,550	0,243	0,056	5,135	0,133	2,321	0,203	8,450

Scale 1:20 Data

Protrusions 1 (1)

Q (l/s)	Depth Y2 (m)	q (m ³ /s.m)	Inception Length (L _i) (m)	Y _c (m)	Y _c /k	L _i /Y _c	L _i /k
20	0,180	0,048	0,375	0,061	1,706	6,109	10,422
40	0,270	0,095	0,596	0,097	2,708	6,110	16,547
55	0,320	0,131	0,748	0,121	3,349	6,202	20,771
70	0,335	0,167	0,888	0,142	3,933	6,275	24,678
95	0,420	0,226	1,098	0,174	4,821	6,324	30,487
110	0,480	0,262	1,208	0,191	5,316	6,355	33,550
135	0,520	0,322	1,366	0,219	6,094	6,400	37,952

Protrusions 1 (2)

Q (l/s)	Depth Y2 (m)	q (m ³ /s.m)	Inception Length (L _i) (m)	Y _c (m)	Y _c /k	L _i /Y _c	L _i /k
20	0,190	0,048	0,375	0,061	1,706	6,109	10,422
40	0,270	0,095	0,596	0,097	2,708	6,110	16,547
55	0,320	0,131	0,748	0,121	3,349	6,202	20,771
70	0,340	0,167	0,888	0,142	3,933	6,275	24,678
95	0,420	0,226	1,098	0,174	4,821	6,324	30,487
110	0,480	0,262	1,208	0,191	5,316	6,355	33,550
135	0,525	0,322	1,366	0,219	6,094	6,400	37,952

Protrusions 1 (3)

Q (l/s)	Depth Y2 (m)	q (m ³ /s.m)	Inception Length (L _i) (m)	Y _c (m)	Y _c /k	L _i /Y _c	L _i /k
20	0,205	0,048	0,628	0,061	1,706	6,151	17,438
40	0,270	0,095	0,859	0,097	2,708	6,810	23,872
55	0,325	0,131	1,016	0,121	3,349	7,148	28,217
70	0,365	0,167	1,157	0,142	3,933	7,381	32,150
80	0,395	0,191	1,244	0,155	4,299	7,490	34,542
95	0,440	0,226	1,360	0,174	4,821	7,597	37,788
110	0,480	0,262	1,462	0,191	5,316	7,645	40,621
120	0,500	0,286	1,522	0,203	5,633	7,651	42,281
135	0,535	0,322	1,599	0,219	6,094	7,700	44,428

Protrusions 1 (4)

Q (l/s)	Depth Y2 (m)	q (m ³ /s.m)	Inception Length (L _i) (m)	Y _c (m)	Y _c /k	L _i /Y _c	L _i /k
20	0,200	0,048	0,308	0,061	1,706	4,600	8,547
40	0,270	0,095	0,452	0,097	2,708	4,634	12,551
55	0,320	0,131	0,574	0,121	3,349	4,759	15,937
70	0,370	0,167	0,707	0,142	3,933	4,996	19,650
80	0,400	0,191	0,803	0,155	4,299	5,189	22,308
95	0,440	0,226	0,956	0,174	4,821	5,511	26,568
110	0,480	0,262	1,122	0,191	5,316	5,861	31,155
120	0,505	0,286	1,238	0,203	5,633	6,106	34,395
135	0,545	0,322	1,423	0,219	6,094	6,487	39,529

Protrusions 2 (1)

Q (l/s)	Depth Y2 (m)	q (m ³ /s.m)	Inception Length (L _i) (m)	Y _c (m)	Y _c /k	L _i /Y _c	L _i /k
20	0,200	0,048	0,357	0,061	1,706	5,600	9,929
40	0,305	0,095	0,589	0,097	2,708	5,641	16,364
55	0,330	0,131	0,699	0,121	3,349	5,650	19,428
70	0,355	0,167	0,814	0,142	3,933	5,751	22,618
80	0,390	0,191	0,893	0,155	4,299	5,772	24,814
95	0,435	0,226	1,016	0,174	4,821	5,852	28,211
110	0,470	0,262	1,142	0,191	5,316	5,970	31,734
120	0,500	0,286	1,229	0,203	5,633	6,062	34,152
135	0,550	0,322	1,364	0,219	6,094	6,217	37,883

Protrusions 2 (2)

Q (l/s)	Depth Y2 (m)	q (m ³ /s.m)	Inception Length (L _i) (m)	Y _c (m)	Y _c /k	L _i /Y _c	L _i /k
20	0,240	0,048	0,696	0,061	1,706	9,750	19,333
40	0,310	0,095	1,066	0,097	2,708	9,800	29,615
55	0,345	0,131	1,328	0,121	3,349	9,854	36,886
70	0,385	0,167	1,576	0,142	3,933	9,989	43,780
80	0,405	0,191	1,734	0,155	4,299	10,093	48,166
95	0,440	0,226	1,900	0,174	4,821	10,211	52,778
110	0,475	0,262	2,070	0,191	5,316	10,301	57,500
120	0,500	0,286	2,183	0,203	5,633	10,400	60,633
135	0,545	0,322	2,315	0,219	6,094	10,552	64,302

Protrusions 2 (3)

Q (l/s)	Depth Y2 (m)	q (m ³ /s.m)	Inception Length (L _i) (m)	Y _c (m)	Y _c /k	L _i /Y _c	L _i /k
20	0,230	0,048	0,378	0,061	1,706	6,151	10,494
40	0,305	0,095	0,664	0,097	2,708	6,810	18,444
55	0,340	0,131	0,862	0,121	3,349	7,148	23,938
70	0,370	0,167	1,045	0,142	3,933	7,381	29,030
80	0,400	0,191	1,159	0,155	4,299	7,490	32,201
95	0,430	0,226	1,318	0,174	4,821	7,597	36,623
110	0,470	0,262	1,463	0,191	5,316	7,645	40,643
120	0,495	0,286	1,552	0,203	5,633	7,651	43,099
135	0,545	0,322	1,672	0,219	6,094	7,700	46,449

Protrusions 2 (4)

Q (l/s)	Depth Y2 (m)	q (m ³ /s.m)	Inception Length (L _i) (m)	Y _c (m)	Y _c /k	L _i /Y _c	L _i /k
20	0,230	0,048	0,284	0,061	1,706	4,352	7,898
40	0,315	0,095	0,456	0,097	2,708	5,000	12,678
55	0,350	0,131	0,620	0,121	3,349	5,329	17,222
70	0,395	0,167	0,780	0,142	3,933	5,593	21,664
80	0,410	0,191	0,884	0,155	4,299	5,745	24,569
95	0,450	0,226	1,038	0,174	4,821	5,946	28,843
110	0,480	0,262	1,189	0,191	5,316	6,123	33,014
120	0,510	0,286	1,287	0,203	5,633	6,231	35,739
135	0,550	0,322	1,431	0,219	6,094	6,379	39,741

Standard Steps

Q (l/s)	Depth Y2 (m)	q (m ³ /s.m)	Inception Length (L _i) (m)	Y _c (m)	Y _c /k	L _i /Y _c	L _i /k
20	0,200	0,048	0,693	0,061	1,706	10,150	19,263
40	0,300	0,095	1,110	0,097	2,708	10,180	30,822
55	0,360	0,131	1,388	0,121	3,349	10,250	38,559
70	0,400	0,167	1,638	0,142	3,933	10,300	45,496
80	0,430	0,191	1,788	0,155	4,299	10,350	49,678
95	0,460	0,226	1,990	0,174	4,821	10,500	55,284
110	0,500	0,262	2,163	0,191	5,316	10,701	60,091
120	0,540	0,286	2,263	0,203	5,633	10,750	62,851
135	0,605	0,322	2,315	0,219	6,094	10,752	64,302

Scale 1:30 Data**Protrusions 1 (1)**

Q (l/s)	Depth Y2 (m)	q (m ³ /s.m)	Inception Length (L _i) (m)	Y _c (m)	Y _c /k	L _i /Y _c	L _i /k
22	0,210	0,049	0,290	0,065	2,727	4,438	12,102
30	0,265	0,067	0,396	0,080	3,353	4,926	16,521
41	0,295	0,091	0,539	0,099	4,130	5,443	22,479
52	0,330	0,116	0,679	0,116	4,839	5,848	28,300
66	0,350	0,147	0,852	0,136	5,672	6,260	35,511
77	0,380	0,171	0,985	0,151	6,286	6,526	41,022
88	0,410	0,196	1,114	0,165	6,872	6,752	46,397
99	0,440	0,220	1,239	0,178	7,433	6,947	51,635
110	0,470	0,244	1,362	0,191	7,974	7,115	56,736
120	0,490	0,267	1,470	0,203	8,450	7,249	61,255

Protrusions 1 (2)

Q (l/s)	Depth Y2 (m)	q (m ³ /s.m)	Inception Length (L _i) (m)	Y _c (m)	Y _c /k	L _i /Y _c	L _i /k
22	0,240	0,049	0,336	0,065	2,727	5,129	13,988
30	0,275	0,067	0,439	0,080	3,353	5,450	18,277
41	0,310	0,091	0,580	0,099	4,130	5,855	24,182
52	0,335	0,116	0,722	0,116	4,839	6,220	30,096
66	0,385	0,147	0,903	0,136	5,672	6,635	37,635
77	0,400	0,171	1,046	0,151	6,286	6,931	43,568
88	0,425	0,196	1,188	0,165	6,872	7,205	49,511
99	0,450	0,220	1,331	0,178	7,433	7,462	55,462
110	0,480	0,244	1,474	0,191	7,974	7,703	61,421
120	0,500	0,267	1,604	0,203	8,450	7,911	66,847

Protrusions 1 (3)

Q (l/s)	Depth Y2 (m)	q (m ³ /s.m)	Inception Length (L _i) (m)	Y _c (m)	Y _c /k	L _i /Y _c	L _i /k
22	0,245	0,049	0,363	0,065	2,727	5,540	15,107
30	0,275	0,067	0,474	0,080	3,353	5,891	19,754
41	0,305	0,091	0,625	0,099	4,130	6,308	26,051
52	0,340	0,116	0,774	0,116	4,839	6,663	32,241
66	0,380	0,147	0,959	0,136	5,672	7,045	39,964
77	0,410	0,171	1,102	0,151	6,286	7,303	45,911
88	0,430	0,196	1,242	0,165	6,872	7,531	51,751
99	0,465	0,220	1,380	0,178	7,433	7,734	57,484
110	0,485	0,244	1,515	0,191	7,974	7,915	63,110
120	0,505	0,267	1,635	0,203	8,450	8,063	68,132

Protrusions 1 (4)

Q (l/s)	Depth Y2 (m)	q (m ³ /s.m)	Inception Length (L _i) (m)	Y _c (m)	Y _c /k	L _i /Y _c	L _i /k
22	0,245	0,049	0,308	0,065	2,727	4,712	12,851
30	0,280	0,067	0,397	0,080	3,353	4,929	16,530
41	0,315	0,091	0,518	0,099	4,130	5,230	21,600
52	0,340	0,116	0,640	0,116	4,839	5,515	26,684
66	0,380	0,147	0,796	0,136	5,672	5,848	33,174
77	0,400	0,171	0,919	0,151	6,286	6,091	38,288
88	0,435	0,196	1,042	0,165	6,872	6,318	43,416
99	0,465	0,220	1,165	0,178	7,433	6,533	48,557
110	0,490	0,244	1,289	0,191	7,974	6,736	53,712
120	0,510	0,267	1,402	0,203	8,450	6,912	58,410

Protrusions 1 (5)

Q (l/s)	Depth Y2 (m)	q (m ³ /s.m)	Inception Length (L _i) (m)	Y _c (m)	Y _c /k	L _i /Y _c	L _i /k
22	0,230	0,049	0,380	0,065	2,727	5,129	15,851
30	0,275	0,067	0,447	0,080	3,353	5,560	18,646
41	0,315	0,091	0,539	0,099	4,130	5,855	22,458
52	0,345	0,116	0,679	0,116	4,839	6,220	28,292
66	0,380	0,147	0,852	0,136	5,672	6,635	35,500
77	0,410	0,171	0,985	0,151	6,286	6,931	41,042
88	0,435	0,196	1,114	0,165	6,872	7,205	46,417
99	0,460	0,220	1,238	0,178	7,433	7,462	51,571
110	0,495	0,244	1,399	0,191	7,974	7,703	58,282
120	0,515	0,267	1,554	0,203	8,450	7,911	64,731



Petersona corroborant cultus recti

Protrusions 2 (1)

Q (l/s)	Depth Y2 (m)	q (m ³ /s.m)	Inception Length (L _i) (m)	Y _c (m)	Y _c /k	L _i /Y _c	L _i /k
22	0,225	0,049	0,333	0,065	2,727	5,093	13,889
30	0,275	0,067	0,496	0,080	3,353	5,500	20,669
41	0,305	0,091	0,570	0,099	4,130	5,600	23,734
52	0,335	0,116	0,653	0,116	4,839	5,620	27,194
66	0,355	0,147	0,772	0,136	5,672	5,671	32,169
77		0,171	0,877	0,151	6,286	5,810	36,526
88	0,425	0,196	0,991	0,165	6,872	6,007	41,279
99	0,445	0,220	1,114	0,178	7,433	6,246	46,427
110	0,480	0,244	1,247	0,191	7,974	6,517	51,969
120	0,510	0,267	1,376	0,203	8,450	6,787	57,350

Protrusions 2 (2)

Q (l/s)	Depth Y2 (m)	q (m ³ /s.m)	Inception Length (L _i) (m)	Y _c (m)	Y _c /k	L _i /Y _c	L _i /k
22	0,235	0,049	0,309	0,065	2,727	4,719	12,868
30	0,285	0,067	0,389	0,080	3,353	4,830	16,197
41	0,310	0,091	0,502	0,099	4,130	5,062	20,903
52	0,335	0,116	0,618	0,116	4,839	5,323	25,759
66	0,370	0,147	0,772	0,136	5,672	5,669	32,155
77	0,395	0,171	0,896	0,151	6,286	5,942	37,351
88	0,430	0,196	1,025	0,165	6,872	6,213	42,696
99	0,450	0,220	1,157	0,178	7,433	6,483	48,190
110	0,485	0,244	1,292	0,191	7,974	6,751	53,834
120	0,510	0,267	1,418	0,203	8,450	6,993	59,095

Protrusions 2 (3)

Q (l/s)	Depth Y2 (m)	q (m ³ /s.m)	Inception Length (L _i) (m)	Y _c (m)	Y _c /k	L _i /Y _c	L _i /k
22	0,235	0,049	0,375	0,065	2,727	5,723	15,607
30	0,287	0,067	0,466	0,080	3,353	5,786	19,402
41	0,315	0,091	0,588	0,099	4,130	5,934	24,505
52	0,340	0,116	0,707	0,116	4,839	6,092	29,477
66	0,375	0,147	0,855	0,136	5,672	6,278	35,614
77	0,400	0,171	0,967	0,151	6,286	6,408	40,285
88	0,430	0,196	1,076	0,165	6,872	6,523	44,824
99	0,455	0,220	1,182	0,178	7,433	6,623	49,232
110	0,490	0,244	1,284	0,191	7,974	6,710	53,507
120	0,511	0,267	1,375	0,203	8,450	6,778	57,278



Pedera roburant culus recti

Protrusions 2 (4)

Q (l/s)	Depth Y2 (m)	q (m ³ /s.m)	Inception Length (L _i) (m)	Y _c (m)	Y _c /k	L _i /Y _c	L _i /k
22	0,240	0,049	0,333	0,065	2,727	5,093	13,889
30	0,287	0,067	0,496	0,080	3,353	5,500	20,669
41	0,315	0,091	0,570	0,099	4,130	5,600	23,734
52	0,340	0,116	0,653	0,116	4,839	5,620	27,194
66	0,375	0,147	0,772	0,136	5,672	5,671	32,169
77	0,400	0,171	0,983	0,151	6,286	5,810	40,966
88	0,432	0,196	1,072	0,165	6,872	6,502	44,679
99	0,457	0,220	1,155	0,178	7,433	6,477	48,145
110	0,492	0,244	1,233	0,191	7,974	6,442	51,366
120	0,512	0,267	1,298	0,203	8,450	6,400	54,081

Standard Steps

Q (l/s)	Depth Y ₂ (m)	q (m ³ /s.m)	Inception Length (L _i) (m)	Y _c (m)	Y _c /k	L _i /Y _c	L _i /k
22	0,210	0,049	0,333	0,065	2,727	10,259	27,976
30	0,270	0,067	0,496	0,080	3,353	10,604	35,559
41	0,310	0,091	0,570	0,099	4,130	10,888	44,964
52	0,345	0,116	0,653	0,116	4,839	10,991	53,187
66	0,370	0,147	0,772	0,136	5,672	11,000	61,941
77	0,400	0,171	0,983	0,151	6,286	11,102	67,475
88	0,435	0,196	1,072	0,165	6,872	11,135	71,826
99	0,460	0,220	1,155	0,178	7,433	11,230	74,994
110	0,495	0,244	1,233	0,191	7,974	11,301	76,980
120	0,520	0,267	1,298	0,203	8,450	11,400	77,758

